



UNIVERSITY OF
LEICESTER

N/O₂ and the Granulocyte

Thesis submitted for the degree of

Doctor of Medicine

Simon Scott

Department of Cardiovascular Sciences

Division of Anaesthesia, Critical Care & Pain Management

University of Leicester

Supervisors:

Professor David G Lambert

Professor Jonathan P Thompson

2019

Abstract

Sepsis is a life-threatening syndrome associated with the deaths of 44,000 people in the UK per year. Nociceptin/orphanin FQ (N/OFQ) and its receptor (NOP) have demonstrated associations with sepsis and cells of the immune system. This thesis describes studies examining the expression of mRNA transcripts for the NOP receptor and the N/OFQ precursor ppNOC. It further describes the development of a novel live-imaging assay for the study of N/OFQ release from single human granulocytes *in vitro*. mRNA experiments demonstrated that ppNOC is predominately expressed in eosinophils. Decreased expression of mRNA for NOP in isolated human PMNs was seen following 20 hours of exposure to 0, 1, 2.5 and 5 $\mu\text{g ml}^{-1}$ LPS *in vitro*. NOP expression in PMNs after whole blood exposure to 5 hours of LPS at 0, 0.01, 0.1 and 1 $\mu\text{g ml}^{-1}$ for 5 hours was decreased. The decrease in expression between 0 and 1 $\mu\text{g ml}^{-1}$ for whole blood treated samples was ~ 200 -fold; for isolated PMN treated samples it was 3-fold. There was an apparent rightward shift in the concentration-response curve. Other factors in whole blood are likely involved in modulation of NOP expression in PMNs to LPS. Determination of PMN release of N/OFQ was achieved through development of a novel bioassay. Chimeric hNOP CHO $\alpha_{i/q}$ were loaded with Fluo-4 to detect N/OFQ-associated $[\text{Ca}^{2+}]_i$ increases by fluorescence. Confocal microscopy was used to co-image CHO cells and live human PMNs, also loaded with Fluo-4. Fluorescence of PMNs was observed in fMLP-activated PMNs. Subsequent fluorescence was observed in individual CHO cells indicating release of N/OFQ by stimulated PMNs. Exposure of CHO cells alone to fMLP-stimulated PMN supernatant was tested in the presence of a NOP antagonist (TRAP-101) and / or purinergic type 2 receptor antagonist (PPADS). Fewer CHO cells fluoresced to supernatant in the presence of TRAP-101 compared with PPADS, suggesting fMLP-stimulated PMN supernatant contains N/OFQ. These data demonstrate for the first time the visualised real-time release of N/OFQ from human immune cells. PMNs both produce and respond to N/OFQ. Further work will determine the cell types involved and their relevance to sepsis.

Acknowledgements

No thesis is written in isolation, no experiment performed without the support of friends and colleagues. My family have provided encouragement, support, and demonstrated extraordinary levels of patience. Mum, Dad, Dheya, Karen and Henry, none of this would have been possible without you – I will be forever grateful.

Dr Jonathon Willets and Shashi Rana taught me how to use the confocal microscope, manage its temperament, generate images worth talking about, and how not to break it. Their equanimity in the face of my struggles, curses, and bemusement was truly admirable. Thank you both for holding my hand.

Thank you Dr Mo Al-Hashimi, my friend and fellow lecturer for many years, for providing so much encouragement and humour. Thank you, Dr Chris Hebbes, for further developing this assay and reviewing my work. Thank you, Dr Mark Bird, for teaching me the dark arts of cell culture and cell biology, and regularly making my attempts at laboratory work less painful. Thank you, Dr John McDonald, for being there every step of the way, whether it be teaching me how to perform PCR or understand dilutions. I remain genuinely grateful for your wisdom and patience.

My supervisors are a testament to all that is excellent about academia. Without Professor Jonathan Thompson and Professor Dave Lambert, this thesis would still be an assorted collection of confused ramblings lost somewhere in a cupboard. The last few years have been incredibly challenging, and they have my eternal gratitude for ensuring that this thesis was not lost in the chaos of life. It has been a genuine privilege working with you both, and an honour to have found your friendship.

Finally, I thank Leodeb, my four-year-old son. He has spent far less time recently with his father than either he or I would have liked. To him I dedicate this thesis, this story of N/OFG and the Granulocyte.

Contents

List of figures.....	vii
List of tables.....	x
List of Abbreviations	xi
1. Introduction	1
1.1. Opioids and their receptors	1
1.2. The Nociceptin System	3
1.3. N/OFQ and Inflammation	5
1.4. Immunocytes	7
1.4.1. Animal Experiments.....	12
1.5. Sepsis.....	14
1.6. Cytokines.....	17
1.7. Therapeutics	19
1.8. Models of Sepsis	20
1.9. The Nociceptin System and Sepsis.....	23
1.10. Studying the nociceptin system.....	30
1.11. Summary and remaining questions.....	30
1.12. Hypothesis and aims	31
STUDIES OF NOCICEPTIN GENE EXPRESSION IN IMMUNOCYTES.....	33
2. Methodology.....	33
2.1. Reagents and equipment.....	33
2.2. Whole blood separation techniques.....	37
2.3. Isolating PMNs and PBMCs	37
2.3.1. Blood separation protocol 1: Ficoll-Paque™ PLUS.....	40
2.3.2. Blood separation protocol 2: Polymorphprep™	41
2.3.3. Red cell lysis protocol	41
2.3.4. Magnetic Activated Cell Sorting (MACS)	42
2.4. Haemocytometer	45
2.5. Studies of mRNA expression	46

2.5.1. mRNA extraction.....	48
2.5.2. RNA quantification and purity	49
2.5.3. Removal of genomic DNA	51
2.5.4. Reverse transcription.....	52
2.5.5. Real-time quantitative PCR (RT-qPCR).....	52
2.6. Whole blood mRNA	58
2.7. Data analysis and statistics	59
3. Results from RNA analysis	60
3.1. Granulocyte mRNA expression	60
3.1.1. Results of cell separation.....	61
3.1.2. Measures of RNA concentration and purity	61
3.1.3. Results of qPCR	62
3.2. Modulated expression of NOP in PMNs	64
3.3. Housekeeper validation	67
3.4. LPS stimulation of whole blood	73
3.5. Whole blood mRNA	79
3.6. Conclusions	82
STUDIES OF N/O ₂ RELEASE FROM PMNs USING LIVE CELL IMAGING	85
4. Methodology.....	85
4.1. Reagents used.....	85
4.2. Introduction	87
4.3. Assay development with fluorimetry	90
4.4. Confocal Microscopy.....	94
4.5. Imaging G _{αi/q} CHO cells	101
4.5.1. Culture and seeding	101
4.5.2. Fluo-4	102
4.6. Adherence of PMNs with Cell-Tak™	104
4.7. Imaging PMNs	105
4.8. Co-imaging of PMNs and CHO cells	106

4.9. Assay development.....	107
5. Results of live cell imaging.....	108
5.1. Fluorimetry	108
5.2. CHO cells as biosensors in confocal microscopy	111
5.3. Confocal imaging of polymorphonuclear cells	119
5.4. Confocal imaging of PMNs and CHO $\alpha_{i/q}$ cells	125
5.5. Stimulation of CHO-biosensors in the presence of antagonists.....	138
5.6. Conclusions	150
6. Discussion.....	151
6.1. Summary of results	151
6.2. Studies of gene expression	153
6.2.1. Limitations in studies of gene expression.....	154
6.3. Development of a novel bioassay.....	159
6.3.1. Biosensors.....	160
6.3.2. Imaging of viable PMNs	163
6.3.3. Co-imaging	167
6.3.4. Supernatant experiments	171
6.4. Further work	172
6.5. Concluding thoughts	174
7. References	175
8. Publications and grants relating to this thesis.....	188

List of figures

Figure 1.2.1 Cellular effects of N/OFQ binding to NOP.	3
Figure 1.2.2 Key structural similarities between N/OFQ and dynorphin A.	4
Figure 1.2.3 The pleiotropic nature of N/OFQ.....	5
Figure 1.3.1 Overview of cellular interactions in inflammation	7
Figure 1.4.1 The haemopoietic pathway	8
Figure 1.4.2 FACS analysis showing spread of cell populations	9
Figure 1.4.3 Pulmonary eosinophils in the nociceptin system.	11
Figure 1.4.4 Changes over time in body weight of experimental mice.....	12
Figure 1.4.5 Muscle infiltration of immunocytes	13
Figure 1.5.1 Immunologic response of three hypothetical patients with sepsis	17
Figure 1.9.1 N/OFQ in rat survival after CLP	24
Figure 1.9.2 Effects of N/OFQ and UFP-101 on cytokine levels in CLP rats.....	25
Figure 1.9.3 N/OFQ levels in sepsis:	26
Figure 1.9.4 N/OFQ in septic patients	28
Figure 1.9.5 Whole blood mRNA differences between patients	29
Figure 2.3.1 Whole blood separation by centrifugation	38
Figure 2.3.2 Different blood separation methods using density-gradient techniques ..	39
Figure 2.3.3 Cell isolation using MACS.....	44
Figure 2.5.1 From sample to PCR.....	48
Figure 2.5.2 Example spectra from NanoDrop 2000.	51
Figure 2.5.3 Summary process for RT-qPCR.	54
Figure 2.5.4 Labelled example of StepOne PCR output.....	56
Figure 2.5.5 Labelled example of StepOne PCR output.....	56
Figure 3.1.1 Results of gene expression in isolated granulocytes.....	63
Figure 3.2.1 Graphs of PMN NOP expression with LPS	66
Figure 3.3.1 Data used in NormFinder®	68
Figure 3.3.2 Output of the online tool RefFinder	69
Figure 3.3.3 Frequency distributions of raw Ct values for tested housekeeper genes..	71
Figure 3.4.1 Data from whole blood samples of 6 volunteers with subsequent stimulation with LPS.	76

Figure 3.4.2 Comparison of log transformed fold-change data (mean, SD)	77
Figure 3.4.3 Normality probability plots.....	78
Figure 3.5.1 Reduced NOP mRNA expression from whole blood.....	81
Figure 4.2.1 Principles of using CHO $G\alpha_{i/q}$ cells in live-imaging assay.....	89
Figure 4.2.2 Diagram representing key components of assay.	89
Figure 4.3.1 Excitation spectra for Ca^{2+} bound and unbound Fura-2.....	91
Figure 4.4.1 Fluorescent microscopy:.....	95
Figure 4.4.2 The confocal microscope	97
Figure 4.4.3 Illustration of perfusion system.....	99
Figure 4.4.4 Pictures of the perfusion system	100
Figure 4.5.1 Fluorescence spectra of Fluo-4.....	103
Figure 5.1.1 Mean change in $[Ca^{2+}]_i$ of CHO $G\alpha_{i/q}$ cells measured by fluorimetry.....	109
Figure 5.2.1 Mean global fluorescence of CHO $\alpha_{i/q}$ cells before and after addition of N/OFQ 10^{-6} M.....	113
Figure 5.2.2 Mean global fluorescence of CHO $\alpha_{i/q}$ cells before and after addition of N/OFQ 10^{-6} M.....	114
Figure 5.2.3 Calculation of area under the curve	115
Figure 5.2.4 AUC analysis:.....	117
Figure 5.3.1 Graphs of fluorescence	123
Figure 5.4.1 Graph demonstrating a loose relationship between the ratio of PMNs to CHOs.....	127
Figure 5.4.2 Sequence of images from a typical experiment co-imaging CHO-biosensors and PMNs.....	128
Figure 5.4.3 Experiment H2.	129
Figure 5.4.4 Experiment E3.....	130
Figure 5.4.5 Experiment D2.	131
Figure 5.4.6 Experiment A1.	135
Figure 5.5.1 Two experiments demonstrating the response of CHO-biosensors to different concentrations of N/OFQ (experiment A), and ATP (experiment B).....	140
Figure 5.5.2 Flow of experiments using supernatant from fMLP-stimulated PMNs to stimulate CHO-biosensors	141
Figure 5.5.3 Experiment E1b.....	144

Figure 5.5.4 Experiment A3.	145
Figure 5.5.5 Experiment (cells from D1) demonstrating that supernatant stimulation of CHO-biosensors is antagonised by the combination of PPADS & TRAP-101.....	146
Figure 5.5.6 Mean fluorescence for CHO-biosensors (n=33) illustrating a sensitive response to fMLP-stimulated PMN supernatant.....	148
Figure 6.1.1 Summary of key findings and development process of a novel live-imaging bioassay.....	152
Figure 6.2.1 Gene expression in a model system	158
Figure 6.3.1 Sigmoid curves superimposed on graphs to help identify genuinely responding PMNS to fMLP	166
Figure 6.3.2 ERK1/2 phosphorylation (pERK = phosphorylated ERK, tERK = total ERK) in EoL-1 cells	169
Figure 6.3.3 Eosinophil regulation of neutrophils	171

List of tables

Table 1.1.1 Summary of opioid receptors and their ligands with associated systemic effects.	2
Table 1.5.1 Sequential Organ Assessment Failure Score.....	15
Table 1.5.2 Sepsis-3 definitions	15
Table 1.5.3 Quick SOFA criteria	16
Table 1.6.1 Pro-inflammatory and anti-inflammatory mediators of sepsis	19
Table 3.1.1 Cell count for cells extracted from separation layers.....	61
Table 3.1.2 Summary of nucleic acid concentrations and their ratiometric purity.	62
Table 3.2.1 Summary of nucleic acid concentrations.....	65
Table 3.3.1 Stability values acquired from NormFinder®	69
Table 3.4.1 Summary of nucleic acid concentrations.....	74
Table 3.4.2 Mean Δ Ct (SD) values for PMN NOP mRNA expression	75
Table 3.5.1 Summary of mRNA yields from whole blood mRNA extraction.	79
Table 5.1.1 Summary of fluorimetry experiments	110
Table 5.2.1 Results of four passages of CHO $\alpha_{i/q}$ cells stimulated with 10^{-6} M N/OFO.	112
Table 5.4.1 Co-imaging results.....	126
Table 5.5.1 Summary contingency tables.....	142
Table 5.5.2 Results from supernatant experiments arranged by first antagonist.	143
Table 6.2.1 Mean raw Ct values from RT-qPCR for control and LPS-exposed samples.	155

List of Abbreviations

18S	18S ribosomal RNA
ACTB	Actin beta
ADP	Adenosine diphosphate
AM	Acetoxymethyl
AMP	Adenosine monophosphate
ANOVA	Analysis of variance
ARDS	Adult respiratory distress syndrome
ATP	Adenosine triphosphate
AUC	Area under the curve
B2M	Beta-2-microglobulin
BODIPY	Boron-dipyrromethene
cAMP	Cyclic AMP
CARS	Compensatory anti-inflammatory response syndrome
CCL5	Chemokine (C-C motif) ligand 5; also RANTES
cDNA	Copy DNA
CHO	Chinese Hamster Ovary cell
CLP	Caecal ligation and puncture
Ct	Cycle threshold
DAG	Diacyl glycerol
DMEM	Dulbecco's Modified Eagle Medium
DMSO	Dimethylsulfoxide
dNTP	Deoxynucleotidetriphosphates
DOP	Delta opioid receptor
DSS	Dextran sulphate sodium
EDTA	Ethylenediaminetetraacetic acid
EGTA	Ethylene glycol-bis(β -aminoethyl ether)-N,N,N',N'-tetraacetic acid
ELISA	Enzyme linked immunosorbent assay
ERK1/2	Extracellular signal-regulated kinase
FACS	Fluorescence activated cell sorting
FITC	Fluorescein isothiocyanate
fMLP	N-Formylmethionine-leucyl-phenylalanine
GAPDH	Glyceraldehyde 3-phosphate dehydrogenase
GOI	Gene of interest
GPCR	G-protein couple receptor
GRK	G-protein coupled receptor kinase
HEPES	4-(2-hydroxyethyl)-1-piperazineethanesulfonic acid
HKG	Housekeeper gene; also reference gene
HPRT-1	hypoxanthine phosphoribosyltransferase 1
ICU	Intensive Care Unit
IL-	Interleukin
KOP	Kappa opioid receptor
LPS	Lipopolysaccharide; also endotoxin

MACS	Magnetic activated cell sorting
MAPK	Mitogen-activated protein kinase
MIF	Macrophage inhibitory factor
MOP	Mu opioid receptor
mRNA	Messenger RNA
N/OFQ	Nociceptin/orphanin FQ
NADPH	Reduced form of nicotinamide adenine dinucleotide phosphate
NET	Neutrophil extracellular trap
NF- κ B	Nuclear factor kappa-B
NK cells	Natural killer cells
NOP	Nociceptin opioid receptor
ORL-1	Opioid receptor like-1; see NOP
PAMP	Pathogen-associated molecular pattern receptor
PBMC	Peripheral blood mononuclear cells
PBS	Phosphate buffered saline
PCR	Polymerase chain reaction
PCT	Procalcitonin
PIP-2	Phosphatidylinositol 4,5-biphosphate
PKG-1	Protein kinase G-1
PLC	Phospholipase C
PMA	Phorbol myristate acetate
PMN	Polymorphonuclear cells; also granulocyte
PMT	Photomultiplier tube
PPADS	Pyridoxalphosphate-6-azophenyl-2',4'-disulfonic acid
ppNOC	Pre-pro nociceptin/orphanin FQ; also pp-N/OFQ, pNOC
RANTES	Regulated on activation, normal T cell expressed and secreted; also CCL5
RIA	Radioimmunoassay
ROI	Region of interest
RPLP0	Ribosomal protein lateral stalk subunit P0
RPMI media	Roswell Park Memorial Institute media
RT-qPCR	Real-time quantitative PCR
SEB	Staphylococcal enterotoxin B
SIRS	Systemic inflammatory response syndrome
SOFA	Sequential organ failure assessment score
TLR	Toll-like receptor
TNF- α	Tumour necrosis factor
TRAP-101	1-[1-(cyclooctylmethyl)-1,2,3,6-tetrahydro-5-(hydroxymethyl)-4-pyridinyl]-3-ethyl-1,3-dihydro-2Hbenzimidazol-2-one hydrochloride
UFP-101	[NPhe1, Arg14, Lys15]N/OFQ-NH2
UTP	Uridine triphosphate

1. Introduction

Sepsis kills approximately 44,000 people every year in the UK alone.¹ Although there has been significant progress in understanding sepsis, there are still no effective specific therapeutics. This thesis explores the association of the endogenous opioid N/OFQ (nociceptin/ orphanin FQ) with granulocytes, important modulators of sepsis, and its possible role within the sepsis syndrome.

1.1. Opioids and their receptors

Endogenous opioid receptors are widely distributed throughout the human body. They are primarily associated with anti-nociception: their activation inhibits neurotransmission of nociceptive signals. They are G-protein coupled receptors (GPCRs) that when bound to opioid ligands decrease calcium ion conductance, reduce cyclic AMP (cAMP) formation and stimulate an efflux of potassium ions hyperpolarising the cell membrane. Opioid receptors were originally named after the compounds used to discover them or their discovered anatomical location; *mu* receptors from *morphine*, *kappa* receptors from *ketocyclazocine* and *delta* receptors from *vas deferens*. Current terminology is based on the International Union of Pharmacology (IUPHAR) nomenclature: MOP (mu opioid peptide), mu or μ ; KOP, kappa or κ ; DOP, delta or δ .² Opioid drugs have widespread effects on the gastrointestinal (constipation and nausea), respiratory (respiratory depression), cardiovascular (hypotension), immune (immunosuppression with long-term use) and other systems (see Table 1.1.1).

In 1995 a further opioid receptor ORL-1 was deorphanised following the discovery in mammalian brain tissue of its endogenous peptide ligand nociceptin/orphanin FQ (N/OFQ).^{3 4} Despite sharing many of the characteristics of classical opioid receptors (amino acid sequence homology, being a GPCR, negative coupling with adenylate cyclase), opioid receptor like-1 (ORL-1) or NOP as it is now known, does not bind classical opioid ligands. N/OFQ binding is also not reversible by the opioid antagonist naloxone.⁵

Ligands	Receptor subtype			
	MOP (μ , μ)	KOP (κ , κ)	DOP (δ , δ)	NOP (ORL-1)
Endogenous				
β -endorphin	+++	+++	+++	0
Endomorphin	+++	0	0	0
Leu-enkephalin	+	0	+++	0
Met-enkephalin	++	0	+++	0
Dynorphin A/B	++	+++	+	+
N/OFQ	0	0	0	+++
Agonists				
Morphine	+++	+	+	0
Meperidine	+++	+	+	0
Diamorphine	+++	+	+	0
Fentanyl / remifentanyl	+++	+	0	0
Antagonist				
Naloxone	+++	++	++	0
Effects				
CNS	Analgesia Sedation Euphoria HPA axis Thermo- regulation	Sedation Dysphoria Hallucinations Analgesia / antanalgesia	Analgesia Opioid tolerance Possible antidepressant effects	Spinal analgesia Supraspinal analgesia Opioid tolerance
Cardiovascular	Bradycardia Hypotension			Vasodilation
Respiratory	Depression		Depression	
Gastrointestinal	Nausea Vomiting Constipation		Constipation	
Genitourinary	Urinary retention	Diuresis	Urinary retention	Antidiuresis
Immune system	Depression (HPA)			Possible pro- inflammatory effects
Dermal	Pruritis	Antipruritis		

Table 1.1.1 Summary of opioid receptors and their ligands with associated systemic effects. Selectivity of ligands expressed as +++ = high affinity, ++ = intermediate affinity, + = low affinity, x = no affinity. N/OFQ = nociceptin/orphanin FQ; CNS = central nervous system; HPA = hypothalamic-pituitary axis (adapted from McDonald and Lambert 2015).⁶

Subsequent research has demonstrated that NOP is distributed amongst many physiological systems, particularly pain and inflammatory pathways, in common with other endogenous opioids.

1.2. The Nociceptin System

The nociceptin system comprises N/OFQ (a 17 amino acid peptide), its precursor pre-pro nociceptin/orphanin FQ (pp-N/OFQ) and its receptor NOP. Following the de-orphanisation of NOP, an accumulating body of data implicate the role of this non-classical opioid system in pathways such as nociception, the hypothalamopituitary axis (HPA), acute and chronic inflammation, as well as cancer.^{7,8}

N/OFQ is a neuropeptide, existing in plasma at low concentrations (10 pg ml^{-1}). Its effects on NOP are similar to those of other opioid-receptor interactions, i.e. inhibition of cAMP formation, closure of voltage-gated calcium channels and the opening of potassium channels resulting in a decrease in intracellular calcium and decreased membrane excitability (illustrated in Figure 1.2.1). Proteolytic processing of the precursor pp-N/OFQ forms N/OFQ and two additional proteins (nocistatin and O/FQ2, which may

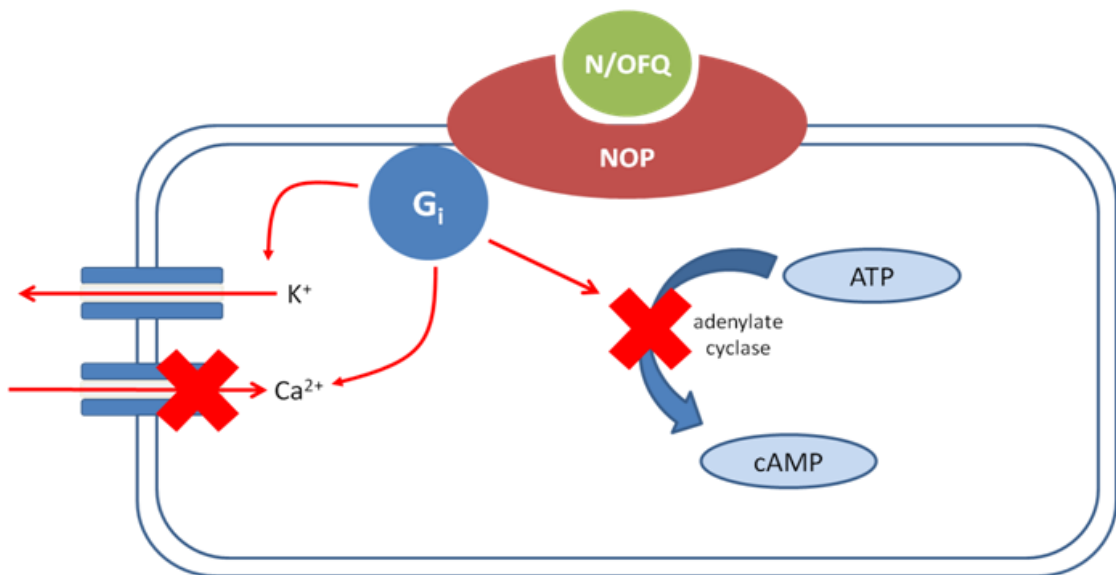


Figure 1.2.1 Cellular effects of N/OFQ binding to NOP. NOP is Gi-coupled, therefore the binding of the agonist N/OFQ leads to a decrease in calcium conductance, increased potassium permeability, and reduced conversion of ATP to cAMP via inhibition of adenylate cyclase.

have regulatory functions). N/OFQ is similar in structure to the endogenous opioid KOP agonist dynorphin A (see Figure 1.2.2).

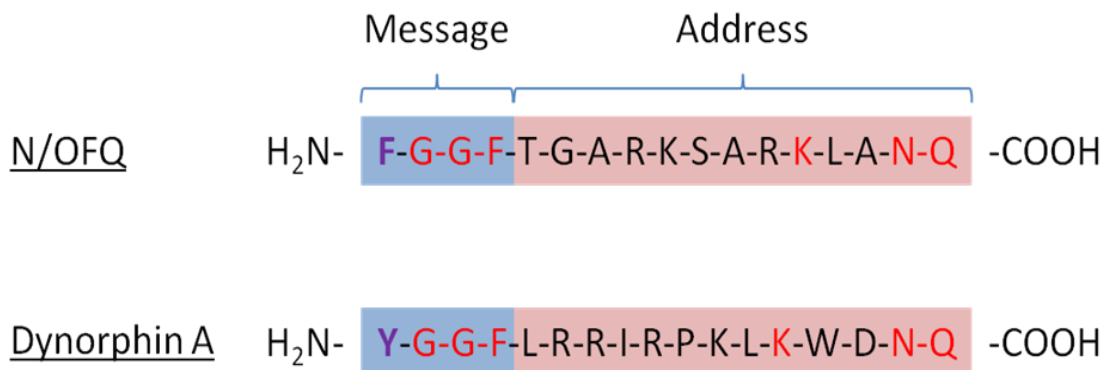


Figure 1.2.2 Key structural similarities between N/OFQ and dynorphin A. Similar to a range of peptides, their structure can be loosely divided into a message sequence (receptor activation) and address sequence (receptor occupation). Red letters represent preserved amino acid sequences between N/OFQ and dynorphin A - the substitution of tyrosine in dynorphin A (Y) with phenylalanine (F) confers NOP specificity (adapted from Lambert, 2008).⁷

The nociceptin system is distributed widely (see Figure 1.2.3). Its components have been determined in central, peripheral and sensory nervous systems, as well as in various regions such as the pulmonary system, myocardial cells, and immunocytes.^{7 9 10} Initial work considered its role in nociception. Spinal administration of N/OFQ is associated with antinociception (except at very low doses), but in rodents intracerebroventricular injections have been shown to be pronociceptive.^{4 11 12} Spinal administration is associated with analgesia in non-human primates - even at very low doses.¹³ However, in contrast to rodents, supraspinal administration of N/OFQ in primates is antinociceptive.¹⁴ The potential therapeutic role of modulating the nociceptin system in acute and chronic pain states continues to receive considerable interest.

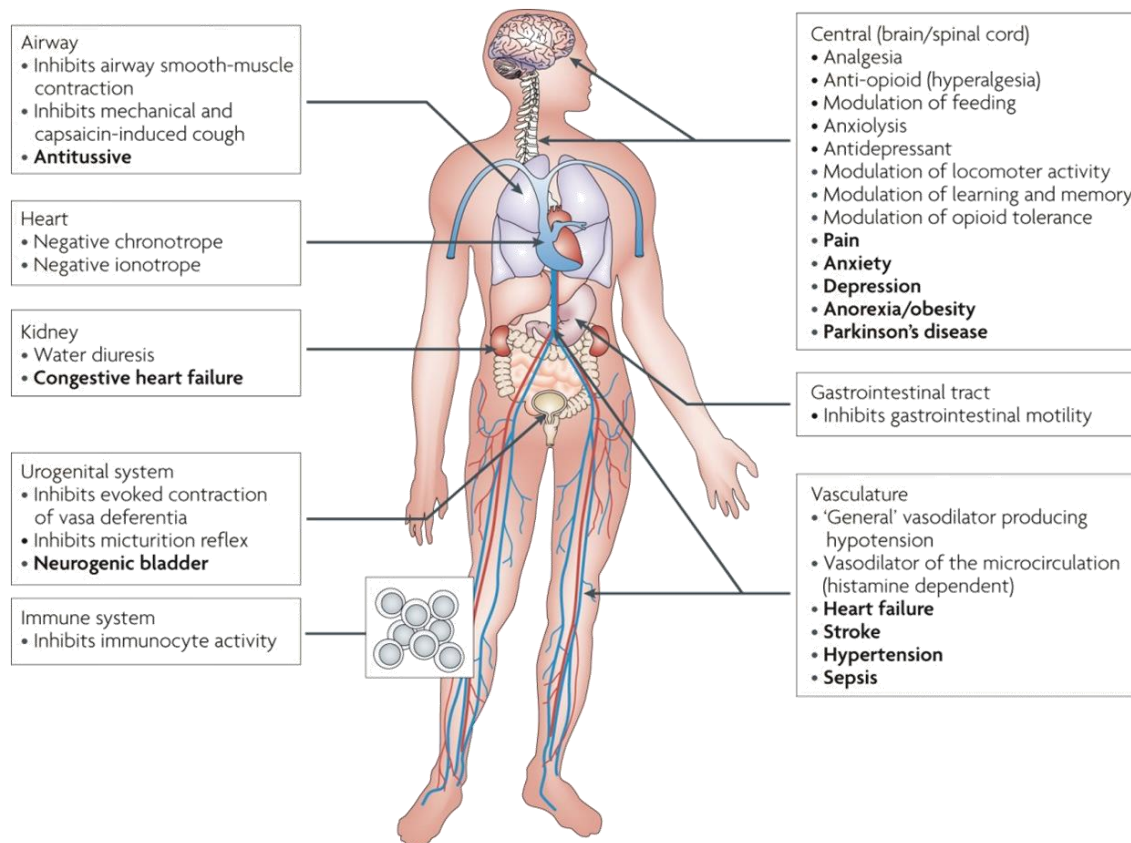


Figure 1.2.3 The pleiotropic nature of N/OFQ (from Lambert, 2008).⁷ Bold type represents potential clinical applications.

1.3. N/OFQ and Inflammation

Pain and inflammation are intimately connected, having been recognised in the 1st century AD by Celsus in *De Medicina* – ‘calor, dolor, rubor, and tumor’. With early reports of classical opioid receptors expressed in human leucocytes (since disputed) as well as the widely documented immunosuppressive effects of opioids, it is perhaps not surprising that the nociceptin system has an increasingly recognised role in immunomodulation.^{15–19}

Inflammation is mediated via immune cells, specifically leucocytes and their subpopulations. In summary, immune cells local to the site of the inflammatory stimulus (e.g. macrophages, histiocytes) recognise antigenic molecular patterns or tissue damage, are activated and release inflammatory mediators (e.g. nitric oxide) resulting in vasodilation and increased vascular permeability. Leucocytes (predominately neutrophils) migrate to the site of inflammation, and a further cascade of reactions

occurs (e.g. complement activation, fibrinolysis), propagating the inflammatory process. This innate immune response continues until the inflammatory stimulus is removed or eradicated. The innate immune system also activates the adaptive immune response via stimulation of lymphocytes, specifically T-cells. Immune cells from the innate system, such as dendritic cells or macrophages, can present foreign antigen on their cell surface through coupling with specific cell surface receptors (major histocompatibility complex) that are recognised by T-cells. This results in T-cell activation, the release of cytokines, and further propagation of the immune response. B-cells are also crucial to this system and form the basis of humoral immunity. In a similar manner to dendritic cells, B-cells phagocytose foreign protein and present foreign protein to T-cells. These T-cells then stimulate the B-cells to form antibody-producing plasma cells. Antibodies then bind to specific foreign antigens, enhancing their eradication by phagocytes (opsonisation) and further acting as a stimulus to complement.²⁰ This process is illustrated in Figure 1.3.1.

Important mediators of the inflammatory system are cytokines (see below), as well as other mediators (e.g. nitric oxide). There is an increasing body of *in vitro* and *in vivo* evidence that suggests that the nociceptin system has an important modulatory role in the inflammatory response.

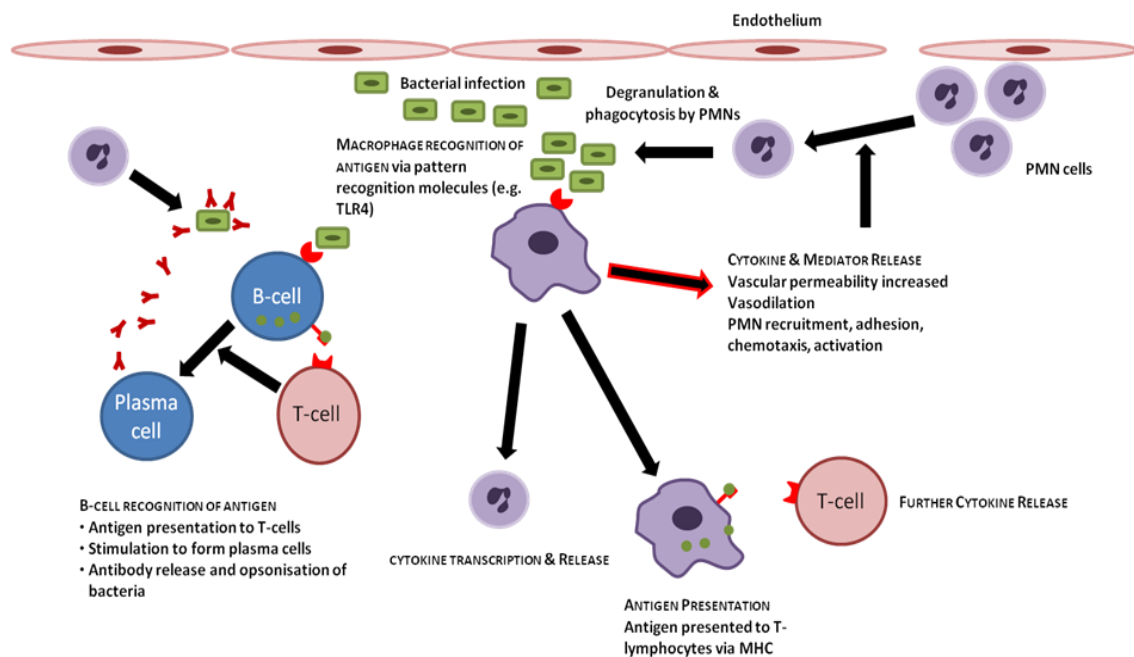


Figure 1.3.1 Overview of cellular interactions in inflammation: Macrophages (or other antigen-presenting cells, APCs) recognise foreign protein via pattern recognition molecules. Cytokines are released that promote local recruitment of phagocytic cells (neutrophils) as well as stimulating systemic changes (e.g. vasodilation, endothelial changes). APCs also activate circulating T-cells by binding with major histocompatibility complex (MHC) surface receptors, also inducing further cytokine release. Circulating B-cells also act as APCs and form antibody secreting plasma cells.

1.4. Immunocytes

A summary of the evidence for the role of inflammatory cells in the nociceptin system is shown in Figure 1.4.1. Much of the cellular evidence is based around the extraction of messenger RNA (mRNA) and analysis of copy DNA (cDNA) transcripts for components of the nociceptin system, i.e. NOP and pp-N/OFQ (termed ppNOC in this thesis). Key to this is the determination of mRNA for nociceptin components in leucocytes, the key cellular mediators of inflammation.

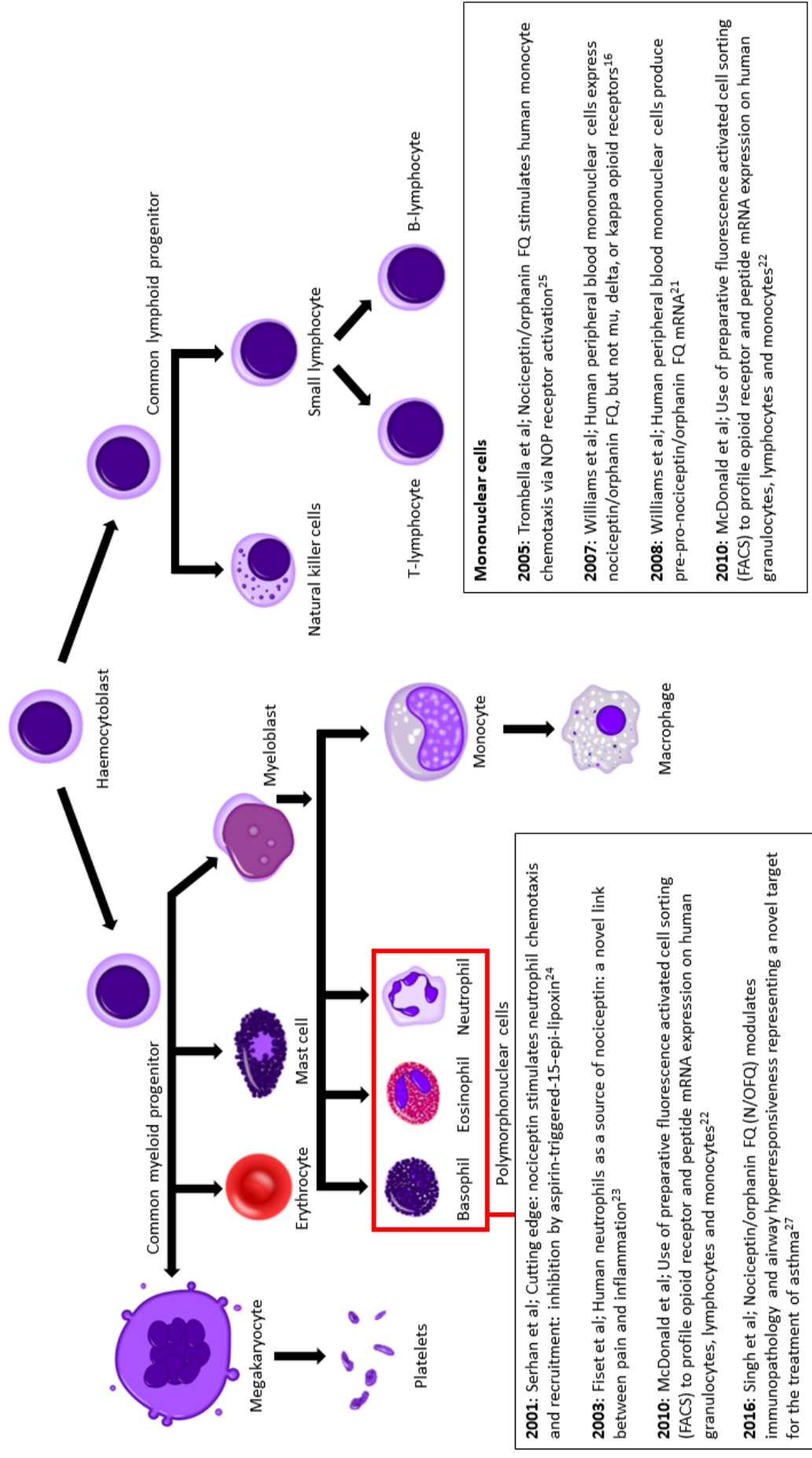
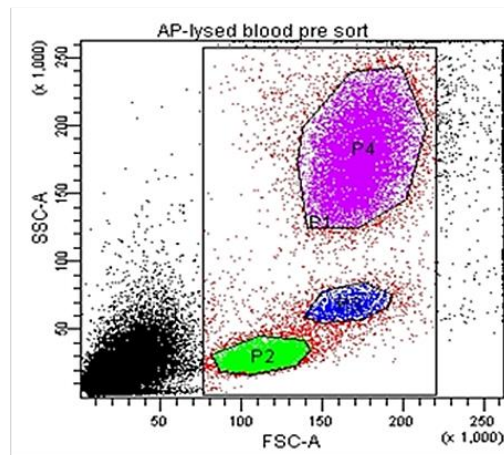


Figure 1.4.1 The haemopoietic pathway illustrating the key cells of inflammation with a summary of evidence for the association of myeloblastic derivatives with the nociceptin system.

Our own laboratory has determined that mRNA for NOP and ppNOC is produced by peripheral blood mononuclear cells (PBMCs), i.e. macrophages, monocytes, and lymphocytes, through use of quantitative polymerase chain reaction (qPCR) analysis.¹⁶ Furthermore, our research group did not identify mRNA transcripts for any of the traditional opioid receptors. Fluorescent-naloxone also did not bind to PBMCs, assessed using fluorescence-activated cell sorting (FACS); a negative finding that was also seen when using a radio-labelled opioid receptor agonist (³H)diprenorphine).¹⁶

Similar work has provided evidence for NOP and ppNOC on granulocyte and monocyte populations. Within our own laboratory, peripheral polymorphonuclear cells (PMNs), lymphocytes, and monocytes (precursors of macrophages) were isolated using FACS. After mRNA extraction and reverse transcription to cDNA, qPCR was performed using TaqMan probes to MOP, NOP and ppNOC. Once again, no mRNA could be determined for MOP in any leucocyte whilst mRNA for NOP, and ppNOC (although at low levels), was shown to be expressed. These data are shown in Figure 1.4.2.²²



Cell Type	MOP Δ Ct	NOP Δ Ct	pp-N/OFQ Δ Ct
Granulocyte	Not detected	5.93(2.44-8.92)	10.37(6.50-11.3)
Monocyte	Not detected	6.33(5.07-7.99)	8.37(6.95-10.27)
Lymphocyte	Not detected	6.78(5.64-9.26)	6.28(5.05-11.45)

Figure 1.4.2 FACS analysis showing spread of cell populations (P2/green=lymphocytes, P3/blue=monocytes, P4/pink=granulocytes) with table showing subsequent MOP, NOP and pp-N/OFQ (ppNOC) qPCR expression displayed as delta CT values (McDonald et al, 2010).²²

These data only demonstrate that cellular DNA is transcribed into mRNA for NOP receptors and ppNOC, and not that any protein is produced or is functional; that such transcription does occur correlates well with further *in vitro* work and functional studies in animals. Fiset and colleagues not only confirmed the presence of NOP and ppNOC mRNA transcripts in stimulated PMNs via Northern Blot analysis, but also demonstrated that degranulated PMN supernatants contained N/OFQ as determined by enzyme-linked immunoabsorbent assay (ELISA).²³ In the same paper this group also demonstrated that cAMP levels were attenuated in stimulated PMNs when exposed to N/OFQ.

Evidence of NOP receptor function is further supported by chemotaxis experiments. Serhan and colleagues identified mRNA transcripts for NOP, detected NOP surface receptors (using ¹²⁵I-labelled N/OFQ), and used a microchamber migration assay to assess the effect of synthetic N/OFQ on PMN migration.²⁴ Compared with a chemoattractant (fMLP), N/OFQ was shown to be at least 100-fold more potent in evoking PMN chemotaxis. Such chemoattraction was confirmed *in vivo* using an established animal model of leucocyte infiltration, the murine dorsal air pouch. N/OFQ induced significant leucocyte recruitment. Trombella and colleagues performed similar *in vitro* experiments, determining that N/OFQ was a potent chemoattractant of monocytes.²⁵ Whilst their data did not support N/OFQ being a chemoattractant of neutrophils, they were able to demonstrate that N/OFQ promotes the release of lysozyme from neutrophils.

Some further *in vitro* studies in mouse cells suggest that N/OFQ also has antibody suppressing activity.²⁶ A plaque-forming assay combining antigenic sheep red cells with spleen tissue from mice was used to assess antibody formation in the presence of increasing doses of N/OFQ. The ability for the splenic cells to mount an appropriate antibody response was suppressed by a dose range of N/OFQ (10^{-14} to 10^{-11} M). Naloxone did not reverse this antibody suppression. Whilst these findings have not yet been replicated in human tissues, they support a potential role for the nociceptin system in modulating the adaptive immune response.

More recently, evidence has been published that suggests, in the pulmonary system, eosinophils may have an important role in the nociceptin system. Singh and colleagues determined that the NOP receptor is expressed in human and mouse immune and airway cells.²⁷ Furthermore, they determined that ppNOC transcripts were expressed in eosinophils, with the number of cells demonstrating a weak correlation with sputum N/OFQ peptide concentrations as determined by radioimmunoassay (RIA) (see Figure 1.4.3). N/OFQ peptide was isolated in human sputum, and its concentrations were increased in patients with asthma. The authors also administered N/OFQ to mice and determined that the peptide reduced airway constriction and immunocyte trafficking to the lung. N/OFQ was also associated with a reduction in inflammatory mediators (IL-4, IL-5, IL-12 and IL-13) and the production of mucin.

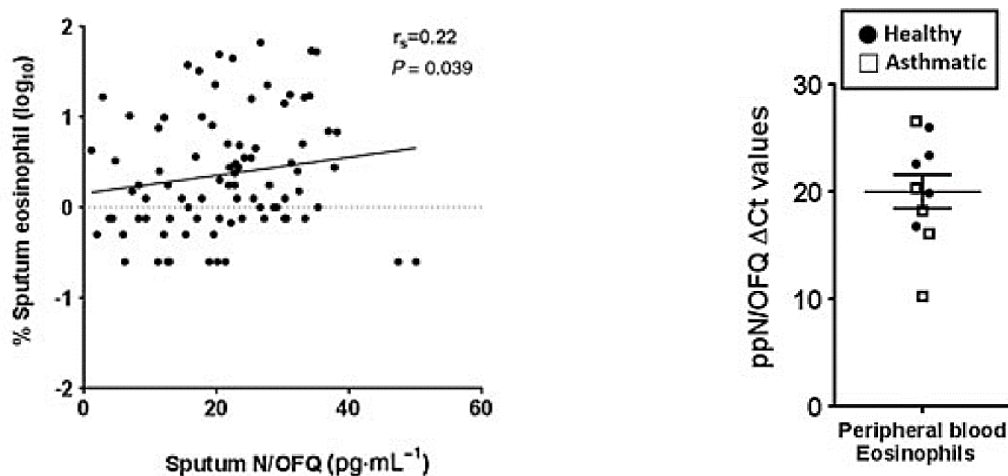


Figure 1.4.3 Pulmonary eosinophils in the nociceptin system. The left-hand graph demonstrates a weak correlation between eosinophil count and sputum N/OFQ. On the right, the graph demonstrates plasma eosinophil mRNA ΔC_t values for the N/OFQ precursor. Both suggest that pulmonary eosinophils are involved in the nociceptin system (Singh et al, 2016).²⁷

1.4.1. Animal Experiments

Evidence from NOP-knockout mice provides a compelling argument that the nociceptin system has a functional role in inflammation.²⁸ Dextran sulphate sodium (DSS) was administered to mice to induce inflammatory colitis. Experimental mice comprised NOP-deficient mice and wild-types, with or without oral DSS treatment. The colon of each mouse was surgically removed under anaesthesia after twenty days and examined for histological damage. Wild-type mice developed signs of colitis as well as significant weight loss, whilst NOP-deficient mice did not (see Figure 1.4.4). Furthermore, colons extracted from the untreated wild-type mouse group and NOP-deficient mouse group displayed no histological changes, whereas those from the wild-type treated mouse group showed significant histological changes consistent with acute colitis.

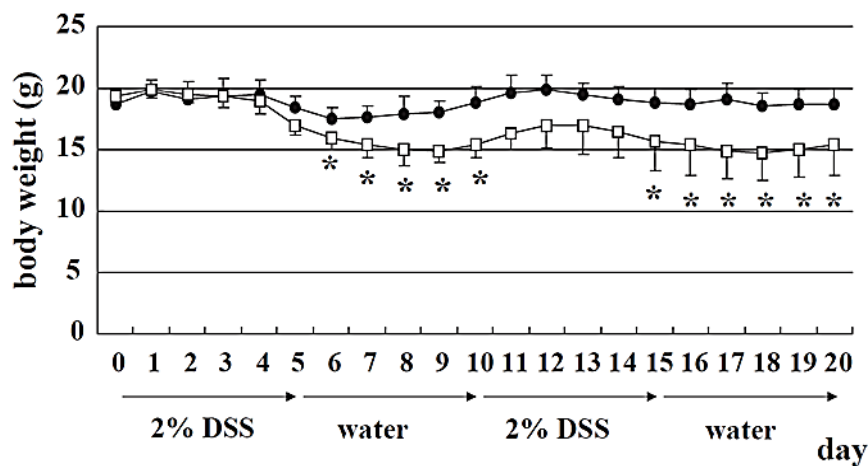


Figure 1.4.4 Changes over time in body weight of experimental mice. Black-circles = NOP-deficient mice; squares = wild-type. Results expressed as mean +/- SD. * = $p < 0.005$ compared with day 0. (Data from Kato et al, 2005).²⁸

Immunohistochemical analysis of the colon samples using polyclonal antibodies to N/OFQ revealed significant upregulation of the peptide in DSS-treated mice as compared with untreated and NOP-deficient mice. Immunocyte infiltration was also significantly increased in DSS-treated wild-type mice, particularly amongst lymphocytes (see Figure 1.4.5).

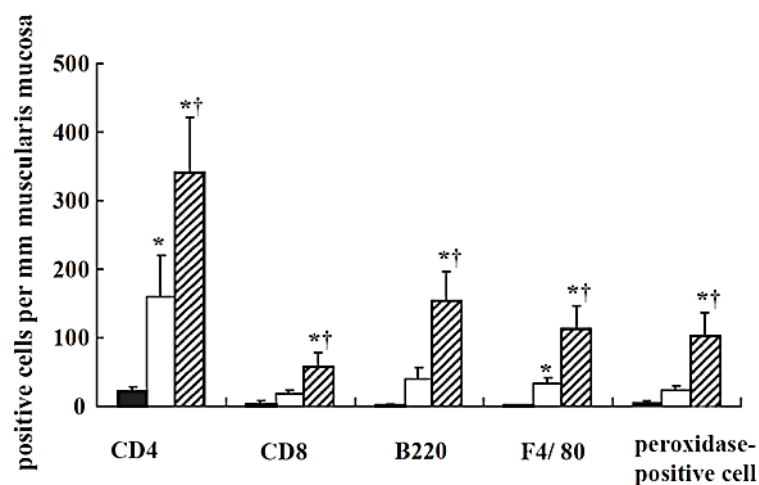


Figure 1.4.5 Muscle infiltration of immunocytes for DSS-treated wild-type mice (hatched columns), untreated NOP-deficient mice (white columns) and DSS-treated NOP-deficient mice (black columns). (Data from Kato et al, 2005).²⁸

The implication of this work is that mice lacking NOP are resistant to the colonic inflammatory process induced by DSS, thus suggesting a key inflammatory role for NOP.

Further evidence for the nociceptin system having a functional role in inflammation comes from work in rat mesenteric vessels.²⁹ After surgical exteriorisation of the terminal ileum, a series of experiments assessing vascular and endothelial changes in response to N/OFQ, UFP-101 (a N/OFQ antagonist), and histamine antagonists were performed. *In vitro* pressure myography experiments were also performed to determine changes in vascular luminal diameter in response to topical stimulation by N/OFQ. Brookes and colleagues demonstrated that N/OFQ administered intravenously caused hypotension, an increase in endothelial permeability, leucocyte recruitment, and vasodilation – features consistent with systemic inflammation. N/OFQ-induced endothelial permeability and vasodilation were reversible by UFP-101, as well as histamine antagonists, suggesting a role for histamine (a well-recognised mediator of inflammation) in mediating the systemic effects of N/OFQ.

Other cardiovascular effects have also been demonstrated in rats. The intravenous administration of N/OFQ to anaesthetised healthy rats resulted in a dose-dependent

reduction in heart rate and blood pressure. The mechanisms for this were postulated as involving the autonomic nervous system – guanethidine combined with bilateral vagotomies prevented any N/OFQ induced cardiovascular effects.³⁰

It is clear that the nociceptin system has a functional role within the inflammatory process. However, how and where it fits within the inflammatory cascade remains poorly understood. There are also data that suggest a key role for the nociceptin system in mediating the clinically important systemic inflammatory process of sepsis.

1.5. Sepsis

Sepsis is defined as ‘life-threatening organ dysfunction caused by a dysregulated host response to infection’.³¹ The health impact of sepsis is significant: sepsis affects millions of people every year with a mortality of approximately 25%, and it accounted for more than \$20 billion of total US hospital costs in 2011. The diagnosis of sepsis has traditionally been stratified into sepsis, severe sepsis and septic shock using physiological criteria in the presence of infection. However, the sepsis criteria were widely recognised as being non-specific and in essence only reflected a host’s systemic inflammatory response to an insult. There is no diagnostic test for sepsis, yet its early diagnosis and management are key to patient survival.

Recent work has attempted to improve diagnosis of sepsis, with a focus on early recognition and management, and the importance of organ dysfunction. The currently accepted definitions – Sepsis-3 consensus – are based on a comprehensive review of 1.3 million clinical encounters within the University of Pittsburgh Medical Center health system.³¹ They recognise the importance of organ dysfunction as measured by the Sequential Organ Failure Assessment Score (SOFA), detailed in Table 1.5.1. The definitions from Sepsis-3 are given in Table 1.5.2. Recognising the importance of early diagnosis, qSOFA (see Table 1.5.3) has also been developed from this data set, designed to improve the rapid identification of patients with suspected sepsis.

System	Score				
	0	1	2	3	4
Respiratory					
PaO ₂ /FiO ₂ mmHg (kPa)	≥400 (53.3)	<400 (53.3)	<300 (40)	<200 (26.7) & respiratory support	<100 (13.3) & respiratory support
Coagulation					
Platelets ×10 ³ /μL	≥150	<150	<100	<50	<20
Liver					
Bilirubin mg/dL (μmol/L)	<1.2 (20)	1.2-1.9 (20-32)	2.0-5.9 (33-101)	6.0-11.9 (102-204)	>12.0 (204)
Cardiovascular					
MAP (mm Hg) Vasopressor (μg kg ⁻¹ min ⁻¹ for ≥1 hr)	MAP ≥70	MAP <70	DA <5 or dobutamine (any dose)	DA 5.1-15 or Adr ≤0.1 or NA ≤0.1	DA >15 or Adr >0.1 or NA >0.1
Central nervous system					
Glasgow Coma Scale	15	13-14	10-12	6-9	<6
Renal					
Creatinine mg/dL (μmol/L)	<1.2 (110)	1.2-1.9 (110-170)	2.0-3.4 (171-299)	3.5-4.9 (300-440)	>5.0 (440)
Urine output mL/d				<500	<200
Notes: DA=dopamine, Adr=adrenaline, NA=noradrenaline					

Table 1.5.1 Sequential Organ Assessment Failure Score; a score of ≥2 is associated with a 10% increased mortality risk when associated with infection (Singer et al, 2016).³¹

Sepsis:
A life-threatening organ dysfunction caused by a dysregulated host response
Organ dysfunction:
Acute change in total SOFA score ≥ 2 points consequent to infection
qSOFA:
Identification of patients with infection likely to have a prolonged ICU stay or die
Septic shock:
Subset of sepsis in which underlying circulatory and cellular/metabolic abnormalities are profound enough to substantially increase mortality. Persistent hypotension requiring vasopressors to maintain MAP ≥ 65 mm Hg and having a serum lactate level > 2 mmol l ⁻¹ despite adequate volume resuscitation. Mortality in excess of 40%.

Table 1.5.2 Sepsis-3 definitions (abbreviated from Singer et al, 2016).³¹

qSOFARespiratory rate $\geq 22 \text{ min}^{-1}$

Altered mentation

Systolic blood pressure $\leq 100 \text{ mm Hg}$ **Table 1.5.3 Quick SOFA criteria (qSOFA) for rapid identification of patients who, in the presence of infection, are likely to have a prolonged ICU stay or die (Singer et al, 2016).³¹**

These definitions illustrate the problem that sepsis is a complex clinical syndrome rather than a definitive diagnosis. The Sepsis-3 consensus also recognises that our understanding of sepsis, whilst still limited, has improved from original concepts of hyper-inflammation mediated by cytokines. It was originally thought that the lethality of sepsis was due to an exaggerated and uncontrolled cytokine storm. In 1974 Lewis Thomas wrote *“the microorganisms... that seem to have it in for us... turn out... to be rather more like bystanders... It is our response to their presence that makes the disease. Our arsenals for fighting off bacteria are so powerful... that we are more in danger from them than the invaders”*.³² However, recent advances in our understanding of sepsis suggest that hypo-inflammation also has an important role in survival from infection. One model describes sepsis as an initial inflammatory response followed by a relative period of immunosuppression preceding recovery. Importantly, the degree of hyper and hypo-inflammation is dependent on host factors, such as co-morbidities.³³ This concept is illustrated in Figure 1.5.1.

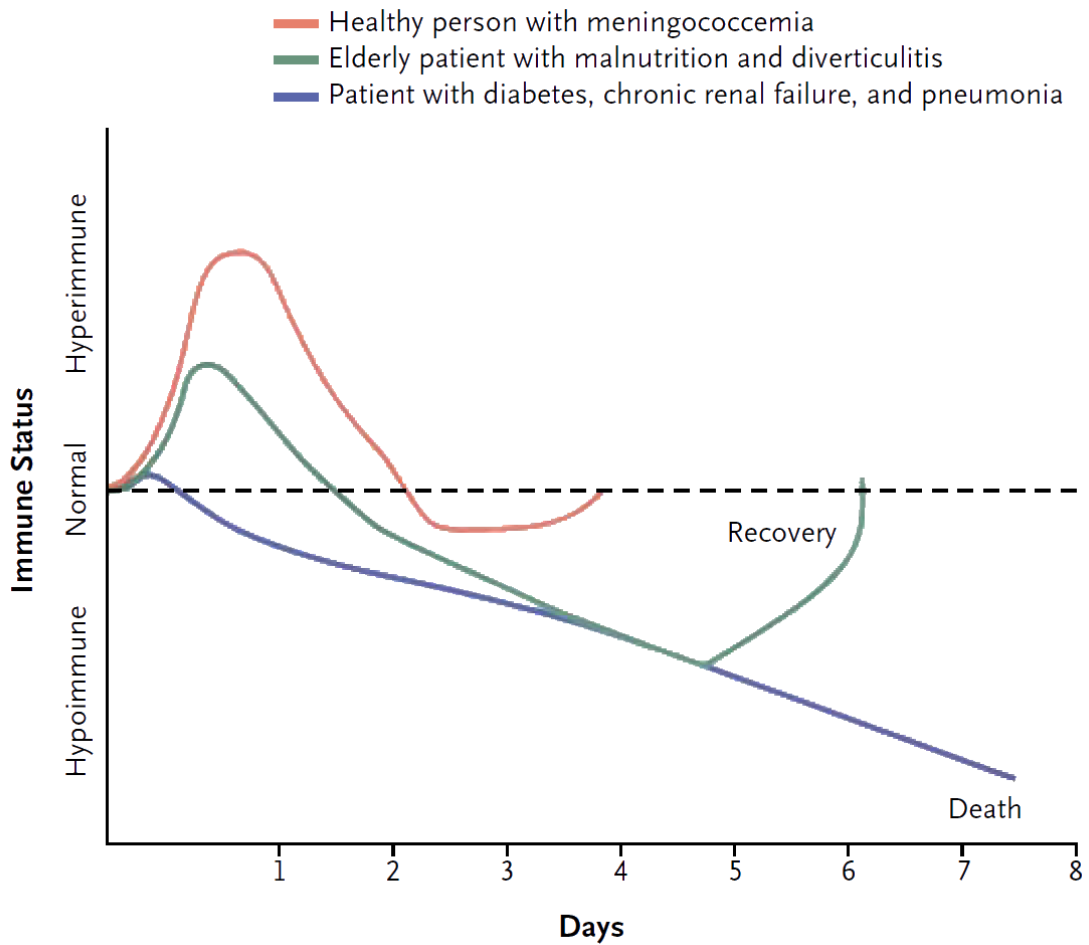


Figure 1.5.1 Immunologic response of three hypothetical patients with sepsis (Hotchkiss and Karl, 2003).³³

1.6. Cytokines

The response to sepsis is driven and mediated by extrinsic and intrinsic factors. An extrinsic bacterial source is the most common cause, though viruses and fungi can produce a similar and no less lethal clinical picture. The traditional model of the sepsis response is based around the Gram-negative bacterial endotoxin. This is a lipopolysaccharide (LPS) that is a potent stimulator of the inflammatory process via the innate immune response, though Gram-positive bacteria induce an almost identical response. In summary, endotoxin stimulates immunocytes and the complement system to release the key cytokines of sepsis: tumour necrosis factor (TNF- α), the interleukins (IL) 1, 6 and 8, and macrophage migratory inhibitory factor (MIF), in addition to non-cytokine mediators such as complement, platelet activating factor (PAF) and nitric oxide (NO).³⁴ Furthermore, LPS binds to the cell surface receptor CD14 activating neutrophils,

macrophages and monocytes, mobilising, recruiting and stimulating them to increase nuclear synthesis of further cytokines via nuclear factor kappa-B (NF- κ B). The binding of CD14 and subsequent intracellular effects requires the transmembrane protein Toll-like receptor (TLR), receptors that also recognise and bind endotoxin independently by functioning as pathogen-associated molecular pattern receptors (PAMP). These TLRs and the role of PAMPs have received considerable interest as therapeutic targets.³⁵ Non-infective stimuli, such as burns, trauma, or surgery can also stimulate immune cells and a similar inflammatory response involving the same mediators.

Cytokines have numerous and varying effects as intrinsic mediators of the inflammatory response, having both pro-inflammatory and anti-inflammatory functions, and are summarised in Table 1.6.1.³⁶ Cytokines amplify the initial inflammatory response and are also key to the compensatory anti-inflammatory response (CARS), the balance between pro-inflammation and CARS maintaining homeostasis. Understanding how this balance is disrupted is another area of sepsis research.

Pro-inflammatory	Anti-inflammatory
<p><i>Cytokines:</i></p> <ul style="list-style-type: none"> TNF alfa IL-1β, IL-2, IL-6, IL-8, IL-15 Granulocyte-macrophage colony-stimulating factor (GM-CSF) IFN-γ Chemokines 	<p><i>Cytokines:</i></p> <ul style="list-style-type: none"> IL-1Ra IL-4 IL-10 IL-13
<p><i>Other mediators:</i></p> <ul style="list-style-type: none"> Neutrophil elastase Thromboxane PAF Vasoactive neuropeptides Phospholipase A₂ Plasminogen activator inhibitor-1 Prostaglandins Prostacyclin Soluble adhesion molecules H₂S, NO 	<p><i>Other mediators:</i></p> <ul style="list-style-type: none"> Type II IL-1 receptor Transforming growth factor β Epinephrine Soluble TNF-α receptors Soluble recombinant CD14 LPS binding protein

Table 1.6.1 Pro-inflammatory and anti-inflammatory mediators of sepsis: TNF=tumor necrosis factor, IL=interleukin, IFN=interferon, PAF=platelet activating factor, H₂S=hydrogen sulphide, NO=nitric oxide, LPS=lipopolysaccharide (adapted from Devi Ramnath et al, 2006).³⁶

1.7. Therapeutics

Despite a considerable volume of research into the functions of cytokines and the understanding of their key role in both inflammatory and anti-inflammatory processes, therapies that target these processes have been mainly unsuccessful. Furthermore, correlations between circulating cytokine concentrations and severity of sepsis are inconsistent, particularly between different pathogens and, of specific concern to research methodology, between species.³⁷ For example, in animal models of severe sepsis the cytokine TNF- α is reliably increased and associated with death.³⁸ However,

clinical trials in humans with drugs targeting TNF- α failed to demonstrate survival benefit, in part due to TNF levels not being significantly raised in septic patients enrolled in the trials.³⁹ Other therapies that target different parts of the sepsis cascade have also proved disappointing, with two sepsis-specific drugs – the TLR antagonist eritoran tetrasodium and activated-protein C - being abandoned or withdrawn in 2011 despite promising earlier trials.^{35 40 41}

1.8. Models of Sepsis

Studying sepsis remains a challenging area of research. The lack of a specific diagnostic test, and it being a physiological syndrome rather than a clearly defined disease have made human observational and interventional data difficult to interpret. Models of sepsis can assist understanding and the development of therapeutics. They fall into three main categories: *in vitro* methods, animal studies, and human studies.

In vitro models of sepsis

The sepsis response comprises many interacting inflammatory and neuroendocrine pathways and cascades which cannot be effectively modelled outside of a host. However, *in vitro* purified cell types including neutrophils, monocytes, macrophages, endothelial and epithelial cells have greatly increased understanding of cell-specific mechanisms which may be relevant to sepsis.³⁴ Similarly, studies of cells taken from patients suffering from a severe infection have improved understanding of the homeostatic dysregulation that occurs.⁴²

Lipopolysaccharide (LPS) is perhaps the most studied stimulus of the septic response. LPS, or endotoxin, forms an integral part of the outer cell wall of gram-negative bacteria and is the main trigger for gram-negative septic shock. There is an abundance of studies using LPS and they have led to much of our understanding of cytokine cascades, as well as the roles of PAMPs, neutrophil extracellular traps (NETs), and the crucial function of TLRs.^{43–45} Other stimulants have also been used to simulate gram-positive infection,

examples being the cell wall components peptidoglycan and teichoic acid.⁴⁶ Alternatively, leukocytes can be 'activated' *in vitro* using known stimulants. These include the leukocyte chemoattractant and degranulator fMLP (formyl-methionyl-leucyl-phenylalanine), PMA (phorbol myristate acetate), components of complement (fragment C5a, for example, inhibits neutrophil apoptosis), and cytokines (e.g. TNF α , IL-8).^{47 48}

Animal models of sepsis

The most commonly used animal in preclinical studies of sepsis is the mouse. Mice are relatively easy to manage for laboratory staff, and can be genetically modified to explore the relevance of particular proteins and receptors to the pathogenesis of sepsis. They can also be made more human by transplanting human haematopoietic stem cells into neonatal mice, leading to the development of human innate and adaptive immune cells (e.g. NK cells, T cells, B cells, monocytes).⁴⁹ Modelling sepsis in mice (and other animals) has usually been achieved with direct injection of LPS (either intravenous or intraperitoneal), caecal ligation and puncture (CLP), or the intraperitoneal introduction of faecal slurry or bacteria.

Studies of LPS in mice are extensive and gave rise to much of the understanding of TNF α , TLR-4 and the cytokine cascade. LPS can be administered either as a bolus or as an infusion. Bolus doses do not accurately mimic the human response to sepsis: the immediate hypodynamic cardiovascular response in mice to LPS is different to the hyperdynamic response to sepsis seen in humans.⁵⁰ Infusions preserve the hyperdynamic aspect of the human response, but modulation of T-cell mediated cytokine release does not occur.⁵¹ Further, mice are considerably more resistant to endotoxaemia than humans. The lethal dose of LPS for 50% of mice (LD₅₀) is approximately a million times larger than needed to induce symptoms in humans.⁵² Further, a comparison of the genomic response of mice with humans to the inflammatory insults of burns, trauma and endotoxaemia, demonstrated significant

differences between species.⁵³ Such discrepancies suggest that therapeutics developed using murine models of mice may not be effective in humans.

Animal CLP studies are relatively simple to produce. The technique involves performing a laparotomy then ligating the caecum before puncturing it with a needle, allowing faeces to enter the peritoneum.⁵⁴ CLP models generate physiological responses seen in humans, e.g. hyperdynamic cardiovascular system, acute lung injury and increased macrophage and monocyte activity. These models are also resistant to therapies such as TNF α antibodies, similarly to human studies.⁵⁵ However, translational research from murine CLP studies has remained unsuccessful. Not only is the genomic response in mice different to that of humans, but also mortality from sepsis in humans occurs predominately at the extremes of age.⁵³ Co-morbidity also predisposes to mortality, and experimental mice are usually young adult animals with no co-morbidity. The timing and duration of sepsis usually occurs over days in experimental animals, unlike humans where the course of the disease may be prolonged by extensive resuscitation and organ support.

Another relatively reproducible animal model of sepsis involves the intraperitoneal introduction of human faecal material or bacteria. This removes the need for a laparotomy as in the CLP technique, and allows introduction of a fixed dose of contamination into the peritoneum. Rabbits have a similar immune response and sensitivity to LPS as humans. Using this peritonitis model in rabbits, tifacogin (a recombinant tissue factor pathway inhibitor) was shown to be an effective pharmaceutical treatment.⁵⁶ However, as with other potential therapies arising from animal data, the results of clinical trials in humans were disappointing.⁵⁷

Fundamentally, the inflammatory response of mice and other animals is different to that of humans. Animal studies are therefore useful for understanding the mechanisms of the sepsis response, as many of the pathways described in animal models have been

found to be applicable in humans. However, translating interventional studies from animals to humans require caution: history suggests they are unlikely to be successful.

Human models of sepsis

Modelling sepsis in humans has mainly been by injections or short duration infusions of endotoxin to healthy volunteers in the range of 1 – 4 ng kg⁻¹. Endotoxin experiments do not replicate the complex and severe, life-threatening syndrome of sepsis, but they have provided useful mechanistic data that have greater relevance for humans than those gained from animal models. The features of the human response to endotoxaemia are similar to sepsis: fever, malaise, myalgia, leucocytosis and a hyperdynamic cardiovascular response or hypotensive shock at higher doses. Studies using this model have increased our understanding of cytokines, leukocyte activation and regulation, and gene regulation.^{58–60} Interventions targeting LPS antigen presentation, cytokine responses, coagulation and neuroendocrine effects have also been studied in the endotoxin human model of sepsis.^{61–64}

Other human models of sepsis have focused on extracting activated human inflammatory cells in localised areas of inflammation in the form of blisters.⁶⁵ There have also been recent advances in computer simulations of inflammation that may improve the development of effective therapies.⁶⁶

1.9. The Nociceptin System and Sepsis

The health and economic burden of sepsis is significant, and despite disappointing results from drug trials, considerable advances continue to be made regarding the pathophysiology of the syndrome. Increasing amounts of research point to a key association between the endogenous N/OFQ system and the inflammatory process of sepsis.

Perhaps the most convincing piece of evidence comes from the work of Carvalho and colleagues who used an animal model of sepsis to demonstrate the profound effects of N/OAQ on survival.⁶⁷ A group of anaesthetised rats underwent laparotomy with caecal ligation and perforation (CLP) followed by abdominal wound closure. A control group of rats – sham – underwent laparotomy without CLP. The CLP rats were divided into groups that received increasing concentrations of N/OAQ (0.001 mg kg⁻¹ to 0.1 mg kg⁻¹). Another set of CLP rats were also exposed to varying concentrations of UFP-101 (N/OAQ antagonist). Both sets of rats were compared against sham. All rats received fluid and antibiotics. Mortality was 100% for CLP rats exposed to 0.1 mg kg⁻¹ N/OAQ, whereas rats exposed to the N/OAQ antagonist showed improved survival. This is shown in Figure 1.9.1.

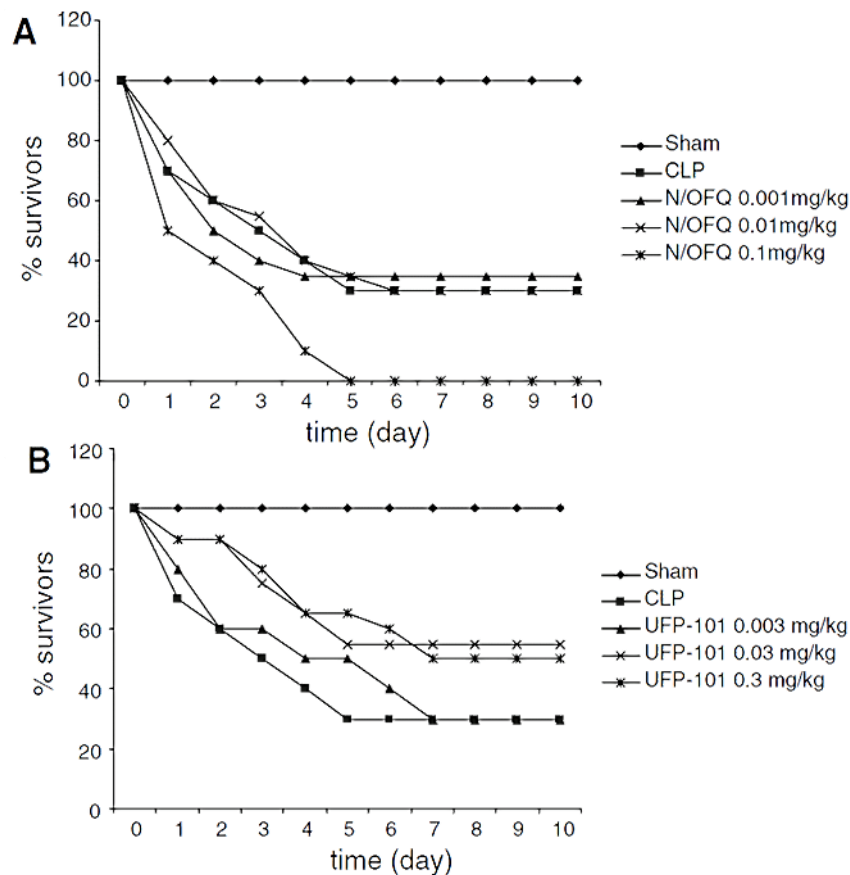


Figure 1.9.1 N/OAQ in rat survival after CLP: A) Rats exposed to CLP and N/OAQ over 10 days. Mortality was 100% for rats exposed to 0.1mg kg⁻¹ N/OAQ compared with sham. B) CLP rats exposed to UFP-101 showing improved survival in the presence of the N/OAQ antagonist (Carvalho et al, 2008).⁶⁷

Carvalho et al also compared the mortality data with biochemical analyses of CLP rats that were exposed to similar doses of N/OFQ and UFP-101 following CLP and then killed 12 hours following surgery. Plasma concentrations of the pro-inflammatory cytokines (TNF- α and IL-1 β) increased with 0.01 mg kg⁻¹ and 0.1 mg kg⁻¹ of N/OFQ, and were reduced by 0.03 mg kg⁻¹ of UFP-101; this is shown in Figure 1.9.2. UFP-101 was also shown to impair leucocyte migration into the peritoneal cavity as well as distant spread. The anti-inflammatory cytokine IL-10 was minimally affected by N/OFQ or UFP-101.

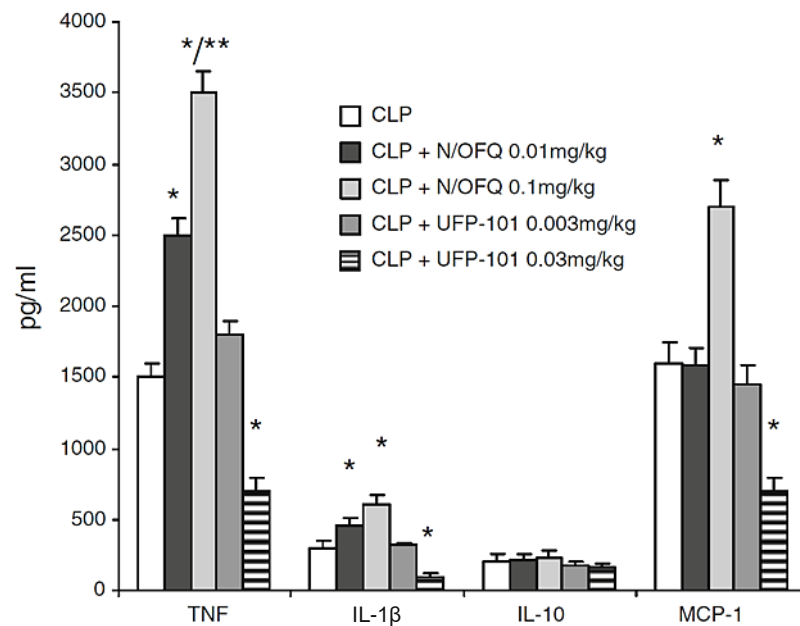


Figure 1.9.2 Effects of N/OFQ and UFP-101 on cytokine levels in CLP rats, showing a stimulatory effect with higher levels of N/OFQ of pro-inflammatory mediators, and an inhibitory effect with UFP-101 (TNF; IL-1 β ; IL-10; MCP-1, monocyte chemotactic protein 1). (Carvalho et al, 2008).⁶⁷

These data are strongly suggestive of N/OFQ having a key role in the pro-inflammatory phases of sepsis, and the therapeutic potential for N/OFQ antagonists. However, it is important to note that the CLP model is one of acute sepsis manipulated at the time of onset. This is rarely the case with patients in clinical practice who frequently present hours or days after the onset of sepsis.

However, there is evidence from human studies that adds weight to there being an important role for N/OFQ in sepsis. Our group performed an observational pilot study examining plasma N/OFQ concentrations in patients admitted to ICU with sepsis.⁶⁸ Of

samples taken from these patients after recovery from their critical illness. mRNA transcripts for ppNOC and NOP were decreased ($p=0.019$ and $p<0.0001$ respectively) compared with matched control volunteers. Cytokine levels were increased on day 1 compared with healthy volunteers and recovery samples ($p<0.0001$). Figure 1.9.4 summarises the findings. In CPB patients, mRNA for NOP showed no significant change in expression up to 24 hours after surgery, but ppNOC showed a significant decrease ($p<0.001$) at 3 and 24 hours after CPB. There was a 35% increase in plasma N/OFQ levels ($p=0.0058$) at 3 hours that returned to basal levels at 24 hours. Whilst it is not clear why NOP expression in septic patients did not match volunteer samples after recovery, or why plasma N/OFQ concentrations were similar in volunteer patients compared with septic patients, taken as a whole these data do suggest that the nociceptin system is modulated in states of sepsis or inflammation.

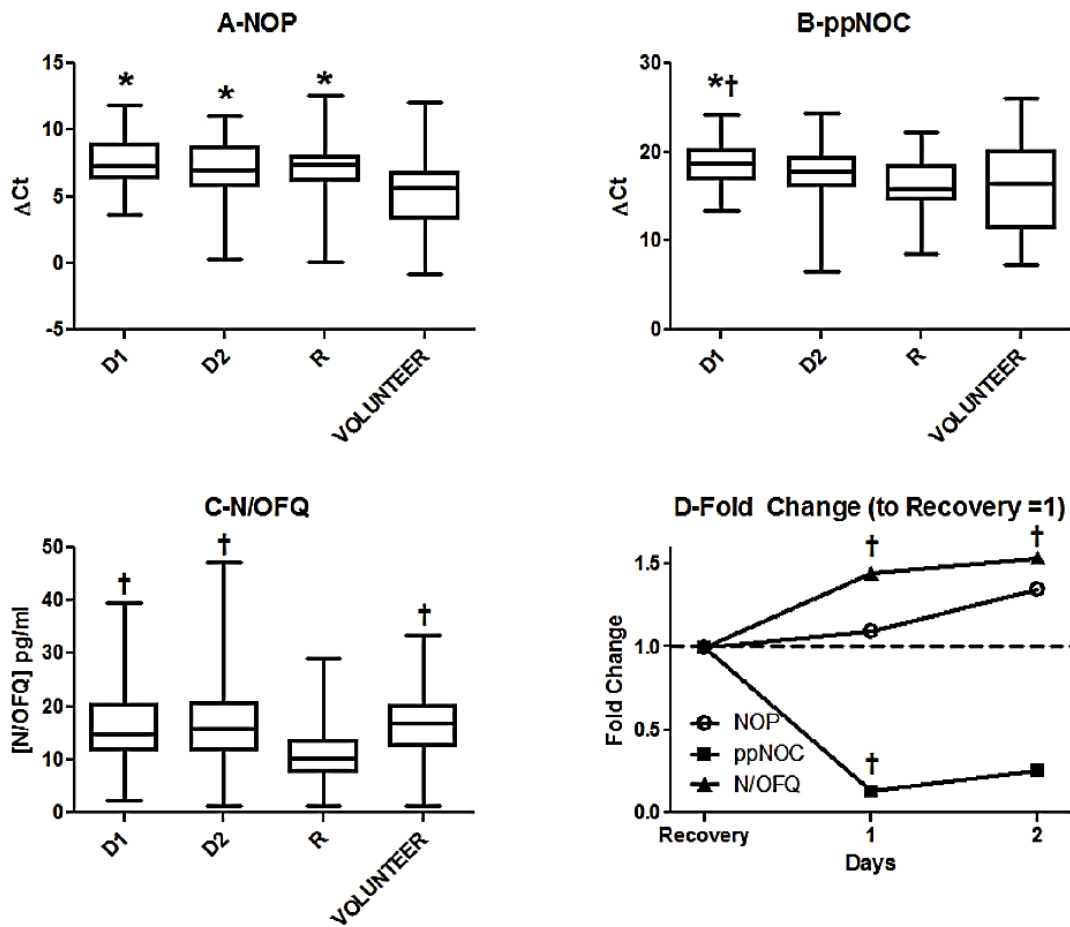


Figure 1.9.4 N/OFQ in septic patients: Data from Thompson and colleagues (2013) demonstrated that NOP mRNA expression was decreased (higher Δ Ct) in patients with sepsis on day 1, 2 and in the recovery period compared with healthy volunteers (A). ppNOC mRNA expression was also reduced, significantly at day 1 (B). Plasma N/OFQ concentrations were increased compared with recovery samples (C). Panel (D) shows the fold-change in NOP, ppNOC and N/OFQ peptide concentrations compared with recovery samples: ppNOC expression decreases with increases in N/OFQ peptide concentrations.⁶⁹

An earlier paper by Stamer and colleagues provides additional evidence for the role of the nociceptin system in systemic inflammation.⁷⁰ In this study, whole blood was taken from patients following major elective surgery (n=20), following admission to ICU with severe sepsis (n=18), or with advanced cancer (n=113). Patients with sepsis had their blood taken on admission, day 3, day 5 and after recovery from multiorgan dysfunction. The key difference with this research was the isolation of mRNA transcripts from whole blood for NOP, pNOFQ (equivalent to ppNOC), and a reference (housekeeper) gene HPRT, rather than from isolated leukocytes as performed by our research group.⁶⁹ Compared with healthy control volunteer blood samples, NOP expression was

significantly increased in ICU patients at admission, the highest values being found in patients who did not survive their admission. This corroborates previous work by Williams and colleagues, but is in contrast to our own findings in 2013.^{68 69} Post-operative surgical patients and cancer patients also showed increased expression for NOP, as shown in Figure 1.9.5. The degree of ppNOC expression was significantly decreased in septic and cancer patients. The authors also compared N/OFQ and ppNOC transcripts with pro-calcitonin (PCT, a biochemical marker of systemic inflammation) and the pro-inflammatory cytokine IL-6. Expression for ppNOC was significantly decreased when plasma levels of PCT and IL-6 were raised – no association was seen for NOP (see Figure 1.9.5).

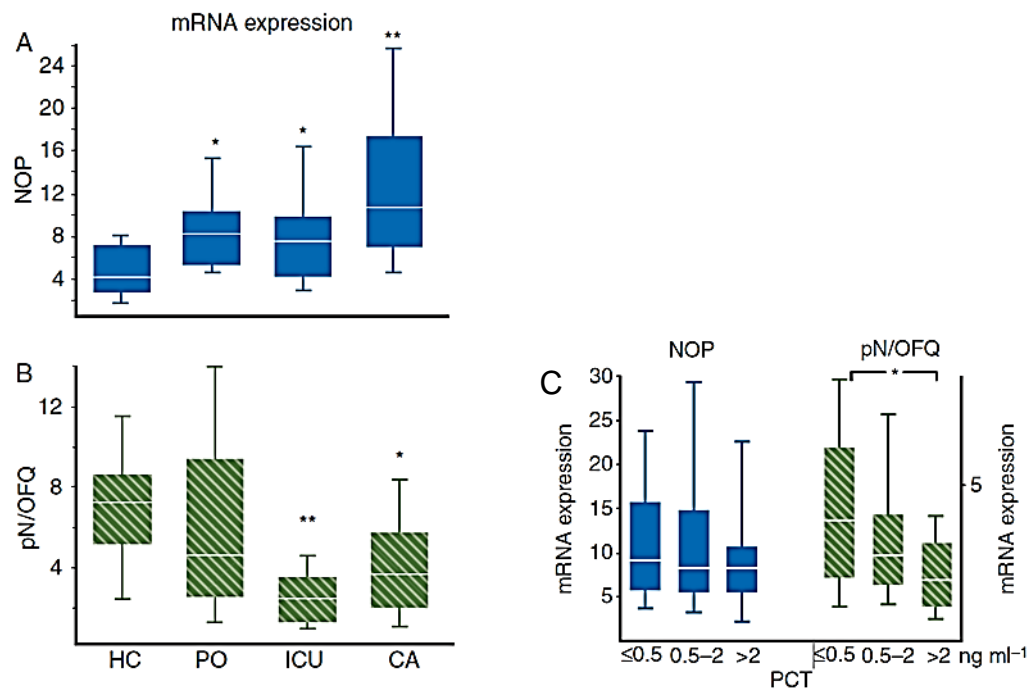


Figure 1.9.5 Whole blood mRNA differences between patients: mRNA expression for NOP (A) and pN/OFQ (equivalent to ppNOC) (B) in whole blood showing significant increases in NOP and decreases in pN/OFQ expression in post-operative patients (PO), septic patients (ICU) and patients with cancer (CA) when compared with healthy controls (HC) (*= $p < 0.05$, **= $p < 0.001$). Graph C illustrates the significant reduction in pN/OFQ expression in all patients associated with 3 different levels of pro-calcitonin (PCT). No such change was demonstrated for NOP expression (Stamer et al, 2011).⁷⁰

These data from Stamer and colleagues point to a significant association between systemic inflammatory states and the nociceptin system. Whilst patients with advanced cancer showed the highest expression for NOP from whole blood (not correlated with

pain states), the authors accept the heterogenous nature of the cancer patients and that the concomitant presence of infection could not be excluded. Furthermore, these were mRNA transcripts recovered from whole blood rather than isolated inflammatory cells; cells from organ systems may be contributing to changes in receptor and precursor expression, independent of any inflammatory process. Nevertheless, for the three modes of inflammation examined, expression of NOP is clearly relevant. This is further supported by the association of ppNOC with the acute inflammatory states, i.e. post-operative, severe sepsis, corroborated by associations with PCT and IL-6.

1.10. Studying the nociceptin system

The majority of *in vitro* and *in vivo* work in this area has been based round mRNA transcripts, chemotaxis experiments and techniques to measure plasma levels of the opioid N/OFQ (e.g. radioimmunoassay (RIA), mass spectrometry). A key technique frequently used to study peptide concentrations is enzyme-link immunosorbent assay (ELISA), and would be expected to form part of the evidence supporting N/OFQ release from immune cells. However, in our experience, no commercially available ELISA kit is reliable enough to measure N/OFQ in plasma. Further, antibodies developed 'in-house' were also unreliable in this assay.⁷¹ Our laboratory has used RIA to quantify plasma N/OFQ levels, but it remains time-consuming and limited by the short shelf-life of radiolabelled antigens. Furthermore, plasma levels of N/OFQ are in the picogram per ml range. This contrasts with work by Fiset (see Section 1.4), where measurements of secreted N/OFQ were in the nanogram per ml range.²³ However, this is an order of magnitude above plasma, CSF and serum measurements of N/OFQ made by other authors.⁷²

1.11. Summary and remaining questions

The literature suggests that the nociceptin system has an immunomodulatory role in states of inflammation. Although some of the data on mRNA expression are conflicting, the results from animal studies, observational human studies, and *in vitro* work on whole blood and leukocytes provide compelling evidence that N/OFQ and its receptor have a

functional role in inflammation and immune modulation. However, it is not clear how exactly N/OFQ acts as a mediator. Furthermore, much of the work has been confined to animal studies, the interpretation of which should be made with the appropriate degree of caution.

It is unclear how cellular measurements of nociceptin components correlate with the clinical picture of sepsis, nor indeed which cell or cells are key to any mediation. It is known that neutrophils play a crucial role in sepsis and particularly the associated pulmonary complication of adult respiratory distress syndrome (ARDS).⁷³ However, data are absent connecting neutrophils (as opposed to PMNs) with nociceptin components, and whether such components are correlated with sepsis severity.

1.12. Hypothesis and aims

The primary hypothesis of the work described in this thesis was **that polymorphonuclear cells are significant mediators of the nociceptin response to sepsis, both producing and responding to N/OFQ.** Exploring this hypothesis would provide cellular data in support of human observational data, and further expand on current data regarding mRNA NOP and ppNOC expression in PMNs. A key aim of this thesis was also the development of a real time, live-cell assay to demonstrate the release of N/OFQ from PMNs following activation, independent of the ELISA techniques that had so far proved unreliable.

This thesis is therefore divided into two main sections.

1. The first section addresses the expression of NOP and ppNOC transcripts in PMNs, and how exposure to an established *in vitro* model of sepsis – lipopolysaccharide – modulates their expression. Further work sought to identify whether these transcripts are universally expressed amongst the granulocytes that make up PMNs, namely basophils, eosinophils and neutrophils.
2. The second, and largest section describes the development of a live cell assay for visualisation of N/OFQ release from activated PMNs using confocal microscopy

and a biological sensor of N/OFQ. The assay was designed to confirm that N/OFQ is released from activated PMNs.

STUDIES OF NOCICEPTIN GENE EXPRESSION IN IMMUNOCYTES

2. Methodology

2.1. Reagents and equipment

Solutions and reagents used in subsequent experiments are given below (in alphabetical order):

2.i Blood sample bottles

All blood samples were collected into 7.5ml Monovette® collection tubes (Sarstedt AG & Company, Nümbrecht, Germany) containing EDTA to a final concentration of 1.6 mg ml⁻¹.

2.ii cDNA Reverse Transcription Kit (Life Technologies LTD, Paisley, UK)

Kit for conversion of isolated mRNA to copy DNA (cDNA) containing MultiScribe™ reverse transcriptase, RNase inhibitor, dNTP mix, RT buffer and random primers.

2.iii Eppendorf Biophotometer (Eppendorf UK Limited, Stevenage, UK)

Spectrophotometer for measurement of mRNA purity and concentration, used in our laboratory prior to acquisition of the NanoDrop™ ND2000.

2.iv Eppendorf Mastercycler gradient thermocycler (Eppendorf UK Limited, Stevenage, UK)

System for heating and cooling (thermocycle) mRNA samples in the presence of reverse transcriptase and nucleic acids to produce copy DNA (cDNA) for subsequent PCR analysis.

2.v Ficoll-Paque™ PLUS (GE Healthcare Life Sciences, Buckinghamshire, UK)

A mixture of Ficoll® PM400 (a commercial product) comprising a non-ionic polymer of sucrose and epichlorohydrin that is hydrophilic, and sodium diatrizoate, with a density of 1.077 g ml⁻¹; used for separation of whole blood into plasma, PBMCs, PMNs and erythrocytes.

2.vi Krebs-HEPES solution

The constituents of Krebs-HEPES solution were:

- Sodium chloride (NaCl): 143.5 mM
- Glucose (C₆H₁₂O₆): 11.7 mM
- HEPES buffer: 10.0 mM
- Potassium chloride (KCl): 4.7 mM
- Monopotassium phosphate (KH₂PO₄): 1.2 mM
- Magnesium sulphate heptahydrate (MgSO₄.7H₂O): 1.2 mM
- Calcium chloride dihydrate (CaCl₂.2H₂O): 2.6 mM

The resultant solution was then brought to pH 7.4 at room temperature with the addition of HCl or NaOH.

2.vii Lipopolysaccharide (LPS) ((Sigma-Aldrich, Dorset, UK)

Endotoxin derived from *E. coli* 0111:B4 bacteria to simulate sepsis *in vitro*.

2.viii Miltenyi buffer

A buffer solution recommended by Miltenyi Biotech for use in MACS[®]. It comprises:

- Phosphate buffered saline
- 0.5% bovine serum albumin
- 2 mM EDTA

2.ix mirVana™ miRNA Isolation Kit (Applied Biosystems, Paisley, UK)

Kit for isolating mRNA from tissues and cells using organic extraction and a glass fibre filter method, effective for isolating small RNAs as well as larger RNA molecules. Contains mirVana™ lysis buffer, miRNA homogenate additive, acid-phenol:chloroform and wash solutions.

2.x NanoDrop™ ND2000 (ThermoFisher Scientific, Leicestershire, UK)

Spectrophotometer for measurement of mRNA concentration and purity, that uses 2 µL volume of sample and generates a spectrophotograph in addition to 260/280 ratio information.

2.xi Peripheral blood mononuclear cells (PBMCs)

Leukocytes within peripheral blood that contain a single nucleus. These cells include lymphocytes, dendritic cells, monocytes, macrophages and natural killer (NK) cells. It is also from this population that basophil granulocytes can be isolated using a combination of density gradient extraction and magnetic activated cell sorting.

2.xii Phosphate buffered saline (PBS)

This was reconstituted from a commercially produced tablet that was dissolved in the ratio of one tablet to 200 ml deionised water. The resultant solution had 0.01 M phosphate buffer, 0.0027 M potassium chloride, and 0.137 M sodium chloride with a pH of 7.4 at room temperature.

2.xiii Polymorphonuclear cells (PMNs)

Inflammatory granulocytes comprising predominately neutrophils and eosinophils. Whilst basophils are also granulocytes and therefore also PMNs, their isolation is more complex and separate from standard PMN isolation. In this thesis PMNs refer only to neutrophils and eosinophils.

2.xiv Polymorphprep™ (Axis-Shield, Dundee, UK)

A high osmolality media comprising sodium diatrizoate and the polysaccharide dextran 500 with a density of 1.113g ml⁻¹, used in the separation of whole blood into plasma, PBMCs, non-adherent PMNs, and erythrocytes.

2.xv Red-cell Lysis Solution (BD Pharm Lyse™)

A buffered, ammonium chloride-based lysing agent, that specifically causes erythrocytes to lyse whilst leaving leukocytes relatively untouched.

2.xvi Ribopure™-Blood kit (Invitrogen™, ThermoFisher Scientific, Leicestershire, UK)

Kit for the isolation of mRNA directly from whole blood. Uses a lysis solution, and then a combination of organic and glass fibre filter methods for extraction of purified RNA.

2.xvii RPMI 1640 media (Sigma-Aldrich, Dorset, UK)

Standard culture media for growth of cultured cells

2.xviii StepOne RT-qPCR system (ThermoFisher Scientific, Leicestershire, UK)

A 48-well PCR instrument containing an LED-based optical system for recording fluorescence from VIC® and FAM® dyes used in TaqMan® assays in duplex.

2.xix TaqMan® fluorescent probes for human NOP and ppNOC (Life Technologies LTD, Paisley, UK)

Assay ID: Hs00173471_m1 for NOP; Hs00173823_m1 for ppNOC

2.xx TaqMan® fluorescent probes for human reference genes (Life Technologies LTD, Paisley, UK)

GAPDH: Glyceraldehyde 3-phosphate dehydrogenase; B2M: beta-2-microglobulin; PKG-1: protein kinase G-1; HPRT-1: hypoxanthine phosphoribosyltransferase 1, RPLP0: ribosomal protein lateral stalk subunit P0; 18S: 18S ribosomal RNA; and ACTB: actin beta.

2.xxi TaqMan® PCR master mix (Life Technologies LTD, Paisley, UK)

Kit containing DNA polymerase, dNTPs, buffers and a passive reference dye.

2.xxii Turbo DNA-free® kit, (Life Technologies Ltd, Paisley, UK)

Kit for removal of genomic DNA from mRNA samples containing buffer, DNase, nuclease-free water and an inactivation agent.

The following methods describe the collection and separation of blood necessary for gene expression experiments as well as for live-cell imaging assay. The methodology for gene expression experiments is then described as well as the theory behind their use.

2.2. Whole blood separation techniques

Blood samples for PCR (and subsequent live cell imaging assay development) were collected from volunteers from within or affiliated with the research group. Following University of Leicester volunteer ethical approval, informed consent was obtained for the 63 samples that were collected. No more than 30 ml samples of blood were obtained from volunteers (median 4.5 samples per person, IQR 1 – 7, range 1 – 11; median 63 days between sampling, IQR 38.5 – 175, range 2 – 400). There was a total of 14 volunteers, comprising 8 male and 6 females.

2.3. Isolating PMNs and PMBCs

Density gradient techniques were used to separate whole blood into PMNs (neutrophils and eosinophils), and PMBCs (monocytes, lymphocytes, dendritic cells). The principle behind these techniques is that cell populations within whole blood have differing densities, and through use of a centrifuge, can be separated. The 'lightest', or lowest specific gravity component is plasma, followed by platelets, then leukocytes, and finally packed red blood cells, as illustrated in Figure 2.3.1. The blood needs to be anticoagulated (with EDTA, for example) to prevent clot-formation that would otherwise cause cell aggregation preventing separation.

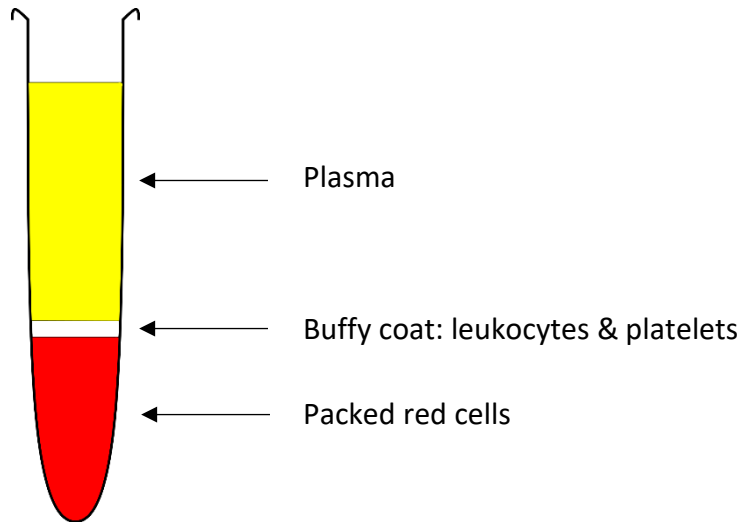


Figure 2.3.1 Whole blood separation by centrifugation results in three layers.

Such blood fractionation is used in clinical medicine to produce components for blood transfusion. However, for these experiments separation of the leukocytes into PMNs and PBMCs was required, which cannot be achieved through centrifugation alone. The densities of leukocytes are similar: monocytes and lymphocytes have densities between 1.067 and 1.077 g ml⁻¹, and PMNs are 1.088 g ml⁻¹ or greater. Separation of the leukocytes therefore needs to be through media with a density of between 1.077 and 1.088 g ml⁻¹. One commonly used medium is Ficoll-Paque™ PLUS. The process requires anticoagulated whole blood that is first diluted with an equal volume of a balanced salt solution. This is then carefully layered onto the Ficoll-Paque™ PLUS solution. After centrifugation, a bottom layer of erythrocytes is formed, aggregated by the Ficoll PM400. Immediately above this sediment are granulocytes, with sufficient density (increased by the osmotic pressure of the Ficoll-Paque™ media) to migrate through the media. There is then a layer of Ficoll-Paque™, and where this interfaces with the uppermost layer of plasma, mononuclear cells are present and can be extracted (as shown in Figure 2.3.2).

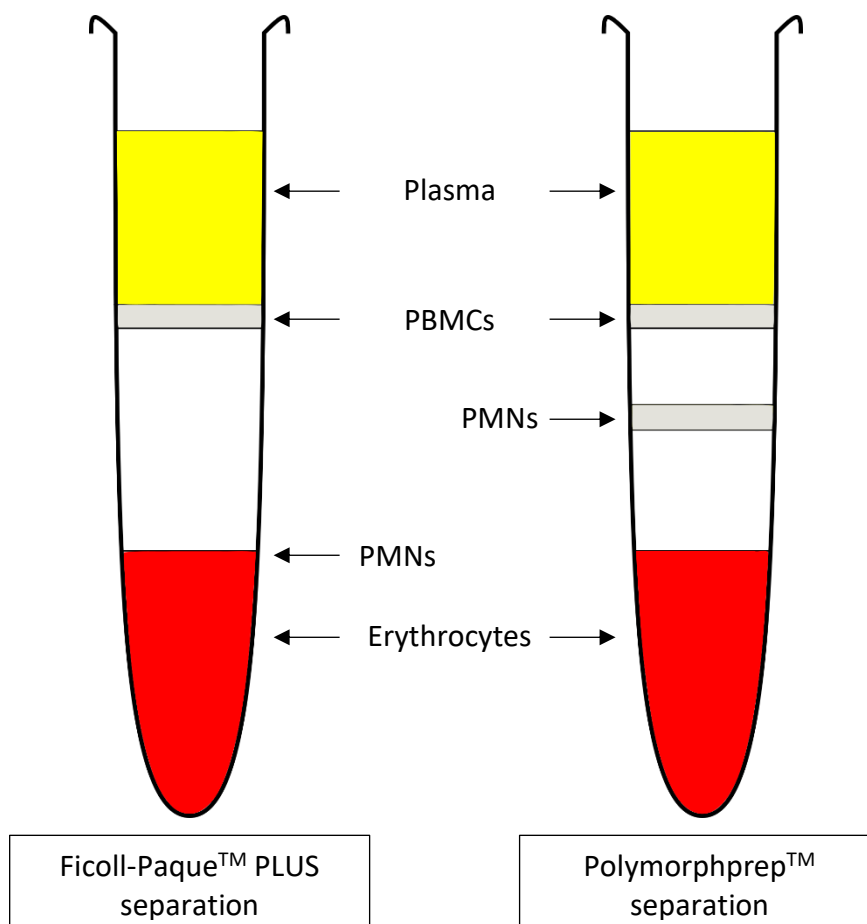


Figure 2.3.2 Different blood separation methods using density-gradient techniques. The Ficoll-Paque™ PLUS separation effectively isolates PBMCs, but leaves PMNs adherent to the erythrocytes. Polymorphprep™ isolates both PBMCs and PMNS, although in reality the separation is not as clearly-defined as illustrated.

Whilst this technique can be used to isolate granulocytes, it is difficult to remove the granulocytes that are adherent to the erythrocytes without significant red cell contamination. One option is to wash any removed cells with a red-cell lysis solution. In these experiments BD Pharm Lyse™ was used. It is a buffered, ammonium chloride-based lysing agent that specifically causes erythrocytes to lyse whilst leaving the granulocytes relatively untouched. Another option is to use a different density solution for cell separation. Our laboratory routinely uses Polymorphprep™, high osmolality media comprising sodium diatrizoate and the polysaccharide dextran 500 with a density of 1.113 g ml^{-1} . The osmolality of the solution (445 mOSM) cause the erythrocytes to lose water and shrink, thereby increasing their effective density and, together with dextran-mediated aggregation, rapidly sediment. The osmotic gradient declines as the erythrocytes sediment through the media; erythrocytes lose water into the media,

thereby diluting it. This dilution alters the density of the media (highest density at the bottom of the media), generating a density gradient that allows separation of the leukocytes into a PMBC layer and a PMN layer (as shown in Figure 2.3.2).

2.3.1. Blood separation protocol 1: Ficoll-Paque™ PLUS

This protocol was primarily used for cell isolation in experiments involving Magnetic Activated Cell Sorting (MACS).

1. Divide 40 ml of Ficoll-Paque™ PLUS (FP+) media into 9 ml volumes within 25 ml Sterilin tubes and allow to reach room temperature.
2. Dilute whole blood samples from Monovettes® containing EDTA with PBS in a 1:1 ratio.
3. Carefully layer 12 ml of blood-PBS solution onto the FP+ within the Sterilin tube using Pasteur pipettes, ensuring that there is minimal mixing of the blood-PBS solution with the FP+.
4. Centrifuge the Sterilin tubes at 400 g for 35 min at 18-20°C ensuring there is no brake on the centrifuge.
5. Carefully remove the Sterilin tubes and identify the layers for further extraction (Figure 2.3.2).
6. The lymphocyte-monocyte-platelet (PMBC) layer contains the basophils, and the eosinophil and neutrophils are found as a thin-white layer adherent to the red-cell layer.
7. Collect the PBMC layer into fresh Sterilin tubes and dilute with PBS in a 1:1 ratio. Centrifuge at 300 g for 10 min at room temperature with brake, and re-suspend the pellets in 2 ml Miltenyi buffer.
8. Carefully aspirate the granulocyte layer from the adherent red-cell layer and perform red blood cell lysis (Red cell lysis protocol, 2.3.3).
9. Following red blood cell lysis and centrifugation, re-suspend pellets in 2 ml of Miltenyi buffer.

2.3.2. Blood separation protocol 2: Polymorphprep™

The protocol for the separation of blood into PMNs (neutrophils and eosinophils, not basophils) and PBMCs was as follows:

1. Prepare 15 ml centrifuge tubes with 7.5ml Polymorphprep™ solution.
2. Carefully layer 7.5ml of whole blood from Monovettes® containing EDTA onto the solution using Pasteur pipettes, ensuring minimal mixing of blood with the solution.
3. Centrifuge tubes at 600 g at 20°C for 45 min, with a gentle acceleration and no deceleration brake.
4. Carefully remove and discard the plasma layer.
5. Carefully extract the monocyte layer with sterile Pasteur pipettes and either keep or discard depending on the experiment.
6. Similarly extract the PMN layer.
7. Wash cell populations with an equal volume of PBS and centrifuge at 20°C at 500 g for 10 min.
8. Re-suspend pellets with PBS or Krebs-HEPES buffer depending on subsequent experiments.

2.3.3. Red cell lysis protocol

1. Re-suspend pellets in 1 – 2 ml appropriate buffer solution (PBS or Krebs-HEPES).
2. Add ten times the volume of lysis solution (diluted in ten times the volume of distilled water) and incubated the mixed solution at room temperature in the dark for 10 min, with intermittent inversions and gentle mixing of the solution.
3. Centrifuge the sample at 300 g for 10 min. Aspirating and discarding the supernatant leaves a residual pellet of live cells for further experiments or storage.

2.3.4. Magnetic Activated Cell Sorting (MACS)

MACS® is a well-established immunological technique designed to specifically select cell populations of interest, developed by Miltenyi Biotech GmbH (Bergisch Gladbach, Germany). Superparamagnetic nanoparticles are attached to cells through antibodies to specific cell surface receptors on cells of interest. The nanoparticles are supplied coated with antibodies, and after incubating a sample with these nanoparticles, or MicroBeads, the sample is passed through a column surrounded by a strong magnetic field. Cells attached to the MicroBeads via antibodies are retained within the column and its magnetic field, whilst those unlabelled cells are allowed to pass through. The labelled cells are then washed off the column by removing it from magnetic field, and then passing buffer under pressure through the column. Thereby a negative and positive fraction of cells are acquired: the negative fraction untouched by antibodies, and the positive fraction attached to the MicroBeads.

PMNs comprise neutrophils and eosinophils, and whilst both share the CD15 cell-surface receptor, only neutrophils amongst PMNs express the CD16 receptor. Separation of PMNs was therefore performed using CD16 MicroBeads to produce a negative selection of eosinophils and a positive selection of neutrophils.

Basophils have a different density to other granulocytes and are not isolated into a PMN layer with either Polymorphprep™ or Ficoll-Paque™ PLUS. They remain within the PMBC layer so require a different set of antibodies to isolate them from PMBCs. This was performed using the Miltenyi Basophil Isolation Kit that comprises a Fc-receptor (FcR) blocking reagent, a biotin-conjugated antibody cocktail, and anti-biotin MicroBeads. The principle is that non-basophils within the PBMC layer are labelled first with biotin-conjugated monoclonal antibodies to CD3, CD4, CD14, CD15, CD16, CD36, CD45RA, HLA-DR and CD235a, and then with an anti-biotin monoclonal antibody that is conjugated to MicroBeads. By passing the mixed-cell population through the appropriate column within a magnetic field, the non-basophils are depleted (held within the column by the magnetic field) and unlabelled basophils pass through the column.

The FcR blocking reagent improves the quality of antibody-binding, ensuring that MicroBeads only bind to the desired cell-surface receptors, and not any Fc receptor protein (common amongst PBMCs and basophils).

The procedure for MACS[®] was as described in the product literature. Ficoll-Paque[™] PLUS procedure was used (Blood separation protocol 1, 2.3.1) to isolate granulocytes and PBMCs as recommended in the Miltenyi literature.

1. Once isolated, keep the PMNs on ice, and use cold solutions for the remaining isolation procedures.
2. Following extraction, perform a cell count on the resultant PMNs. (Between 2.1×10^7 and 11×10^7 PMNs were extracted in experiments).
3. Centrifuge the samples for 10 min at 300 g, and re-suspend the resultant pellet in 50 μ L Miltenyi buffer per 5×10^7 cells.
4. Add 50 μ L per 5×10^7 cells of CD16 MicroBeads, mixing well and incubating for 30 min at 4-8°C.
5. Wash cells with 1 – 2 ml of Miltenyi buffer per 10^7 cells and centrifuge at 300 g for 10 min at room temperature.
6. Resuspend pellet in 500 μ L of Miltenyi buffer.
7. Use appropriate columns as supplied by Miltenyi (Figure 2.3.3). (LS columns were used in experiments because the maximum number of labelled cells were less than 10^8 based on earlier cell counts).
8. Prepare the separation column by rinsing with 3 ml of Miltenyi buffer and then placing it within a magnetic field (as supplied by Miltenyi).
9. Add the sample cell suspension to the column and collect the resultant effluent: this effluent contains unbound cells i.e. eosinophils, and the CD16+ bound cells remain bound to the column within the magnetic field.

10. Wash the column with 3 ml of Miltenyi buffer three times and collect the effluent.
11. To remove the CD16+ cells (neutrophils) from the column, remove the column from the magnetic field and force 5 ml of Miltenyi buffer through the column to extract the bound neutrophils.
12. Centrifuge both effluents at 300 g for 10 min to give two pellet samples: unbound eosinophils (CD16-) and bound neutrophils (CD16+).



Figure 2.3.3 Cell isolation using MACS. The LS column is on the left and was used for isolation CD16- and CD16+ cells from a PMN sample. The MS column is on the right and used for basophil isolation.

These samples were kept on ice and used for further experiments. For basophil extraction, the Basophil Isolation Kit was used on the PBMC separation layer. The procedure was as follows:

1. Following a cell count, centrifuge the PBMC suspension for 10 min at 300 g.
2. Re-suspend the subsequent pellet in 30 μL Miltenyi buffer per 10^7 cells. To this add 10 μL FcR Blocking Reagent per 10^7 cells, followed by 10 μL Basophil Antibody Cocktail per 10^7 cells.
3. Mix samples well and incubate at 2-8°C for 10 min.
4. After this period, add 30 μL of Miltenyi buffer per 10^7 cells to the samples, followed by 20 μL of Anti-Biotin MicroBeads per 10^7 cells. Incubate the samples at 2-8°C for 15 min.
5. Wash samples with 1-2 ml Miltenyi buffer per 10^7 cells, and centrifuge for 10 min at 300 g.
6. Re-suspend the pellet in 500 μL buffer per 10^8 initial cells.
7. Use a MS column for MACS separation (Figure 2.3.3).
8. Rinse the MS column with 500 μL Miltenyi buffer and discard the effluent.
9. Add the labelled cell suspension to the column and retain the effluent containing unlabelled basophils.
10. Wash the column 3 times with 500 μL buffer, collecting the effluent into the same sample tube, a process that takes approximately 45 min.
11. Centrifuge the effluent for 10 min at 300 g, and use the resultant pellet for further experiments.

2.4. Haemocytometer

Cell counts were performed using a haemocytometer. This consists of a microscope slide containing a chamber on which there is a grid of laser-etched perpendicular lines. The grid is made up of nine 1 x 1 mm squares, with each 1 x 1 square divided into 16 smaller

squares (0.25 x 0.25 mm). There are smaller divisions in the centre of the slide. A cover slip is placed on the haemocytometer slide. It is raised 0.1 mm above the chamber, such that in a 16 square grid the volume of cells contained is 100 nL. A sample of isolated PMNs can then be counted. This is done by taking 100 μ L of the sample and allowing capillary action to draw some of the sample under the coverslip. Using a 10x microscope objective, cells within a grid of 16 squares can then be counted using a hand counter. The 100 μ L sample may need diluting further if too many cells are clumped together or are too numerous for an accurate count. The number of cells contained within 16 squares multiplied by 10^4 is equivalent to that number of cells in 1 ml. Any dilution factor then needs to be accounted for, and a final multiplication for the volume of the original PMN sample. Accuracy can be improved by repeating the count in different areas of the slide and dividing by the number of observations.

2.5. Studies of mRNA expression

Initial experiments were focused on establishing the expression of messenger RNA for granulocyte populations in control and stimulated blood samples. Whilst DNA contains the code for all proteins within a cell, the steps between DNA being translated into functional protein involves messenger RNA (mRNA). Conceptually as the demand for a certain protein increases, so does expression of mRNA. Therefore, measuring the mRNA for specific proteins of interest should first identify which proteins are required by the cell, and to what extent protein production is modulated in response to changes in the cellular environment. However, cellular mRNA is produced in very small amounts. Therefore, to extract and analyse mRNA requires amplification of the RNA code via a process known as Polymerase Chain Reaction (PCR). This first requires conversion of mRNA to copy DNA (cDNA) using reverse transcription. Specific probes that bind to regions of interest within the cDNA genetic sequence are then used to identify the relevant regions, and through a process of heating and cooling in the presence of DNA polymerase (cycles), are amplified to a level they can be detected (cycle threshold). For these experiments, commercially available TaqMan probes specific to regions of interest were used. These probes contain a fluorophore which fluoresces when cleaved from the probe, enabling detection. This allows real-time quantitative analysis (RT-qPCR) with

specific equipment that detects the fluorescence with the degree of fluorescence relating to the amount of relevant genetic material; detection during the PCR process or cycles is the cycle threshold, and the earlier the cycle threshold is reached the more starting genetic material (see Figure 2.5.4).

However, the amount of originating mRNA is also dependent on the amount extracted from samples, a factor that is difficult to control, especially in low concentration cell populations such as basophils. To control for this, a housekeeper gene (HKG) is also amplified – that is, a genetic sequence of mRNA that is consistently produced by the cells of interest and not modified by environmental factors. By amplifying and measuring the fluorescence (using different fluorophores) of two mRNA sequences, the difference between the two (the ΔCt) can be used as an assessment of the relative expression of the gene of interest (GOI) compared with the control.

The steps from cell isolation to mRNA amplification and measurement are summarised in Figure 2.5.1: cells are isolated, mRNA extracted, measured, cleaned, converted into copy DNA (cDNA) in the presence of reverse transcriptase, and following incubation with the specific TaqMan probes, amplified and measured using RT-qPCR. A control sample is also used to demonstrate the absence of contaminating DNA.

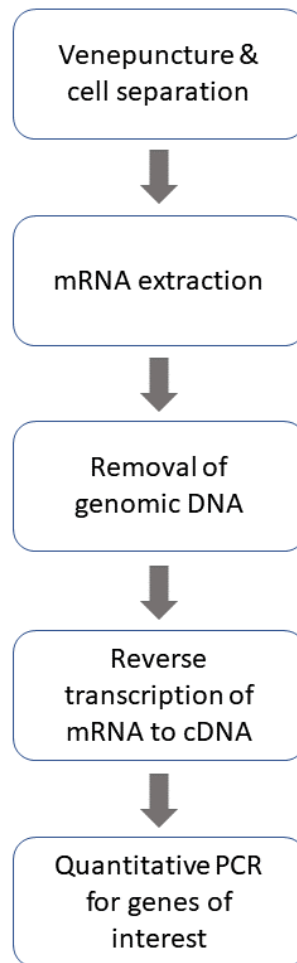


Figure 2.5.1 From sample to PCR: Flow diagram of process from acquiring blood from volunteers to production of ΔC_t values for mRNA expression.

2.5.1. mRNA extraction

Total RNA was isolated from extracted cells using a commercial isolation kit available from *mirVana™* Applied Biosystems. This kit uses a combination of two established techniques to ensure optimal recovery of RNA, from small (15-30 nucleotide lengths) to larger RNA molecules. The first technique is organic extraction. The cell sample is homogenised in the presence of a phenol-based chemical that also inactivates RNases. The sample is then centrifuged, resulting in three phases: a lower layer of organic solution, a middle layer of denatured proteins and genomic DNA, and an upper aqueous layer that comprises RNA. The second technique of solid-phase extraction then extracts

the RNA from this aqueous layer. Ethanol is added to decrease the affinity of RNA for water and increase its affinity for a silica-based filter. The sample is placed in a filter and centrifuged, trapping the RNA on the filter. A wash solution is then used to remove any residual contaminants, and the RNA is finally recovered using PCR-grade (nuclease-free) water. The procedure used is as follows:

1. Wash extracted cells in 1 ml ice-cold PBS and centrifuge at low speed.
2. Remove the supernatant, and to the resultant pellet add 1.2 mL lysis/binding solution for each 7.5 ml blood sample obtained, mixing well to ensure adequate cell lysis.
3. Organic extraction is achieved by adding 120 μ L miRNA homogenate additive, mixing thoroughly and leaving on ice for 10 min, followed by 1.2 ml of acid-phenol:chloroform. Thoroughly mix the sample, and centrifuge at 10000 g for 5 min, allowing recovery of the upper aqueous phase containing the mRNA.
4. RNA is then isolated by adding 1.25 volumes of neat ethanol to the aqueous phase and passing the solution through a filter at 10000 g for 20 sec. Wash the filter using supplied solutions to remove debris and contaminants. To the filter add 100 μ L of pre-heated PCR-grade water, and centrifuge at 10000 g for 30 sec. The filtrate is the recovered RNA.
5. Proceed to measurement of concentration and purity.

2.5.2. RNA quantification and purity

Initial measurements were performed using an Eppendorf Biophotometer, but later a NanoDrop ND2000 was used to enable spectrophotometric assessment of RNA.

The principle of RNA analysis is that nucleic acids absorb ultraviolet light at a wavelength of 260 nm (A_{260}). Passing light at this wavelength through the sample onto a photodetector enables an assessment of nucleic acid concentration: the more light that passes through to the photodetector, the lower the concentration of nucleic acid. However, samples are frequently contaminated with other proteins and extraction

chemicals (e.g. phenol). Contaminating proteins absorb light at 280 nm (A_{280}), so by measuring absorption at 260 nm and comparing with absorption at 280 nm it is possible to make an assessment of RNA purity: the A_{260}/A_{280} ratio. A ratio of 1.8 is considered acceptable for RNA purity: lower values suggest either very low concentrations of RNA or significant phenol contamination.

The Eppendorf Biophotometer uses a quartz cuvette through which light is passed. This requires sufficient volume of solution (200 μ l comprising 2 μ l sample and 198 μ l PCR-grade water) and adequate mixing. The NanoDrop ND2000 requires 2 μ l of sample with no dilution and no mixing, and is placed directly into the device. It also generates sample spectra (190 - 840 nm) that enable a visual assessment of purity as shown in Figure 2.5.2.

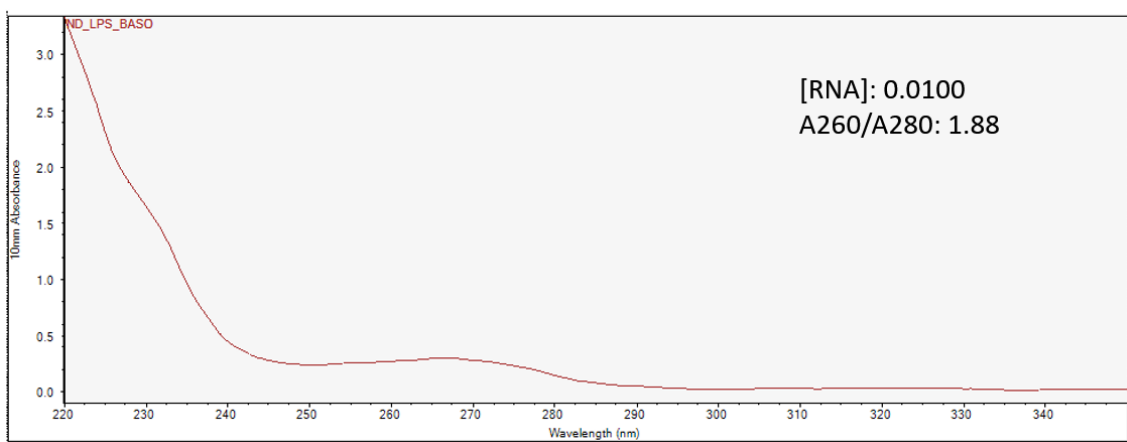
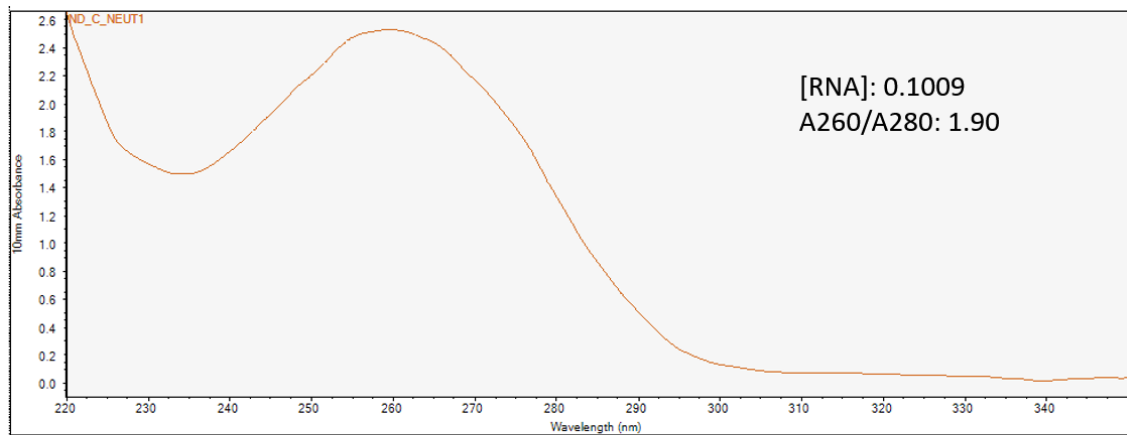


Figure 2.5.2 Example spectra from NanoDrop 2000. The top graphic is illustrative of an acceptable concentration ($\mu\text{g } \mu\text{L}^{-1}$) of RNA with good purity, acquired from neutrophils. The basophil sample (bottom graphic), however, is ten times lower in concentration, although purity is assessed as being acceptable.

2.5.3. Removal of genomic DNA

It is necessary to remove any potential contaminating or genomic DNA before proceeding to reverse transcription. For this the Turbo DNase Kit was used, and involved adding 5 μL of supplied buffer, 1 μL of DNase, the RNA sample (5 μg) and sterile PCR-grade water to make up at total of 50 μL . Samples were then incubated at 37°C for 30 minutes, remixed, and then any remaining DNase inactivated with 5 μL Inactivation Reagent. Where there was less than 5 μg of RNA extracted, the entire sample was used up to a maximum volume of 44 μL . Samples were left at room temperature for 5 min before being centrifuged at 10000g for 1.5 min, resulting in a clear supernatant free of contaminating DNA.

2.5.4. Reverse transcription

Copy DNA is more stable than mRNA, and is necessary for DNA polymerase amplification. Conversion of mRNA to cDNA was achieved using a high capacity cDNA reverse transcription kit. For each sample, a non-template control was prepared, to which no reverse transcriptase was added (RT-), thereby ensuring any subsequent PCR results were purely due to reverse transcribed mRNA rather than any contaminating genomic DNA. In the test samples, reverse transcriptase (RT+; MultiScribe™ reverse transcriptase enzyme, 1 µl) was added to a solution of reverse transcription buffer (2 µl), deoxynucleotidetriphosphates (dNTP) (0.2 µl, 100 nM), random primers (2 µl), RNase inhibitor (1 µl), PCR-grade water (3.2 µl), and the test sample (10 µl). In the RT-control, the volume of RT (1 µL) was replaced with the equivalent volume of PCR-grade water. All samples were incubated in a thermocycler at 25°C for 10 min, 37°C for 2 hr, and finally for 85°C for 5 min.

2.5.5. Real-time quantitative PCR (RT-qPCR)

Analysis of the resultant cDNA was performed using a commercially available TaqMan™ gene expression assay within a StepOne system, as described extensively in previously published data.^{9 16 27 69 74} Although the samples had been cleaned of genomic DNA, TaqMan™ probes span exon junctions and so do not readily amplify genomic DNA, giving further strength to the validity of subsequent results.

The principle of RT-qPCR is that by measuring detection of the gene of interest (GOI) during the PCR reaction cycles, it is possible to assess the relative expression of that gene. That is, a poorly expressed gene will require more cycles of PCR before it is detected. PCR consists of a sequence of heating (95°C) and cooling (60°C) in the presence of DNA polymerase. Heating splits cDNA into single-strands of cDNA, and through the action of DNA polymerase, free nucleotides bind to the cDNA to form new double-stranded cDNA. The cDNA is again heated, and the cycle repeats, and through the process of heating, cooling and new cDNA formation the original cDNA is amplified.

TaqMan™ gene assays consist of a primer and probe for a specific gene of interest. The probe consists of a fluorophore that fluoresces when stimulated with light of a specific wavelength. This fluorophore is bound to an oligonucleotide sequence that binds to single-stranded cDNA and terminates with a quencher molecule. This quencher molecule inhibits fluorescence of the fluorophore when it is stimulated with light. After heating to split cDNA into single-strands, then cooling, the Taq primer for the GOI binds to the cDNA and enables Taq DNA polymerase to start binding free nucleotides to the cDNA. The TaqMan probe binds downstream to the primer, and when Taq DNA polymerase reaches the probe, it cleaves the fluorophore releasing it from the actions of the quencher molecule. The fluorophore then fluoresces in response to light stimulation. With each cycle, more and more fluorophore is released in proportion to the amount of cDNA encoding for the GOI, until a detectable threshold is reached and reported by the StepOne RT-qPCR device. This process is illustrated in Figure 2.5.3.

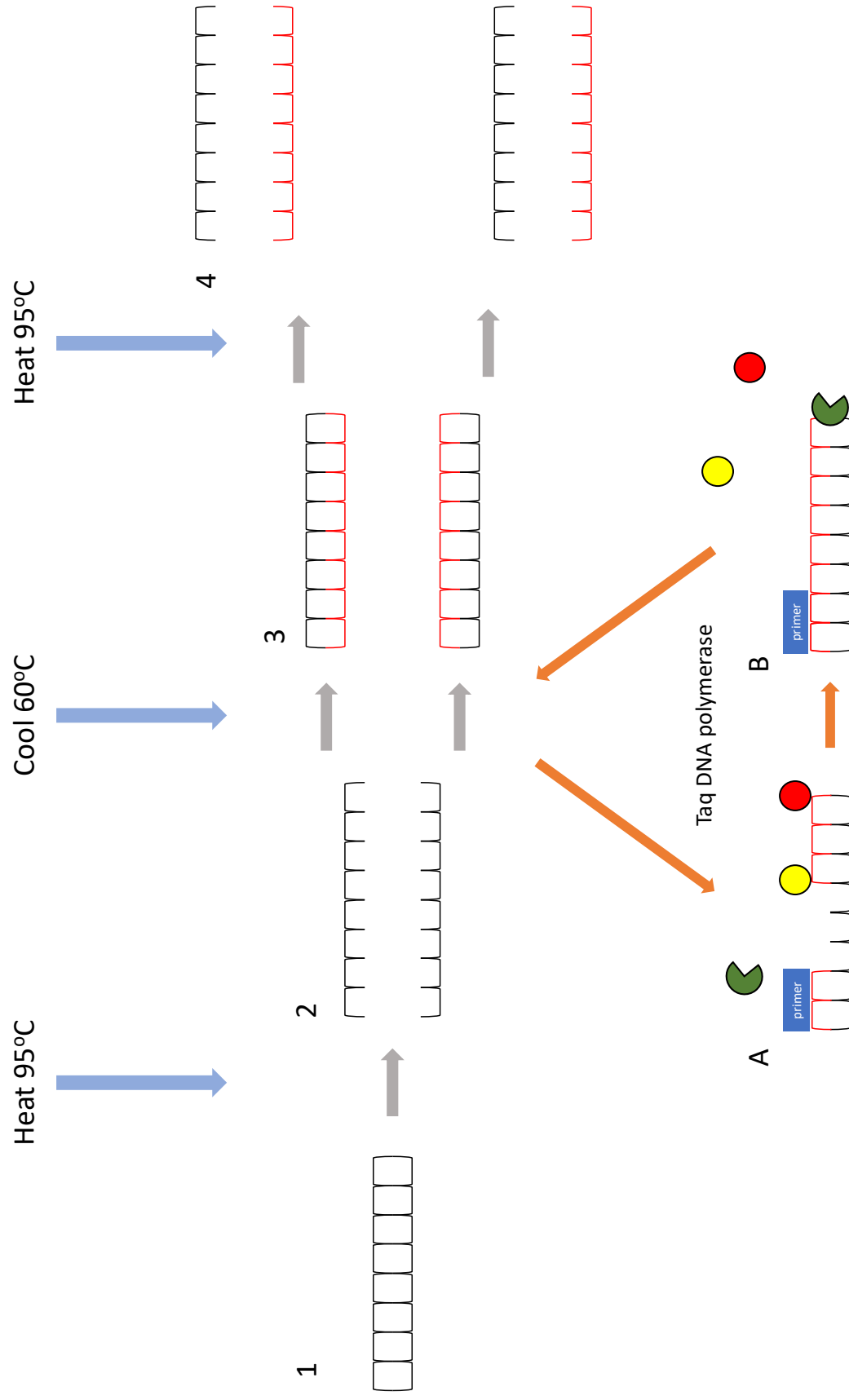


Figure 2.5.3 Summary process for RT-qPCR. cDNA (1) is denatured by heat into single-stranded cDNA (2). During a cooler period (A), a primer and TaqMan™ probe anneal with single-stranded cDNA. Taq DNA polymerase (green icon) anneals further nucleotides until the TaqMan probe is reached, and cleaves the fluorophore (yellow icon), releasing it from the action of the quencher (red icon). The newly completed cDNA (3) is then heated again, to produce further single-stranded cDNA (4). The cycle then repeats for each strand of cDNA, resulting in amplification and fluorescence for each newly created copy of DNA.

Three samples of cDNA were used for each experimental sample: two containing cDNA from the reverse transcription step, and one absent of cDNA (RT+ and RT-). For each cDNA sample (both RT+ and RT-), 10 μ L Gene Expression Mastermix, 1 μ L NOP or ppNOC primer, and 1 μ L of the HKG primer were prepared, to which 6 μ L water and 2 μ L of cDNA sample were added to give a total volume of 20 μ L. For consistency, two samples were prepared for each gene of interest, and one sample with the non-template control. Samples were placed in the StepOne™ system using the thermal profile of 50°C for 2 min, 95°C for 10 min, followed by 40 cycles of 95°C for 15 s and 60°C for 1 min.

The data output for this PCR analysis is presented as cycle thresholds i.e. the number of cycles of PCR heating and cooling to generate expression of the gene of interest. A high number of cycle thresholds indicates low expression of the measured gene. The measurement of gene expression is, however, dependent on the concentration of starting cDNA material. There are sources of error which can influence cDNA concentrations. For example, incomplete conversion to cDNA, pipetting errors, poor quality mRNA can all contribute to differences in cDNA concentrations. Furthermore, because PCR is a process of exponential amplification, small changes in cDNA concentrations can lead to large differences in measured gene expression. One technique to overcome these issues is normalization. This is achieved by using a reference gene or housekeeper gene (HKG). In principle, genes that are natively expressed in cells (usually genes relating to cell integrity or ribosomal function) can be used as reference point by which genes of interest can be measured. This controls for any variability introduced by small differences in cDNA concentrations; a low concentration of cDNA results in low expression of the gene of interest (a high cycle threshold) but also low expression of the housekeeper gene. The difference between cycle thresholds of the housekeeper gene and gene of interest therefore represents the relative abundance of the gene being investigated. This is termed the delta cycle threshold or Δ Ct. Figure 2.5.4 demonstrates this concept for a gene with low expression, and can be compared with Figure 2.5.5 where a lower Δ Ct indicates higher expression of the gene of interest.

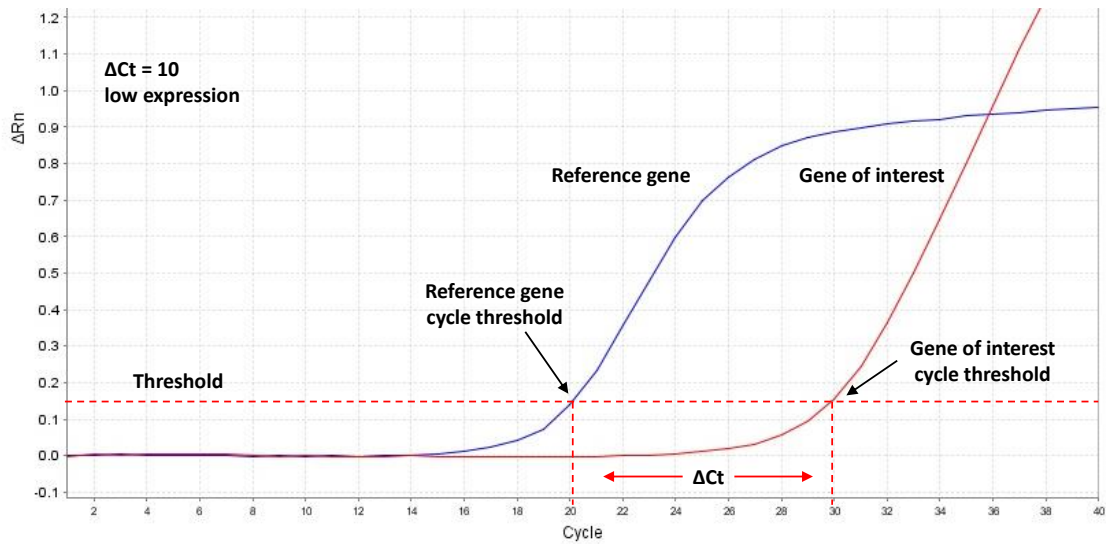


Figure 2.5.4 Labelled example of StepOne PCR output. Amplification of the cDNA sample occurs with each cycle, with fluorescence for the TaqMan® probes increasing with reaction cycles. Fluorescence reaching a detection threshold (dotted red line) is the cycle threshold (Ct) for the probed gene. The lower the Ct the higher the expression of the gene. The difference in cycle thresholds between the reference gene (or HKG) and the gene of interest (GOI) is termed delta CT (ΔCt).

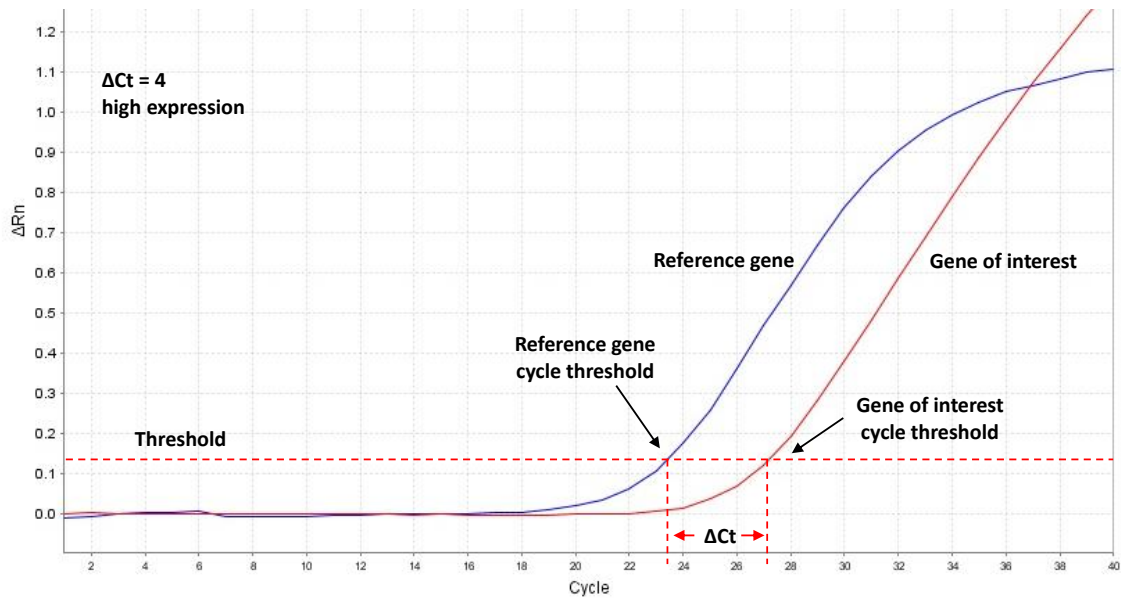


Figure 2.5.5 Labelled example of StepOne PCR output demonstrating a smaller ΔCt than for Figure 2.5.4. This indicates higher expression of the gene of interest.

The experiments described in the next chapter used LPS to simulate sepsis *in vitro*. Analysis of the effect of LPS on gene expression was performed by comparing mean ΔCt values between samples exposed to different concentrations of LPS. It is also possible to express changes in cDNA (and therefore mRNA) expression as fold-change using the $2^{-\Delta\Delta\text{Ct}}$ method which generates a more intuitive result.⁷⁵ The series of steps to do this are given below:

Using example data of:

Control sample: HKG Ct value = 22.05 GOI Ct value = 29.90

Treated sample (e.g. LPS stimulated): HKG Ct value = 20.33 GOI Ct value = 24.10

Enables calculation of ΔCt values using $\Delta\text{Ct} = \text{Ct}(\text{GOI}) - \text{Ct}(\text{HKG})$:

Control $\Delta\text{Ct} = 29.90 - 22.05 = 7.85$

Treated $\Delta\text{Ct} = 24.10 - 20.33 = 3.77$

The $\Delta\Delta\text{Ct}$ is then calculated using $\Delta\Delta\text{Ct} = \Delta\text{Ct}(\text{treated}) - \Delta\text{Ct}(\text{control})$:

Treated $\Delta\Delta\text{Ct} = 3.77 - 7.85 = -4.08$

[Control $\Delta\Delta\text{Ct} = 7.85 - 7.85 = 0$]

The fold change from control is then calculated using $2^{(-\Delta\Delta\text{Ct})}$:

Fold change from control to treated = $2^{(\text{minus}-4.08)} = 16.91$

Therefore, in this example there has been a 16.91-fold increase in gene expression compared with control. Decreases in expression are represented by values between 0 and 1. A $\Delta\Delta\text{Ct}$ of +4.08 is a fold change of 0.06, i.e. gene expression in the treated sample is 0.06 of that of the control, a decrease in expression by 16.91 fold.

2.6. Whole blood mRNA

As an alternative to mRNA extraction from isolated leukocytes, NOP and ppNOC expression from whole blood mRNA was investigated. For these experiments the commercial RiboPure™-Blood kit (see 2.xvi) was used to isolate mRNA directly from whole blood. The procedure for this isolation of mRNA was as follows:

1. Aliquot 0.5 ml of whole blood into 2 ml microcentrifuge tubes.
2. Centrifuge at 1600 g for 1 min and discard supernatant.
3. Add 800 μ L lysis solution and 50 μ L sodium acetate solution to each sample.
4. Mix thoroughly (vortex and inversion).
5. Add 500 μ L of phenol:chloroform to lysate and vortex for 30 s.
6. Rest at room temperature for 5 min, and then centrifuge at 1600 g.
7. Transfer supernatant to new 2 ml microcentrifuge tubes.
8. Add 600 μ L of 100% ethanol to samples and briefly vortex.
9. Warm provided elution solution to 75°C. Each 0.5 ml sample will require 50 μ L of elution solution.
10. Apply 700 μ L of each sample onto individual filters as supplied with kit.
11. Centrifuge for 5 – 10 s.
12. Discard effluent and apply 700 μ L wash solution 1 to each sample filter; centrifuge for 5 – 10 s.
13. Discard effluent and apply 700 μ L wash solution 2/3 to each sample filter; centrifuge for 5 – 10 s.
14. Discard effluent and again apply 700 μ L wash solution 2 / 3 to each sample filter; centrifuge for 5 – 10 s.
15. Centrifuge for 1 min to dry filter.
16. Transfer filters to clean collection tubes.
17. To each filter add 50 μ L of warmed elution solution and rest for 20 s.
18. Centrifuge for 20 – 30 s.
19. Take flow-through and reapply to filter.
20. Centrifuge for 1 min to collect mRNA in solution.
21. Proceed to quantification and assessment of purity.

2.7. Data analysis and statistics

All data were analysed using a combination of Microsoft Excel (for tabulating data) and Graphpad Prism v6 (GraphPad Software, La Jolla California USA, www.graphpad.com; for statistical analysis and graph production).

Analysis of PCR data was based on ΔCt values. Relative quantification uses the transformation $2^{-\Delta\Delta\text{Ct}}$ that generates a ratio, e.g. a relative quantification of 2 equates to a 2-fold increase in expression, a relative quantification of 0.5 equals a halving of expression or a 2-fold decrease. Data expressed as relative quantification do not follow a parametric distribution: decreases in expression have a ratio of between 0 and 1, increases of expression have a ratio of between 1 and ∞ . Therefore, for analysis of fold change data were log transformed. For this thesis log₂ was used for the transformation, which conveniently equates to $-\Delta\Delta\text{Ct}$. Graphical representation of fold-change in this thesis uses log transformed values.

Parametric distribution was assessed using D'Agostino-Pearson analysis. Where there were few data points, normal probability plots with Pearson coefficients (R) were generated to assess distribution (the closer the Pearson coefficient to 1, the increased likelihood of a normal distribution). Parametric analysis was used to compare changes in mRNA expression compared with control. For this ANOVA was used with Dunnett's correction for multiple comparisons, matched samples where appropriate. T-test was used where only two groups were compared.

3. Results from RNA analysis

This chapter describes a series of experiments designed to establish 1) whether there are differences in expression of mRNA transcripts of the nociceptin system between different granulocyte subpopulations, and 2) whether expression is modified by exposure to an *in vitro* model of sepsis using lipopolysaccharide (LPS).

3.1. Granulocyte mRNA expression

Question: Do granulocyte sub-populations express mRNA for NOP and ppNOC?

Previous studies have suggested that polymorphonuclear cells (PMNs) are associated with the nociceptin system (see Introduction 1.4). PMNs are also granulocytes, representing those white blood cells (leukocytes) that contain granules in their cytoplasm. They include neutrophils, eosinophils, basophils and mast cells. Of these, the neutrophils, eosinophils and basophils are found in peripheral blood, whilst mast cells are mainly associated with tissues and mucosal surfaces. The populations of peripheral whole blood granulocytes vary: neutrophils are the most abundant (60 – 65% of circulating leukocytes), followed by eosinophils (1 – 3%) and the comparatively rare basophils (0.5 – 1%). These cells are associated with the inflammatory process (see Figure 1.3.1 in Chapter 1) and so were the focus of experiments.

In these experiments blood samples (no more than 30 ml) were acquired from five healthy volunteers. Blood samples were separated into peripheral blood mononuclear cells (PBMCs) and PMNs using Blood Separation Protocol 1 (see Chapter 2.3.1). Extraction of neutrophils, eosinophils (PMN layer) and basophils (PBMC layer) was achieved using MACS (see Chapter 2.3.4).

Lipopolysaccharide (LPS) was used in all gene expression experiments as a model of sepsis *in vitro*. In this first experiment, isolated cells were exposed to LPS at either 0

(control) or $5 \mu\text{g ml}^{-1}$ for 20 hours at 37°C in the presence of RPMI media. mRNA was extracted and prepared as described in Chapter 2.5. Samples were stored at -80°C (-20°C for cDNA) where necessary during the mRNA extraction and measurement phases. Real-time quantitative PCR (RT-qPCR) was performed using TaqMan® probes for NOP, ppNOC and the housekeeper gene (HKG) GAPDH. Expression of mRNA for NOP and ppNOC would suggest that inflammatory cells produce protein for NOP and the N/OFQ precursor. Data were generated by RT-qPCR as delta-cycle threshold (ΔCt) values (the difference between expression of the gene of interest (GOI) and the HKG GAPDH) for samples. Note that a low ΔCT represents higher GOI expression than for a high ΔCt .

3.1.1. Results of cell separation

As per the blood separation and MACS methodology, neutrophils and eosinophils were extracted from PMN layer, basophils from the PBMC layer. Total cell counts of the PMN and monocyte layer were made using a haemocytometer and are shown below in Table 3.1.1.

Sample	Volume of blood (ml)	PBMC Layer ($\times 10^7$ cells)	PMN Layer ($\times 10^7$ cells)
A	30	5.7	8.1
B	30	6.6	14.0
C	30	11.6	15.0
D	25	3.4	6.0
E	30	2.1	7.7

Table 3.1.1 Cell count for cells extracted from separation layers for each volunteer. Differences in cell counts in samples are likely related to Ficoll-Paque™ PLUS yields as well as variation inherent with haemocytometry.

3.1.2. Measures of RNA concentration and purity

Spectrophotometry enabled an evaluation of the resulting concentrations of nucleic acids and their relative purity to contaminating protein, as shown in Table 3.1.2.

		Control		LPS	
		mRNA concentration ($\mu\text{g } \mu\text{L}^{-1}$)	260/280 ratio	mRNA concentration ($\mu\text{g } \mu\text{L}^{-1}$)	260/280 ratio
SAMPLE A	Basophil	0.01	1.6	0.0119	1.79
	Eosinophil	0.0404	1.78	0.015	1.67
	Neutrophil	0.2379	1.95	0.1591	1.95
SAMPLE B	Basophil	0.0466	1.44	0.0456	1.6
	Eosinophil	0.0344	1.87	0.0222	1.68
	Neutrophil	0.2185	1.9	0.2589	1.93
SAMPLE C	Basophil	0.0253	1.53	0.0247	1.62
	Eosinophil	0.0347	1.72	0.0328	1.87
	Neutrophil	0.1778	1.95	0.1349	1.95
SAMPLE D	Basophil	0.014	1.84	0.01	1.88
	Eosinophil	0.0208	1.68	0.0338	1.66
	Neutrophil	0.1817	1.94	0.4097	1.95
SAMPLE E	Basophil	0.015	1.87	0.01	1.7
	Eosinophil	0.02	1.95	0.035	1.97
	Neutrophil	0.199	1.94	0.279	1.91

Table 3.1.2 Summary of nucleic acid concentrations and their ratiometric purity.

A 260/280 ratio approximating 1.8 suggests minimal protein contamination, and a concentration of nucleic acid $>0.1134 \mu\text{g } \mu\text{L}^{-1}$ provided an optimal $5 \mu\text{g}$ material for removal of genomic contamination. These results show that for eosinophils and basophils extracted nucleic acid concentrations were consistently below this threshold. This makes interpretation of changes in mRNA expression difficult.

3.1.3. Results of qPCR

The qPCR data suggested that NOP was expressed in all granulocyte populations, despite low levels of extracted mRNA. However, ppNOC was preferentially expressed, albeit at high ΔCTs (low expression), in the eosinophil population (Figure 3.1.1). The isolated granulocytes had been incubated in the absence or presence of LPS ($5 \mu\text{g ml}^{-1}$ for 20 hours at 37°C). The universally low concentrations of mRNA in basophils and eosinophils made assessment of the effect of LPS difficult. However, these data do suggest that all granulocytes do express mRNA for NOP, and that ppNOC is preferentially expressed in eosinophils (particularly when compared with the higher concentrations of extracted mRNA for neutrophils).

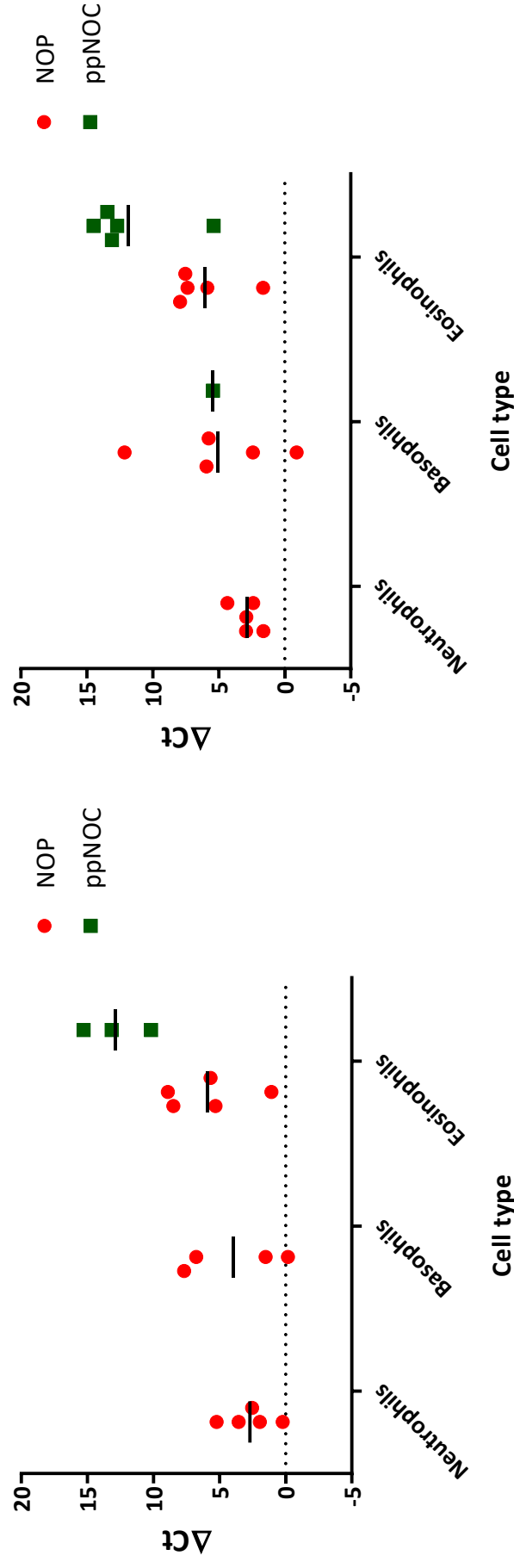


Figure 3.1.1.1 Results of gene expression in isolated granulocytes: Median and spread of ΔCt (GOI – GAPDH) values for mRNA expression of granulocyte populations in control samples (left) and LPS-stimulated samples (right). Higher ΔCt values represent reduced expression of the gene of interest. In two of the unstimulated basophil samples expression of NOP could not be measured, likely due to low mRNA yields associated with rarity of the cells. Expression of ppNOC was either low or unmeasurable in these samples. Where detected, ppNOC was predominately identified in eosinophils, with only one basophil sample containing mRNA for ppNOC. Neutrophils did not appear to express ppNOC at all.

3.2. Modulated expression of NOP in PMNs

Question: Is the expression of NOP in PMNs modified by increasing concentrations of LPS?

Initial experiments suggested that NOP was expressed in granulocytes, and that ppNOC was predominately identifiable in eosinophils, accepting the limitations of initial experiments. The issues of low mRNA concentrations, and the difficulties in reliably acquiring sufficient numbers of granulocyte subpopulations, meant that the focus of subsequent experiments was on PMNs (a mixture of eosinophils and neutrophils in the cell preparation), as these would be the cells of interest in the development of a live-cell imaging assay. Based on previous laboratory work, a technique for acquiring sufficient numbers of PMNs had already been established (i.e. PolymorphPrep™) and processes in place for reliably measuring mRNA expression using RT-qPCR.⁶⁹ Furthermore, MACS separation – as used in initial experiments – necessarily binds CD16 antibodies to neutrophils (leaving eosinophils unbound), potentially modifying their response to LPS.

These subsequent experiments were performed using 30 ml blood samples taken from nine volunteers. PMNs were extracted (Chapter 2.3.2 Blood Separation Protocol 2), and samples incubated with increasing concentrations of LPS: 0, 1, 2.5 and 5 µg ml⁻¹ for 20 hours at 37°C in the presence of RPMI media and 10% Fetal Calf Serum. Nucleic acid extraction was as for the first experiments, and all samples were analysed for concentration and purity using the NanoDrop™ 2000 spectrophotometer. Quantities and purities for extracted nucleic acids were generally better than for the first set of experiments (see Table 3.2.1).

For real-time quantitative PCR, the HKG Beta-2-microglobulin (B2M) was used to generate ΔC_t for NOP and ppNOC. Data are also presented as log transformed fold change (see Chapter 2.7) as this produces a more intuitive result (Figure 3.2.1).

	LPS concentration ($\mu\text{g ml}^{-1}$)	mRNA concentration ($\mu\text{g }\mu\text{L}^{-1}$)	260/280 ratio
SAMPLE A	0	0.067	1.9
	1	0.091	1.81
	2.5	0.098	1.84
	5	0.106	1.79
SAMPLE B	0	0.125	1.91
	1	0.036	2.0
	2.5	0.154	1.9
	5	0.215	1.9
SAMPLE C	0	0.056	2.01
	1	0.068	1.93
	2.5	0.101	1.94
	5	0.333	1.91
SAMPLE D	0	0.331	1.9
	1	0.207	1.9
	2.5	0.377	1.91
	5	0.237	1.91
SAMPLE E	0	0.369	1.91
	1	0.120	1.9
	2.5	0.173	1.9
	5	0.113	1.91
SAMPLE F	0	0.260	1.92
	1	0.252	1.92
	2.5	0.119	1.92
	5	0.060	1.95
SAMPLE G	0	0.133	1.41
	1	0.078	2.0
	2.5	0.071	1.78
	5	0.057	1.94
SAMPLE H	0	0.238	1.91
	1	0.110	1.84
	2.5	0.095	1.93
	5	0.113	1.87
SAMPLE I	0	0.222	1.93
	1	0.067	1.94
	2.5	0.057	2.04
	5	0.053	2.03

Table 3.2.1 Summary of nucleic acid concentrations and their associated 260/280 ratios. Values highlighted in red are those nucleic acid concentrations where there was less than the minimal sample concentration ($0.1134 \mu\text{g }\mu\text{L}^{-1}$) expected for removal of genomic DNA.

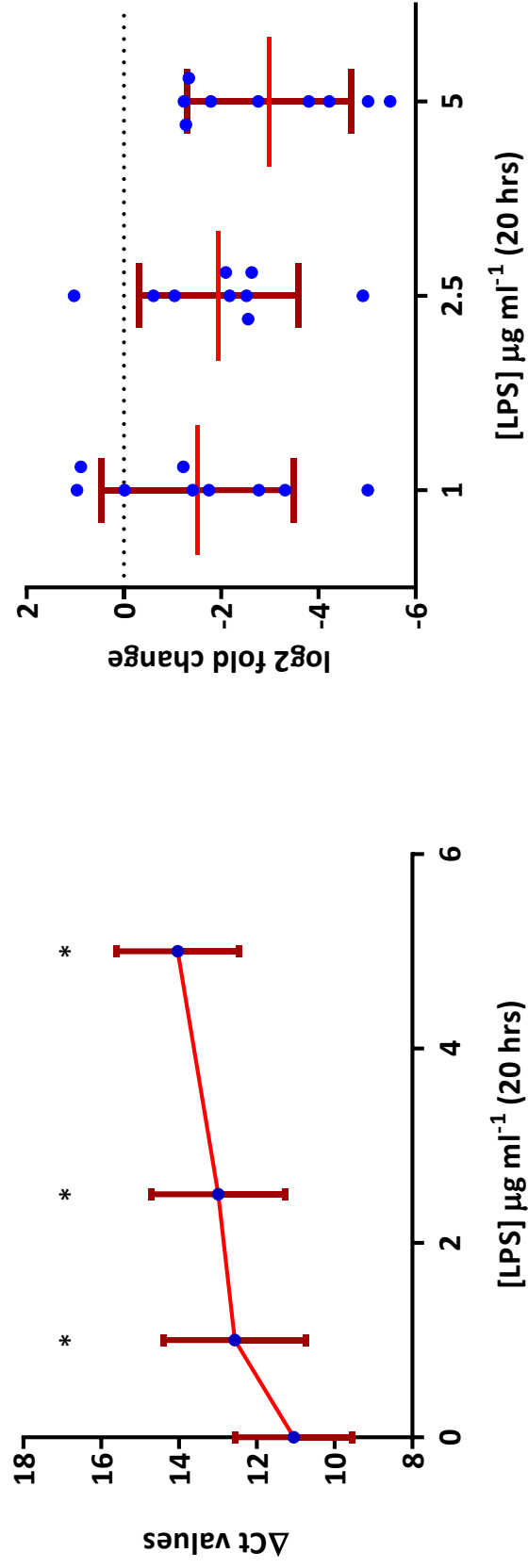


Figure 3.2.1 Graphs of PMN NOP expression with LPS: there was reduced NOP expression (mean ΔCt [SD, HKG B2M]) in PMNs exposed to increasing concentrations of LPS. An increase in ΔCt values represents a decrease in NOP mRNA expression (left), with there being a significant ($p=0.0005$) difference - indicated with * - in expression between PMNs exposed to all concentration of LPS and control (ANOVA with Dunnett's). When represented as log transformed fold change (right), reduced expression can be observed more clearly. Note that the control of 0 $\mu g\ ml^{-1}$ LPS is represented as a control line at 0 on the y-axis.

Mean control Ct values for NOP were 31.1 and for B2M 20.0. Δ Ct values were normally distributed (D'Agostino-Pearson), and comparison of the means using matched 1-way ANOVA (Dunnett's multiple comparison) demonstrated a significant difference ($p=0.0005$) in NOP mRNA expression between PMNs exposed to all concentrations of LPS and control. As illustrated by the fold change, there is a reduction in NOP mRNA expression with increasing concentrations of LPS exposure in isolated PMNs.

Of note, whilst ppNOC expression was tested in these experiments, it was barely measurable. Only 3 volunteer PMN isolates expressed ppNOC, and only at cycle thresholds greater than 35. This may reflect the quality and quantity of mRNA isolated, but given the results in the first experiments, suggests that ppNOC is minimally expressed in a mixed PMN population of neutrophils and eosinophils.

3.3. Housekeeper validation

Housekeeper genes (HKG) represent those genes constitutively expressed in DNA that should demonstrate stable expression despite environmental conditions. That is, the ideal HKG should be expressed at the same level irrespective of other gene expression, and so provides a reference against which relative expression of the gene of interest can be measured. In reality, most HKGs are not so stable and thus liable to change. The ideal HKG should be one that is expressed more than the gene of interest (i.e. with lower Ct values) and not subject to variation.

The HKG GAPDH was used in the first experiments for reasons of familiarity and previous published work.^{9 74} However, the literature suggested that in studies of PMNs Beta-2-microglobulin (B2M) should be more stable than GAPDH and highly expressed.⁷⁶ This was studied using six of the volunteer samples from experiment 3.2, performing RT-qPCR to examine expression of available HKGs GAPDH, B2M, PKG-1, HPRT-1, RPLPO, 18s and ACTB (see Chapter 2.xx). Data were first analysed with the commonly used algorithm

NormFinder®.⁷⁷ Comparisons of HKG expression were made for samples exposed to LPS 0 µg ml⁻¹ (control) and exposed to all concentrations of LPS.

NormFinder® is a Microsoft Excel add-in that examines variation in HKG expression from linearized relative quantities (RQ) derived from mean Ct values for each HKG using the formula:

$$RQ = 1/2^{(Ct\ value - \min\ Ct\ value)}$$

The results of these calculations were then grouped into control samples (group 1) or samples exposed to any concentration of LPS (group 2). NormFinder® was then run. Figure 3.3.1 shows how the data were presented for NormFinder®.

Raw Ct values																								
Sample	A	B	C	D	E	F	A LPS	B LPS	C LPS	D LPS	E LPS	F LPS	A LPS	B LPS	C LPS	D LPS	E LPS	F LPS	A LPS	B LPS	C LPS	D LPS	E LPS	F LPS
GAPDH	25.636	26.835	24.432	27.537	27.995	28.139	28.624	28.803	29.797	28.071	24.992	23.308	23.995	29.523	29.502	28.923	22.585	23.323	28.264	24.408	31.832	26.645	21.967	24.560
HPRT-1	32.055	32.492	30.313	32.457	33.514	33.171	33.997	32.947	35.043	32.591	31.158	30.393	30.605	34.447	32.782	32.896	30.419	29.483	33.503	29.695	35.743	31.441	29.714	31.118
RPLO	28.678	29.567	27.279	29.092	30.719	31.930	31.427	30.886	33.693	30.898	29.050	27.644	28.072	32.338	32.941	30.722	27.406	27.308	32.584	26.124	36.212	27.924	26.573	29.893
18s	14.813	15.175	11.049	14.561	13.910	14.368	16.865	16.295	19.967	20.358	11.877	8.584	12.351	20.830	14.720	16.736	10.497	9.351	14.968	14.771	18.783	13.237	9.566	16.262
B2M	20.716	22.607	20.192	22.845	20.569	22.304	22.126	22.846	25.345	21.407	19.930	17.868	19.420	23.642	22.840	23.697	17.969	18.248	22.356	18.238	25.202	21.531	17.317	19.278
PKG-1	26.577	29.706	24.903	27.032	26.114	27.327	28.465	27.961	30.539	28.609	25.211	23.086	24.929	29.801	29.232	28.889	23.008	23.860	27.540	24.426	30.403	26.686	22.560	24.539
ACTB	23.410	24.163	23.116	26.459	26.865	26.875	25.131	29.259	24.995	28.587	24.378	21.347	23.147	29.431	31.744	29.939	21.089	21.872	27.158	29.823	35.146	26.195	20.313	23.938
	1	1	1	1	1	1	2	2	2	2	2	2	2	2	2	2	2	2	2	2	2	2	2	2
Relative quantities																								
Sample	A	B	C	D	E	F	A LPS	B LPS	C LPS	D LPS	E LPS	F LPS	A LPS	B LPS	C LPS	D LPS	E LPS	F LPS	A LPS	B LPS	C LPS	D LPS	E LPS	F LPS
GAPDH	0.079	0.034	0.181	0.021	0.015	0.014	0.010	0.009	0.004	0.015	0.123	0.395	0.245	0.005	0.005	0.008	0.651	0.391	0.013	0.184	0.001	0.039	1.000	0.166
HPRT-1	0.168	0.124	0.563	0.127	0.061	0.078	0.044	0.091	0.021	0.116	0.313	0.532	0.459	0.032	0.102	0.094	0.523	1.000	0.062	0.863	0.013	0.257	0.852	0.322
RPLO	0.170	0.092	0.449	0.128	0.041	0.018	0.025	0.037	0.005	0.037	0.132	0.349	0.259	0.013	0.009	0.041	0.411	0.440	0.011	1.000	0.001	0.287	0.733	0.073
18s	0.013	0.010	0.181	0.016	0.025	0.018	0.003	0.005	0.000	0.000	0.102	1.000	0.073	0.000	0.014	0.004	0.265	0.587	0.012	0.014	0.001	0.040	0.506	0.005
B2M	0.095	0.026	0.136	0.022	0.105	0.032	0.036	0.022	0.004	0.059	0.163	0.682	0.233	0.012	0.022	0.012	0.636	0.524	0.030	0.528	0.004	0.054	1.000	0.257
PKG-1	0.062	0.007	0.197	0.045	0.085	0.037	0.017	0.024	0.004	0.015	0.159	0.695	0.194	0.007	0.010	0.012	0.734	0.406	0.032	0.274	0.004	0.057	1.000	0.254
ACTB	0.117	0.069	0.143	0.014	0.011	0.011	0.035	0.002	0.039	0.003	0.060	0.488	0.140	0.002	0.000	0.001	0.584	0.339	0.009	0.001	0.000	0.017	1.000	0.081
#REF!	1	1	1	1	1	1	2	2	2	2	2	2	2	2	2	2	2	2	2	2	2	2	2	2

Figure 3.3.1 Data used in NormFinder® for samples exposed to control and to LPS concentrations. The groups are numbered 1 (control) and 2 (LPS – all concentrations). Raw Ct values were entered into an Excel spreadsheet and converted to relative quantities (RQs). The Excel add-in then used these RQs to generate stability values.

The results of these analyses are shown in Table 3.3.1. GAPDH was the most stable HKG amongst the tested samples, in contrast to what was expected.⁷⁶

Gene name	Stability value
GAPDH	0.206
HPRT-1	0.272
RPLPO	0.307
PKG-1	0.329
B2M	0.342
18s	0.397
ACTB	0.483

Table 3.3.1 Stability values acquired from NormFinder® analysis of HKG expression in response to all concentrations of LPS. Genes are in order of stability, with lower values representing reduced variance.

Another technique for assessing HKG stability is the web-based tool (www.leonxie.esy.es/RefFinder) based on work by Xie and colleagues in 2012.⁷⁸ This tool uses the algorithms of Genorm, Norfinder, BestKeeper and the comparative delta-Ct method to analyse all measured HKG Ct values. The output of this online tool generated a comprehensive ranking for HKGs (see Figure 3.3.2).

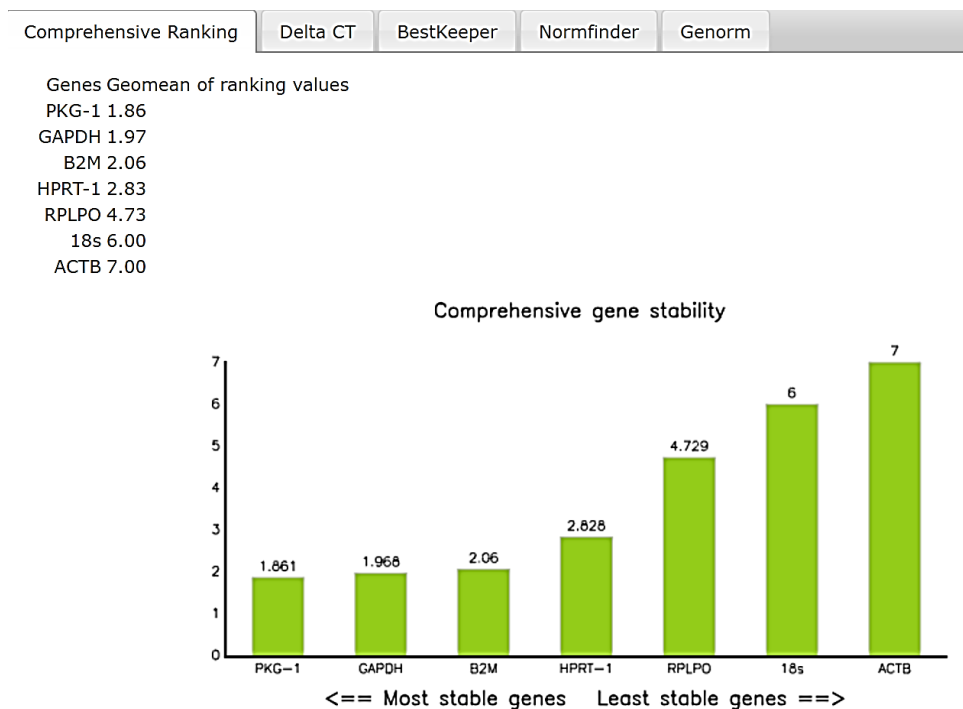


Figure 3.3.2 Output of the online tool RefFinder that brings together some of the commonly used algorithms in assessing HKG stability.

This tool does not test by grouping, however, and so assesses overall stability irrespective of the conditions of the experiment.

Whilst NormFinder[®] and RefFinder seek to identify the most stable HKG from a set of genes, it does not answer whether a HKG is sufficiently stable on its own. For this histograms were generated for the Ct values for each HKG and compared with Gaussian distributions (see Figure 3.3.3) as advocated by Mane and colleagues in 2008.⁷⁹ In essence, gene expression that remains close to the mean (low SD) and follows a Gaussian distribution irrespective of experimental conditions is likely to represent a preserved HKG. This analysis suggested that B2M met the criteria of having high expression (mean Ct 21.19), a relatively low SD (2.32), and minimal skew (-0.03, where a skew of 0 represents a Gaussian distribution).

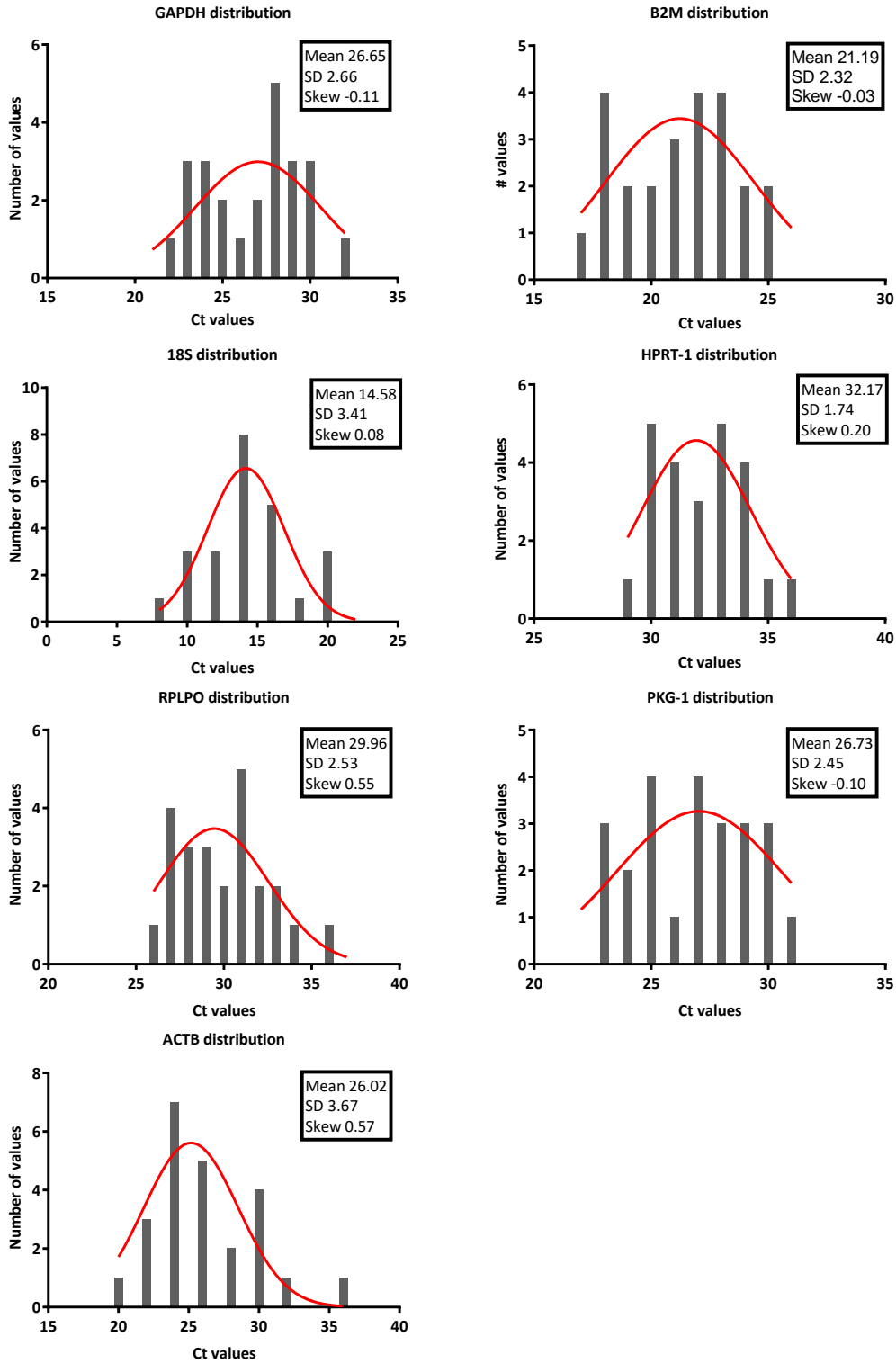


Figure 3.3.3 Frequency distributions of raw Ct values for tested housekeeper genes. Gaussian curves have been overlaid. Mean, SD and skew are included to demonstrate spread of data around the mean. Values with a normal distribution and reduced variance would suggest stability of the HKG.

B2M was the HKG used in LPS experiments following those in 3.1. Gaussian curve analysis suggested that B2M was comparatively stable. However, because validation analysis of these reference genes used the same samples used for measuring NOP expression, concentrations of mRNA (and therefore cDNA) were variable (see Table 3.2.1). It is possible that variations in HKG expression may have represented variations in cDNA concentration rather than variations caused by LPS exposure. Another reason for using B2M was that its expression was higher (lower Ct values, 21.19 SD 2.32) compared with GAPDH (mean Ct 26.65, SD 2.66). Further, RefFinder suggested there was little difference in stability between PKG-1, GAPDH and B2M. Minimum Information for Publication of Quantitative Real-Time PCR Experiments (MIQE) guidelines strongly recommend the use of two or more HKGs or reference genes as well as normalisation studies being performed for each experimental assay.⁸⁰ These experiments did not adhere to these specific recommendations, in part due to difficulties in extracting sufficient concentrations of mRNA to ensure cDNA concentrations were consistent.

3.4. LPS stimulation of whole blood

Question: How is NOP expression modulated when whole blood is exposed to LPS?

So far, experiments had been based on the analysis of mRNA expression in isolated granulocytes subsequently exposed to LPS. Subsequent studies now considered whether LPS-stimulated whole blood, followed by extraction of mRNA from PMNs, would generate similar results. The literature also suggested that LPS could be used at much lower concentrations for shorter periods of time to generate a marked 'septic' response.⁸¹ Previous work by our laboratory also suggested that PBMCs also expressed mRNA for NOP and ppNOC.¹⁶

These experiments were performed on whole blood acquired from 6 healthy volunteers according to Blood Separation Protocol 2 (see Chapter 2.3.2). PMNs and PBMCs were isolated from blood samples that had been exposed to LPS for 5 hours at 37°C at concentrations of 0, 0.01, 0.1 and 1 µg ml⁻¹. mRNA was extracted, prepared and measured as previously described. All samples were analysed for concentration and purity using the NanoDrop™ 2000 spectrophotometer. Nucleic acid yields were again low in some PMN samples (i.e. less than 0.1134 µg µl⁻¹ required for optimal removal of genomic DNA). Purity was acceptable for both PMNs and PBMCs (see Table 3.4.1).

	LPS concentration ($\mu\text{g ml}^{-1}$)	PMNs		PBMCs	
		mRNA concentration ($\mu\text{g } \mu\text{L}^{-1}$)	260/280 ratio	mRNA concentration ($\mu\text{g } \mu\text{L}^{-1}$)	260/280 ratio
SAMPLE A	0	0.387	2.05	0.219	2.23
	0.01	0.185	1.82	0.214	2.29
	0.1	0.262	1.89	0.272	2.24
	1	0.033	2.01	0.306	2.23
SAMPLE B	0	0.135	1.95	0.083	2.05
	0.01	0.034	1.83	0.256	2.15
	0.1	0.145	1.82	0.224	2.09
	1	0.094	1.84	0.172	2.08
SAMPLE C	0	0.140	1.95	0.332	2.07
	0.01	0.132	1.9	0.280	2.05
	0.1	0.147	1.92	0.416	2.03
	1	0.092	1.88	0.325	2.07
SAMPLE D	0	0.132	1.88	0.304	2.02
	0.01	0.098	1.73	0.207	1.96
	0.1	0.107	1.69	0.214	2.01
	1	0.075	1.71	0.210	2.02
SAMPLE E	0	0.052	1.83	0.196	2.15
	0.01	0.072	1.68	0.196	2.21
	0.1	0.097	1.74	0.194	2.16
	1	0.086	1.63	0.197	2.15
SAMPLE F	0	0.470	1.93	0.408	2.02
	0.01	0.516	1.90	0.435	2.00
	0.1	0.286	1.96	0.536	1.96
	1	0.215	1.96	0.438	2.01

Table 3.4.1 Summary of nucleic acid concentrations and their associated 260/280 ratios for PMNs and PBMCs. Values highlighted in red are those nucleic acid concentrations where there was less than the minimal sample concentration ($0.1134 \mu\text{g } \mu\text{l}^{-1}$) expected for removal of genomic DNA.

The HKG in these experiments was B2M. Mean PMN Ct values in control samples for NOP were 31.1 and for B2M 22.9; for PBMCs mean Ct values were 29.9 for NOP and 20.0 for B2M. There was again a reduction in mRNA expression for NOP with increasing concentrations of LPS in both PMNs and PBMCs. This is seen in Figure 3.4.1 where log transformed fold-change in mRNA expression has been plotted. As per previous experiments, mRNA for ppNOC was poorly expressed, either being unmeasurable or with cycle thresholds consistently greater than 35.

Statistical analyses were performed on ΔCt values. There were too few volunteer samples to test for or observe a parametric distribution. However, NOP mRNA ΔCt values in section 3.2 from the same pool of volunteers and similar experimental conditions of LPS were normally distributed. Further, normal probability plots suggested that these data were normally distributed, with Pearson coefficients (R) of a minimum of 0.93 (see Figure 3.4.3). Therefore, parametric ANOVA was performed with Dunnett's multiple comparisons correction for matched samples. This analysis demonstrated that for PMNs and PBMCs there was a significant difference between all exposures of LPS compared with control ($p < 0.0001$ for both analyses).

When put together with experiments in 3.2, there was a marked reduction when compared with isolated PMNs despite the reduced concentration of LPS and the shorter duration of exposure (Figure 3.4.2). The decrease in PMN NOP expression seen in whole blood samples exposed to 0 and 1 $\mu\text{g ml}^{-1}$ LPS was significantly different from that seen in isolated PMNs (t-test, $p = 0.0001$, see Table 3.4.2). This suggests that the other factors within whole blood are involved in modulating PMN NOP expression.

WB PMNs mean ΔCt (SD) (n=6)			Isolated PMNs mean ΔCt (SD) (n=9)			t-test
LPS 0 $\mu\text{g ml}^{-1}$	LPS 1 $\mu\text{g ml}^{-1}$	$\Delta\Delta\text{Ct}$	LPS 0 $\mu\text{g ml}^{-1}$	LPS 1 $\mu\text{g ml}^{-1}$	$\Delta\Delta\text{Ct}$	
8.19 (2.13)	15.82 (1.36)	7.63 (2.45)	11.06 (1.50)	12.57 (1.83)	1.51 (1.98)	$p = 0.0001$

Table 3.4.2 Mean ΔCt (SD) values for PMN NOP mRNA expression in whole blood LPS stimulation compared with isolated PMN stimulation. The change in expression from control is represented by $\Delta\Delta\text{Ct}$. Analysis using t-test on all $\Delta\Delta\text{Ct}$ values suggests a significant difference in the change in NOP expression.

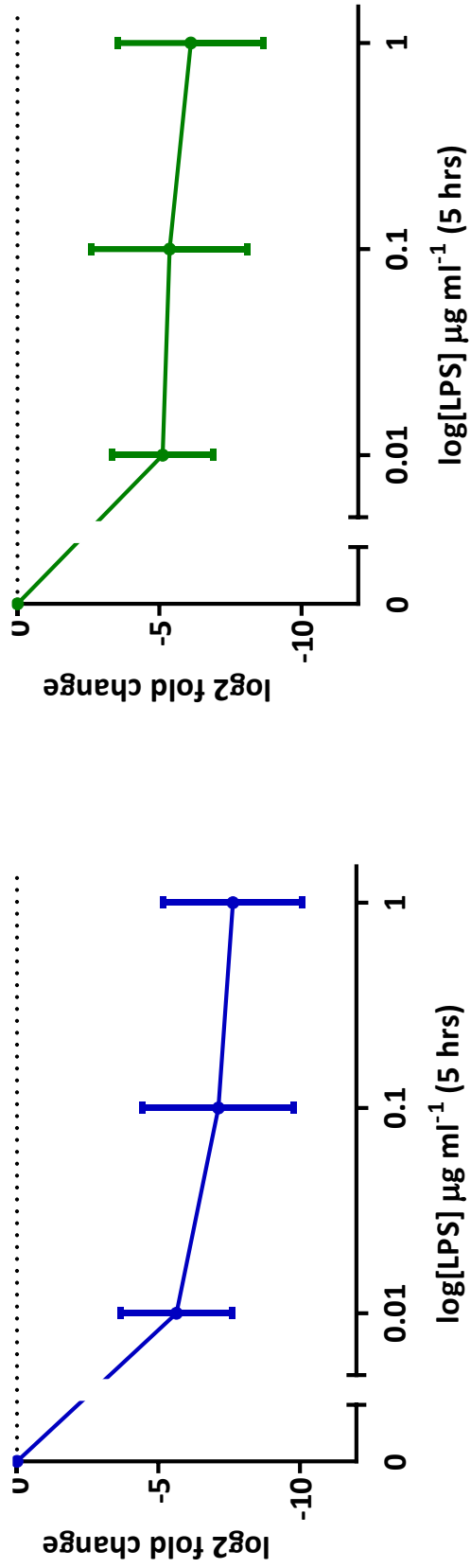


Figure 3.4.1. Data from whole blood samples of 6 volunteers with subsequent stimulation with LPS. These graphs represent log₂ fold changes (mean, SD) and illustrate reduced NOP expression with 10-fold increases in LPS concentration, with a 5 hour exposure. The mean fold change for PMNs was 0.0051 (log₂ -7.63) at 1 µg ml⁻¹; this is a 198-fold reduction in mRNA expression from control. For PBMCs, the fold-change at 1 µg ml⁻¹ LPS was 0.015 (log₂ -6.1); a 67-fold reduction in mRNA expression.

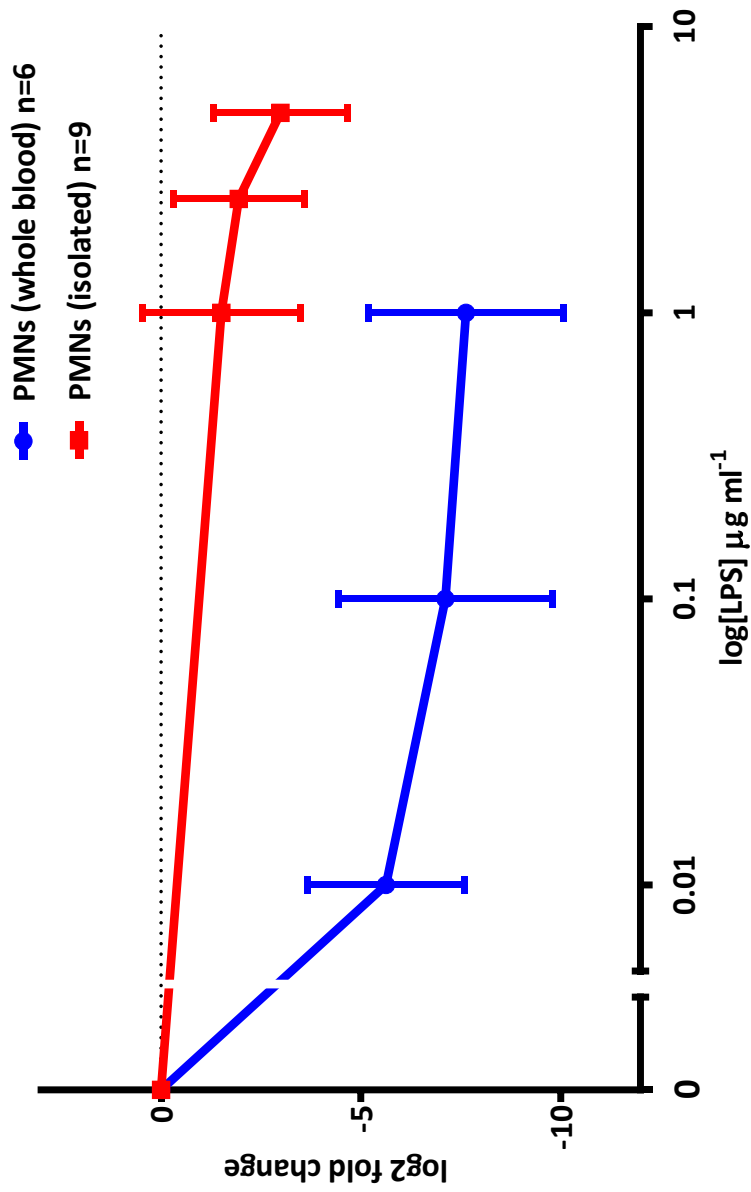


Figure 3.4.2 Comparison of log transformed fold-change data (mean, SD) for PMN NOP mRNA expression between whole blood samples stimulated with LPS (n=6), compared with LPS stimulation of isolated PMNs (n=9) taken from experiment 3.2. Whole blood stimulation was associated with a marked decrease in NOP expression in PMNs (significant between 0 and 1 $\mu\text{g ml}^{-1}$ LPS). The fold-change at 1 $\mu\text{g ml}^{-1}$ was 198 compared with a maximum 8-fold decrease in NOP mRNA expression from LPS-stimulated isolated PMNs. Furthermore, decreased expression occurred at a lower concentration of LPS administered over a shorter duration. This suggests that there are likely other factors within whole blood that modulate the nociceptin response to a septic stimulus.

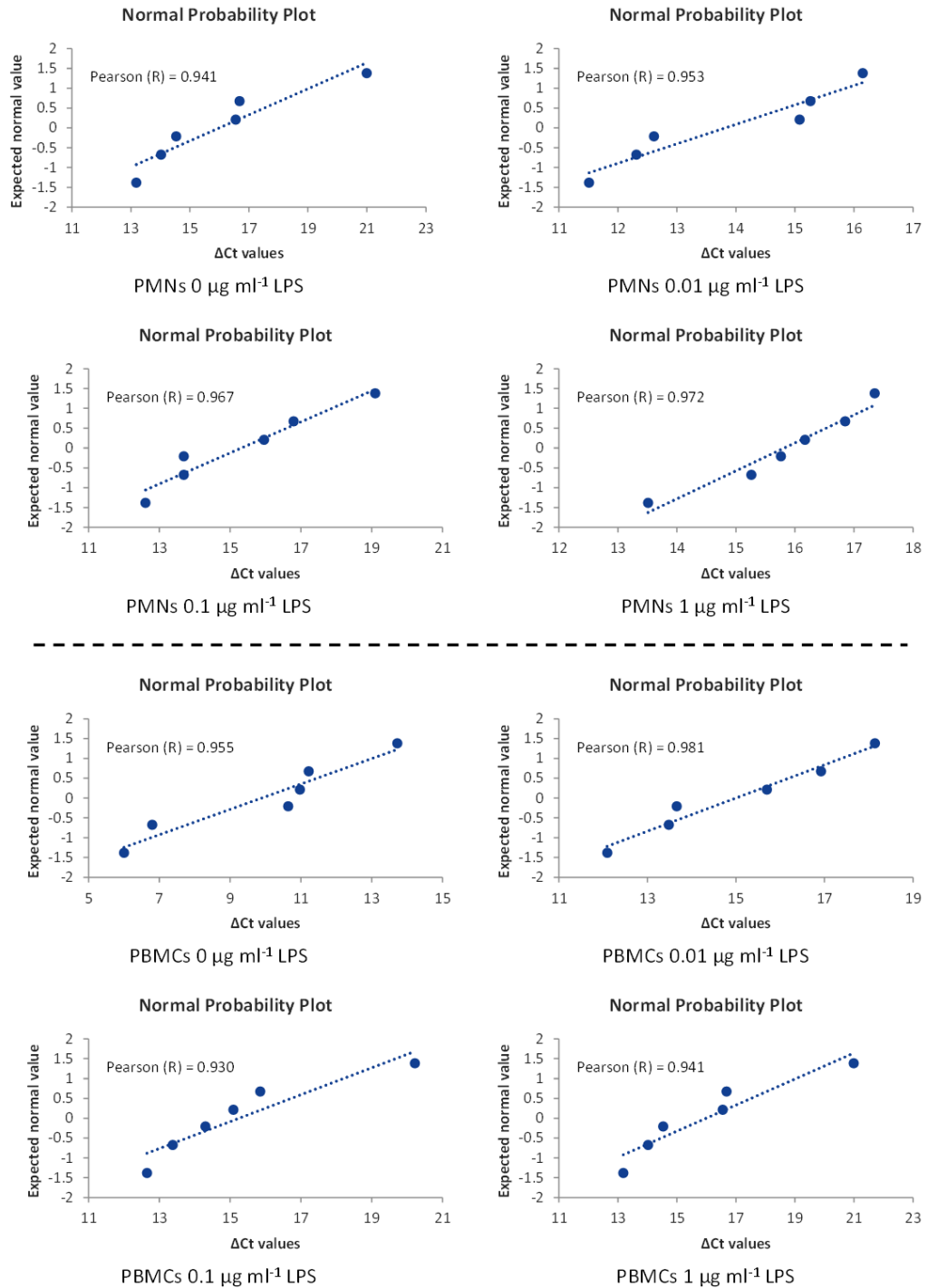


Figure 3.4.3 Normality probability plots for NOP ΔC_t values from experiment 3.4. These are ΔC_t values ranked in order then plotted against a linear representation of an ideal Gaussian distribution. The closer to the line the distribution, the increased likelihood of data being normally distributed. Pearson co-efficients of >0.930 in these data suggest that the ΔC_t values follow a normal distribution.

3.5. Whole blood mRNA

Question: Is NOP mRNA extracted from whole blood modulated similarly to isolated leukocytes?

Previous experiments had focussed on predominately granulocytes, but also PBMCs (lymphocytes, monocytes and dendritic cells). However, blood contains other components involved in systemic inflammation e.g. platelets, plasma proteins, that potentially interact and modulate the nociceptin response to a septic stimulus.

In a limited pair of experiments, mRNA was extracted from whole blood (see Methods 2.6) that had been stimulated for 5 hours with LPS at concentrations of 0, 0.01, 0.1 and $1\mu\text{g ml}^{-1}$. Two volunteers provided blood samples (30 ml volume). Assessments of mRNA yield and purity, reverse transcription and qPCR were as previously described. As seen in Table 3.5.1, mRNA yields were predictably higher as cell isolation was not required for these experiments.

		Whole blood	
LPS concentration ($\mu\text{g ml}^{-1}$)		mRNA concentration ($\mu\text{g }\mu\text{L}^{-1}$)	260/280 ratio
SAMPLE A	0	0.181	1.95
	0.01	0.256	1.95
	0.1	0.283	1.94
	1	0.244	1.95
SAMPLE B	0	0.289	2.03
	0.01	0.252	2.02
	0.1	0.250	2.01
	1	0.261	2.03

Table 3.5.1 Summary of mRNA yields from whole blood mRNA extraction. Overall yields of mRNA were improved compared with previous experiments.

Results from these experiments demonstrated a marked reduction in NOP mRNA expression (Figure 3.5.1). It was again difficult to determine expression of mRNA for

ppNOC, with values being either unobtainable or with cycle thresholds of 35 or more. As these data come from a such a small data set it is difficult to draw any specific conclusions. However, the similarity in NOP mRNA modulation does point to whole blood mRNA isolation being a useful technique for further exploring NOP expression in response to a septic stimulus.

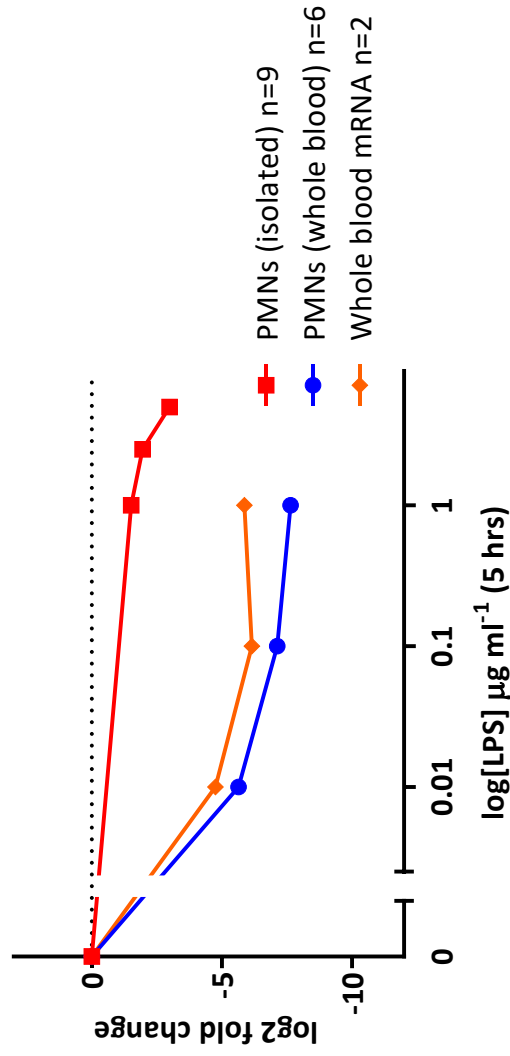
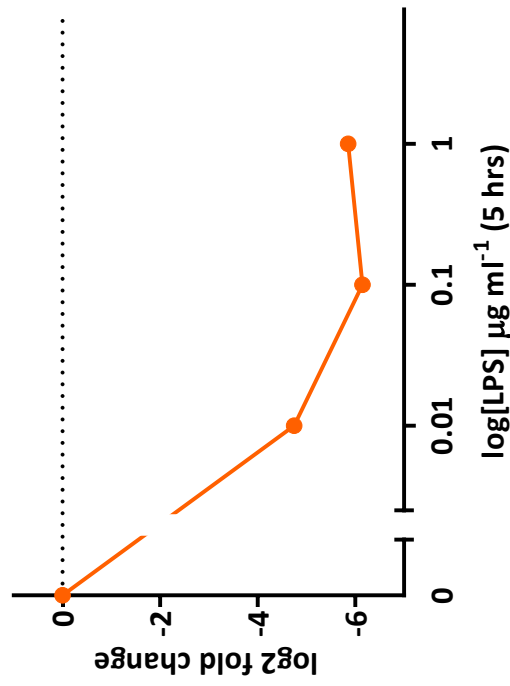


Figure 3.5.1 Reduced NOP mRNA expression from whole blood (n=2 blood samples) with increasing concentrations of LPS displayed as a fold-change on a logarithmic scale (left). The maximum mean fold-change was 67 from control ($2^{-\log_2(0.015)}$) at an LPS concentration of $0.1 \mu\text{g ml}^{-1}$. This was a similar decrease in NOP expression as seen in PMNs from stimulated whole blood, but a marked contrast with NOP expression following stimulation of isolated PMNs (right graph).

3.6. Conclusions

Together, these data suggest that mRNA for NOP is expressed in immune cells and within subpopulations of granulocytes. Perhaps surprisingly, mRNA for ppNOC was difficult to isolate. This may be because it is localised to only a few immune cells, with preliminary data suggesting eosinophils. This finding is supported by other published data that suggests ppNOC is predominately expressed in eosinophils.²⁷ Alternatively, the relatively low yields of mRNA for these experiments may have affected the ability to measure ppNOC expression. Still, NOP mRNA was detectable in all experiments, and expression of this receptor in immune cells suggests a function.

These data also indicate that NOP mRNA expression is modifiable. By using a standard *in vitro* septic stimulus (LPS), these experiments demonstrate that NOP mRNA expression is reduced as a consequence of LPS exposure. That this was seen in PMNs, PBMCs and whole blood indicates that NOP is widely expressed and influenced by inflammation. Further, there was a significantly larger decrease in PMN NOP expression for LPS-stimulated whole blood (198-fold) compared with LPS-stimulated PMNs (2.8-fold) for equivalent concentrations of LPS ($1 \mu\text{g ml}^{-1}$). This suggests that LPS-induced NOP modulation is influenced by immune cell and blood component interactions. Given the role of immunocyte signalling in sepsis (see Figure 1.3.1 Chapter 1), this is not unexpected.

These data are based on the use of a single normalisation gene / HKG (B2M) and it would have been preferable to use at least two normalisation genes in accordance with MIQE guidance. However, these data are consistent with other published data in this area. Zhang, Stuber and Stamer published in 2013 and demonstrated significant suppression of NOP transcripts in leukocytes following whole-blood exposure to LPS at a concentration of $0.01 \mu\text{g ml}^{-1}$ for 0, 3, 6 and 24 hours.⁸² This group used a single HKG, HPRT. The same group, however, previously published conflicting evidence in 2011. Stamer and colleagues demonstrated *increased* transcripts for NOP in patients admitted to ICU, those with cancer and post-operative patients; essentially inflammatory states.⁷⁰

Again, a single HKG (HPRT) was used. Despite the conflicting data, it is reasonable to conclude that mRNA for the nociceptin system is modulated in inflammatory states. Increased or decreased expression of NOP may reflect influences of circulating cytokines, the differences between *in vivo* and *in vitro* environments, and the type of stimulus (LPS or non-specific sepsis). Although Stamer's group used standard curves to calibrate their RT-qPCR experiments, it would be useful to investigate the most appropriate HKGs for studies of PMNs exposed to LPS.

Another issue was the relatively low yields of mRNA. Our laboratory has published data using PolymorphPrep™ to isolate PMNs, but other PMN isolation techniques (e.g using Ficoll-Paque™ Plus) might have improved mRNA yields. Low mRNA yields lead to variable concentrations of cDNA. Whilst normalisation should control for low cDNA concentrations, generating data to justify housekeeper gene selection is more difficult with variable starting cDNA product. Alternatively, larger blood volumes from volunteers could have been acquired, but samples necessarily came from a relatively small pool of volunteers, and larger blood volumes would have been difficult to justify on ethical grounds. Future experiments considering the effect of LPS on NOP expression could be performed on whole blood without cell isolation, as in experiment 3.5. The limited data above demonstrate a very similar reduction in NOP expression as for isolated PMNs, and likely would be a valid, and arguably more representative assay for observing changes in NOP and ppNOC expression to models of *in vitro* sepsis. The data from Thompson and colleagues in 2013 used PolymorphPrep™ to isolate PMNs before extracting mRNA and saw similar reductions in NOP expression as demonstrated above.⁶⁹ This contrasts with work by Stamer's group who analysed whole blood mRNA.⁷⁰ Stamer's finding of increased NOP expression also conflicts with the findings in experiment 3.5 analysing whole blood mRNA. However, with such a small sample size it is difficult to draw conclusions.

These experiments used endotoxin / LPS to simulate sepsis. LPS is well established as a stimulator of an immune response and activator of neutrophils.⁸³ It is major component

of the cell wall of gram negative bacteria and mimics gram negative sepsis, yet there are other sources for sepsis. For example, staphylococcal enterotoxin B (SEB) and streptococcal pyrogenic exotoxin can be used *in vitro* to mimic gram positive sepsis, and agonists such as N-Formylmethionine-leucyl-phenylalanine (fMLP) or (phorbol myristate acetate, PMA, an agonist of protein kinase C) can directly stimulate neutrophils.^{84–86} Furthermore, human models of sepsis are possible using LPS or dermal procedures (see Introduction 1.8). For example, cantharidin (a potent vesicant) blisters, skin windows and intra-dermal injections of UV-killed *E. coli* are techniques that allow acquisition of neutrophils that have been activated *in vivo*.⁶⁵ In these dermal techniques, blisters are either chemically generated (cantharidin) or formed on an area of human skin by suction and the inflammatory exudate aspirated for analysis. These generated neutrophils appear to respond in a similar manner to LPS-stimulated neutrophils, and it would be interesting to see whether NOP and ppNOC expression are similarly modulated.

Whilst these and other data on the mRNA expression of NOP and ppNOC are useful for understanding the role of the nociceptin system in inflammation, they do not address the function of the N/OFQ peptide or NOP receptor. Furthermore, expression of mRNA for NOP and ppNOC does not necessarily correlate with protein synthesis. mRNA is subject to modification by small regulatory RNAs (miRNA) that can prevent or enhance translation, and there are no data as to how this affects translation to functional protein.⁸⁷ Furthermore, translation is subject to other cellular regulatory processes. For example, eukaryotic initiation factor-2 (eIF-2) is necessary for initiating translation at ribosomes and is itself regulated by phosphorylation.⁸⁸ Therefore, the next stage was to develop an assay that allowed the study of N/OFQ in live human cells, forming a basis for future experiments that could better characterise the role of the nociceptin system in leukocytes.

STUDIES OF N/OAQ RELEASE FROM PMNs USING LIVE CELL IMAGING

4. Methodology

4.1. Reagents used

Solutions and reagents used in subsequent experiments are given below (in alphabetical order):

4.i Cell culture media (Sigma-Aldrich, Dorset, UK)

CHO-biosensors were grown from stock using cell culture media comprising DMEM:F12 with 10% Foetal bovine serum (100 IU ml^{-1}), streptomycin ($100 \mu\text{g ml}^{-1}$), fungizone ($2.5 \mu\text{g ml}^{-1}$). Selection media comprised G418 (geneticin) ($\mu\text{g ml}^{-1}$) and Hygromycin B ($\mu\text{g ml}^{-1}$).

4.ii Corning® BD Cell-Tak™ (Fisher Scientific, Loughborough, UK)

An adherent protein solution comprising polyphenolic proteins extracted from marine mussels, used to coat coverslips for adherence of unstimulated PMNs.

4.iii EGTA (Sigma-Aldrich, Dorset, UK)

Ethylene-bis(oxyethylenenitrilo)tetraacetic acid, a calcium chelating agent used to generate R_{min} for calibration of fluorimetry (200 μl of 90 mM EGTA).

4.iv Fluo-4 (Fisher Scientific, Loughborough, UK)

A single-emission fluorescent Ca^{2+} indicator associated with high fluorescence when bound to Ca^{2+} . Its excitation spectrum is very close to the wavelength of the argon laser (488 nm) used in confocal microscopy.

4.v fMLP (Sigma-Aldrich, Dorset, UK)

N-Formylmethionine-leucyl-phenylalanine, a standard stimulator of PMN degranulation and chemotaxis. Acts on formyl peptide GPCRs to increase intracellular calcium via phospholipase C.

4.vi Fura-2 (Sigma-Aldrich, Dorset, UK)

A ratiometric fluorescent Ca^{2+} indicator, presented as an acetoxymethyl (AM) ester.

4.vii Harvest buffer

Solution used for harvesting CHO-biosensor cells from cell culture. Comprises 10 mM HEPES buffered saline (0.09%), 0.05% EDTA, adjusted to a pH of 7.4 with sodium hydroxide.

4.viii Krebs-HEPES

Standard buffer solution previously described in Chapter 2.vi.

4.ix Modified Chinese Hamster Ovary (CHO) cells

CHO cells expressing the human NOP receptor and co-expressed with $G\alpha_{i/q}$ provided by T Costa, Istituto Superiore di Sanità, Rome, Italy via G Calo, University of Ferrara, Italy. Details of transfection and culture previously published by Camarda and colleagues.⁸⁹

4.x PPADS (Sigma-Aldrich, Dorset, UK)

Pyridoxalphosphate-6-azophenyl-2',4'-disulfonic acid, a non-specific antagonist of P2 receptors native to CHO cells.

4.xi Trap-101 (G Calo, University of Ferrara, Italy)

A selective competitive antagonist of the NOP receptor.

4.xii Triton-100X (Sigma-Aldrich, Dorset, UK)

Non-ionic surfactant used as a cell lysis agent used to generate R_{max} for calibration of fluorimetry (50 μ l of 4% Triton-100x).

4.2. Introduction

The mRNA experiments were designed to demonstrate not only the presence of mRNA for NOP and ppNOC, but also that expression could be modulated by a standard *in vitro* sepsis stimulant. However, mRNA expression does not necessarily confer functional protein, and there are few data about the role of the nociceptin system in inflammation at the cellular level. Research in this area has been hampered by the unreliability of ELISA in plasma samples, the inability to effectively culture granulocytes, as well as complexities with migration assays.⁷¹ Whilst there is some evidence to suggest polymorphonuclear cells do release N/OFQ, confirmation of this was sought by designing a completely new bioassay utilising live-cell imaging to visually demonstrate immune cell release of functional N/OFQ.²³ This could be used to study the inflammatory role of N/OFQ consistent with other experimental data (see Introduction 1.4).

Key to this novel assay was a sensor for detecting N/OFQ release distinct from ELISA or radioisotopes. Measuring calcium using fluorescence is well established in the study of GPCRs and in the high throughput screening of GPCR ligands.⁹⁰⁻⁹² Whilst studies of G_q coupled receptors using fluorescent calcium indicators are reasonably straightforward, G_i coupled receptors decrease intracellular calcium in response to ligand binding. To overcome this, G_i proteins can be forced to signal via the phospholipase C (PLC) pathway by co-expressing with chimeric $G\alpha_{i/q}$ proteins, thereby increasing intracellular calcium. The NOP receptor, in common with other opioid receptors, is G_i coupled. Studies have demonstrated that CHO cells transfected to express NOP with chimeric $G\alpha_{i/q}$ efficiently signal through G_q to increase intracellular calcium.^{89 93} **This thesis, therefore, explored whether such modified CHO cells could be used to detect endogenous N/OFQ produced by stimulated granulocytes.**

CHO cells have a long track-record in cell biology. They divide rapidly and are susceptible to genetic manipulation. However, CHO cells also express native purinergic receptors. These are a class of receptors that bind adenosine (P1) or nucleotides ATP, UTP or ADP (P2), with P2 receptors being subsequently subdivided into P2Y (GPCRs) and P2X (ligand-

gate ion channels).⁹⁴ There are further classes of P2Y and P2X receptors determined pharmacologically. CHO cells express P2Y and P2X receptors and increase intracellular calcium in response to nucleotides (e.g ATP, UTP).^{95 96} For the modified CHO cells to function as a biosensor to endogenous N/OFQ these receptors would need to be blocked to prevent purinergic-mediated increases in intracellular calcium. PPADS is a relatively non-selective antagonist of P2X receptors and some P2Y subtypes (including P2Y1 expressed on CHO cells).⁹⁷ PMNs release nucleotides when stimulated, therefore, blocking the native CHO cell P2 receptors with PPADS should enable increases in CHO intracellular calcium due to N/OFQ to be distinguished from increases due to nucleotide binding.⁹⁸

This assay, therefore, would use increases in intracellular calcium as determined by fluorescence as an indicator of N/OFQ binding to NOP expressed on CHO $\alpha_{i/q}$ cells. PMNs also increase intracellular calcium on activation and this rise in calcium is associated with PMN secretion.^{99 100} Therefore, this assay would also use fluorescence to indicate PMN activation. Detection of fluorescence would be by confocal microscopy as this would enable real-time imaging of changes in fluorescence. This assay, therefore, would allow single cell visualisation of PMN activation and any CHO-biosensor fluorescence in response to PMN release of N/OFQ. This concept is summarised by Figure 4.2.1, and the proposed assay system is illustrated in Figure 4.2.2.

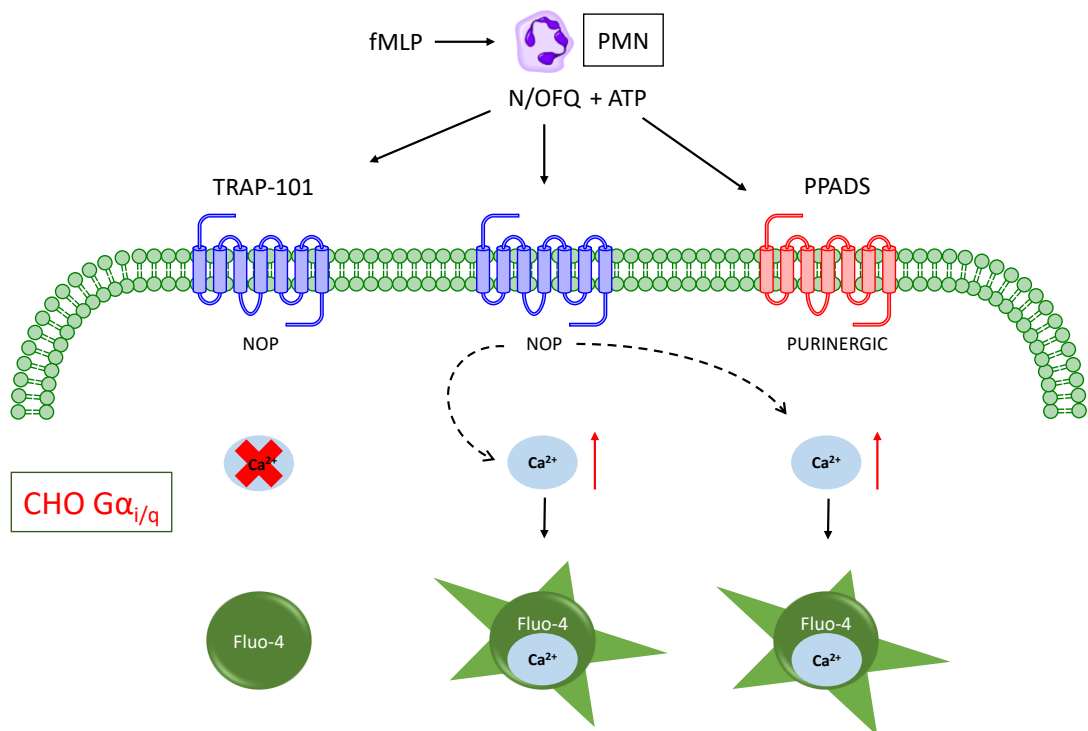


Figure 4.2.1 Principles of using CHO $G\alpha_{i/q}$ cells in live-imaging assay. N/OFQ released from stimulated PMNs binds to NOP receptors to increase intracellular calcium, resulting in fluorescence of the calcium indicator Fluo-4 (see 4.5.2). This effect is blocked by TRAP-101. PPADS ensures that rises in CHO intracellular calcium are not due to nucleotide stimulation of native purinergic receptors.

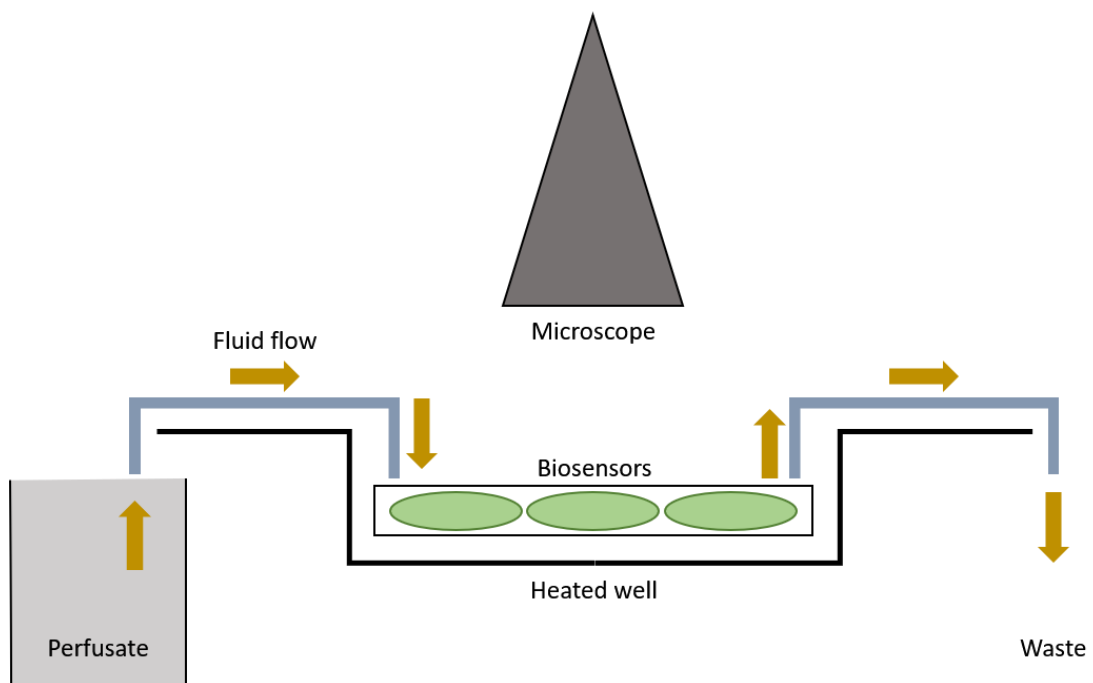


Figure 4.2.2 Diagram representing key components of assay. Biosensor cells reside within a heated well, where they can be imaged by the microscope. Warmed perfusion fluid is passed via a pump across the biosensors, and excess fluid removed into waste. Reagents can be administered either with the perfusion fluid or added directly onto the biosensors. Cells of interest can also be placed with the biosensors.

4.3. Assay development with fluorimetry

The success of this assay was dependent on functional CHO cells that would act as a biosensor to nanomolar concentrations of N/OFQ. Through collaboration with researchers in Italy modified CHO $\alpha_{i/q}$ cells were acquired (T Costa, Istituto Superiore di Sanità, Rome, Italy via G Calo, University of Ferrara, Italy).

The suitability of these CHO cells as biosensors of N/OFQ peptide was assessed by examining them using conventional cuvette-based fluorimetry. CHO cells were stimulated with differing concentrations of N/OFQ and fluorescent responses, indicating increased intracellular calcium, were measured. The dual-excitation calcium indicator Fura-2 was used for these experiments.

Fluorescence describes the property of a material that emits light following absorption of light or other electromagnetic radiation. Usually the emission wavelength is longer than that of the stimulating wavelength, i.e. less energetic, and relates to the transfer of energy that occurs when an excited electron returns to its lowest energy state. This energy for fluorophores (molecules that fluoresce) is seen as light. Fluorophores are widely seen in nature (e.g. in species of fish, squid, jellyfish, frogs, butterflies etc.), contrasting with bioluminescence which describes the emission of light following a chemical reaction. Natural fluorescence can be used to identify minerals and gems, organic liquids, and also describes the atmospheric phenomena of auroa (e.g. aurora borealis). There are many applications in science that depend on fluorescence, including spectroscopy, microscopy and fluoroscopy.

Fura-2 is one of the most commonly used fluorescent probes for the measurement of intracellular calcium (Ca²⁺). It readily binds calcium and importantly this binding is largely pH insensitive. It is a dual-excitation indicator: stimulation of the fluorophore occurs at two wavelengths of light depending on the degree of calcium binding. At levels of low calcium Fura-2 shows excitation spectra between 300 and 400 nm (peak at 370 nm).

After binding with calcium, the excitation spectra move further into the ultraviolet region of light. Therefore, exciting the fluorophore at 340 nm will show increased fluorescence on binding with calcium, and a decrease in fluorescence on stimulating at 380 nm. This change in emission spectra allows the use of ratiometric measurements. Cycling excitation of the sample at 340 nm and 380 nm enables a ratio of emission signals (measured at 510 nm) to measure changes in calcium. This principle is illustrated in Figure 4.3.1.

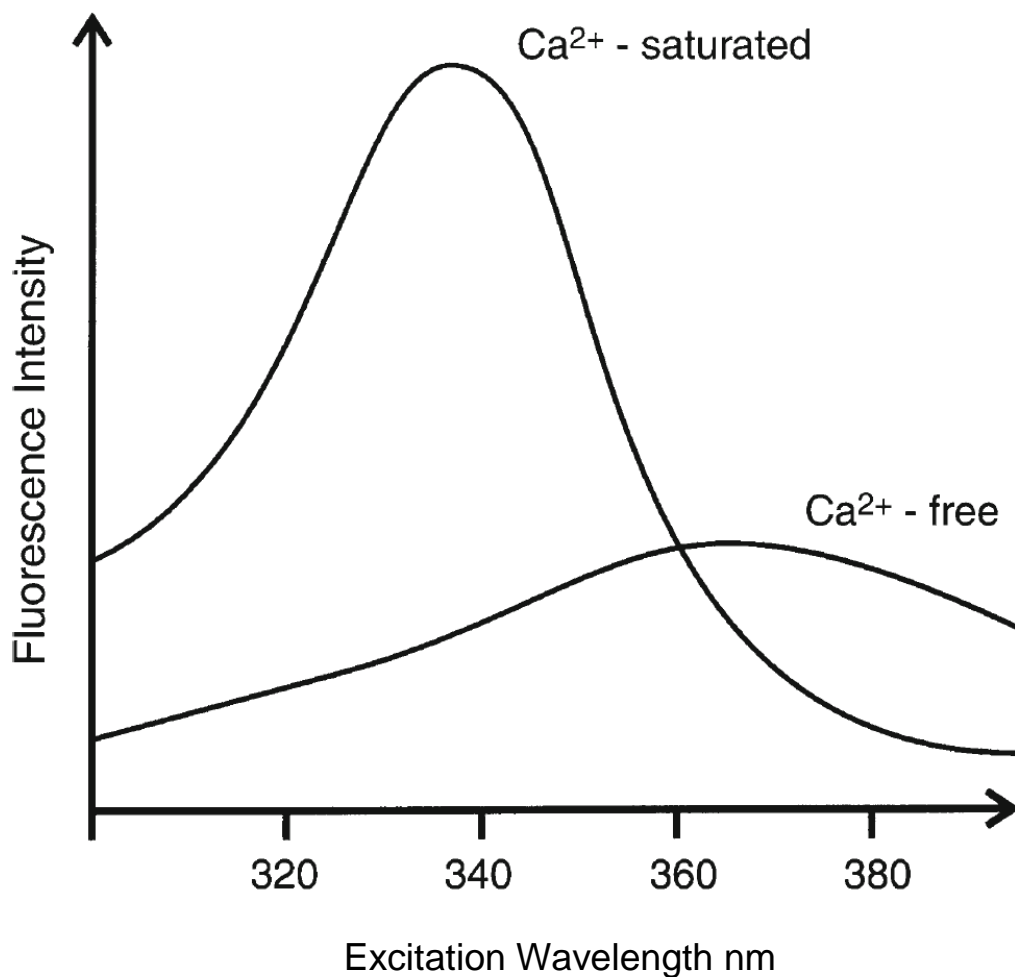


Figure 4.3.1 Excitation spectra for Ca²⁺ bound and unbound Fura-2. When bound, maximal emission intensity occurs with excitation at 340 nm, whereas unbound emission is highest with excitation at 370 nm. Cycling between excitation wavelengths of 340 nm and 380 nm generates a ratiometric measure of Ca²⁺ (Simpson A from Lambert and Rainbow, Calcium Signalling Protocols 3rd Ed.).¹⁰¹

The concentration of intracellular calcium is proportional to the 340/380 ratio as described by the Grynkiewicz equation.¹⁰² This equation considers the affinity of Fura-2 for calcium (K_d), with the 340/380 ratio in experimental conditions (R) and at calibration (R_{max} and R_{min}), finally correcting for baseline fluorescence (Sfb – the ratio of baseline fluorescence in calcium free and calcium bound conditions).

$$[Ca^{2+}]_i = K_d \times [(R - R_{min})] / [(R_{max} - R)] \times Sfb$$

The advantage of ratiometric measurement is that errors related to indicator concentration (affected by leakage and bleaching), optical path length, and illumination intensity affect both excitation wavelengths. Therefore, a more accurate measurement of calcium concentration is possible than would be possible with a single-excitation indicator.

Calibration is a crucial step for deriving calcium concentrations from measures of fluorescence. This is achieved by measuring fluorescence at maximum and minimum calcium concentrations. Fluorescence measurement at maximum calcium concentration (R_{max}) is achieved by damaging the cells of interest so that all intracellular dye is released into extracellular calcium-containing solution. Triton X-100 is a detergent used for this process that causes complete cell lysis. Free calcium is then chelated by a high affinity chelating agent (EGTA), binding all free calcium enabling measurement of R_{min} .

Fluorescent indicators of calcium are unable to pass through cell membranes due to ionisation. However, esterification renders them lipophilic, and so are usually supplied as acetoxymethyl (AM) esters. Cells can therefore be loaded with indicator by incubating them for between 15 min and 2 hr. Living cells contain esterases; these remove ester groups and so return the indicators to an ionised state, thereby trapping them within the cell.

A Perkin-Elmer LS50B fluorimeter (Beaconsfield, UK) using FLDM software was used for these experiments. This equipment comprised a Xenon discharge lamp for sample

excitation, appropriate emission filters, a gated photomultiplier for light emission detection, a cuvette holder surrounded by a water jacket, and a magnetic stirrer.

The following procedure for measuring fluorescence of $G_{\alpha i/q}$ CHO cells when stimulated by N/OAQ was used:

1. Discard culture media and rinse $G_{\alpha i/q}$ CHO cells once with harvest buffer.
2. Add no more than 20 ml of harvest buffer and incubate at 37°C for 5 min, agitating intermittently until cells are non-adherent and in suspension.
3. Transfer cells to 25 ml sterilin and fill with Krebs-HEPES solution.
4. Centrifuge at 1500 g for 2 – 3 min at room temperature.
5. Resuspend cells with Krebs-HEPES solution and repeat centrifugation.
6. Resuspend with 2 ml Krebs-HEPES solution and 5 μ M Fura-2 (10 μ l of 1 mM Fura-2/AM). Load cells for 30 min at 37°C, mixing halfway through loading process.
7. Fill with Krebs-HEPES solution and keep in dark conditions for 20 min to allow intracellular de-esterification of Fura-2.
8. Centrifuge cells at 500 g, discard supernatant, and wash cells three times with Krebs-HEPES, with 500 g centrifugation between washes. Resuspend cells to a volume of 2 ml per experiment.
9. Place quartz cuvette containing a magnetic stirrer into the fluorimeter. The sample should be kept at 37°C using the water jacket.
10. Add 2 ml of sample and measure 340 and 380 nm excitation fluorescence (measured at 510 nm) until a stable baseline is achieved (approximately 175 s).
11. Add desired concentration of exogenous N/OAQ (10^{-8} to 10^{-6} M).
12. After completing fluorescence measurements for all samples, perform calibration using a clean cell suspension. To this suspension add 0.1% Triton-X100 (50 μ l of 4% Triton-X100) to induce complete cell lysis. Measure fluorescence to give R_{max} . Now add 4.5 mM EGTA (200 μ l 90 mM EGTA). This chelates free calcium to give R_{min} .
13. Export data from fluorimeter and analyse as appropriate.

4.4. Confocal Microscopy

The properties of fluorescence as described above can be used in microscopy. Cells of interest can be appropriately labelled or stained with fluorescent molecules, and when stimulated with the specific wavelength of light, can be easily visualised. This has seen wide application in cellular studies. For example, fluorescent microscopy has been used to image myofilaments in cells, nucleic acids, and sub-cellular structures such as microtubules. Optical fluorescent microscopes utilise an illumination light (a xenon arc lamp or mercury-vapor lamp) to stimulate the sample of interest. This light is passed via an excitation filter and then reflected by a dichroic mirror (selectively reflects or passes through specific colour spectra) through the objective to the sample. Emitted fluorescence (usually of a longer wavelength) passes back through a spectral emission filter, selecting only for the emission wavelength, through the dichroic mirror, and finally to the viewfinder or photodetector. This setup is illustrated in Figure 4.4.1.

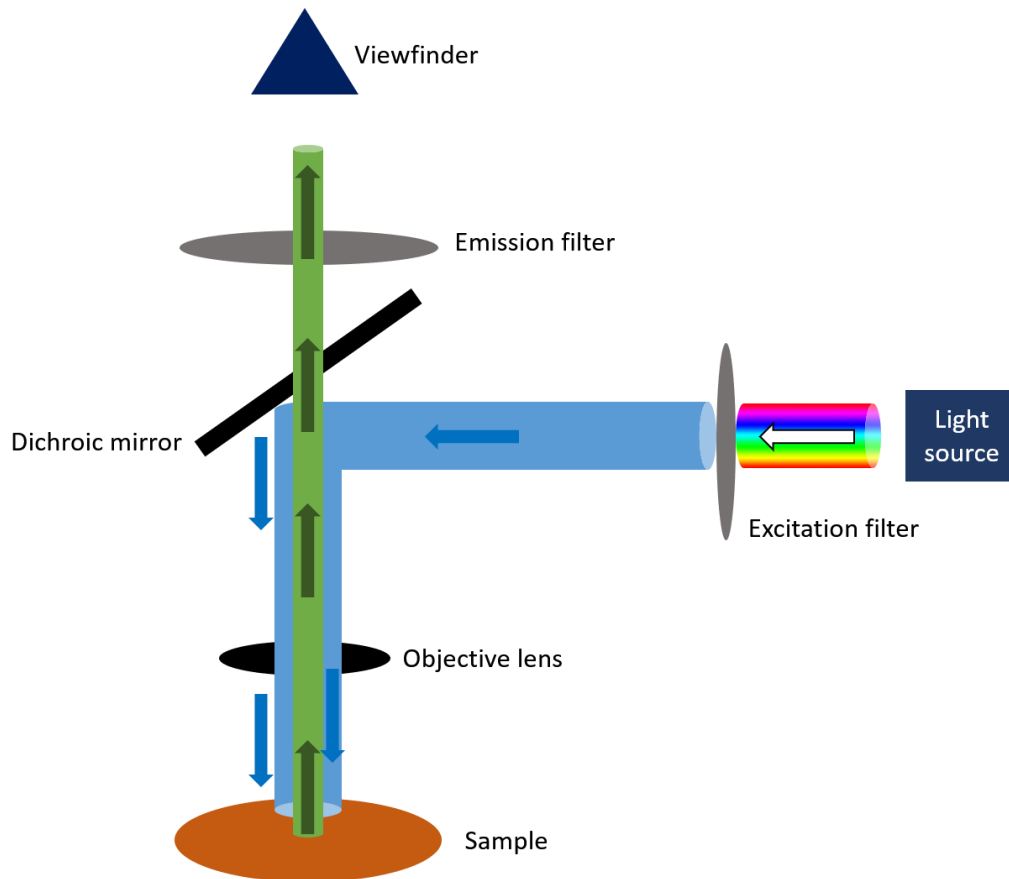


Figure 4.4.1 Fluorescent microscopy: light passes through the excitation filter selecting for a specific wavelength (above blue) determined by the fluorophore being used. The excitation light reflects onto the specimen via the dichroic mirror. Emitted fluorescence (above green) returns through the dichroic mirror, through the emission filter to the viewfinder.

The advantage of fluorescence microscopy is that intracellular structures can more easily be resolved than would otherwise require electron microscopy. Furthermore, unlike electron microscopy, it is a non-destructive process. It can also be used to generate real-time images of live cell systems so that dynamic cellular processes can be visualised.

Confocal microscopy is an extension of conventional fluorescence microscopy. In fluorescence microscopy the entire sample is bathed in light, stimulating all areas within the optical path. This is problematic for calcium-sensitive fluorescent molecules; the process of incomplete de-esterification and leaching results in calcium indicators interacting with calcium-containing perfusion solutions, causing background fluorescence and interfering out-of-focus light. Furthermore, when studying calcium changes within cells it is important to be able to focus purely on the point of interest.

without contaminating light from excited fluorophores throughout the rest of the sample. Confocal microscopy overcomes these issues through use of two pinholes in the light path. The first pinhole is in front of the light source, which generates a sharp focus of light, free of scatter, onto a single point of the sample. The light then stimulates the fluorophores which then emit light from this single focal point. A second pinhole then filters emitted light. This prevents the passage of light from outside the focal plane (i.e. out-of-focus light), improving resolution of the image. The way in which both pinholes ensure light is focussed on the sample, and only emitted light from the point of focus is detected, gives rise to the term confocal. This is illustrated in Figure 4.4.2.

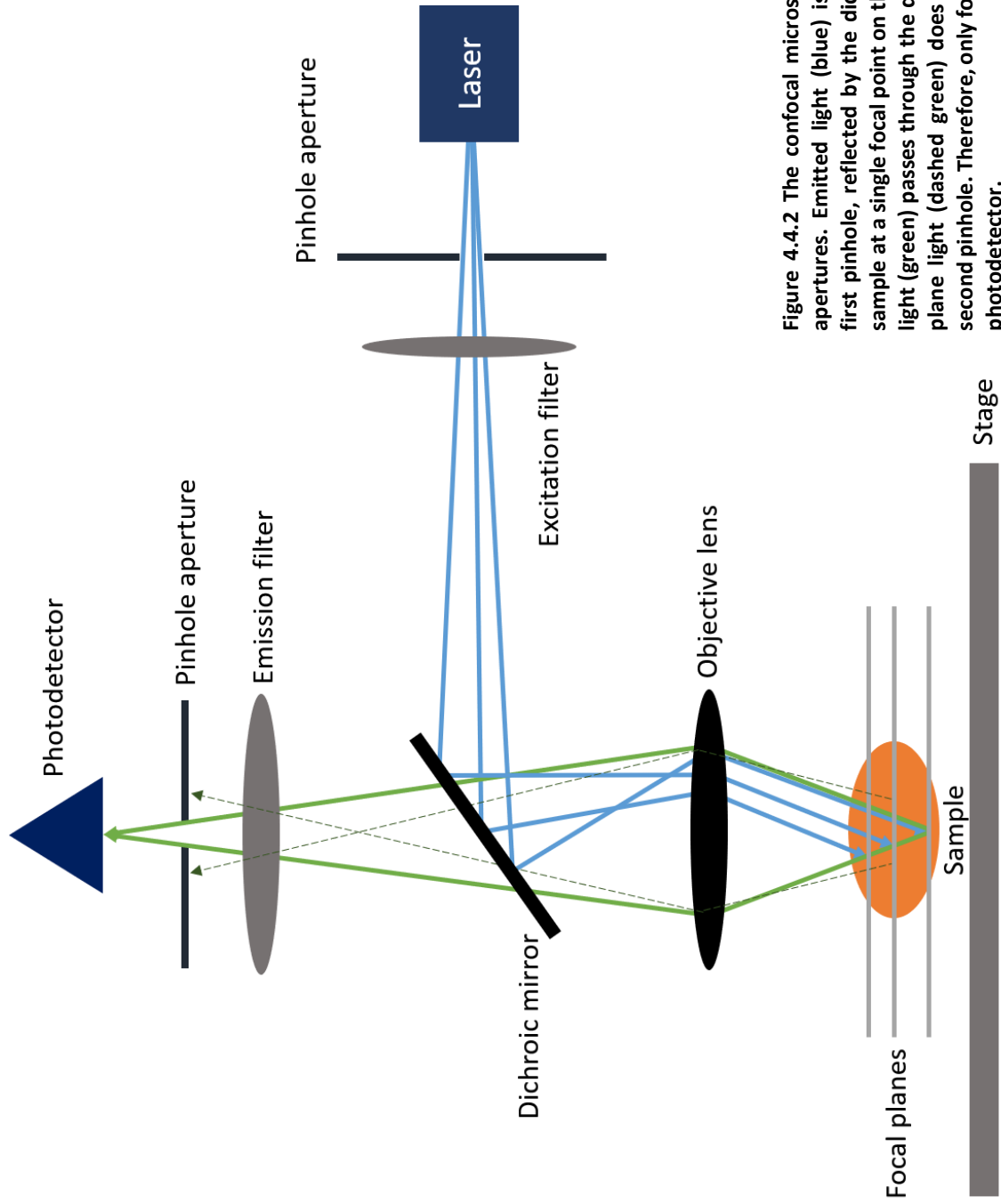


Figure 4.4.2 The confocal microscope has two pinhole apertures. Emitted light (blue) is focused through the first pinhole, reflected by the dichroic mirror onto the sample at a single focal point on the focal plane. Emitted light (green) passes through the dichroic mirror. Out-of-focus light (dashed green) does not pass through the second pinhole. Therefore, only focused light reaches the photodetector.

There are two practical problems to confocal microscopy. Firstly, the pinholes block light, therefore a high intensity excitation light is required (in practice lasers are used), and a photomultiplier system and/or sensitive photodetector is required for detecting emitted light. The second issue is that either the light needs to scan across the sample to generate an interpretable image, or the sample needs to move across the light path. The original confocal microscope passed the stage containing the sample across the beam, and some systems in the microchip industry use this approach. Systems devised for biological imaging scan a stationary sample through use of a single laser beam being directed by computer-controlled mirrors. A two-beam scanning system is also in commercial use that uses specially designed spinning disks.

A limitation of confocal microscopy is the intensity of the laser light. This can cause photobleaching. This is the irreversible damage of calcium indicator fluorophores, indicated by a fixed fluorescence of the molecule. Furthermore, the laser can damage live-cells and tissues themselves.

A feature of confocal microscopy not used as part of this thesis is optical slicing. Due to the highly focused nature of the microscope, focal points are often within the three-dimensional structure that comprises a cell. Therefore, moving the focal plane vertically and horizontally enables a series of slices to be imaged. These can then be recreated with software as a three-dimensional image.

The confocal microscope used in experiments was a Nikon C1Si confocal laser scanning microscope. This system comprises a laser light source, a sensitive photomultiplier tube (PMT) detector, and a computer which controls the scanning mirrors as well as the configuration of the laser and pin hole apertures. The computer also acquires images in real-time allowing for monitoring of any experiment, and acquisition for later analysis. The microscope used a 60x oil immersion objective (CFI Plan Apochromat VC 60x (NA=1.4)).

In addition to the confocal microscope a method for keeping the live cells viable for the subsequent experiments was needed. For this a custom-built perfusion system was used. This comprised a water-bath to keep perfusate and solutions warm, a rotary pump that delivered the perfusate to the objective and removed excess fluid, and a peltier heater to maintain cells in the objective at the desired temperature. An illustration for this setup is given in Figure 4.4.3.

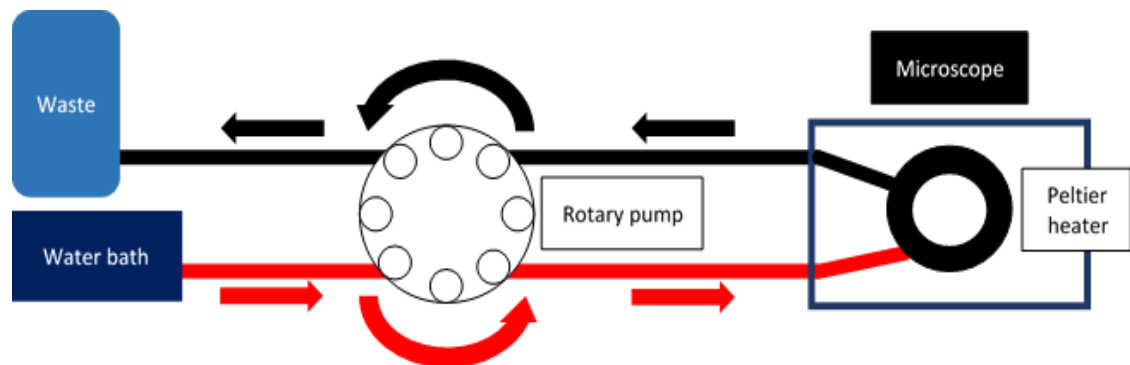


Figure 4.4.3 Illustration of perfusion system. Reagents are kept warm in the water bath, and connected to the perfusion system as required for the experiment.

Pictures of the actual system used are given in Figure 4.4.4. This had been custom-made for the laboratory in which the experiments were performed. The perfusion system had been previously calibrated to maintain perfusion fluid level during experiments and to prevent flooding of the stage and microscope.

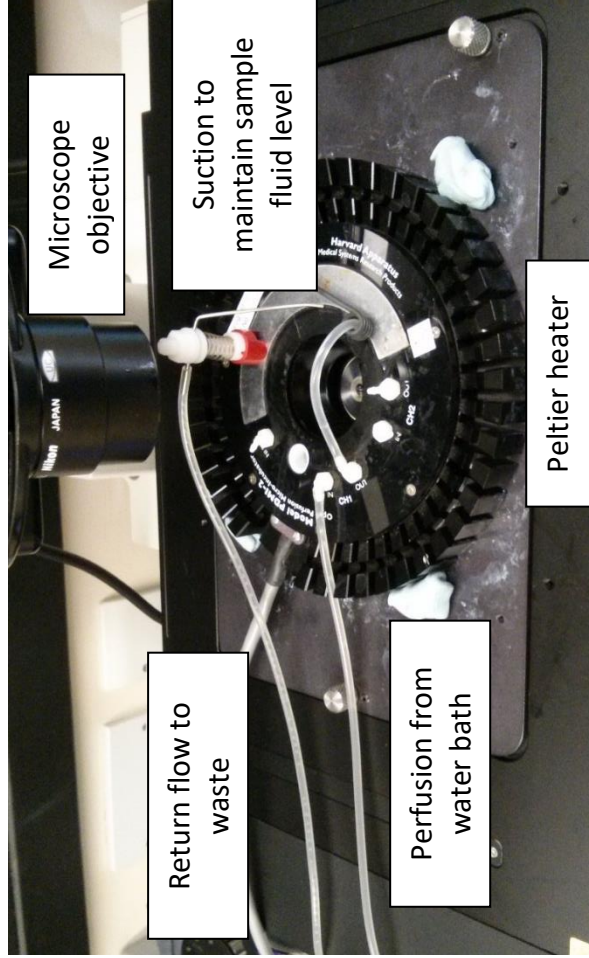
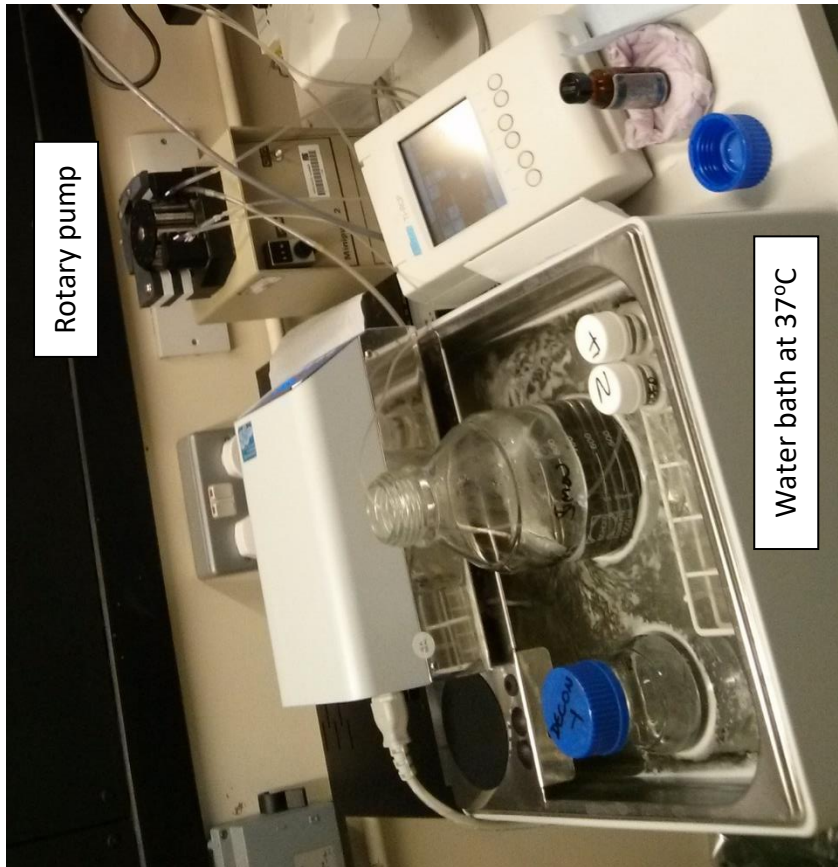


Figure 4.4.4 Pictures of the perfusion system used in confocal microscopy experiments

Having established a system by which to examine the cells, the next stage was to verify the CHO cells could be used within this system and remain viable during imaging. This was more challenging than with standard fluorimetry as visualisation of individual cells was needed to demonstrate an increased calcium response to N/OFQ binding to the modified CHO cell surface NOP receptors. A successful experiment would also validate the fluorimetry results.

4.5. Imaging $G_{\alpha i/q}$ CHO cells

The key processes for achieving successful dynamic images of the biosensor cells were: culture and seeding of cover slips for placement in the microscope, 48 hours of cell growth, loading of the cells with an appropriate calcium sensitive fluorophore, transfer of viable cells to the objective, and imaging during perfusion.

4.5.1. Culture and seeding

Stock chimeric CHO cells were cultured following standard cell culture protocols. The feed media was DMEM:F12 with 10% Foetal bovine serum (100 IU ml^{-1}), streptomycin ($100 \text{ } \mu\text{g ml}^{-1}$), fungizone ($2.5 \text{ } \mu\text{g ml}^{-1}$). Selection media comprised G418 (geneticin, $400 \text{ } \mu\text{g ml}^{-1}$) and Hygromycin B ($200 \text{ } \mu\text{g ml}^{-1}$).

Confocal experiments required that a stable, adherent population of CHO cells that could be perfused without displacing the cells from view. Seeding of the cells took place on coverslips, one for each well of a six-well plate. CHO cells by themselves are relatively adherent, and coverslips required no further preparation. Each well was seeded with $0.1 \times 10^6 \text{ ml}^{-1}$ cells taken from a stock culture, determined empirically to avoid over-confluence. The cells were then incubated at 37°C for 48 hr in feed media. Optimal confocal imaging was possible when CHO cells were not confluent.

4.5.2. Fluo-4

The calcium indicator Fluo-4 was used for confocal microscopy experiments. This indicator is particularly suited to confocal microscopy. First, it is a single-excitation indicator. Whilst this makes calibrated measurements of calcium changes more challenging and subject to error (see Fura-2), it is better suited to confocal microscopy systems that generally only stimulate at one wavelength. Second, it is stimulated in the visible light spectrum rather than the ultraviolet spectrum. The advantage of this over Fura-2 is that the lower energy of longer wavelength light is less damaging to cells, and also reduces photobleaching. Furthermore, cell autofluorescence is minimised compared with using ultraviolet excitation light. Third, Fluo-4 has a high affinity for calcium with minimal fluorescence at low levels and is more fluorescent at calcium saturation (more than a 100-fold increase in fluorescence). The AM ester form of Fluo-4 is also non-fluorescent – any esterified Fluo-4 that remains outside of the cell will not contribute to background fluorescence. Fluo-4 AM is also relatively easy to load, requiring half the time and half the concentration of the similar indicator Fluo-3. Finally, peak excitation of Fluo-4 (491 nm [Ca^{2+}] unbound – 494 nm [Ca^{2+}] bound) occurs very close to the wavelength of the argon laser (488 nm) used in the confocal microscopy. This is illustrated in Figure 4.5.1.

In a similar manner to Fura-2, the loading of Fluo-4 into cells is achieved using a cell-permeable acetoxymethyl (AM) ester derivative that is cleaved by intracellular esterases, thereby trapping the free Fluo-4 within the cell. Fluo-4 is reconstituted with dimethylsulfoxide (DMSO) due to its low water solubility. For the experiments, a 1 mM solution was prepared (50 μg Fluo-4 made up in 50 μl DMSO). 4 μl aliquots (final concentration 4 μM) were then used to load CHO cells for 30 min at room temperature in dark conditions.

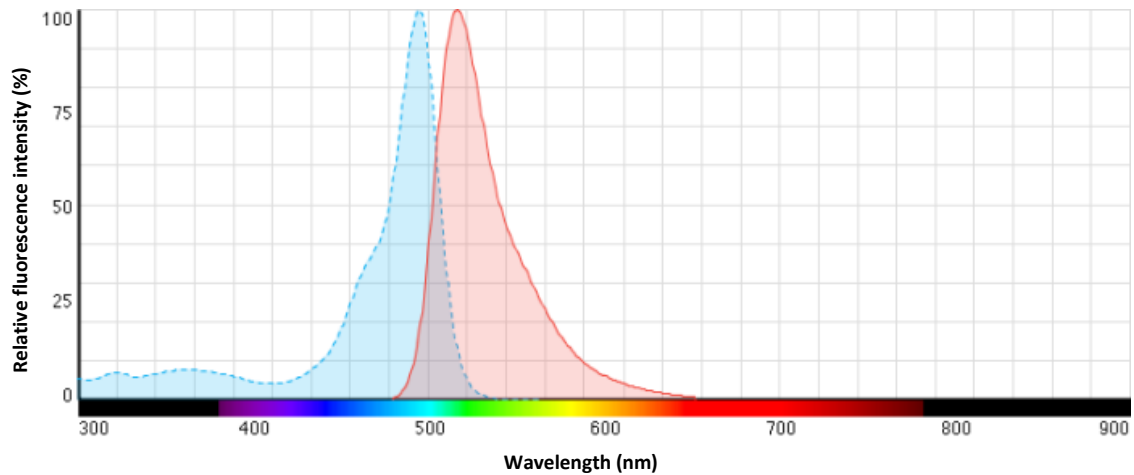


Figure 4.5.1 Fluorescence spectra of Fluo-4 showing excitation spectra (blue) and emission spectra (red) (adapted from ThermoFisher product catalogue).

The following procedure was used for preparing and loading cells for confocal microscopy:

1. Warm all experiment solutions in water-bath set at 40°C. Solutions warmed in this bath would approximate 37°C by the time they reached the stage of the microscope.
2. Take a single cover-slip and gently place into 2 ml Krebs-HEPES solution to wash off residual media. This can be done in an appropriately sized petri-dish (e.g. 35 x 10 mm).
3. Mix 4 µl pre-prepared Fluo-4 in 1 ml Krebs-HEPES solution (final concentration 4 µM) and add to a different petri-dish.
4. Transfer CHO coverslip to petri-dish containing Fluo-4.
5. Place in darkness at room temperature for 30 min. Optimal loading occurs at room temperature; at higher temperatures CHO cells extrude calcium indicators.
6. Use loading time to prepare confocal microscope and perfusion system, particularly testing for leaks.
7. Transfer loaded CHO cell coverslip to sample well, add 1 ml of Krebs-HEPES solution, and check for any leaks. Place onto stage within the warmed peltier heater and begin perfusion system using Krebs-HEPES solution.
8. Use 60x oil immersion lens (CFI Plan Apochromat VC 60x (numerical aperture=1.4)).

9. Focus sample using standard light. Check focus using laser but keep duration to a minimum to avoid photobleaching. Finally, confirm focus with scanning laser using supplied computer software and optimise to achieve desired focal plane.
10. Setup microscope with following adjustments:
 - a. Argon laser 488 nm
 - b. Excitation strength 10 – 11%
 - c. Adjust photodetector gain to achieve acceptable view with minimal noise
 - d. Set scanning speed as one scan per second or two seconds, depending on time course of planned experiment
 - e. Set emission pinhole to large
 - f. Set detector filter to FITC (fluorescein isothiocyanate). This filter selection will allow transmission of Fluo-4 fluorescence (516 nm) to the photodetector.
11. Perform series of experiments (see Chapter 5.2).

4.6. Adherence of PMNs with Cell-Tak™

The aim of this assay was to co-image CHO-biosensor cells and live PMNs, and by stimulating the PMNs, establish whether N/OAQ was released by measuring CHO-biosensor fluorescence. This required being able to image live, viable PMNs adherent to the coverslip during perfusion.

Coverslips were prepared so that they would adhere the PMNs. An adherent protein solution – Corning® BD Cell-Tak™ – was used to coat the coverslips prior to seeding with the CHO-biosensors. The adherent solution comprised polyphenolic proteins extracted from marine mussels that act as a tissue glue to coat such surfaces as glass, plastics and metals. The procedure for preparing coverslips for the CHO-PMN experiments was as follows (adapted from the protocol supplied with Cell-Tak™):

1. Prepare a buffer solution of 0.1M sodium bicarbonate with a pH of 8.0. Filter-sterilise before use.
2. Plan a coverage density of $3.5 \mu\text{g cm}^{-2}$ with Cell-Tak™.
3. Calculate mass of Cell-Tak™ required for a six well plate with total expected growth area of 9.6 cm^2 ; e.g. assuming stock of Cell-Taq is 2.1 mg ml^{-1} , take $16 \mu\text{l}$ ($33.6 \mu\text{g}$) and dilute to 3 ml with buffer solution. This allows 0.5 ml of solution per well.
4. Sterilise cover slips with ethanol or methanol. Ensure full evaporation of liquid before preparing with Cell-Tak™.
5. To each cover slip, add 0.5 ml of Cell-Tak™ solution as made above, ensuring full surface area coverage but avoiding spillage beyond edge of cover-slip.
6. Incubate at 37°C for 20 min.
7. Aspirate off any remaining solution, and wash with sterile water to remove residual bicarbonate.
8. These coverslips can be stored for two weeks at a temperature of $2-8^\circ\text{C}$

4.7. Imaging PMNs

PMNs cannot be cultured (do not divide), so fresh human PMNs were necessary for these experiments. Polymorphonuclear cells were isolated from whole human blood provided by volunteers with ethics approval. Isolation was performed using Blood Separation Protocol 2 (see Chapter 2.3.2), and all PMNs used on the day they were extracted. PMNs were diluted into 1 ml Krebs-HEPES solution and kept on ice.

Loading of PMNs was with Fluo-4. A Cell-Tak™ prepared coverslip was placed in a petri-dish and 1 ml of warmed Krebs-HEPES added. To this $4 \mu\text{l}$ of 1 mM Fluo-4 was added (final concentration $4 \mu\text{M}$). $100 \mu\text{l}$ of PMN suspension was then added to this coverslip and left at room temperature in darkness for 10 min.

Cells were transferred to a sample well, 1 ml of Krebs-HEPES added, and the well checked for leaks. The well was then placed onto the confocal microscope stage within the peltier heater. Visible light microscopy was performed to focus cells, then the perfusion system started. Focus was again checked using the laser light source, and a suitable area for study identified. Finally, focus was confirmed with scanning laser using C1Si software to view images. Studies of PMN responses to fMLP stimuli were then performed as described in Chapter 5.3.

4.8. Co-imaging of PMNs and CHO cells

Imaging of both PMNs and CHO cells required a non-confluent layer of CHO cells, and a layer of PMNs with minimal clumping and relatively even distribution amongst CHO cells. CHO cells were prepared as previously described except for these experiments they were seeded onto Cell-Tak™ prepared coverslips.

The calcium indicator Fluo-4 was used to load CHO cells as previously described. The loading time was 20 min before the CHO cell coverslip was transferred to the confocal microscope and 1 ml Krebs-HEPES solution added. At this point the perfusion system was not turned on. PMNs were then layered on the CHO cell coverslip. An initial volume of 100 μ l was added initially, but if too few PMNs were visible this volume was doubled for further experiments. Conversely, if the initial sample showed too many cells obscuring the CHO cells, the sample was diluted before adding 100 μ l of the diluted sample to CHO cells. A further 10 min was then allowed for loading of PMNs by residual Fluo-4. Whilst this would provide a lower concentration of Fluo-4 for PMN-loading, layering and loading the PMNs with the CHO cells prior to transferring to the microscope would have risked displacing PMNs during the transfer process. After this period, the cells were visualised as previously described and perfusion started. Laser microscopy was then used to identify an area of interest, i.e. one where there was a relatively even distribution of CHO cells and PMNs. The scanning laser was then used to finally focus the cells using the C1Si software for image viewing.

4.9. Assay development

The next chapter describes a series of experiments designed to establish whether CHO cells would work as effective biosensors. It then proceeds to detail experiments establishing CHO cell responsiveness to exogenous N/OFQ within the confocal microscope system. The development of the assay then continues with imaging of PMNs and stimulation by fMLP, followed by imaging of both CHO cells and PMNs and the effects of PMN degranulation. A final set of experiments were performed using the supernatants of fMLP-stimulated PMNs to stimulate CHO cells in the presence or absence of NOP and purinergic antagonists (TRAP-101 and PPADS).

5. Results of live cell imaging

This chapter contains a series of experiments conducted to develop a novel live-cell assay for detecting the release of N/OFQ from human granulocytes.

5.1. Fluorimetry

Question: Are chimeric $G\alpha_{i/q}$ CHO cells responsive to exogenous N/OFQ?

Assessment of CHO-biosensor responsiveness was made using fluorimetry, as described in Methods (Chapter 4.3). Using the ratiometric intracellular $[Ca^{2+}]_i$ indicator Fura-2, experiments were performed using 5 different passages of cells to test the responsiveness of the CHO $G\alpha_{i/q}$ cells. Fluorescence was measured at 510 nm after stimulation at 340 nm ($[Ca^{2+}]_i$ -bound) and 380 nm ($[Ca^{2+}]_i$ -free). Each experiment underwent calibration steps as described in Chapter 4.3. $[Ca^{2+}]_i$ levels were calculated by FDLM software using the Grynkiewicz equation. Maximum response was analysed using GraphPad Prism 6. For each experimental run, any baseline drift was returned to zero using linear regression across the period of drift to the inflection point. Figure 5.1.1 represents the baseline-corrected response of CHO $G\alpha_{i/q}$ cells at tested concentrations of N/OFQ (10^{-6} M, 10^{-7} M, and 10^{-8} M), with graph D representing baseline-correction methodology. Values are given as a change in $[Ca^{2+}]_i$ from a corrected baseline of 0 nM.

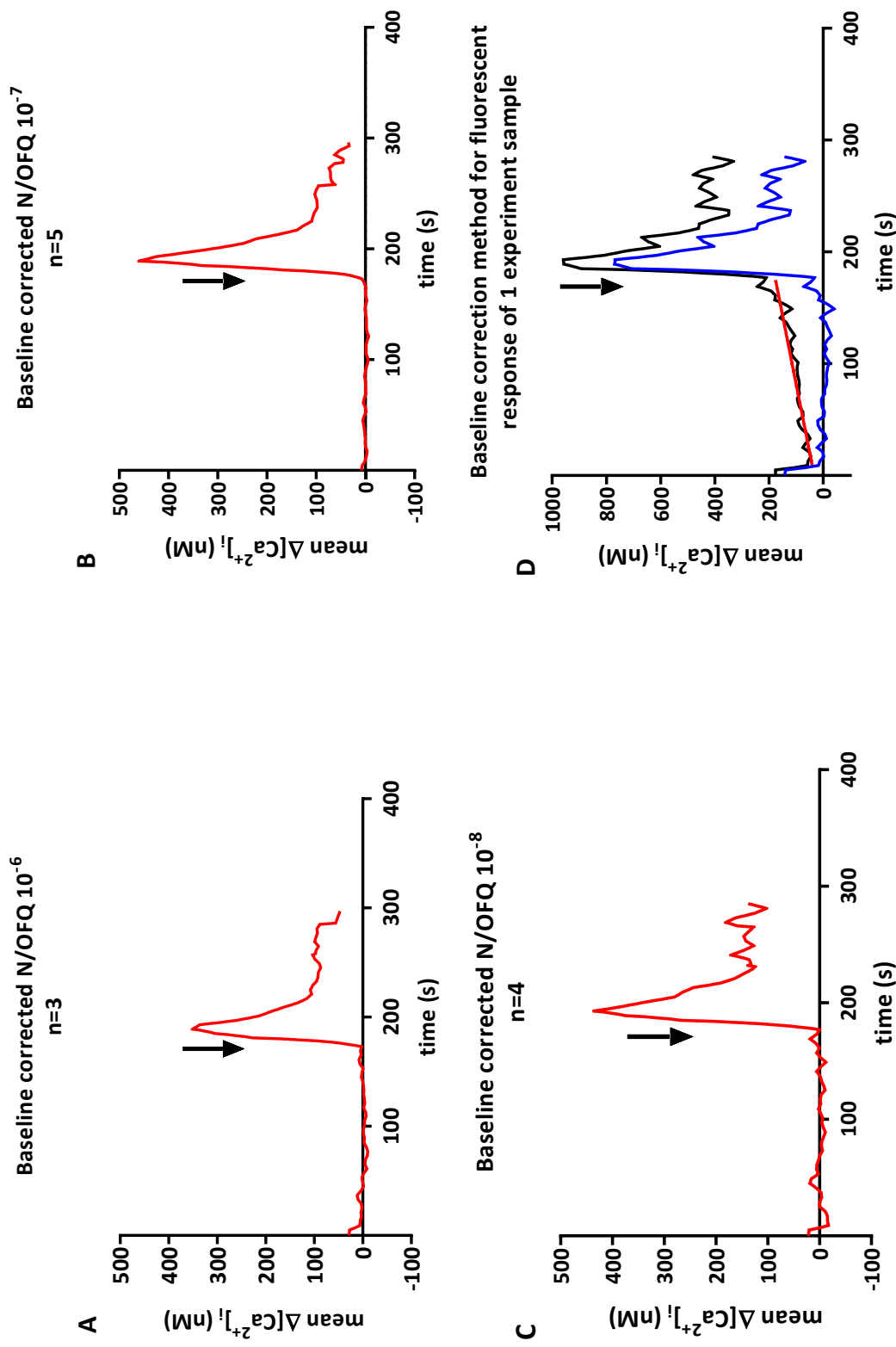


Figure 5.1.1.1 Mean change in $[Ca^{2+}]_i$ of CHO $G\alpha_{i4}$ cells measured by fluorimetry for stimulation with 10^{-6} , 10^{-7} , and 10^{-8} M N/OFQ (graphs A, B and C). n = represents number of experiments at each concentration. Arrow marks addition of N/OFQ. Graph D demonstrates base-line correction methodology, with the linear regression line in red and the new baseline-corrected graph in blue.

These first experiments were designed to establish whether proposed CHO-biosensor cells would increase calcium in response to agonist binding to the surface NOP receptor. Cuvette fluorimetry provided a straight-forward technique for testing these cells and ensuring that they could theoretically function as useable biosensors. These data demonstrate that the chimeric CHO $\alpha_{i/q}$ cells are reactive to the application of exogenous N/OFQ, and therefore suitable as a biosensor. There was considerable baseline drift in some of the experiments, which likely represents the leakage of Fura-2 out of the CHO cell via active mechanisms. This is particularly evident when cells are in suspension, exacerbated by any extracellular calcium that will saturate leaked indicator. Linear regression enabled the return of the baseline to zero, but is a mathematical process that necessarily attenuates peak values. The addition of probenecid (an organic anion transport inhibitor, 2.5 mM) can minimise leakage, but can also attenuate peak responses following agonist binding.

There was poor relationship between changes in $[Ca^{2+}]_i$ concentrations and concentrations of N/OFQ (see Table 5.1.1). Whilst the range of tested concentrations was limited, there are issues with using cuvette-based fluorimetry in assessing CHO cell fluorescence in a moving suspension. Problems include incomplete de-esterification, insufficient loading, autofluorescence, ultraviolet radiation damage to cells and Fura-2 leakage into calcium-rich fluid, in addition to it being a hostile environment for CHO cells.

Experiment	N/OFQ concentration (M)		
	10^{-6}	10^{-7}	10^{-8}
A	373	292	120
B		437	770
C		632	658
D	511	553	
E	245	570	236

Table 5.1.1 Summary of fluorimetry experiments for determining CHO $\alpha_{i/q}$ response to concentrations of N/OFQ. Table values represent peak $\Delta[Ca^{2+}]_i$ (nM) determined by fluorimetry.

The next phase of experiments was to explore the use of the CHO-biosensors in confocal microscopy. Cuvette fluorimetry is a comparatively crude technique as it is only able to measure total fluorescence from the sample. This means that if only some cells react to a low concentration of N/OAQ, the total fluorescence may not peak above baseline. Cell viability is also difficult to assess with cuvette fluorimetry, whereas microscopy allows specific regions to be identified where cells appear adequately loaded with calcium indicator and have maintained morphology. It also allows for repeated testing of cells which can be used to assess any apparent receptor desensitisation. Cuvette fluorimetry would also not satisfy the overall aim of observing cell-to-cell interactions between human polymorphonuclear cells and CHO-biosensors.

5.2. CHO cells as biosensors in confocal microscopy

Question: Can CHO $\alpha_{i/q}$ cells be used as a N/OAQ-responsive biosensor in confocal microscopy?

The next series of experiments focused on whether CHO $\alpha_{i/q}$ cells would function as an effective biosensor in a confocal microscope setup. For these experiments CHO-biosensors were prepared as described in Chapter 4.5.1. After 48 hours, the CHO cells were prepared for confocal microscopy, loading with Fluo-4 as described in Chapter 4.5.2. Experiments were performed across four passages of CHO $\alpha_{i/q}$ cells. For each experiment, the cells were perfused with Krebs-HEPES buffer solution and 10^{-6} M N/OAQ introduced into the perfusion system. Confocal imaging was performed as previously described in Chapter 4.5.2.

A total of 173 cells were imaged across these experiments. Data files from the Nikon C1Si software were exported (.ids image files and .ics text metadata files), and analysed using the Fiji distribution of ImageJ (an open-source image processing package widely used in analysing fluorescent microscopy images).¹⁰³ Initial analysis considered global change in fluorescence: the whole visual field was selected as a region of interest (ROI)

and mean fluorescence over time measured. These data are shown in Table 5.2.1. Subsequently, individual cells were identified manually and a ROI within the cytoplasm of each CHO cell selected. Mean fluorescence was then measured from each ROI over time.

Measurements of global fluorescence were exported from Fiji into GraphPad Prism v6. As with fluorimetry experiments, baseline drift was corrected using linear regression. Graphs of fluorescence over time were generated and included with images demonstrating cell fluorescence before and after addition of N/OEQ, shown in Figure 5.2.1 and Figure 5.2.2.

Experiment	Global change in mean fluorescence (baseline corrected, arbitrary units)	CHO respond	CHO not responding	Total cells in view
A	392.5	99	0	99
B	266.6	23	1	24
C	1782	23	1	24
D	14.23	5	21	26

Table 5.2.1 Results of four passages of CHO $\alpha_{i/q}$ cells stimulated with 10^{-6} M N/OEQ. In experiment D fewer biosensors responded compared with non-responders, resulting in a reduced global change in fluorescence. This illustrates the value of confocal microscopy in identifying variable responses within a cell population.

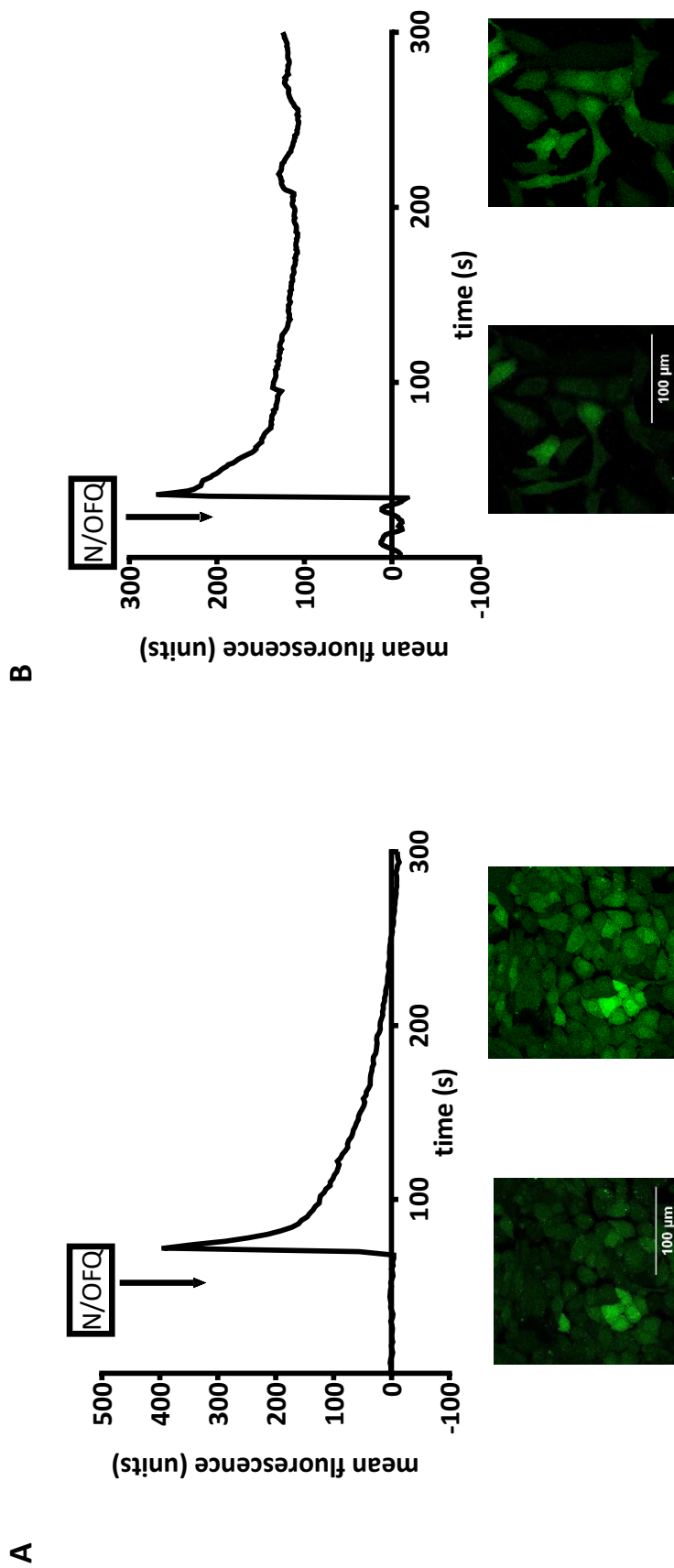


Figure 5.2.1 Mean global fluorescence of CHO $\alpha_{v/4}$ cells before and after addition of N/OFQ 10^{-6} M. The images are representative of the increase in fluorescence that was subsequently measured to produce the associated graphs.

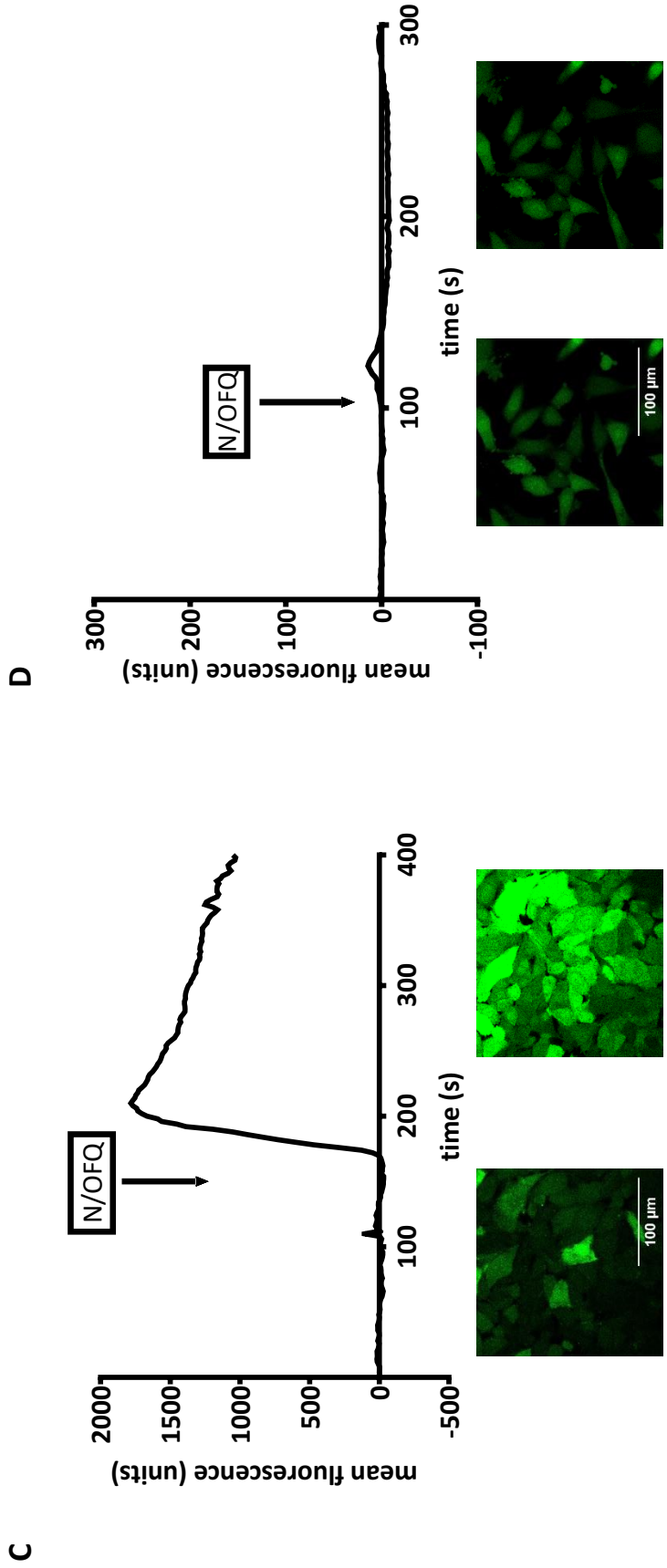


Figure 5.2.2 Mean global fluorescence of CHO $\alpha_{1/q}$ cells before and after addition of N/OFQ 10^{-6} M. In (C) fluorescence saturated the photodetector, suggesting that these cells were either better loaded with Fluo-4, or that they were more responsive (possibly due to increased expression of NOP receptors). In (D) there was a minimal measurable or visible increase in fluorescence, as can be seen in the associated images.

Identification of individual responding cells based on measured changes in fluorescence was performed using the Area Under Curve (AUC) function within GraphPad Prism. This function identifies peaks based on deviation from a baseline value. GraphPad calculates the area under the curve between adjacent points on the x-axis by forming a trapezoid and converting it into a rectangle with the same area as the trapezoid (see Figure 5.2.3). The area under the curve between the two x-values is therefore the difference in x (Δx) multiplied by $(y_1 + y_2)/2$.

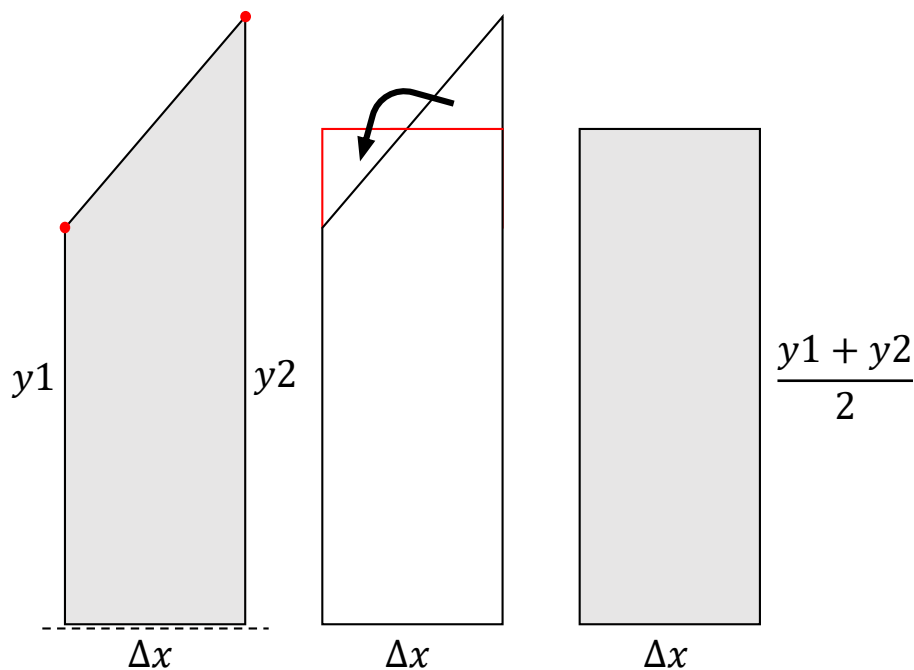


Figure 5.2.3 Calculation of area under the curve by GraphPad Prism for identifying peaks in CHO-cell fluorescence over time (adapted from GraphPad Statistics Guide)

These calculations are then replicated for the rest of the curve. Peaks are determined by a positive deflection from a set baseline that are greater than a set threshold from the minimum y value of the baseline. In these experiments the baseline was determined as an average of fluorescence values over the time period prior to stimulation with N/OFQ (in non-responders the earliest time point of inflection taken from responding cells). The deflection threshold was set at 50% deflection from baseline as the threshold for a positive response. All peaks identified by AUC analysis were visually checked against a graph of fluorescence for each cell, and further against the images from the confocal microscope where there was doubt. The table in Figure 5.2.4 is an example of the output from AUC analysis. The values of interest are the time when a peak occurs

(first x) and the height of that peak (peak y – baseline). Below the table is the graph from which the AUC output is determined.

The figure also demonstrates the limitations of AUC analysis. The first point is that peaks in fluorescence occurring prior to N/OFQ administration can lead to genuine N/OFQ stimulated peaks being missed if relying on AUC analysis alone. The blue line on the graph represents CHO cell P from one set of experiments. There is a small peak at x = 28 preceding the N/OFQ-stimulated peak at x = 35. Because the baseline was taken as an average over the first 30 s, peaks in this range increase the baseline value calculated by the AUC analysis. In this case, setting the deflection threshold at 60% rather than 50% of an increase from baseline would have resulted in omission of this positive result. The second point is that a steep decrease in baseline fluorescence can lead to a similar omission of genuine N/OFQ-stimulated peaks. In this example, cell D at x = 0 has a fluorescence value of 1243 units. It then steeply decreases to 791 units prior to N/OFQ-stimulation, when peak fluorescence reaches 1690 units. The decreasing baseline is probably due to Fluo-4 leak which has the double effect of decreasing cell fluorescence whilst increasing background fluorescence as the Fluo-4 interacts with free calcium in the Krebs-HEPES perfusate. Again, changing the deflection threshold to 60% would have led to omission of this genuine N/OFQ-stimulated peak. Therefore, whilst AUC analysis was a useful tool for quickly identifying peaks in fluorescence, its specificity is significantly affected by the threshold value and the stability of the baseline. This necessitated manually checking each cell against its individual graph and confocal images.

AUC		A	B	C
		cell D	cell M	cell P
		Y	Y	Y
1	Baseline	1121	638.7	838.9
2	Total Area	24475	38603	12016
3	Total Peak Area	6382	36555	4612
4	Number of Peaks	1.000	1.000	1.000
5				
6	Peak 1			
7	First X=	34.34	34.08	34.46
8	Last X=	55.50	100.0	60.04
9	Peak X=	35.00	36.00	36.00
10	Peak Y=	1690	1622	1203
11	Peak Y - Baseline =	568.9	983.1	364.3
12	Area=	6382	36555	4612
13	%Area=	100.0	100.0	100.0

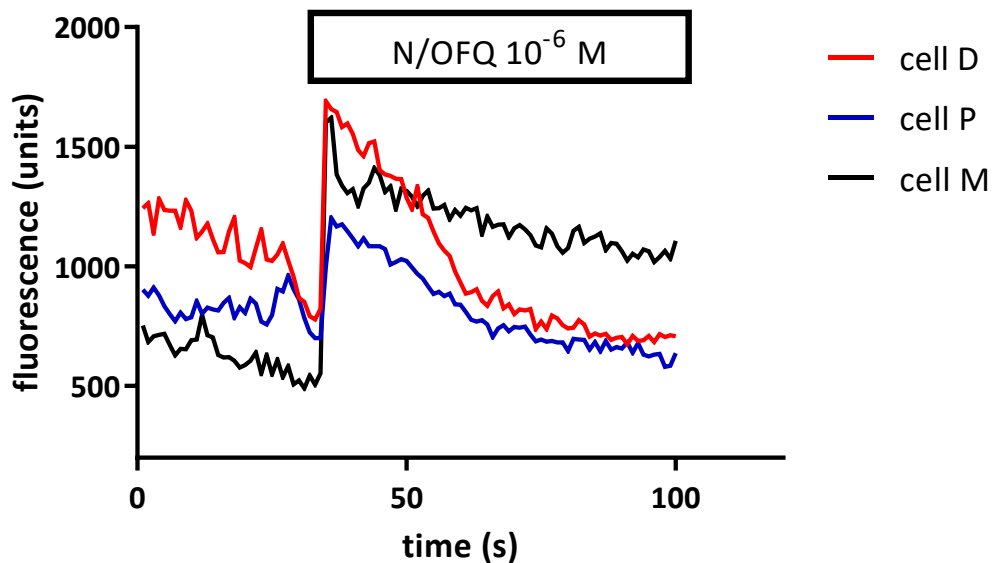


Figure 5.2.4 AUC analysis: The top table is a typical output for AUC analysis, with peaks identified based on their difference (>50% used here) from an averaged baseline up to N/OFQ administration. This is graphically represented with mean fluorescence values for each cell over time, before and after N/OFQ administration. CHO Cell M represents a response that is readily detected by AUC analysis. CHO Cell P demonstrates a positive N/OFQ response that would not have been detected had the AUC analysis threshold been changed from 50% to 60% from baseline. This is due to the small peak prior to the N/OFQ-associated peak raising the baseline (the average of fluorescence values during the first 30 s). Similarly, the CHO cell D response would have been missed due to a rapidly decreasing baseline that is not entirely corrected by averaging over 30 s. These examples demonstrate the limitations of using AUC analysis when the baseline is variable.

These data demonstrate that the CHO $\alpha_{i/q}$ cells can be used in confocal microscopy for the detection of N/OFQ. The cells successfully load with Fluo-4, generally remain viable, and increases in calcium are readily visualised using laser scanning confocal microscopy. The assay, however, is not without issues. First, the response of CHO cells to similar concentrations of N/OFQ is variable. Peak global fluorescence (baseline-corrected) in experiment C was 1782 units, more than four times greater than the next highest peak fluorescence (experiment A). Furthermore, experiment D demonstrated that the CHO cells were almost entirely unresponsive to N/OFQ despite apparently normal morphology and loading of Fluo-4. Possible reasons for this difference include small variations in Fluo-4 loading conditions, increased skill in transferring the cells to the confocal system, or small differences in their culture and preparation. However, it is also likely that the NOP receptor is not uniformly expressed between cells, and that there may be differences between cell batches in the efficacy of transfection to generate chimeric signalling.

This variability in response led to the modifications to planned experiments. First, calibration of Fluo-4 against calcium concentrations was not performed. There are many factors that are hard to control within this experimental assay (e.g. biosensor reactivity, transferring cells to the confocal system, loading of Fluo-4, cell viability, perfusion uniformity, N/OFQ distribution). Further, there are significant technical challenges in using ratiometric indicators in confocal microscopy (Fura-2, Indo-1). For example, available ratiometric fluorophores are excited in the non-visible ultraviolet region of light. The use of ultraviolet light incurs expense and complexity in confocal microscopy design, and such a system with perfusion capability was not available. Second, it was not possible to correlate biosensor fluorescence intensity with N/OFQ concentration. Originally it had been hoped that confocal microscopy would allow estimates of PMN-secreted N/OFQ peptide concentration. However, the variable response to 10^{-6} M N/OFQ suggested that it would be difficult to justify associated intensity of CHO-biosensor response to N/OFQ concentrations. Therefore, assay development proceeded using CHO $\alpha_{i/q}$ cells as binary biosensors; that is, they would be used to detect the presence of N/OFQ, not the quantity.

The next step in assay development was determining whether viable and active human PMNs could be isolated and visualised in the confocal microscope system. This would then lead to imaging both PMNs and CHO-biosensors simultaneously.

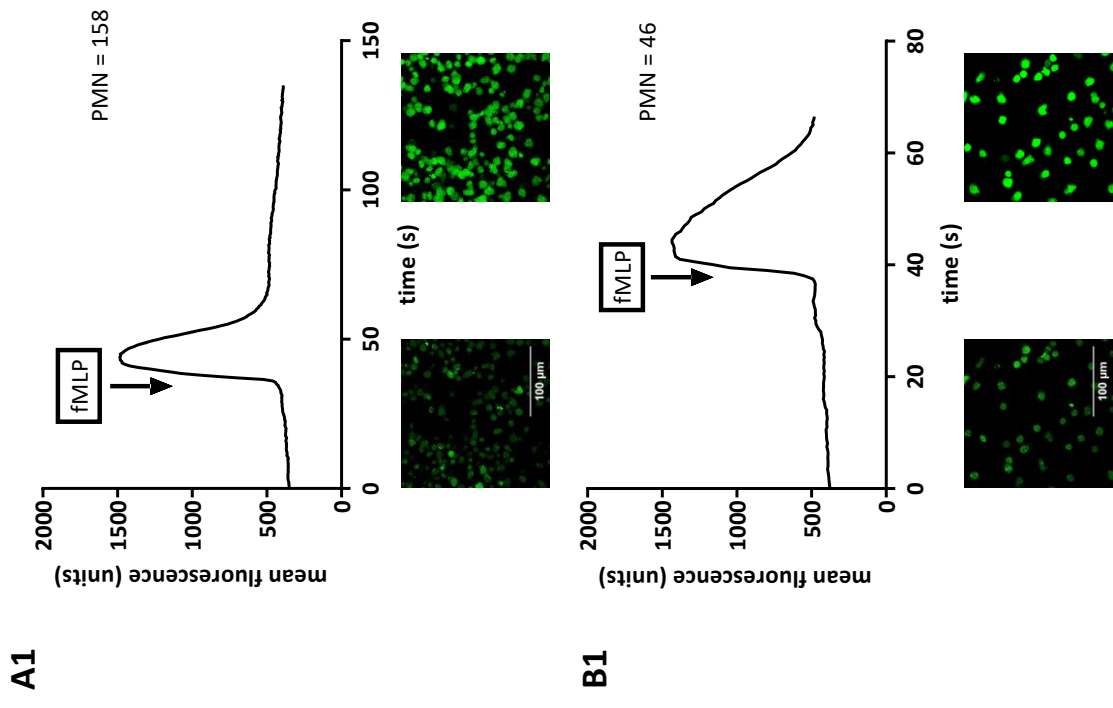
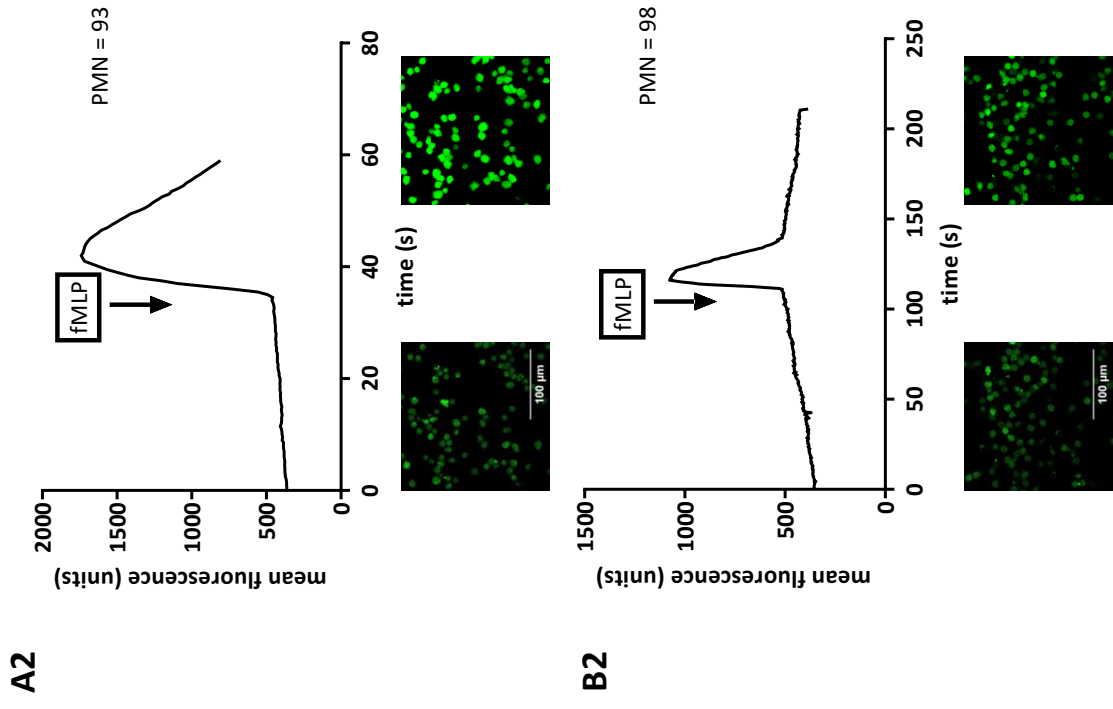
5.3. Confocal imaging of polymorphonuclear cells

The main challenges in imaging PMNs were first acquiring PMNs that were viable and would respond to exogenous stimulation, and second could remain fixed on the coverslip during perfusion. Unlike CHO cells, PMNs do not grow; they are terminally differentiated cells. They are also very easily activated (undergoing oxidative burst and degranulation) and whilst can be stored on ice, should be used as soon as possible after isolation. They also do not naturally adhere to glass so require preparation of glass coverslips before use.

For the following experiments blood was acquired from healthy volunteers with University of Leicester ethics approval. Cells were isolated using Polymorphprep™ according to Blood separation protocol 2 with additional red cell lysis (see Chapter 2.3.2 and 2.3.3). Coverslips were prepared ahead of time using BD Cell-Tak™ (see Chapter 4.6). Once acquired and isolated, human PMNs were kept on ice in the presence of Krebs-HEPES solution and used the same day in all experiments. PMNs were placed on coverslips, loaded with Fluo-4 and imaged as described in Chapter 4.7.

PMNs were stimulated with fMLP. This is a potent activator of PMNs acting via formyl peptide receptors to increase intracellular calcium via phospholipase C (PLC).¹⁰⁴ A total of 9 experiments were performed using PMNs from 5 different volunteers. This represents 1116 cells. Fluorescence was measured over time for a ROI within each cell. These data were then exported into GraphPad Prism to generate an overall average fluorescence for all the cells over time for each experiment, as shown in Figure 5.3.1.

These experiments demonstrate that PMNs can be isolated, fixed in place and visually shown to increase intracellular calcium in response to fMLP. This suggests that PMNs are activated and degranulate as expected. Importantly these data demonstrate that the majority of isolated PMNs are viable.



121 Figure 5.3.1

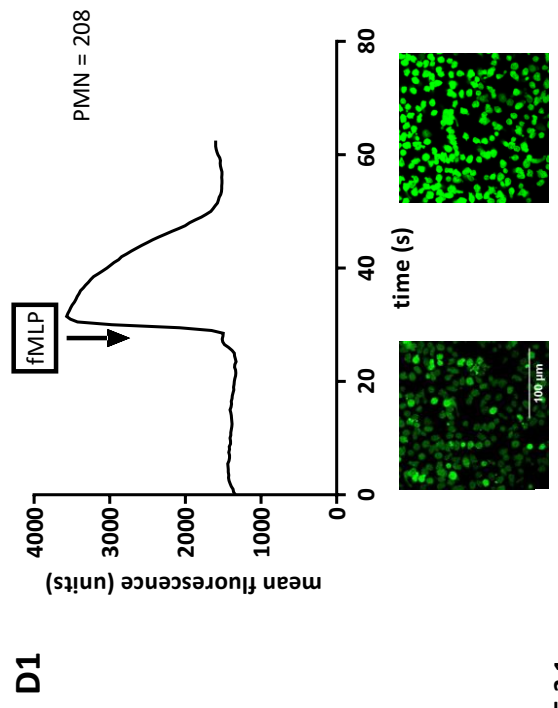
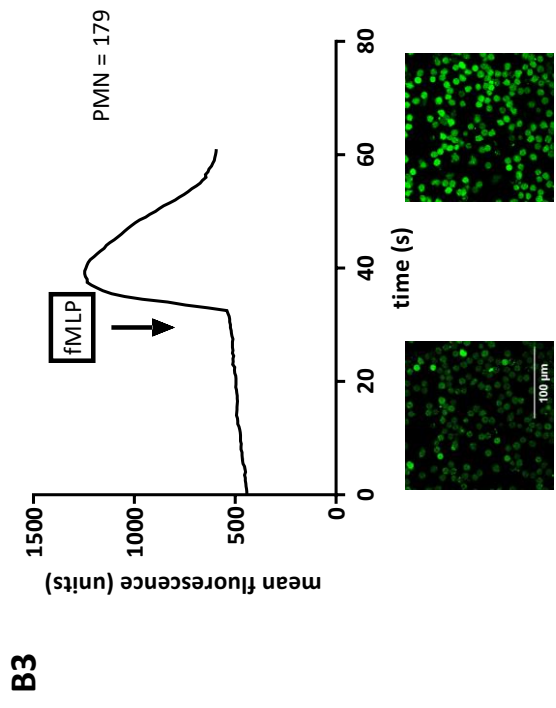
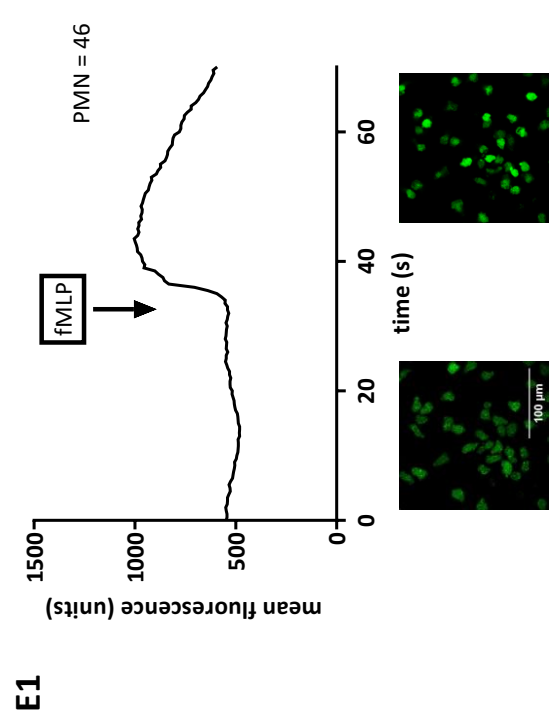
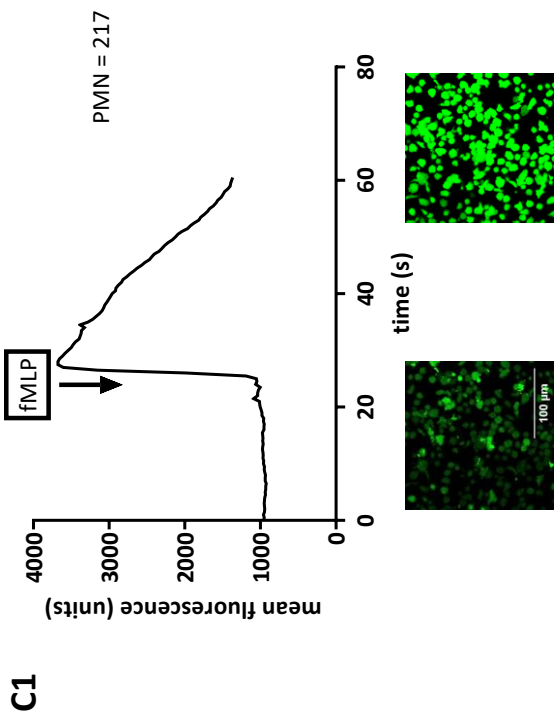


Figure 5.3.1

E2

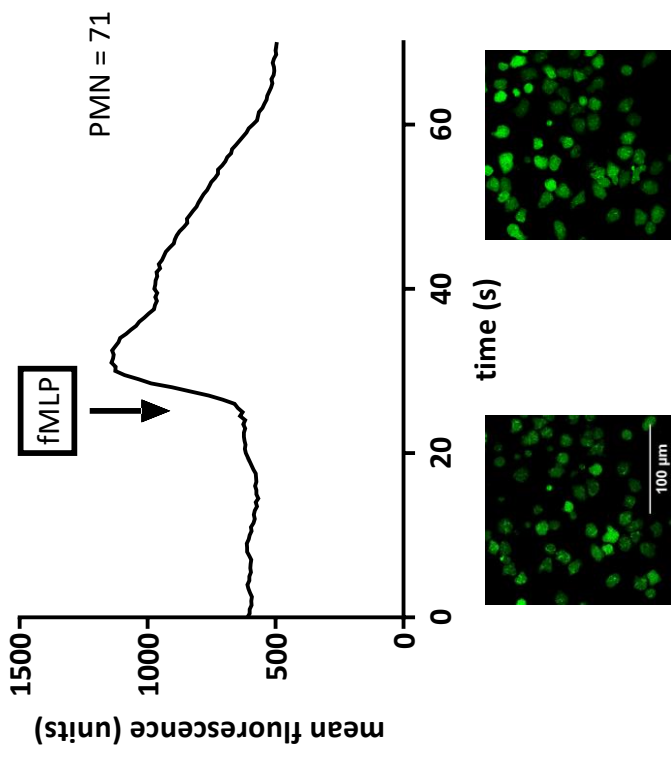


Figure 5.3.1 Graphs of fluorescence with associated images for 9 experiments stimulating PMNs with fMLP. The letter of the label corresponds to the volunteer blood sample, the number to the experiment. Overall there is marked increase in fluorescence associated with fMLP administration. Experiments E1 and E2 demonstrate an atypical response and likely reflect reduced PMN viability.

One concern with these experiments was the observation of unstimulated fluorescence of PMNs. This may represent autofluorescence in response to laser stimulation but could also represent spontaneous degranulation. Another important issue was that whilst the PMNs remained static during perfusion, after stimulation with fMLP they would frequently change in morphology or migrate across the field of view. This made measuring fluorescence over time challenging; because fluorescence was measured from a static ROI, the PMNs would sometimes move outside this ROI, resulting in abnormal measured fluorescence values. A final issue was a consequence of the very thin focal planes achieved with confocal microscopy. Cells above or below would migrate into the focal plane following fMLP stimulation; again, this is difficult to measure using static ROIs. These issues made identifying responding and non-responding PMNs more difficult, and frequently where an AUC or nonlinear regression analysis had identified a potential non-responder, it could be seen that in fact a cell's change in morphology or location had led to an inaccurate measurement of fluorescence.

Accepting these limitations, the next phase of assay development was co-imaging of PMNs and CHO-biosensors. The PMNs would then be stimulated with fMLP and observations made of PMN degranulation and subsequent CHO-biosensor fluorescence, indicating N/OFQ binding to $G\alpha_{i/q}$ NOP receptors. Whilst measurements of fluorescence would be challenging, it was hoped that images of PMNs interacting with CHO-biosensors would provide valuable information regarding the release of N/OFQ from human immunocytes.

5.4. Confocal imaging of PMNs and CHO $\alpha_{i/q}$ cells

Question: Do fMLP-stimulated PMNs induce an increase in intracellular calcium in CHO $\alpha_{i/q}$ cells?

The aim of the following experiments was to co-image PMNs and CHO-biosensors, and observe the putative release of N/OFQ from the PMNs. In these experiments CHO-biosensors were seeded on Cell-TakTM treated coverslips and allowed 48 hours for cell growth, as described in Chapter 4.8. Blood was acquired from healthy human volunteers as isolated PMNs as per Blood Protocol 2 (Chapter 2.3.2). CHO cells and subsequently PMNs were loaded with Fluo-4 following the protocol in Chapter 4.8. The confocal perfusion system was as previously described, with Krebs-HEPES buffer as the perfusate. PMN stimulation was with fMLP 10^{-6} M, and N/OFQ 10^{-6} M was also used to confirm CHO-biosensor responsiveness following fMLP administration.

A total of 21 experiments were performed. Confocal images were exported from the Nikon C1Si microscope and mean fluorescence over time for ROI within cell cytoplasm was measured using Fiji software. Data were analysed in Graphpad Prism v6, grouping fluorescence data for CHO cells and PMNs. As previously, AUC analysis was used to identify CHO-biosensors that appeared to fluoresce at a similar time-point to the PMN response to fMLP. Verification of AUC analysis was performed by looking at a graph of the data as well as reviewing the original confocal images. Given the known variability of CHO-biosensor responsiveness to N/OFQ, an estimation was made of whether administering 10^{-6} M N/OFQ induced an absent, weak, moderate, or strong fluorescence response in the CHO-biosensors.

Table 5.4.1 is a data summary. PMNs reliably responded to fMLP with those fluorescing being counted. Experiments occurring on the same day are given the same letter. The PMN count is important because as the experiments progressed it was observed that a

higher ratio of PMNs to CHO cells appeared to increase the likelihood of a CHO response. This is demonstrated in Figure 5.4.1.

Experiment	PMNs responding to fMLP	CHO $\alpha_{i/q}$ responders after fMLP	CHO $\alpha_{i/q}$ non-responders after fMLP	Exogenous N/OFQ response: cells responding (% of total)
A1	19	0 (0%)	16 (100%)	weak: 3 (19%)
A2*	48	0 (0%)	20 (100%)	absent: 0 (0%)
B1	22	5 (8%)	61 (92%)	strong: 65 (98%)
B2	13	11 (16%)	56 (84%)	moderate: 65 (97%)
C1	11	2 (2%)	121 (98%)	strong: 123 (100%)
C2	143	10 (19%)	42 (81%)	moderate: 52 (100%)
C3	19	4 (5%)	80 (95%)	moderate: 81 (96%)
C4	6	22 (29%)	54 (71%)	moderate: 49 (64%)
C5	51	21 (55%)	17 (45%)	weak: 30 (79%)
D1	4	7 (8%)	80 (92%)	strong: 87 (100%)
D2	74	6 (21%)	23 (79%)	moderate: 26 (90%)
D3	41	2 (3%)	64 (97%)	weak: 63 (95%)
E1	62	2 (4%)	44 (96%)	moderate: 46 (100%)
E2	22	1 (4%)	23 (96%)	moderate: 24 (100%)
E3	65	1 (6%)	17 (94%)	moderate: 19 (100%)
E4	55	12 (28%)	31 (72%)	moderate: 40 (93%)
F	80	0 (0%)	5 (100%)	not tested
G1	74	3 (27%)	8 (73%)	not tested
G2	71	6 (38%)	10 (63%)	weak: 6 (38%)
H1	163	4 (10%)	36 (90%)	not tested
H2	140	11 (46%)	13 (54%)	strong: 24 (100%)
TOTAL	1183	130 (14%)	821 (86%)	802 (84%)

Table 5.4.1 Co-imaging results: Summary of data from co-imaging PMNs and CHO-biosensors, and stimulating with fMLP. All experiments demonstrated a CHO-biosensor fluorescent response to exogenous N/OFQ (where tested) except A2*; these cells were probably unviable.

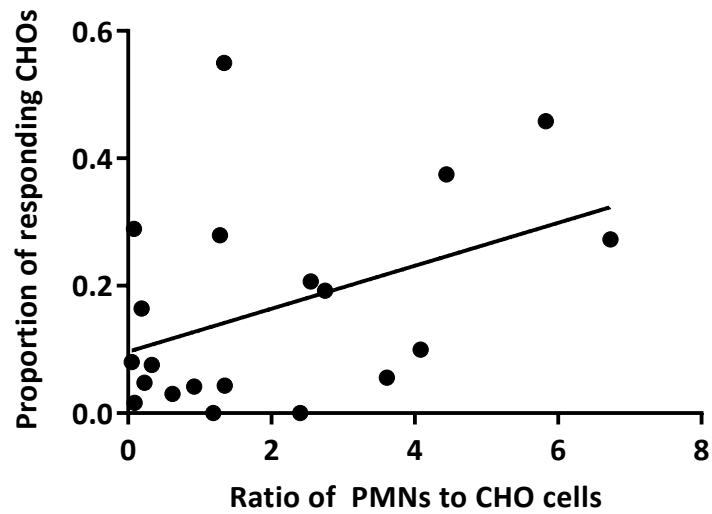


Figure 5.4.1 Graph demonstrating a loose relationship between the ratio of PMNs to CHOs and the proportion of CHOs that fluoresce following fMLP (R^2 0.18, one outlier removed).

The tabulated data suggest that CHO-biosensor stimulation occurs relatively infrequently when PMNs are stimulated by fMLP. However, when considered with images and graphs of fluorescence, it is possible to see that PMN-CHO interactions do occur at time-points consistent with PMN N/OFQ release. Figure 5.4.2 illustrates a field of view of a typical experiment with a region of PMN-CHO interaction highlighted across a sequence of images. Figure 5.4.3, Figure 5.4.4 and Figure 5.4.5 are examples of observed PMN-CHO biosensor interactions during confocal microscopy with associated graphs of fluorescence. These images are taken from regions within the field of view acquired during scanning microscopy, similar to Figure 5.4.2.

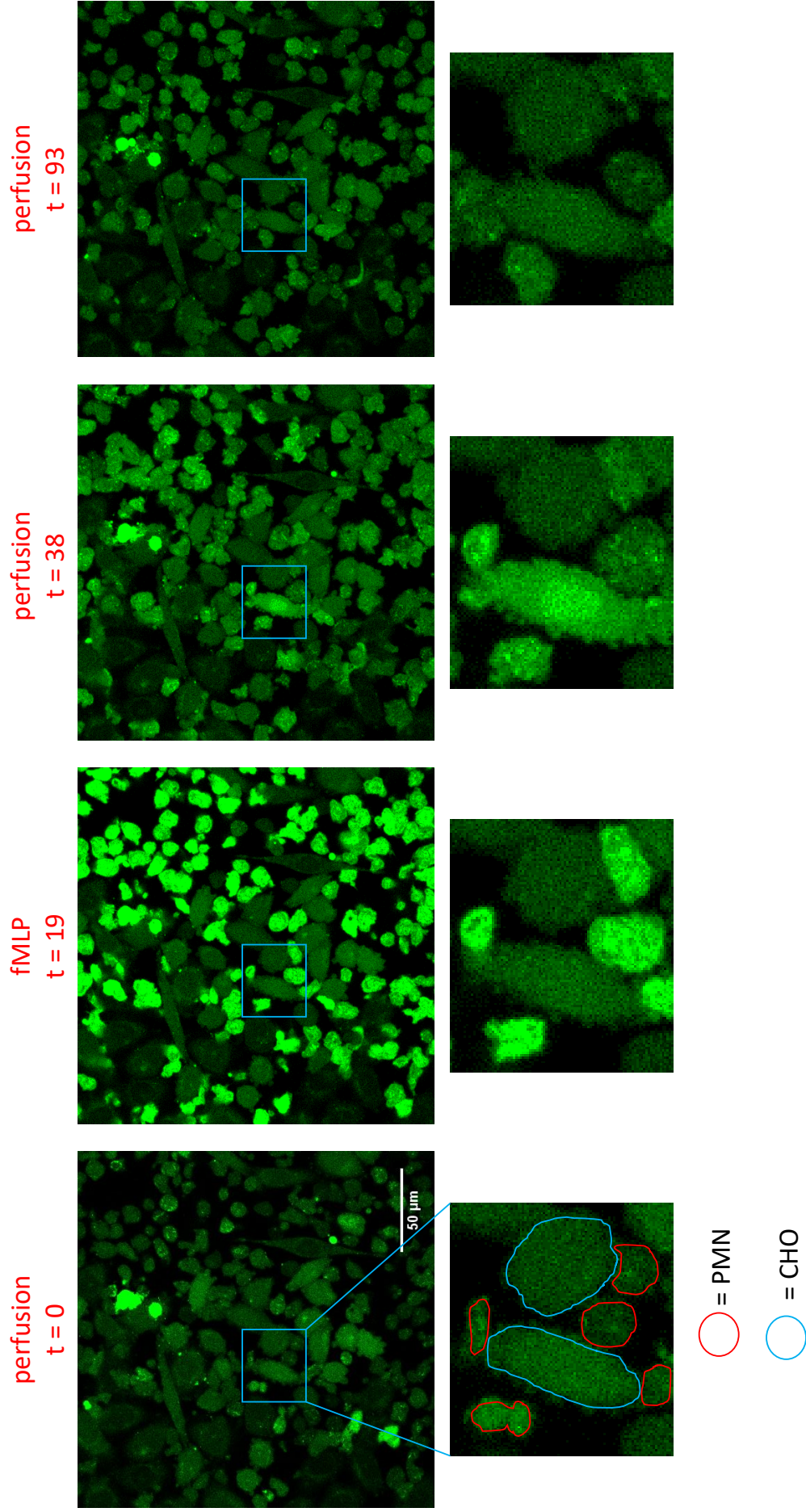


Figure 5.4.2 Sequence of images from a typical experiment co-imaging CHO-biosensors and PMNs. The administration of fMLP generates a universal large fluorescent response in PMNs indicating activation. A CHO cell is then seen as showing maximal fluorescence at 38 s (onset of fluorescence at 31 s), followed by restoration to baseline by end of the experiment.

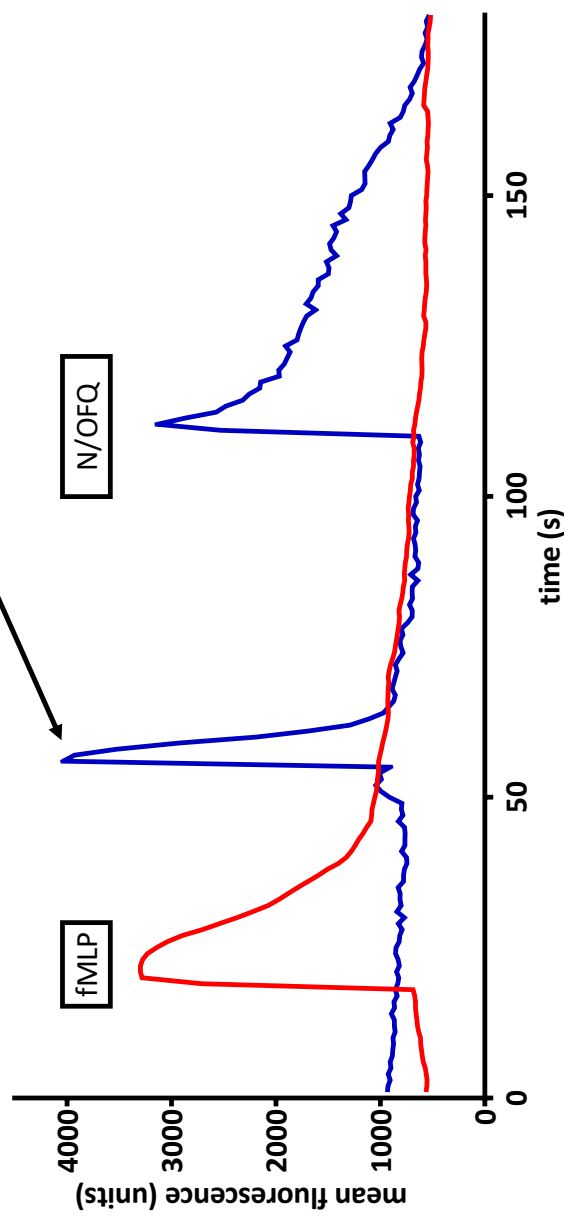
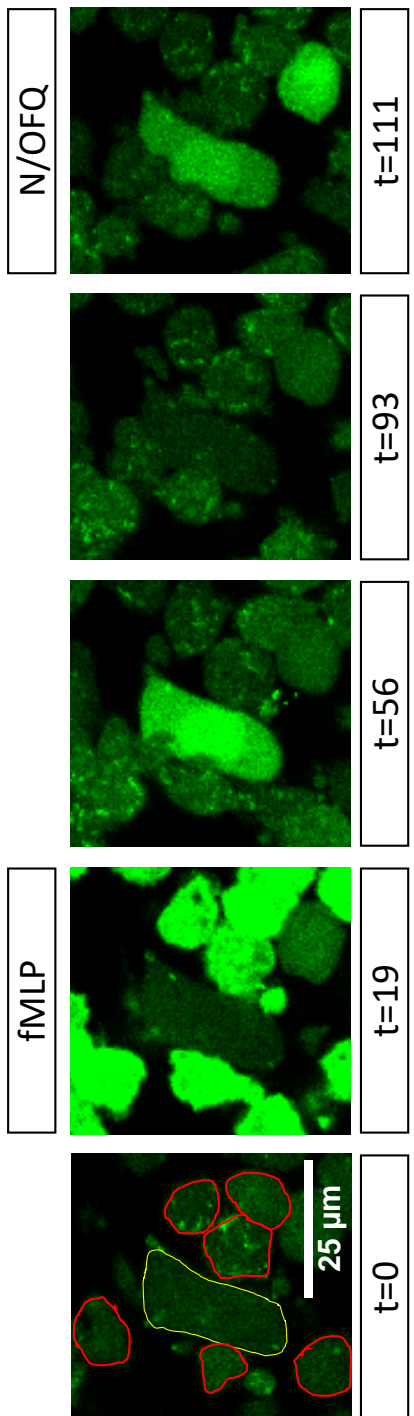


Figure 5.4.3 Experiment H2. The CHO-biosensor (yellow outline) responds following stimulation of PMNs (red outline) with fMLP, with exogenous N/OFQ 10^{-6} M confirming the identity and reactivity of the CHO-biosensor. The graph displays the fluorescence over time for this specific CHO cell (blue line), compared with the averaged fluorescence of all the PMNs in the experiment (red line). There is a clear increase in fluorescence of the CHO cell associated in time with PMN stimulation by fMLP.

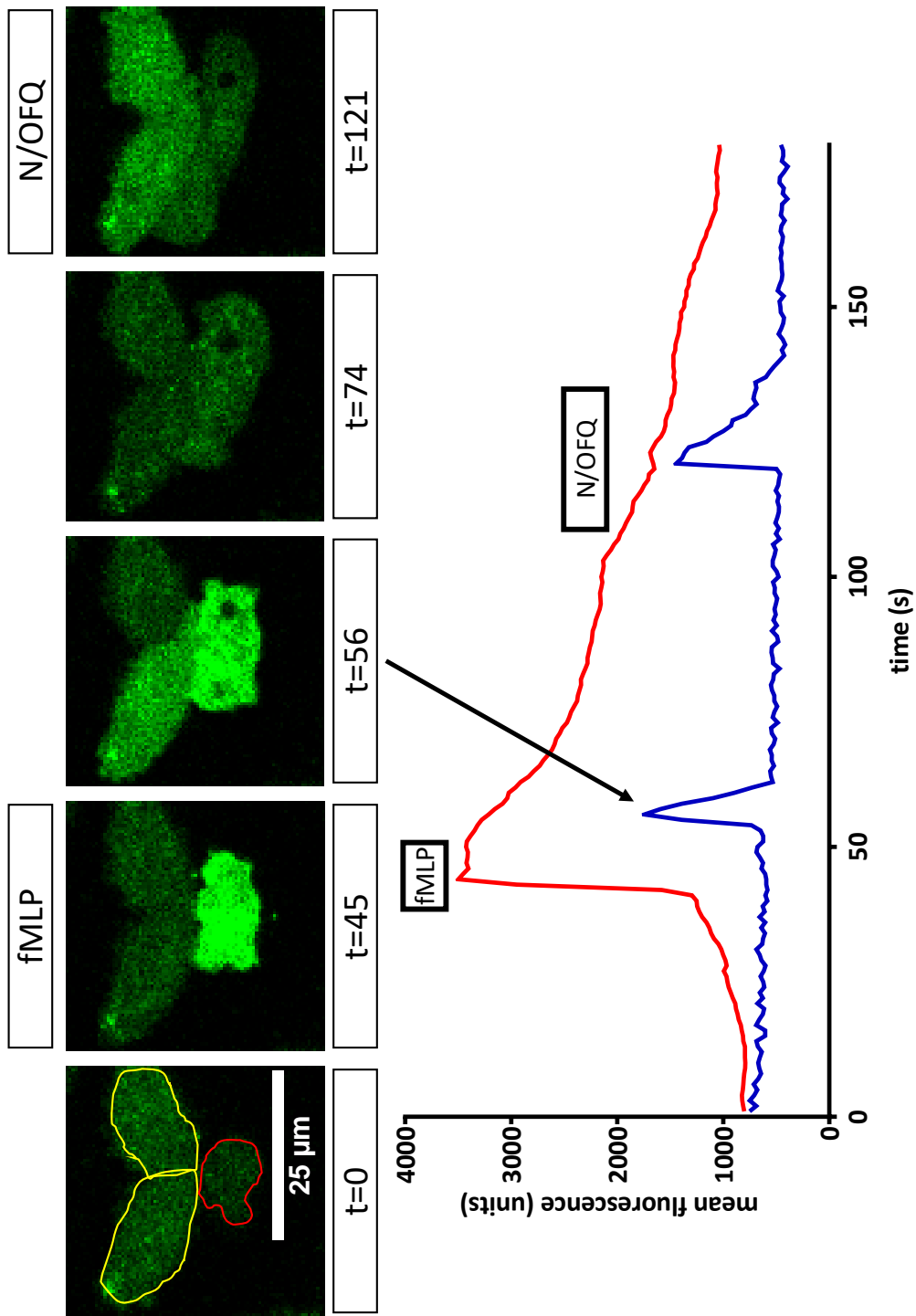


Figure 5.4.4 Experiment E3. The CHO-biosensor (yellow outline) fluoresces following fMLP stimulation of PMNs (red outline, probably 2 cells). Exogenous N/OFQ 10^{-6} M generates a fluorescent response confirming the cell is a CHO-biosensor. The graph demonstrates this fluorescent response of the single reacting CHO cell (blue line) compared with the average fluorescent response of all the PMNs in the experiment. Of note, only one of the two CHO cells fluoresces following PMN activation. Because confocal allows a very thin focal plane, PMNs above or below the focal plane may be contributing to the CHO cell's response, not affecting the other visible CHO cell.

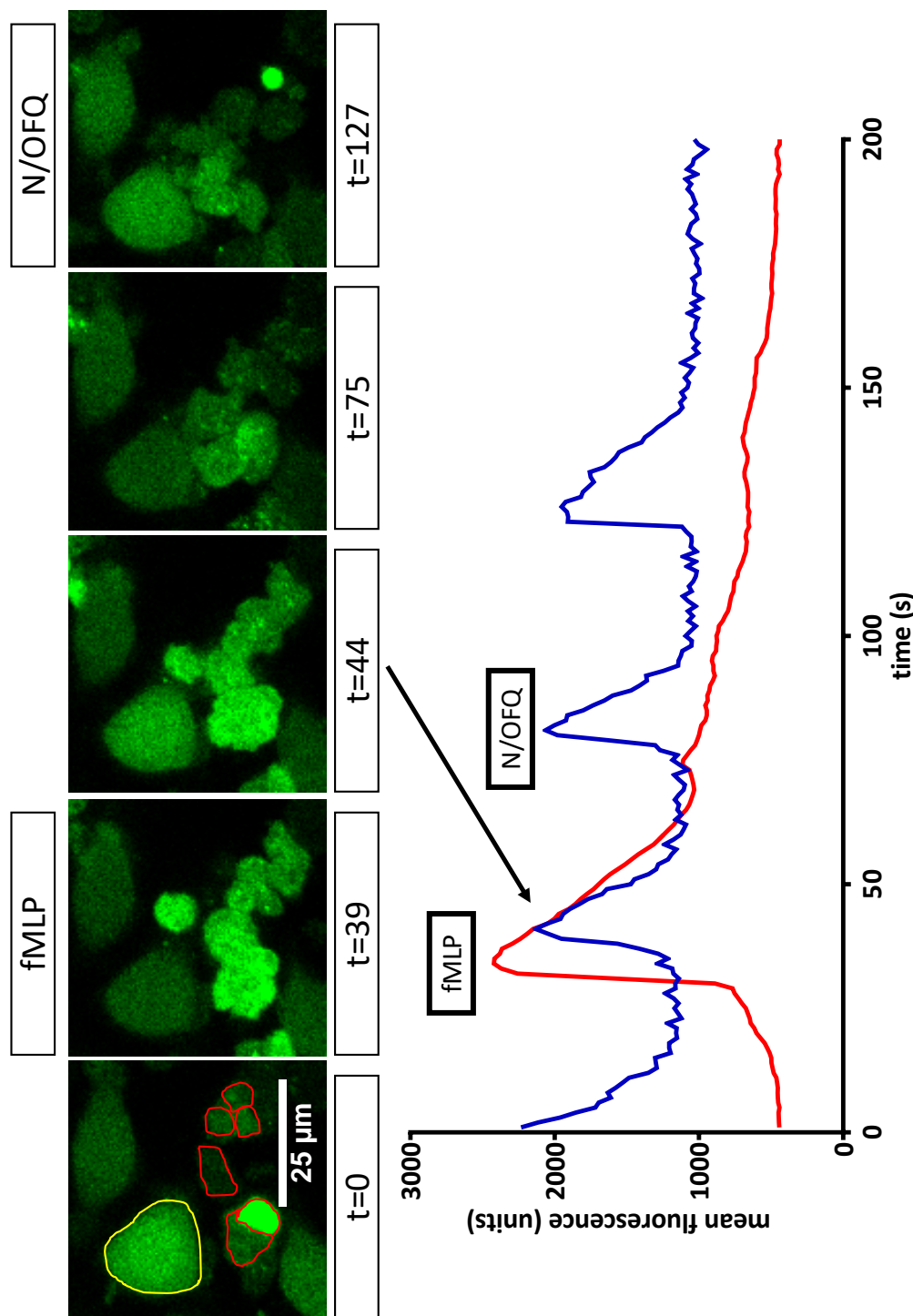


Figure 5.4.5 Experiment D2. The CHO-biosensor (yellow outline) fluoresces rapidly following fMLP stimulation of PMNs (red outline). Exogenous N/OFG 10^{-6} M generates a fluorescent response confirming the cell is CHO-biosensor. The graph compares fluorescence of the single fluorescing CHO cell (blue line) with the average fluorescence of all PMNs in the experiment (red line). Whilst fluorescence of the CHO cell is associated in time with PMIN activation, there are also subsequent similar peaks (one being N/OFG associated). Further, the CHO cell is already fluorescing at time = 0 s. This may represent autofluorescence of the CHO cell, or a response to spontaneous activation of non-visualised PMNs, either outside the field of view, or above or below the focal plane.

Overall these experiments demonstrate that the co-imaging of live, reactive PMNs and CHO cells is possible. Furthermore, these data demonstrate that PMNs can be stimulated to degranulate and the effects of degranulation visualised by changes in calcium concentrations in a different non-human cell. These effects, however, were not universal, with a 14% of all CHO cells fluorescing in a time-associated manner following fMLP degranulation of PMNs. There are a number of possible explanations for this low rate of responsiveness.

PMNs

PMNs in this assay included neutrophils and eosinophils, with approximately 10% expected to be eosinophils.¹⁰⁵ fMLP is primarily an activator of neutrophils and although eosinophils do respond to fMLP, they do so with a lower maximal response than for neutrophils.¹⁰⁶ The initial mRNA transcript experiments raised the suggestion that eosinophils may be involved in N/OFQ release (see Chapter 3.1), further confirmed by Singh and colleagues.²⁷ It is possible, therefore, that the biosensors were only responding to eosinophil release of N/OFQ. It was not possible in this assay to determine whether cells were neutrophils or eosinophils. However, future experiments should explore either techniques for distinguishing between cells (for example, using a distinguishing eosinophil or neutrophil fluorescent indicators), or isolated eosinophils (separated by MACS or FACS). Furthermore, known degranulators of eosinophils (e.g. eotaxin, RANTES / CCL5) could be used instead of fMLP.^{107 108}

A second issue, discussed in 5.3, was that measuring PMN fluorescence is technically more challenging than for CHO cells. The reason is that the PMNs demonstrated chemotaxis (despite CellTak™ preparation) and morphological changes following fMLP stimulation. Fluorescence measurement is conventionally achieved using static regions of interest to measure mean fluorescence within the ROI. When the cell moves or significantly changes morphology, the static ROI measures fluorescence from a different part of the cell. PMN migration could also lead to the static ROI no longer being within

the cell at all, or even falling within an adjacent migratory cell. This meant that some PMN responses were probably missed or inaccurate. Whilst there are Plugins for Fiji that attempt to track moving cells, their implementation is more complex. Future experiments would benefit from exploring the feasibility of such software. That said, the fluorescent response of PMNs to fMLP was essentially universal and reliable. Averaging of the fluorescence of all PMNs meant that any errors due to migration or morphological changes in a small number PMNs had a minimal effect on the overall measured fMLP-stimulated response.

It is highly likely that PMNs were degranulating prior to stimulation with fMLP. PMNs are highly reactive cells that respond to small changes in their environment. The process of isolation, transfer, loading with Fluo-4, and exposure to CHO cells would all have been stimulants for PMN degranulation. It is possible that the presence of PMNs also affected the viability of the CHO cells, possibly explaining some of their variability in response. It is also likely that some of the CHO-biosensors were fluorescing prior to stimulation due to the activity of PMNs. It is difficult to distinguish these issues from the phenomenon of autofluorescence that is largely unavoidable in confocal microscopy (see Chapter 4.4). Figure 5.4.5 illustrates this point: is the CHO cell fluorescing due to unstimulated activity of the PMN (in the graph, the fluorescence of the CHO cell at time 0 is similar to subsequent fluorescent peaks), subsequent degranulation effects, or due to autofluorescence? Related to autofluorescence is photobleaching, a consequence of photo-induced damage to the fluorophore, usually visualised as a fixed or fading fluorescence. Therefore, it is possible that some biosensors were reacting to PMN degranulation, but the fluorophore was inactive due to laser-induced damage. This is one reason that the time spent focusing the cells under laser illumination prior to scanning was minimised.

CHO-biosensors

As discussed in Section 5.2, the CHO $\alpha_{i/q}$ cells did not uniformly respond to N/OFQ. This is also demonstrated in Table 5.4.1, where 5 of the exogenous N/OFQ-stimulated responses were either absent or weak. It is likely that even between cells of the same line there was a variation in response. For example, in experiment A1, only 3 out of the 16 CHO-biosensors responded to 10^{-6} M N/OFQ, shown in Figure 5.4.6. This meant there was a degree of uncertainty for each experiment as to whether the biosensors would function as intended. Reasons for such variation may relate to their initial transfection, storage and transport, issues with cell culture and growth, and maintenance of viability when being transferred to the confocal microscope. Future experiments would benefit from trying to improve CHO-biosensor reliability, as well as screening using standard fluorimetry prior to confocal experiments.

The CHO-biosensors express the human NOP receptor, but they also natively express purinergic receptors that increase $[Ca^{2+}]_i$ in response to stimulation by adenosine triphosphate (ATP) and other nucleotides. PMNs release an assortment of cytotoxic chemicals and cytokines as well as adenosine monophosphate (AMP) and ATP when degranulated, some of which could act as an agonist at the CHO purinergic receptor.⁹⁸ That all the viable CHO-biosensors did not react to PMN degranulation is interesting in itself. However, it means that CHO-biosensor activation does not conclusively indicate N/OFQ stimulation. Antagonist experiments would be required.

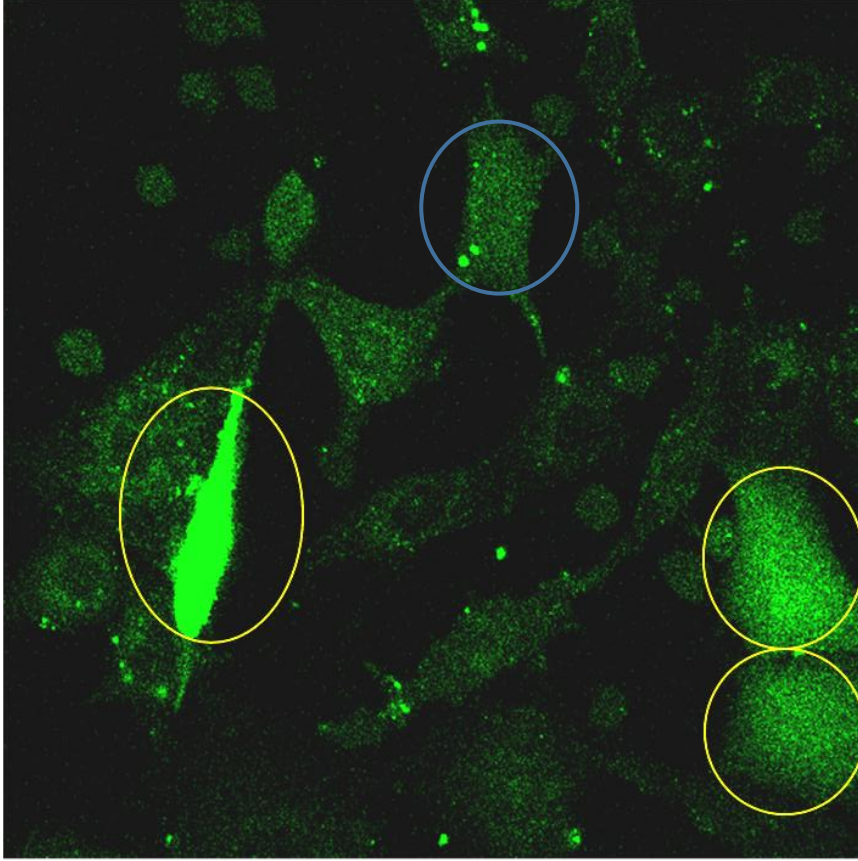
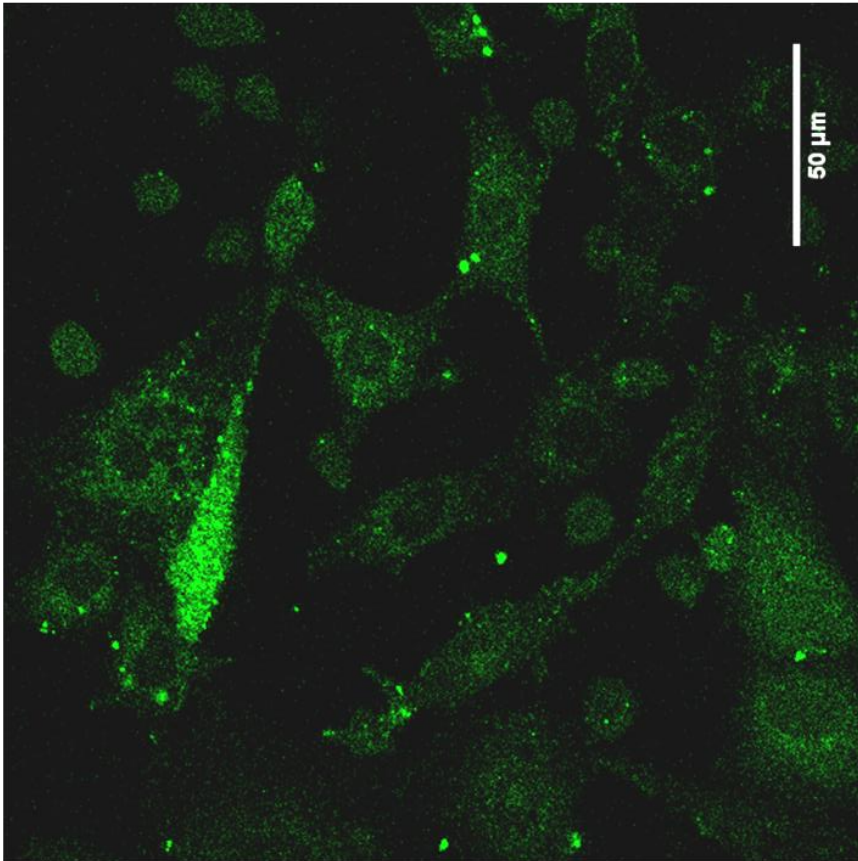


Figure 5.4.6 Experiment A1. Only three CHO-biosensors show a clear change in fluorescence in response to exogenous N/OFQ 10^{-6} M. There is also a change in focus in the cell marked with a blue circle, evidenced by the loss of the cell nucleus. Small changes in volume of perfusate (e.g. when changing reagents or adding boluses of agonist) can change the focal point of the confocal microscope. This can be misinterpreted as fluorescence.

Technical issues

Development of this assay raised significant technical challenges. Proficiency in use of the microscope and perfusion system improved over time, but even so, certain issues remained. A key problem was the layering of PMNs and CHOs. Confocal imaging allows very thin focal planes. The CHOs were adherent to the coverslips, but the PMNs were layered from above on the day of experiment, necessary because of the impossibility of culturing PMNs. Achieving focus of both the PMNs and CHOs in the same focal plane was challenging, and that during imaging and stimulation, morphological and migratory changes meant the PMNs would move in and out of focus. Furthermore, confocal imaging focuses on just one region within the whole sample. Not only will there be cells above and below the focal plane, but there will also be cells in areas not being imaged. This means that stimulation with fMLP necessarily degranulated unseen PMNs, influencing local N/OAQ concentrations for an individual CHO cell. This may explain the single CHO cell fluorescence in Figure 5.4.4 despite being immediately adjacent to another CHO-biosensor. The microscope also only focuses on one area of the entire sample, yet events occurring outside the field of view can still influence those being visualised. Additionally, fMLP and agonist concentrations were unlikely to be entirely uniform throughout the sample.

It was not possible to correlate fluorescence of CHO cells with concentrations of PMN-released N/OAQ peptide. For reasons already discussed, calibration of the assay presents significant technical challenges and the variation in response of the CHO-biosensors discussed in Section 5.2 meant that establishing a standard curve could not be reliably achieved. Further, the use of ratiometric indicators was not possible using this equipment. That said, based on the data in Section 5.2, it is a reasonable estimate that N/OAQ peptide concentrations released from PMNs is $\geq 10^{-9}$ M. Further refinement of this assay may allow for more accurate measurements of N/OAQ concentrations.

In conclusion, these PMN-CHO experiments demonstrate that co-imaging live interacting cells is feasible and possible. The next stage was to determine whether those CHO cells that responded following PMN degranulation were fluorescing in response to N/OFQ-NOP binding or other components released by activated PMNs.

5.5. Stimulation of CHO-biosensors in the presence of antagonists

Question: Are increases in intracellular calcium in CHO-biosensors subsequent to PMN degranulation due to stimulation of the NOP receptor by N/OFQ, or by nucleotide stimulation of purinergic receptors?

Although a proportion of CHO-biosensors had responded following PMN degranulation it was not certain that this response was N/OFQ mediated. Subsequent experiments, therefore, used antagonists to the NOP receptor and the natively expressed purinergic receptors present in CHO cells. Given the relatively low response rate of CHO cells in the presence of degranulating PMNs, it would have been difficult to generate meaningful data using the co-imaging assay. Therefore, an alternative methodology was developed that used the supernatant of isolated, activated PMNs to stimulate a layer of CHO-biosensors in the confocal microscope.

The following experiments were performed using samples of CHO-biosensors loaded with Fluo-4 and placed in the confocal microscope as previously described. CHO-biosensors were then perfused with either an antagonist to NOP (TRAP-101), a non-selective antagonist to purinergic receptors (PPADS), or both. Whole blood (15 ml) was donated by healthy volunteers and PMNs isolated as per Blood Separation Protocol 2 (see Chapter 2.3.2) with additional red cell lysis. A concentration of 10^{-6} M fMLP was administered to the isolated PMNs, which were then incubated at 37°C for 3 min, centrifuged at 300 g for 5 min and then the supernatant aspirated. This supernatant was then kept on ice. Aliquots of 100 μ L to 200 μ L supernatant were then administered to the CHO-biosensors in the presence or absence of antagonists.

TRAP-101 is a non-peptide selective competitive antagonist of the NOP receptor; its pharmacological profile is detailed by Trapella et al.¹⁰⁹ Its potency is the same as J-113397 (IC_{50} 2.3 nM), from which TRAP-101 is derived. For these experiments 600 nM

(6×10^{-7} M) TRAP-101 in Krebs-HEPES was used. An enabling experiment suggested that TRAP-101 (3×10^{-7} M) could prevent N/OAQ stimulation at 10^{-8} M (see Figure 5.5.1). We doubled the concentration of TRAP-101 in subsequent experiments to maximise effective blockade of the NOP receptor. PPADS (pyridoxalphosphate-6-azophenyl-2',4'-disulfonic acid) is a non-selective P2 purinergic antagonist with relatively low potency (IC_{50} 1.0 – 2.6 μ M at P2X, 0.9 mM at native P2Y receptors). For these experiments 30 μ M (3×10^{-5} M) in Krebs-HEPES was used. An enabling experiment (see Figure 5.5.1) suggested that this concentration of antagonist could attenuate the CHO-biosensor response to ATP at 10^{-8} M but not 10^{-6} M.

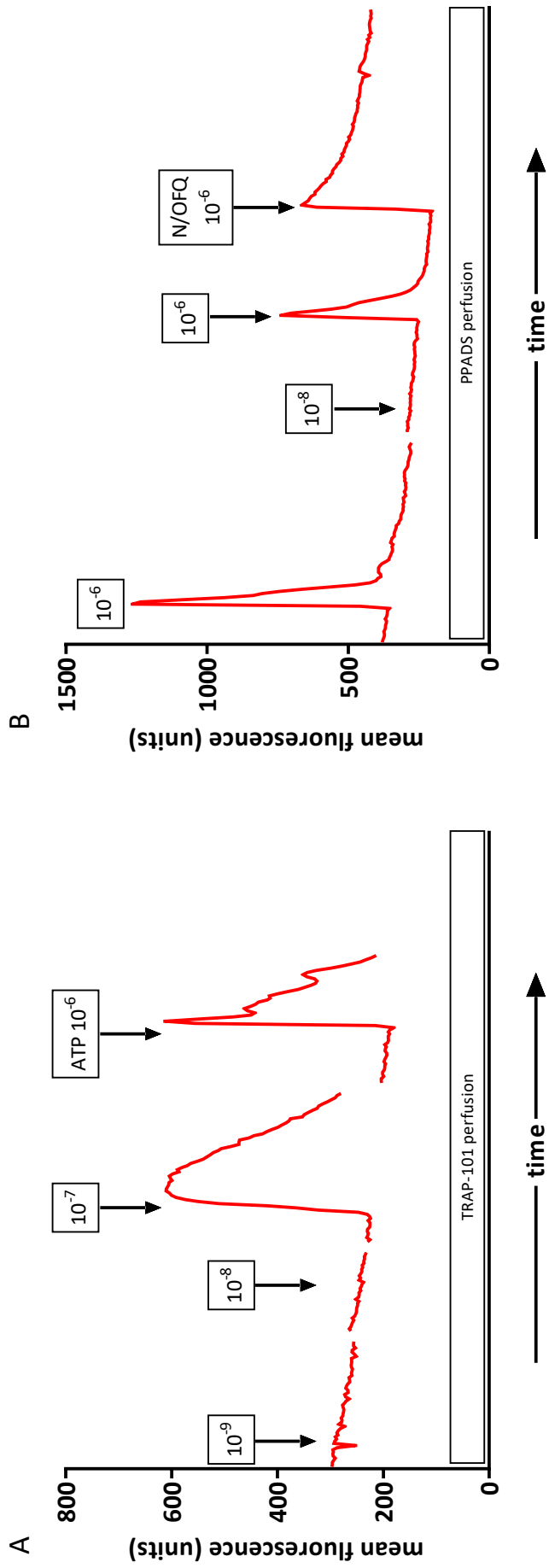


Figure 5.5.1 Two experiments demonstrating the response of CHO-biosensors to different concentrations of N/OFQ (experiment A), and ATP (experiment B). The graphs represent overall mean fluorescence over time taken from each of (A) 82 CHO cells, and (B) 113 CHO cells. The graph of experiment A shows that TRAP-101 (300 nM) inhibits the biosensor response up to N/OFQ 10^{-7} M. The cells remain responsive to ATP (10^{-6} M). In experiment B the data suggest 10^{-6} M ATP overcomes the block of PPADS (300 μ M), with the cells remaining responsive to 10^{-6} M N/OFQ. These data confirm that both N/OFQ and ATP increase $[Ca^{2+}]_i$ in CHO-biosensors, and that TRAP-101 and PPADS can attenuate this response.

Competitive antagonists can be overcome by larger concentrations of agonist. To ensure that supernatant concentrations of purinergic ligands or N/OAQ were not high enough to overcome receptor blockade, serial dilutions of supernatant were made until there was no fluorescence response of the CHO-biosensors in the presence of TRAP-101 and PPADS, or TRAP-101 alone. Subsequent experiments involved testing aliquots of the supernatant against either first PPADS or TRAP-101, then resting the system for 5 – 10 min whilst perfusing with the alternative antagonist. This allowed time for receptor recovery. Further aliquots of supernatant were then tested. Where there was minimal or no response to the supernatant for both the first and second antagonist, cells were tested for viability and responsiveness by administering a large concentration of agonist (exogenous ATP 10^{-6} M, exogenous N/OAQ 10^{-6} M, or neat supernatant). This procedure is illustrated in Figure 5.5.2.

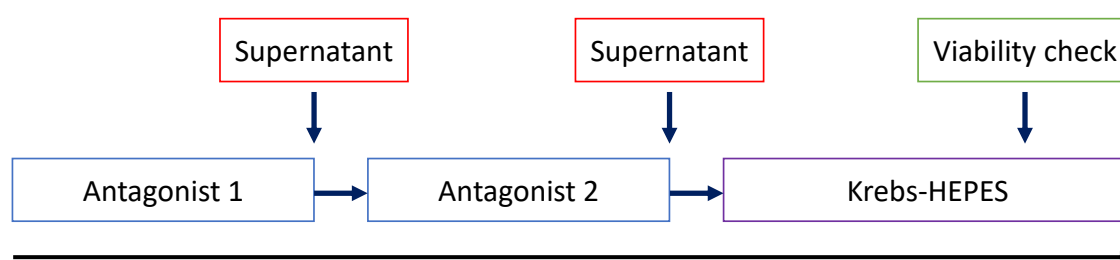


Figure 5.5.2 Flow of experiments using supernatant from fMLP-stimulated PMNs to stimulate CHO-biosensors

A degree of desensitisation was expected during these experiments. The literature suggests that P2 receptors are subject to desensitisation and it is known that NOP GPCRs also desensitise.^{110–113} However, that the cells would remain sufficiently responsive to agonists was determined in the enabling experiment shown in Figure 5.5.1. The initial antagonist was also varied between PPADS and TRAP-101, although overall TRAP-101 was most commonly used as the initial antagonist. This antagonist was associated with a more attenuated response thereby minimising any desensitisation. Furthermore, the onset and offset of the non-specific PPADS was known to be slower than that for TRAP-101, so starting with PPADS may have had a greater influence on subsequent responsiveness despite a 5 – 10 min rest.

Data from 15 experiments using PMNs isolated from 6 volunteers are presented in Table 5.5.2 and were analysed using χ^2 (Fisher's exact) tests. The results were also analysed by groups determined by which antagonist was used first; i.e. PPADS then TRAP-101, or TRAP-101 followed by PPADS. For all data there was a significant difference ($p < 0.0001$) in the CHO-biosensor responses to supernatant in the presence of TRAP-101 compared with PPADS. Where PPADS was the first antagonist the difference was also significant ($p < 0.001$) as it was when TRAP-101 was the first antagonist ($p < 0.001$). Contingency tables are given in Table 5.5.1. Graphs and associated images were also generated to illustrate these changes in responsiveness (see Figure 5.5.3, Figure 5.5.4 and Figure 5.5.5).

All data	Number of CHO cells	
	Fluorescence response	No fluorescence response
PPADS	252	283
TRAP-101	88	429

PPADS as first antagonist	Fluorescence response	No fluorescence response
PPADS	118	20
TRAP-101	48	91

TRAP-101 as first antagonist	Fluorescence response	No fluorescence response
TRAP-101	40	338
PPADS	134	263

Table 5.5.1 Summary contingency tables for all data for the administration of supernatant to CHO-biosensors in the presence of antagonists, and for when PPADS was the first antagonist, and for when TRAP-101 was the first antagonist. Numbers represent the numbers of CHO-biosensor cells that responded or did not respond to supernatant administration.

Experiment	Supernatant dilution	Antagonist 1	CHOs responding (% of total)	Antagonist 2	CHOs responding (% of total)	Viability test	CHOs responding (% of total)
A1	100	PPADS	25 (96%)	TRAP-101	0 (0%)	ATP	21 (81%)
B1a	neat	PPADS	23 (89%)	TRAP-101	20 (77%)	-	
C3	neat	PPADS	23 (92%)	TRAP-101	24 (92%)	-	
E1b	10	PPADS	47 (77%)	TRAP-101	4 (7%)	N/OHQ	47 (77%)
A2	100	TRAP-101	1 (3%)	PPADS	2 (6%)	NOHQ	31 (97%)
A3	100	TRAP-101	1 (3%)	PPADS	31 (100%)	-	
B1b	10	TRAP-101	6 (23%)	PPADS	5 (14%)	-	
B2	neat	TRAP-101	5 (63%)	PPADS	8 (89%)	N/OHQ	5 (56%)
C1	100	TRAP-101	3 (7%)	PPADS	29 (71%)	supernatant	23 (56%)
C2	100	TRAP-101	2 (6%)	PPADS	3 (9%)	N/OHQ	29 (85%)
D1	10	TRAP-101	2 (7%)	PPADS	18 (62%)	-	
D2	100	TRAP-101	8 (15%)	PPADS	23 (42%)	-	
E1a	10	TRAP-101	4 (7%)	PPADS	7 (12%)	N/OHQ	50 (82%)
E2	10	TRAP-101	0 (0%)	PPADS	0 (0%)	ATP	42 (96%)
F1	100	TRAP-101	8 (28%)	PPADS	8 (28%)	N/OHQ	26 (96%)

Table 5.5.2 Results from supernatant experiments arranged by first antagonist. The letters for the experiment label correspond to the sample used to generate the fMLP-stimulated supernatant; the number of the experiment represents each experimental run (B1b and E1a were performed on the same cells as B1a and E2a). Supernatant was used on the day of experiment with none being stored for later use.

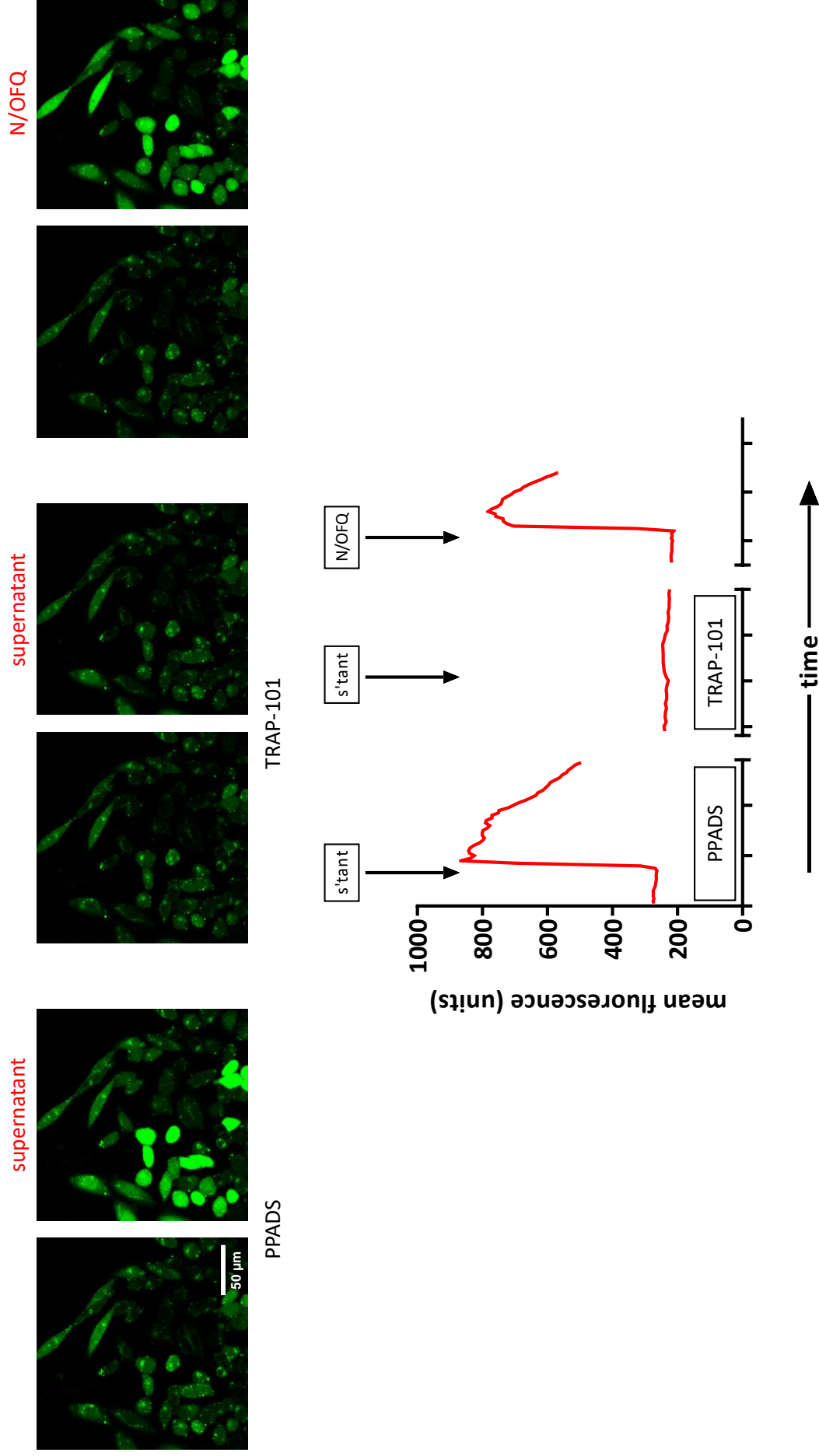


Figure 5.5.3 Experiment E1b. PPADS does not fully remove the fluorescent response of CHO-biosensors to PMN-supernatant. However, the fluorescent response is attenuated by TRAP-101. A micromolar administration of exogenous N/OFQ demonstrates that the CHO-biosensors remain viable. This suggests N/OFQ is contributing to most of the CHO-biosensor response.

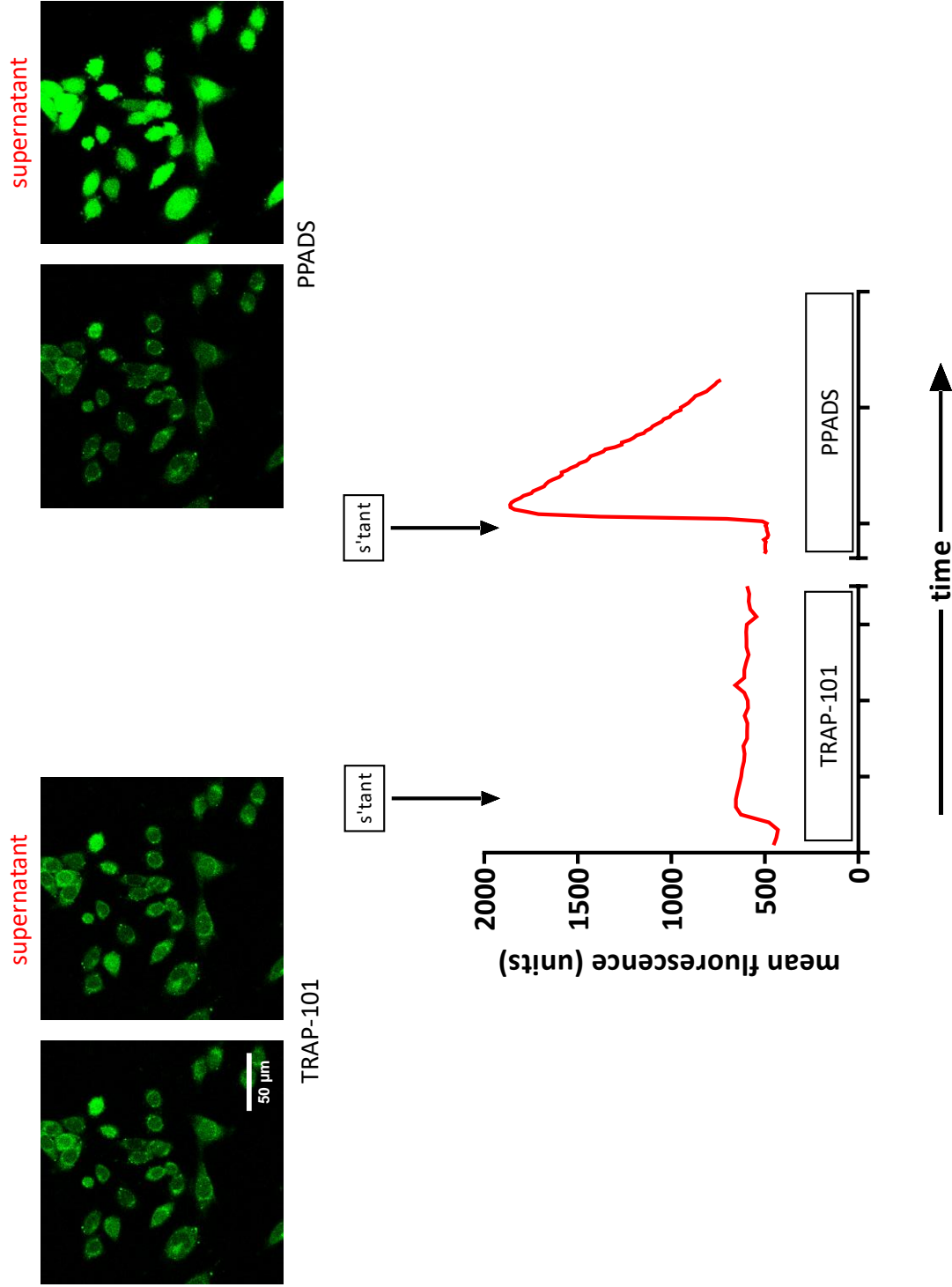


Figure 5.5.4 Experiment A3. The CHO-biosensor fluorescent response to PMN-supernatant is attenuated by TRAP-101. However, the CHO-biosensors strongly fluoresce in response to supernatant in the presence of the antagonist PPADS. This suggests that N/OFQ is present in the supernatant at sufficient concentrations to elicit large increases in $[Ca^{2+}]_i$ in the CHO-biosensors.

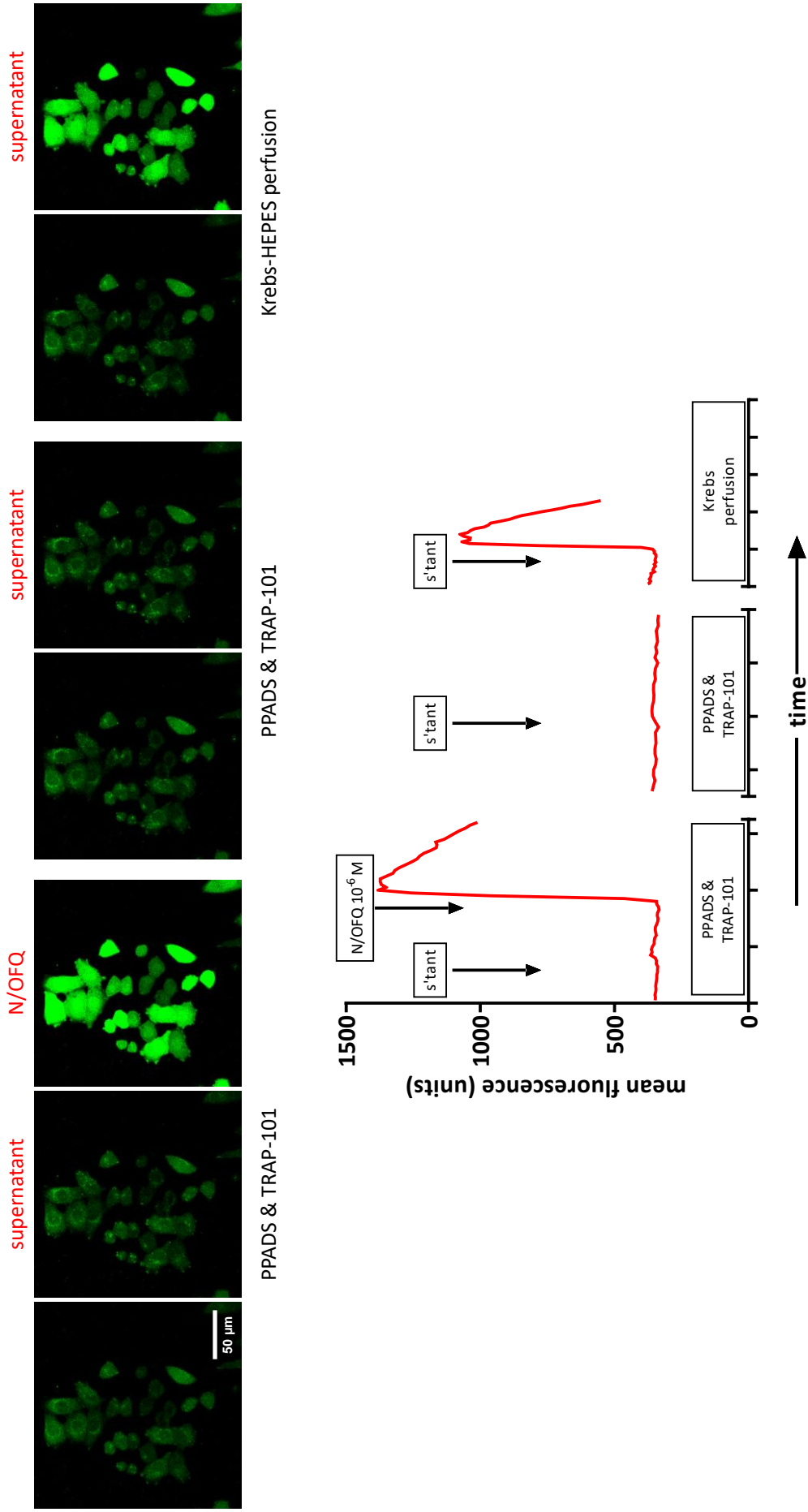


Figure 5.5.5 Experiment (cells from D1) demonstrating that supernatant stimulation of CHO-biosensors is antagonised by the combination of PPADS & TRAP-101. In the first part of the graph, exogenous N/OFG 10^{-6} M ensures that this is not due to CHO-biosensors being unviable. The same cells perfused with PPADS & TRAP-101 do not fluoresce after administration of PMIN-supernatant, but do fluoresce when the antagonists are washed off during perfusion with just Krebs-HEPES solution.

These data suggest that the supernatant of fMLP-stimulated PMNs does contain N/OFQ. Therefore, it is likely that at least some of the individual cell response seen in CHO-biosensors in Section 5.4 was due to N/OFQ.

It is interesting that PPADS and TRAP-101 combined could effectively block the fluorescent response of CHO-biosensors. Degranulated PMNs release numerous active substances other than N/OFQ and nucleotides. In these experiments TRAP-101 inhibited CHO-fluorescence, and the combination of the PPADS and TRAP-101 was effective at completely attenuating the fluorescent response to PMN supernatant. This suggests that other substances had little effect on the CHO-biosensors. However, the products of PMN degranulation can be very short-lived, such as reactive oxygen species (e.g. $[\text{OH}]^\bullet$ with a half-life of 10^{-9} s; 1 ms for H_2O_2).¹¹⁴ Whilst it is likely that the PMN-CHO cell interactions demonstrated in Section 5.4 were due to only a combination of N/OFQ and nucleotides, it is possible that short-lived PMN products were also responsible.

As predicted by previous experiments, the CHO-biosensor response was variable. This necessitated variation in experiments as they proceeded. For example, as shown in Figure 5.5.5, a lack of response to TRAP-101 and PPADs combined could indicate poorly performing biosensors so this was checked by administering 1 μM of N/OFQ before performing further antagonist investigation. Another example was in an experiment illustrated in Figure 5.5.6. In this experiment, dilution of the PMN supernatant was by a factor 10,000 before a fluorescence response could be attenuated by PPADS and TRAP-101. Unfortunately, having done this, the CHO-biosensors became unresponsive, possibly desensitised, so further individual antagonist work on this run could not proceed. It is possible that this was due to particularly high concentrations of N/OFQ and ATP in the supernatant sample. However, it is also possible that these particular CHO cells were more effectively loaded with Fluo-4, or were more responsive due to factors such as higher receptor expression.

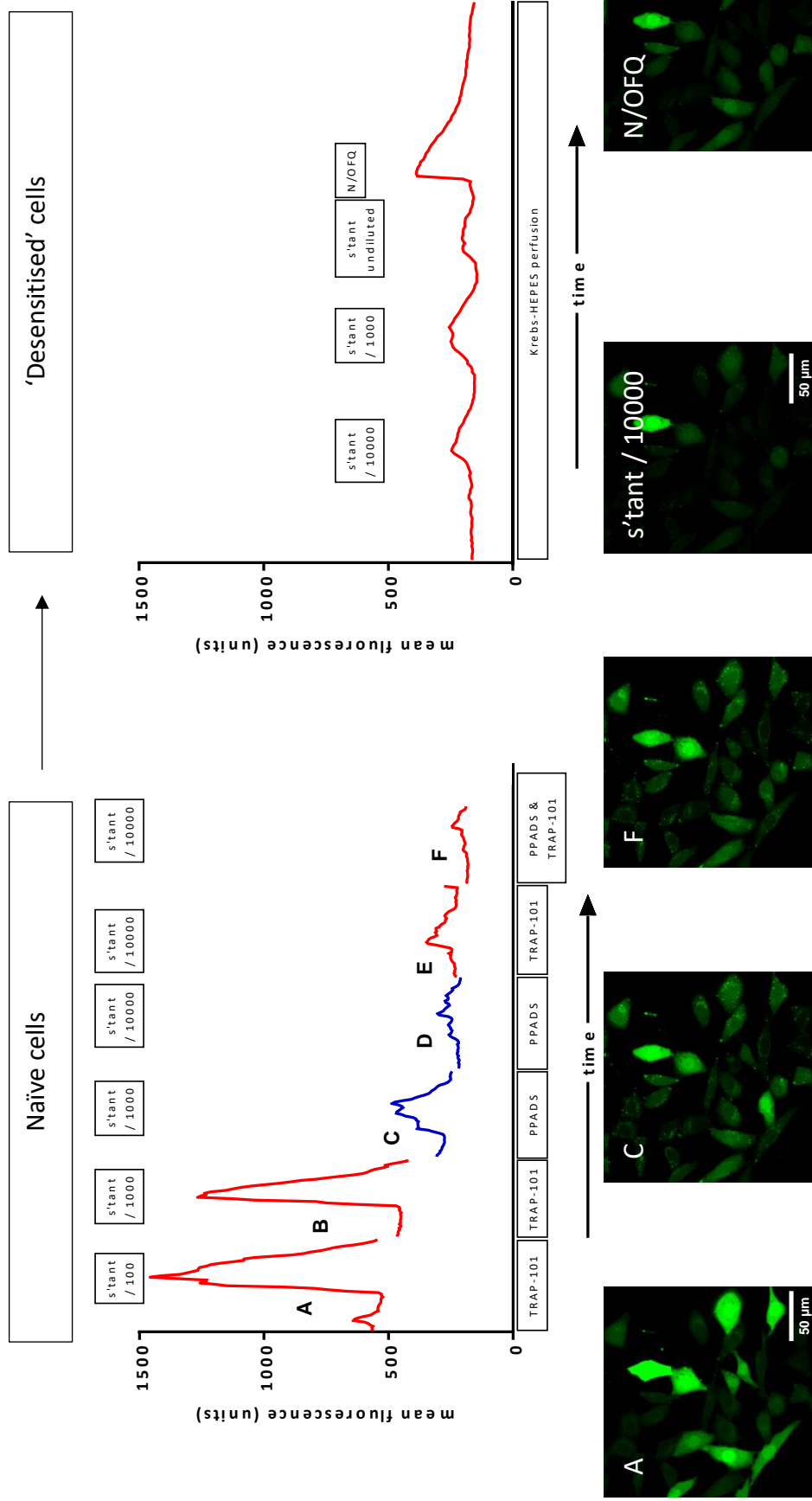


Figure 5.5.6 Mean fluorescence for CHO-biosensors (n=33) illustrating a sensitive response to fMLP-stimulated PMN supernatant. Despite a 10,000x dilution, it was difficult to inhibit all cell fluorescence. Peaks C and D suggest that nucleotides (e.g. ATP) may have been contributing to the peaks seen in A and B, but even when using both antagonists (F) fluorescence remained. There is a visible decrease in baseline fluorescence - rest periods (5 min) may have been insufficient for cell recovery. The consequence of these repeated stimuli was that once an appropriate dilution of supernatant had been reached, the same biosensors were poorly responsive (possibly desensitised), as shown in the second graph.

PPADS was used in these experiments to block the effect of nucleotides on CHO-biosensor stimulation. The advantage of PPADS is that it is poorly selective, simplifying the number of antagonists required to attenuate CHO cell fluorescence mediated by the native P2Y and P2X receptors. However, it is also a low affinity antagonist of purinergic P2 receptors. Whilst PPADS has been used extensively in research of purinergic receptors, it has a relatively slow onset and offset, and displays non-competitive antagonism.¹¹⁵ Its low potency necessitated relatively high concentrations of PPADS (30 μ M), and it was difficult to be certain that PMN-degranulated nucleotide actions were entirely inhibited. One enabling experiment suggested that 10^{-8} M of ATP was inhibited by PPADS, but not 10^{-6} M. The consequence of this is that the effect of degranulated PMN nucleotides on the CHO-biosensors was possibly not entirely removed; that is, the difference in response between TRAP-101 and PPADS perfused CHO-biosensors may actually be smaller than presented. However, for there to be no significant difference between groups in the data, an alternative antagonist would have to have reduced the number of fluorescing biosensors to 117, a 54% reduction in responding cells.

In comparison, TRAP-101 is a highly selective and potent competitive antagonist (although can display inverse agonism) of the NOP receptor, and, in the majority of experiments, effectively attenuated the response of CHO-biosensors to PMN-degranulated N/OFQ (notable exceptions are experiments C3 and F1). Experiments where TRAP-101 made little difference to the numbers of CHO-biosensors responding to supernatant suggest some possibilities. Either the PMN-degranulated supernatant contained no N/OFQ, the concentrations of any N/OFQ were greater than 0.1 μ M, or the nucleotide-mediated response was prominent (even though in C3 and F1 there was a biosensor response in the presence of PPADS, accepting the limitations of this antagonist described above). However, across all experiments there was a significant difference in biosensor responses in the presence or absence of TRAP-101.

Ideally each experimental run would have been calibrated against a concentration-response curve for each antagonist. However, the variable response of the CHOs within

a cell line as well as between cell samples meant that such an endeavour would have been impractical and likely confusing. Further investigative work using antagonists would benefit from further refinement of the CHO $\alpha_{i/q}$ biosensors. It would have also been useful to measure the pharmacokinetics of antagonists in this system. It is likely that a degree of receptor inhibition persisted in the CHO-biosensors after the five minutes of perfusion with Krebs-HEPES. However, there was a need to balance maintaining biosensor viability, PMN supernatant integrity, minimising calcium indicator leak, with time required for complete removal of antagonist and restoration of receptor function.

An alternative strategy to using antagonists would be the use of an enzyme to degrade any nucleotides present in the fMLP-stimulated PMN supernatants. Apyrase is an ATP diphosphohydrolase that catalyses the degradation of ATP to ADP + Pi and ADP to AMP + Pi. It is available commercially, being derived from the red potato *S. tuberosum* with one unit liberating 1 μ mole of Pi from ATP or ADP per minute. If N/OAQ is present in the supernatant of degranulated PMNs, an apyrase-treated supernatant would be expected to stimulate CHO-biosensors, an effect that could be blocked with TRAP-101. Whilst this would be useful additional experiment to what has been presented, without further work refining the CHO-biosensors it is likely that data would be difficult to interpret.

5.6. Conclusions

These data are the first to demonstrate live cell imaging of CHO $\alpha_{i/q}$ cells in the presence of live, viable, human PMNs. The development of this assay through a series of experiments has resulted in a novel assay for visualising cell-to-cell interactions. Further, this assay has generated data supportive of PMNs releasing N/OAQ following activation. Whilst the technique requires refinement, the assay is effective and feasible, and will allow further exploration of the function of N/OAQ in human immune cells.

6. Discussion

6.1. Summary of results

The studies contained within this thesis have explored the role of nociceptin in sepsis in two areas. First, gene expression of NOP and ppNOC was examined. Conclusions were that NOP mRNA transcripts (and not ppNOC) were present in all subpopulations of granulocytes and NOP expression in PMNs was modulated by lipopolysaccharide *in vitro*. The second section of the thesis described the development of a novel live-imaging bioassay. Data from this bioassay suggested that N/OFQ peptide was released by *ex vivo* stimulation of PMNs with fMLP. A summary of these data and the development of this novel bioassay are presented in Figure 6.1.1.

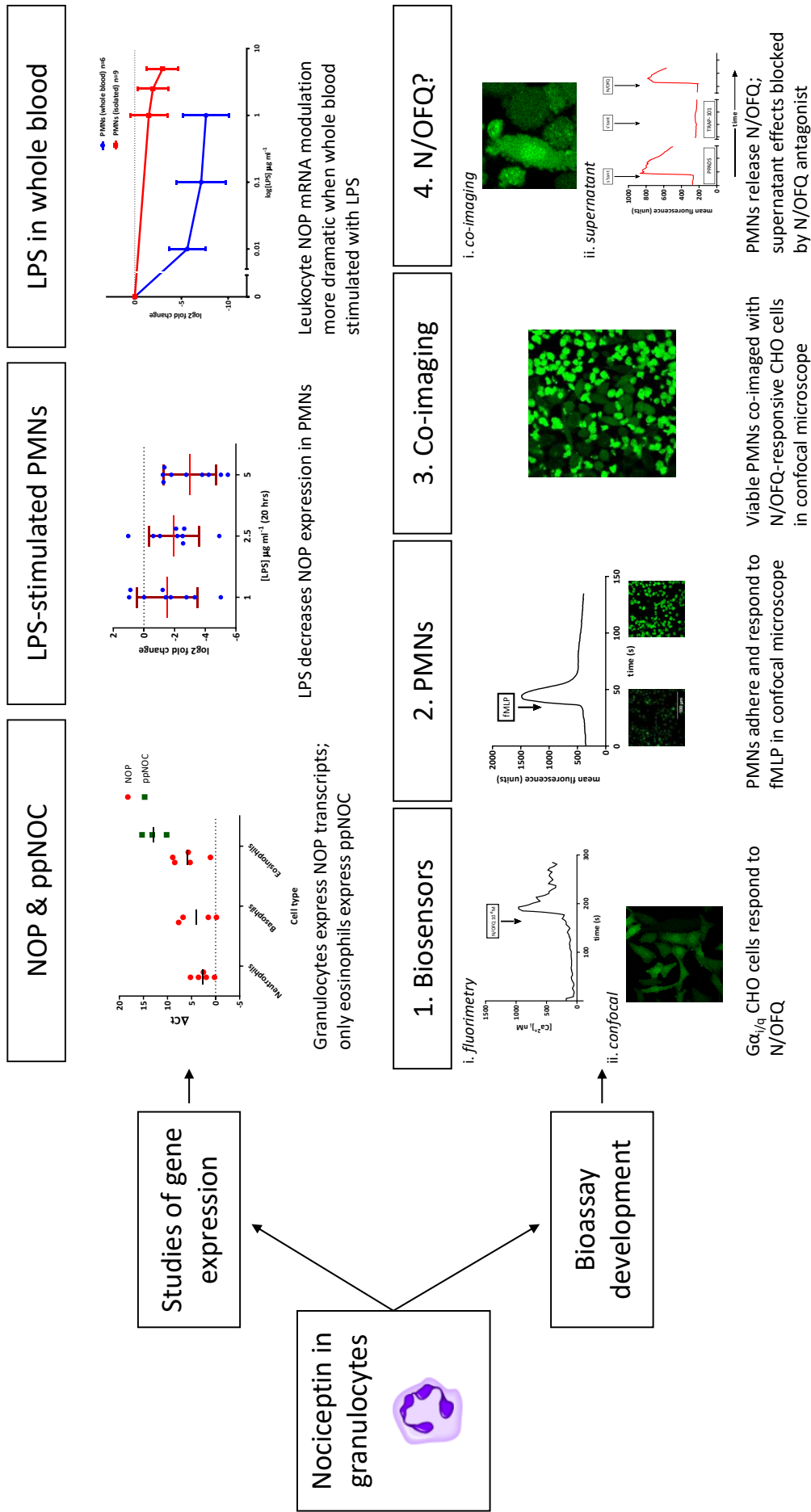


Figure 6.1.1 Summary of key findings and development process of a novel live-imaging bioassay.

6.2. Studies of gene expression

These data add to the published literature on mRNA transcripts in immune cells. Earlier work had determined expression of NOP on monocytes and lymphocytes, and subsequently neutrophils.^{23 24 116 117} Work by McDonald and colleagues (2010) further demonstrated that cells purified using FACS expressed mRNA transcripts for NOP and ppNOC in granulocytes, monocytes and lymphocytes.²² Interestingly, ppNOC expression was lower in granulocytes (average ΔCt 10.37) compared with NOP (average ΔCt 5.93), which is consistent with data presented in this thesis. The data presented here in Chapter 3.1 had ΔCt values for NOP of 2.72 in neutrophils, 3.96 in basophils, 5.91 in eosinophils and ppNOC of 12.89 in 3 eosinophil samples (undetected in the other 2 samples). Both the data from McDonald and colleagues, and data presented here used the HKG GAPDH.

These data are the first to demonstrate mRNA transcripts for NOP in subpopulations of neutrophils, eosinophils and basophils. That ppNOC was predominately expressed in eosinophils is also further supported by recent work performed by Singh and colleagues.²⁷ In that study ppNOC expression was found in eosinophils, but not in human structural airway cells (smooth muscle, epithelial and mast cells). Whilst it is known that lymphocytes and monocytes both express ppNOC transcripts, that it is absent from neutrophils suggests that eosinophil – neutrophil interactions may be important to the nociceptin response to inflammation.

The modulation of NOP expression to LPS is also consistent with the literature. Thompson and colleagues showed reduced NOP expression in PMNs in patients with a clinical diagnosis of sepsis, and Zhang and colleagues demonstrated that LPS reduces NOP expression in PMNs following LPS stimulation.^{69 82} These data, however, conflict with Stamer's earlier work demonstrating NOP expression is *increased* in sepsis, cancer and surgery.⁷⁰ LPS stimulation is not the same as the sepsis (see Chapter 1.8), and it is conceivable that endotoxin modulates NOP expression differently from other sources of sepsis and inflammation. There were also differences in mRNA isolation. In Stamer's

2011 paper mRNA was extracted from whole blood, whereas Thompson and Zhang isolated PMNs before extracting mRNA. Data from Chapter 3 also demonstrated that PMNs isolated from whole blood that had been exposed to LPS show a more profound reduction in NOP expression compared with direct exposure of PMNs to LPS. This points to a more comprehensive nociceptin response to LPS beyond stimulation of PMNs. Whilst fetal calf serum (FCS) provided LPS-binding protein in PMN samples, previously determined ppNOC transcripts in lymphocytes and monocytes indicates that a more comprehensive immune response has a larger impact on PMN NOP expression.¹¹⁸ Given current understanding of the integrated and complex physiological response to sepsis, it is perhaps not surprising that whole blood LPS stimulation modulates NOP expression to a greater extent compared with isolated PMNs.

It is also interesting that whole blood mRNA isolation demonstrated a reduction in NOP expression with LPS stimulation, consistent with PMN mRNA. The data presented in this thesis are limited to the blood of only two volunteers, but do point to an area of future study. Does LPS-stimulation lead to whole blood mRNA changes that differ from Stamer's original observations? A study that repeated the work of Thompson and colleagues but considered both whole blood mRNA and PMN mRNA would be informative. Further, future studies of septic patients would use the more specific criteria set out in Sepsis-3 (see Chapter 1.5) and could lead to more robust conclusions about how nociceptin is involved in sepsis.

6.2.1. Limitations in studies of gene expression

The first experiment of gene expression identified mRNA transcripts for NOP mRNA in all subpopulations of granulocyte (i.e. neutrophils, basophils, eosinophils) separated by MACS. This experiment was designed for detection of transcripts rather than relative abundance, i.e. GAPDH as the HKG gave an indicator of the presence of mRNA in samples, important if transcripts for NOP and ppNOC were not detected. However, gene expression for GAPDH and the genes of interest NOP and ppNOC was low (indicated by high cycle thresholds) in samples as summarised below in Table 6.2.1. Raw Ct values

greater than 35 are difficult to distinguish from artefact and so are conventionally viewed as being of high risk of being a false positive.

N=5	Control			LPS		
	mean Ct (SD)			mean Ct (SD)		
	Neutrophil	Eosinophil	Basophil	Neutrophil	Eosinophil	Basophil
GAPDH	28.5 (3.4)	25.6 (4.6)	30.5 (4.4)	28.9 (3.6)	24.3 (1.5)	29.0 (3.3)
NOP	31.3 (1.8)	31.5 (2.2)	33.8 (2.6) ^a	31.8 (3.2)	30.4 (1.3)	34.1 (2.8)
ppNOC	-	36.1 (2.2) ^b	-	-	36.2 (1.9)	37.1 ^c

Table 6.2.1 Mean raw Ct values from RT-qPCR for control and LPS-exposed samples. Cycle thresholds, even for GAPDH, are high denoting low expression; *a* = detection in 4 samples, *b* = detection in 3, *c* = detection in 1 sample, - = no detection in any sample.

These high Ct values likely reflect the low mRNA concentrations extracted in eosinophil and basophil cells. However, neutrophil samples had acceptable mRNA concentrations ($>0.1134 \mu\text{g } \mu\text{L}^{-1}$) yet still gene expression, even GAPDH, was low. It is not clear why this was the case. It is conceivable that the process of magnetic separation affected mRNA extraction, but there is little in the literature to support this.¹¹⁹ This experiment exposed isolated cells to 20 hours in RPMI with 0 and $5 \mu\text{g ml}^{-1}$ LPS. This latter concentration is high and possibly affected cell viability. The duration of the experiment may have affected cell viability. PMNs are short-lived cells and fragile, with a constitutive tendency to apoptosis.¹²⁰ Further, mRNA degrades rapidly and in the presence of non-viable cells over 20 hours at 37°C it is possible that the integrity of mRNA was affected. Despite this, NOP expression was detectable. These factors, though, might explain why ppNOC expression was undetected.

Subsequent experiments used lower concentrations of LPS and a shorter time-period of 5 hours. It was still difficult to detect ppNOC, and concentrations of mRNA were still low. As previously discussed (see Chapter 3.6), larger blood volumes may have improved mRNA yields but were limited by the small pool of volunteers. These later experiments also used PolymorphPrep™ to isolate PMNs. MACS is effective at producing purified

cells: purities of 98 – 99% eosinophils, 94 – 98% neutrophils, >95% purity basophils.¹²¹
¹²² However, it is time consuming and involves more steps in processing which can affect cell viability. PolymorphPrep™ is associated with at least 94% purity or greater, and is quicker and simpler than MACS.^{69 123} Further, PMNs are very reactive, and any stimulation can lead to spontaneous degranulation and oxidative burst potentially affecting interpretation of relative gene expression. Minimising processing limits their activation.

There are other techniques for cell isolation.¹²⁴ Fluorescence activated cell sorting (FACS) is a technique used by McDonald and colleagues for isolating granulocytes, lymphocytes and monocytes.²² This technique uses fluorescent probes to target cell surface markers such as CD16 (neutrophils) from a suspension of cells (for example whole blood following red cell lysis). The cell suspension is then passed through a flow cytometer and each cell is exposed to a laser. Cells of interest labelled with a fluorophore fluoresce and are detected by fluorescence detectors. The instrument applies a charge to droplets containing fluorescing cells, and an electrostatic deflection system sorts the cells into collection tubes. This technology allows the sorting of highly purified different cell populations based on cell surface markers. However, like MACS, this technology produces labelled cells that theoretically can interfere with downstream experiments. Further, it is a slow process requiring access to specialised equipment. It was briefly explored as a technique for use in initial gene expression studies in this thesis and potentially confocal experiments. However, the lengthy time required for sorting 10^8 cells and limited access to the equipment meant that MACS was an easier and more accessible technique. Another technology is laser capture microdissection, which uses short duration focussed laser pulses to separate out cells identified microscopically. This does require correct identification of cells, which is difficult for subpopulations of granulocytes, and again requires specialist equipment. It is also better suited to isolating cells from tissues. Microfluidics is a relatively new technology that in some respects is similar to MACS. A micro-channel chip is modified with antibodies that can bind the cells of interest, and the sample passed through the micro-channels. Cells of interest are retained on the microchip whilst the remaining cells pass through. Elution then removes

the immobilised cells from the chip. This is not a technology explored in this thesis, but could be explored in future experiments requiring isolated purified cells.

There are valid criticisms of measurement of gene expression that can be made. First, accurate analysis of relative quantities of mRNA require equal PCR reaction efficiencies. Reaction efficiencies were not studied as part of this thesis, but data from our laboratory using NOP, GAPDH and B2M has demonstrated that the TaqMan Gene Expression Assays are 90 – 110% efficient.²²

The choice and use of HKGs in these data are also subject to criticism. HKGs are conceptually a useful way for controlling for variable concentrations of mRNA, a significant issue with experiments described in this thesis. Relative quantification, however, is dependent on the chosen HKG being stable in all experimental conditions. This can be explained with a simulated model of gene expression. In an ideal experiment, identical concentrations of mRNA have been acquired from samples that have been exposed to increasing concentrations of LPS. The Ct value of the gene of interest (GOI) decreases with LPS exposure – i.e. its expression increases – and the HKG remains completely stable. However, if exposure of LPS modifies the HKG by just one cycle, the effect on fold change is amplified by a factor of 2^1 . If the HKG is modified by two cycles, then the amplification factor is 2^2 and so on. This is demonstrated in Figure 6.2.1.

LPS	Ideal HKG Ct	Model GOI Ct	ΔCt	Fold change	Variable HKG Ct	New ΔCt	New Fold change
0	20	30	10	1	20	10	1
1	20	29	9	2	21	8	4
2.5	20	28	8	4	21	7	8
5	20	27	7	8	21	6	16

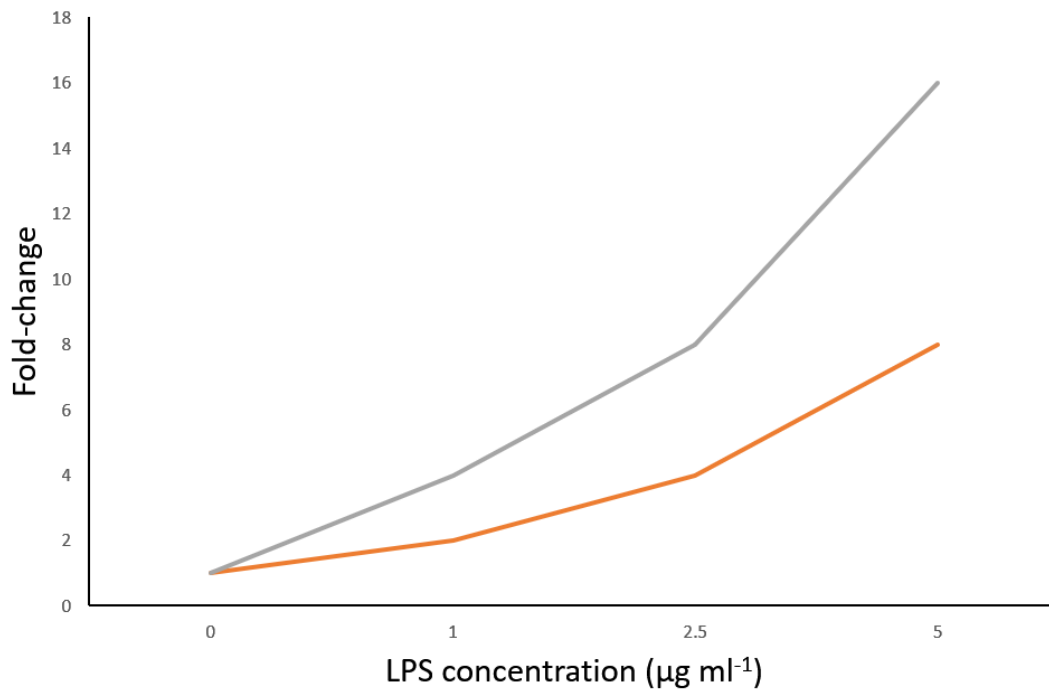


Figure 6.2.1 Gene expression in a model system: A small change in HKG expression has a large effect on fold change in the gene of interest (fold change = $2^{-\Delta\Delta Ct}$). In the table, the left side describes an ideal HKG which has the same Ct value at all concentrations of LPS. The model GOI of interest is affected by LPS with increased expression associated with increased LPS concentration. This is represented on a graph of fold-change by the orange line. On the right side of the table is what happens when the HKG expression increases by one cycle. The fold-change in apparent GOI expression is increased by a factor of 2^1 . This is represented by the grey line on the graph. Small changes in HKG expression can lead to large changes in apparent gene expression.

In reality, there is no perfect HKG, as extensively reviewed by Kozera and Rapacz in 2013.¹²⁵ HKGs that were previously believed to be fundamental to a cell's function have been demonstrated as having altered expression, with variations between tissues (GAPDH and B2M) and in the presence of disease. Even obesity can influence HKG expression. In samples of adipocytes from lean and obese individuals B2M and GAPDH (amongst other HKGs) demonstrated significant variability.¹²⁶ Accepting that HKGs are in fact variable, various algorithms exist that try to determine the most stable gene for specific experimental conditions. These include geNorm (one of the earliest), BestKeeper and NormFinder.^{77 127 128} However, these algorithms are different from one another, and therefore can and do produce different results.

The alternative technique to using HKGs for normalisation and measuring relative quantities is to use absolute calculations. Absolute quantification determines a gene's copy number by comparing it with a standard curve, created by serial dilutions of known concentrations of the test sequence. However, there are significant issues with absolute quantification. These include issues with RNA extraction, storage and maintenance of integrity, pipetting errors (small errors are amplified by PCR), variations in efficiency between samples during reverse transcription, as well as uncontrollable issues such as native reverse transcription and PCR polymerase inhibitors. Contamination can also occur from ribosomal RNA. Relative quantification using HKGs controls for these issues.

The consequence of these concerns with both absolute quantification and relative quantification was the publication of MIQE guidelines.⁸⁰ Normalisation to reference genes requires absolute validation of their stability, either through standard curve analysis, or through robust analysis of stability. Authors in this area now advocate using three reference genes, three stability programs and three repeats for each genotype.^{129–}

131

The choice of HKGs in this thesis do not meet current recommendations. Whilst the data do match other published results, further work in this area requires a more robust assessment of HKGs in PMNs in an LPS-stimulated experimental model. That said, the data presented in this thesis is consistent with other published work, and at the very least points to an important association of NOP receptor expression and LPS.

6.3. Development of a novel bioassay

The experiments investigating gene expression for transcripts of the nociceptin system provided supportive data of NOP modulation and suggested that PMNs would be an important area for further research. The low levels of predominately eosinophil ppNOC expression also warranted further investigation. Additionally, the experiments had

enabled an assessment and development of leukocyte isolation techniques that would be useful in developing a bioassay to assess the nociceptin system in immunocytes.

The study of N/OFQ release from immune cells remains difficult. As discussed in Chapter 1.10, ELISA-based techniques have been unsuccessful in our laboratory, despite forming the basis of an intercalated BSc project using in-house and commercially available N/OFQ antibodies.⁷¹ Mass spectrometry and ELISA have been reported as being successful by Fiset and colleagues.²³ However, these data have not been replicated. Further, the establishment of an effective bioassay would enable our group to investigate other cells, as well as observe cellular interactions contributing to the release of N/OFQ.

The work in this thesis has described the development of a confocal microscopy-based bioassay (see Figure 6.1.1). The key stages in this development were first, identification and testing of a suitable biosensor, then confirming that viable PMNs could be imaged and stimulated, followed by co-imaging of live PMNs and biosensors. Key to this system was the confocal microscope and perfusion system, the details of which are described in Chapter 4.4.

6.3.1. Biosensors

The concept of biosensors is not new and they are widely used in the food industry. The term biosensor refers to 'analytical devices that convert a biological response into an electrical signal'.¹³² The assay developed in this thesis does not strictly meet this definition, but it can be thought of a device (confocal microscope) that uses a biological sensor (CHO cell) that converts a biological response (activation of NOP by N/OFQ) into an electrical signal (a release of light that is detected by the confocal photodetectors and electrically converted to a digital image). Key to this assay was the use of CHO cells transfected to express the human NOP receptor with a chimeric G-protein.

The measurement of calcium signalling using fluorimeters together with calcium-sensitive fluorophores forms the basis of identifying novel GPCR ligands. G_i coupled receptors (e.g. NOP), however, decrease intracellular calcium by inhibition of the production of cAMP from ATP. To overcome this chimeric G proteins have been developed. High throughput screening studies have demonstrated that NOP (and other opioid) receptors co-expressed with chimeric $G\alpha_q$ proteins will signal through G_q and that N/OFQ retains full agonist activity.⁹³ The G_q intracellular pathway is phospholipase C (PLC) which, when activated by agonist binding, cleaves phosphatidylinositol 4,5-bisphosphate (PIP₂) into diacyl glycerol (DAG) and inositol 1,4,5-triphosphate (IP₃). IP₃ binds to IP₃ receptors on calcium channels in the endoplasmic reticulum of the cell, resulting in cytosolic increases in calcium. CHO cells successfully transfected to express the human NOP receptor coupled with $G\alpha_{i/q}$ have been demonstrated to respond to full and partial agonists, as well as antagonists, in studies using fluorimetry.⁸⁹

In this thesis the suitability of CHO- $G\alpha_{i/q}$ cells for use as a biosensor was studied. Data using fluorimetry demonstrated that these cells do fluoresce when appropriately loaded with Fura-2 and stimulated with exogenous N/OFQ. Further, confocal experiments demonstrated that the modified CHO cells in the main remained viable within the perfusion system and reactive to N/OFQ, demonstrated by Fluo-4 mediated changes in fluorescence. In both fluorimetry and confocal imaging CHO- $G\alpha_{i/q}$ cells were seen to increase intracellular calcium concentrations in response to N/OFQ.

However, as previously discussed in Chapter 5, the response of the CHO-biosensors to N/OFQ was variable, particularly in cuvette-based fluorimetry. One reason relates to fluorophore leakage. CHO cells natively have organic-anion transporters in the cell membrane that extrude dye back into the perfusing solution. The result is that background fluorescence increases (because of calcium within the Krebs-HEPES solution) whilst intracellular calcium-mediated fluorescence is diminished, with the net effect of reduced detectable fluorescence in response to increased intracellular calcium. This extrusion can be blocked with addition of probenecid which is a specific inhibitor of

non-specific anion transport. However, probenecid can be toxic to cells and it potentially could have affected PMN function. There are some data suggesting PMN lysosomal enzyme secretion is inhibited by probenecid, although other authors investigating PMN function have used probenecid without adverse effects.^{133–135} Additionally probenecid has agonist actions on the TRPV2 receptor which could affect interpretation of PMN activation.¹³⁶ TRPV receptors are associated with receptor and store operated calcium entry in PMNs, with rises in intracellular calcium associated with neutrophil activation.^{137–140} Investigating whether probenecid enhances or disrupts the assay would be useful.

Another reason for the variable response of the CHO-biosensors could relate to uneven expression of NOP receptors. Whilst transfection is an established process for forcing CHO cells to express human receptors, receptor expression can be uneven. For example, a study by Bjork, Vainio and Scheinin in 2005 demonstrated uneven cellular expression of α_{2A} -adrenoceptors in transfected CHO cells.¹⁴¹ Such uneven distribution could have a significant effect when studying individual CHO-biosensor cell responses to PMN degranulation.

There are technical aspects that may have affected the response of the CHO-biosensors to N/OAQ. For example, loading of Fluo-4 may have been uneven, or CHO cells may have become less viable during the transfer process from incubation to the microscope. Initial experiments were also affected by over-confluence of cells affecting the ability to distinguish between single CHO cells. Some of these factors improved with experience in using this assay. Issues with variable responses however remained. This necessitated modification of planned experiments as described in Chapter 5, and the use of the biosensors as a binary system.

Supernatant experiments required the use of the same CHO cells over time. Cells were successfully stimulated with the supernatant of fMLP-degranulated PMNs in the

presence or absence of antagonists. There was, however, an appreciable fall in the responsiveness of the CHO-biosensors over time. It is probable that this represents receptor desensitisation. GPCRs are known to desensitise – that is the response to agonist binding diminishes with repeated or prolonged administration.¹⁴² Molecular mechanisms include G-protein coupled receptor kinase (GRK) phosphorylation of the activated receptor, arrestins, and receptor downregulation. It has previously been established that both native purinergic receptors and NOP receptors demonstrate desensitisation.^{110 111 113 143} This thesis did not specifically study this, but could be studied in future experiments.

6.3.2. Imaging of viable PMNs

This thesis has demonstrated the successful isolation and imaging of live, viable human polymorphonuclear cells that demonstrate activation and morphological changes following fMLP administration. PMNs are notoriously difficult to work with. They have a short life-span, are highly reactive, and unstimulated are non-adherent. That said, recent years have seen a few publications of live-imaging data of neutrophils fluorescence (including confocal) microscopy. For example, live imaging using confocal microscopy and an environmental chamber has been used to study interactions of murine neutrophils with *Cryptococcus neoformans* with real-time images of neutrophil migration and phagocytosis.¹⁴⁴ Another study has examined the response of human immune cells to labelled fungal spores, and NETosis (a form of neutrophil cell death in which bactericidal neutrophil extracellular traps are released) has been visualised in neutrophils in response to various stimulants (including LPS, PMA, and live bacteria).¹⁴⁵¹⁴⁶ However, using live cell imaging to demonstrate the release of peptide from PMNs to act on a fluorescent biological sensor is unique.

Isolation of PMNs was achieved using PolymorphPrep™. The technology for isolating purified cells has previously been described, but other density gradient techniques are recorded in the literature. These include using Dextran-500 to aggregate erythrocytes followed by Ficoll®-Hypaque, as well as Ficoll-Paque™ PLUS with an erythrocyte lysis

step.¹⁴⁷ However, the advantage of the PolymorphPrep™ technique was that it was relatively quick (approximately 90 minutes in total). PMNs should be used the same day as isolation, and ideally as soon as possible, if they are to remain viable. Using a relatively rapid isolation technique increased the time available for confocal experiments. Further, total cell yields are less important in confocal experiments because only a small number of cells can be imaged at a time. Previous work using this technique in our laboratory had demonstrated >94% purity of PMNs determined by FACS.⁶⁹ Viability of the cells was most easily assessed using the confocal microscope, where visual fluorescent responses to fMLP confirmed viability.

Adherence of PMNs was predicted to be a significant challenge. The literature suggests various techniques for adhering motile PMNs to coverslips. These include coating coverslips with fresh human serum, poly-lysine or fibrinogen.^{148 149} In this thesis Cell-Tak™ - a cell adhesive composed of polyphenolic proteins derived from mussels – was used. An advantage of Cell-Tak™ is that coverslips can be coated ahead of time and stored, improving assay efficiency. Further, the co-imaging assay required 48 hours of CHO culture on coated coverslips. The data from Chapter 5 suggest that despite this period of incubation, Cell-Tak™ could successfully adhere PMNs. There also did not appear to be a significant impact on CHO growth.

In this confocal assay Fluo-4 was used as the calcium indicator in both PMNs and CHO-cells, with increased intracellular calcium being used as an indicator of cell activation. This simplified the assay, minimising confounders when assessing its feasibility. However, future experiments could consider immunostaining PMNs with antibodies to either cell surface markers or intracellular components. This would allow better identification of neutrophils and distinguish them from eosinophils or other cellular contaminants. Further, immunostaining could allow identification of neutrophil cytosolic components key to their antimicrobial function and release of reactive oxygen species. For example, neutrophils can be stained to detect NADPH oxidase subunits p22^{phox} and p67^{phox} and changes in their response to stimulation assessed.^{150 151}

As discussed in Chapter 5.3 measurement of PMN fluorescence over time could be challenging. Some PMNs demonstrated significant motility with stimulation by fMLP and most underwent morphological change. AUC analysis was used to identify cells that appeared to fluoresce by identification of peak fluorescence over time, but this method either incorrectly identify or miss fluorescence peaks in migratory cells. Further, if peaks in fluorescence followed a rapidly diminishing baseline, or the cells demonstrated fluorescence prior to fMLP stimulation, genuine fMLP associated peaks could be missed altogether. This necessitated manual checking of data for each cell against graphs of fluorescence and live cell images. One option would be to perform non-linear regression on individual cell responses to flatten the baseline. However, in the context of over 1000 cells this would be very laborious, although could be made easier through use of scripts in software like R or MATLAB.

Another solution to this issue is to use different analysis to AUC. The difficulty was identifying significant deflections in fluorescence values from a variable, decreasing baseline that sometime contained small peaks, in a large number of cells. One approach briefly explored is to mathematically fit a curve to the average fluorescence values for all the cells, and then measure how well the fluorescence response of individual cells matches the same shaped curve applied to all cells. Amongst the various options for curve fitting provided by non-linear regression models in GraphPad Prism, is a sigmoid curve that that can be set to start immediately prior to stimulation and ends just after a peak value is reached. The model can be constrained to ensure the curve starts above a defined baseline value. Setting the curve immediately prior to stimulation removes the issue of a varying baseline; setting a bottom constraint to be greater than background fluorescence identifies those activated PMNs that move into ROI following stimulation. Where the model curve does not fit the fluorescence response of a cell (defined by an $R^2 < 0.5$) identifies that cell as not responding to stimulation. The use of curve fitting is summarised in Figure 6.3.1. Further work would help establish this technique or whether alternative non-linear regression models (e.g. segmental line) would better fit the graphs of fluorescence.

Alternatively, there is commercial software available that better identifies peaks, for example, MATLAB (MathWorks, Massachusetts, USA). Better identification of responding cells would improve the speed of analysis, and the quality and confidence in acquired fluorescence peaks.

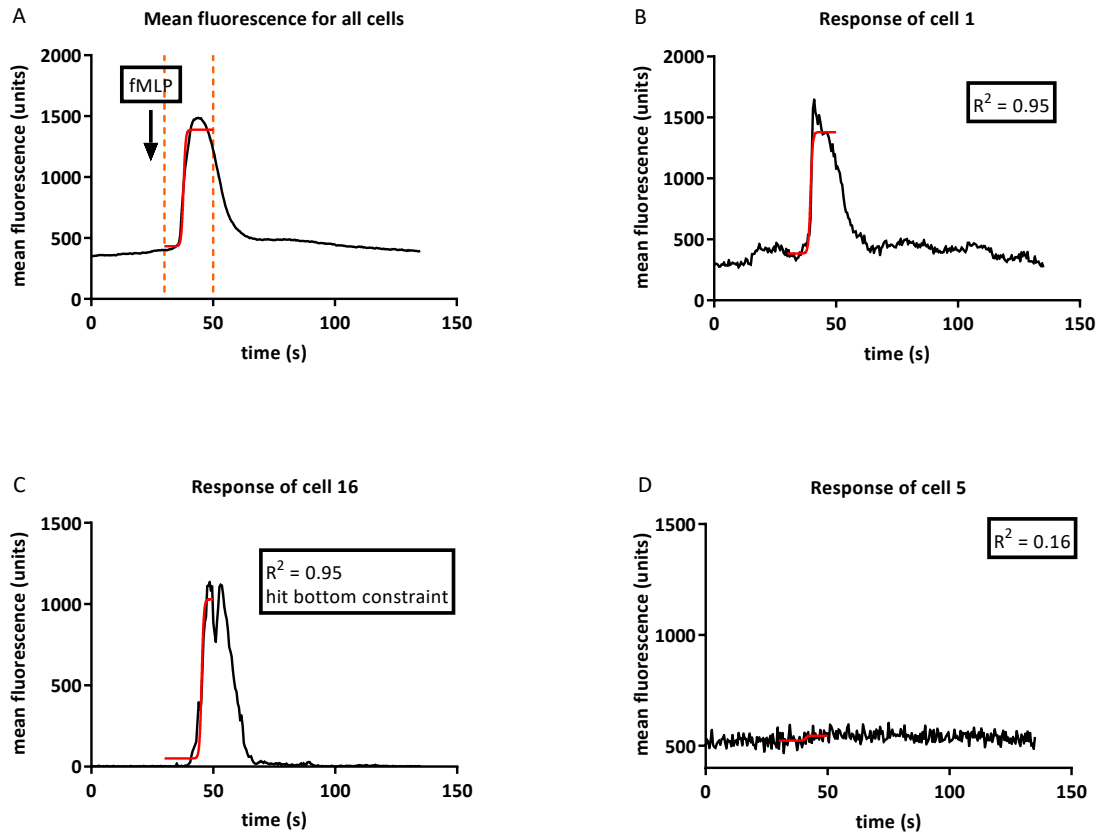


Figure 6.3.1 Sigmoid curves superimposed on graphs to help identify genuinely responding PMNS to fMLP. In A is a graph from which the sigmoid curve is defined: constraints of x between 30 – 50, and a bottom constraint of 50. B is a cell response that meets criteria of $R^2 > 0.5$. Graph C is typical of a cell that moved into measurement range after fMLP stimulation. The bottom constraint identifies this cell as moving into a ROI. In D, the cell has a noisy background fluorescence and does not respond to fMLP. R^2 is far below 0.5 and identified as a non-responder.

In the study of PMN responses to fMLP the calcium indicator Fluo-4 was used. It is conceivable that Fluo-4 either initiated or affected PMN fMLP-associated responses. For example, fluorescent probes, such as BODIPY, have previously been determined as acting as agonists.¹⁵² However, Fluo-4 has been successfully used in other fluorescent experiments of neutrophils, and the data from this confocal bioassay suggests that any Fluo-4 indicator induced fluorescence was minor compared with fMLP.¹⁵³

This confocal assay used fMLP to stimulate PMNs. It is a well-studied, and potent chemotactant and degranulator of PMNs that acts on formyl peptide receptors to increase intracellular calcium.¹⁵⁴ Alternative stimulants are phorbol myristate (PMA, an activator of protein kinase C) and TLR4 receptor agonists like LPS that could be studied in future experiments. One reason for not using LPS in this assay is that the actions of LPS are not specific to PMNs, and the confocal equipment and perfusion system was shared by other research teams. It was important that the perfusion system was not contaminated, but future experimental protocols could involve a thorough decontamination of equipment. Regarding fMLP, Fiset and colleagues reported that fMLP on its own does not fully degranulate PMNs.²³ These authors determined that the addition of cytochalasin B (a mycotoxin) was necessary for the exocytosis of primary and secondary granules from neutrophils. It may be that when co-imaging PMNs and CHO-biosensors the lack of cytochalasin B affected N/OAQ release. However, experiments using supernatants for fMLP-stimulated PMNs did not utilise cytochalasin B, yet data suggest that N/OAQ was present in these supernatants. It would be useful to assess whether cytochalasin B enhances PMN-CHO G $\alpha_{i/q}$ responsiveness in future work.

6.3.3. Co-imaging

The final stage of bioassay development was the co-imaging of CHO-biosensors and PMNs. As discussed, the addition of Cell-Tak™ enabled the co-location of PMNs and CHO-biosensors, and the use of Fluo-4 allowed visualisation of calcium signalling in both CHO-biosensors and PMNs. This is the first description of a bioassay using confocal imaging for the study of NOP GPCR stimulation in the presence of human immune cells. The data in this thesis are supportive of N/OAQ being released from PMNs, and confirm the findings of Fiset and colleagues.²³ Not only has data been presented that demonstrates PMN-CHO interaction, but also that the fMLP-stimulated PMN secretions contain N/OAQ.

A significant issue with co-imaging of PMNs and CHO-biosensors was the very thin focal plane used in confocal microscopy, as discussed in Chapter 4.8. This could potentially

have been improved by allowing more time for PMNs to settle on the coverslip, although this must be weighed against maintenance of PMN viability and loading at environmental conditions of 37°C. Minimising confluence of CHO cells is important to successful co-imaging, and it is possible 48 hours cell growth was too long and better images would be achieved by a growth time of 24 hours.

In these co-imaging experiments the response of CHO-biosensors to fMLP-induced degranulation was not universal, with 14% of CHO-cells responding across all experiments (84% responded to exogenous N/OFQ). Some of this variable response could be due to some of the points described above, i.e. not using probenecid, uneven NOP receptor distribution, absence of cytochalasin B. However, it could indicate that neutrophils are not the source of N/OFQ peptide. The PMNs isolated in these experiments comprised a mixed population of neutrophils and eosinophils, of which eosinophils would be expected to comprise approximately 10%.¹⁰⁵ Combined with the gene expression data, where ppNOC was predominately identified in eosinophils and not at all in neutrophils, suggests that it is the eosinophils that release N/OFQ. Unpublished work from our laboratory that developed following data from this thesis suggests that this may be true. An extracellular signal-related kinase 1/2 (ERK1/2) coupling assay was used with a human cell eosinophil precursor cell line EoL-1 (shown to express NOP and ppNOC). ERK1/2 (previously MAPK) are protein kinases fundamental to cell growth and division, and demonstrate increased activity in response to N/OFQ acting on the NOP receptor of CHO-hNOP cells.¹⁵⁵ Incubating the EoL-1 cells with a NOP antagonist (SB-612,111) resulted in lower basal levels of ERK1/2 and the cells became sensitive to exogenous N/OFQ (see Figure 6.3.2).

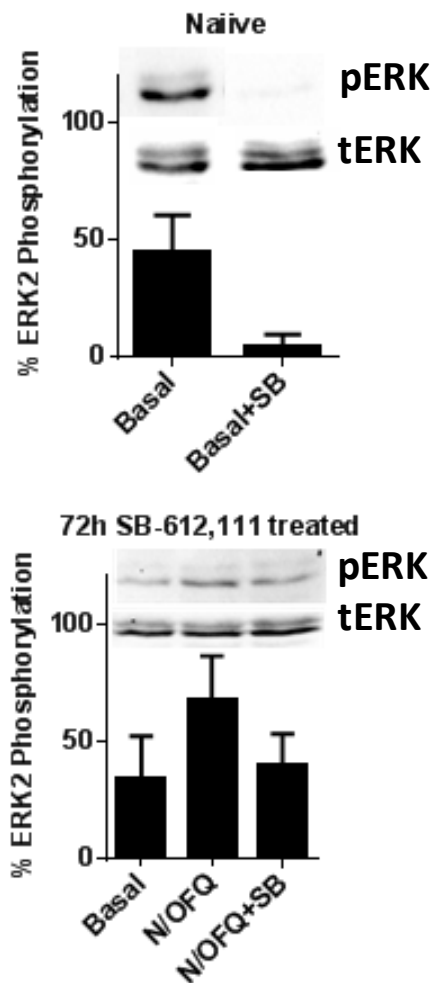


Figure 6.3.2 ERK1/2 phosphorylation (pERK = phosphorylated ERK, tERK = total ERK) in EoL-1 cells was reduced compared with basal levels in the presence of the NOP antagonist SB-612,111. This suggests that EoL-1 cells release N/OAQ that activates NOP receptors to increase basal phosphorylation. Exogenous N/OAQ raises phosphorylation in SB-612,111 treated cells.

These data come from cultured cells, but data from Singh and colleagues in human airway eosinophils (ppNOC expression found on eosinophils and loosely correlates with sputum N/OAQ concentrations) adds further supporting information.²⁷

The concept of eosinophils releasing signalling molecules is not new. For example, eosinophils have been demonstrated as releasing Major Basic Protein that activates neutrophils, and more recently eosinophils have been shown to release protective mediators that inhibit neutrophil migration in a murine model of acute colitis.^{156 157} How

could eosinophils regulate neutrophil function in the nociceptin system? Data from Serhan and colleagues demonstrated that N/OFQ is chemotactic, and Trombetta and colleagues demonstrated that N/OFQ stimulates PMN lysozyme production and significant chemotaxis in monocytes (see Chapter 1.4).^{24 25} However, data from Al-Hashimi and colleagues, suggest that N/OFQ inhibits neutrophil chemotaxis.¹⁵⁸ Eosinophils may then release N/OFQ to modulate neutrophil recruitment to sites of inflammation (see Figure 6.3.3). It is also clinically feasible that eosinophils are a source of N/OFQ. For example, eosinopaenia has been associated with poor outcomes in patients with sepsis, and laboratory work has confirmed that eosinophils have an increasingly recognised role in the host's response to pathogens.^{159–162} More work in this area is required to fully understand how N/OFQ integrates the function of granulocytes. Furthermore, ppNOC transcripts have been determined in lymphocytes and monocytes, suggesting they too secrete N/OFQ.^{21 22} Lymphocyte and macrophage signalling of granulocytes is well documented, and their release of N/OFQ could be further studied using this bioassay.^{34 163}

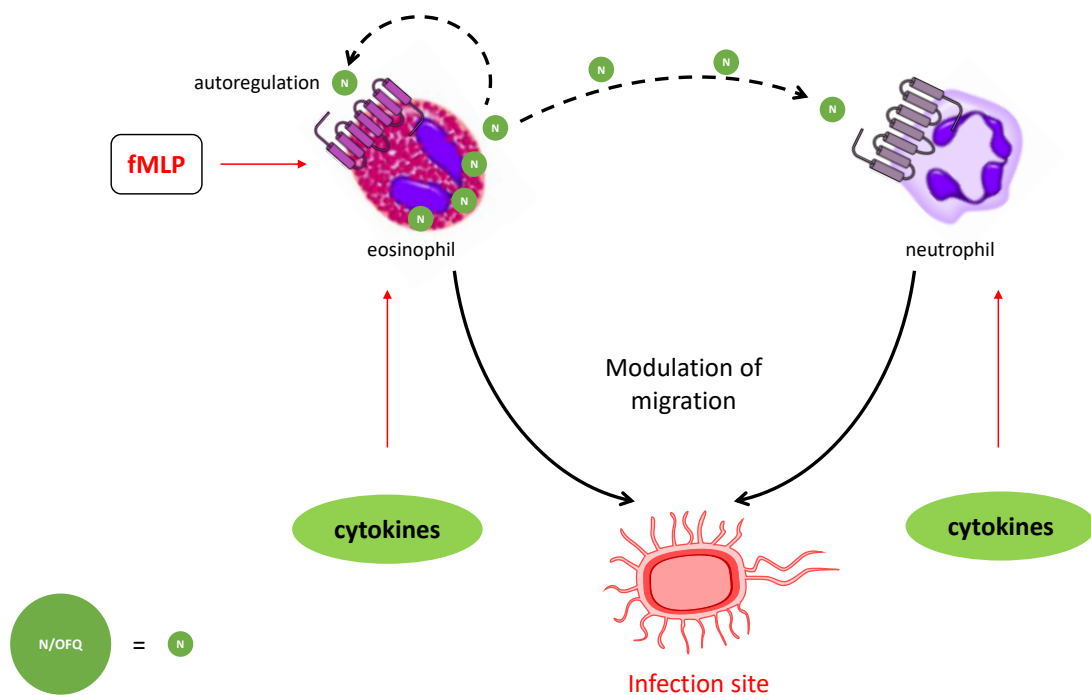


Figure 6.3.3 Eosinophil regulation of neutrophils. A possible regulatory function of eosinophils could be the release of N/OFQ to regulate neutrophil migration to the site of injury or infection. N/OFQ has been demonstrated to induce and prevent chemotaxis in neutrophils (Serhan 2001, Al-Hashimi 2015).^{24 158} Further data are required to fully elucidate the effect of N/OFQ on neutrophil migration.

6.3.4. Supernatant experiments

Chapter 5.5 demonstrated that the supernatant of fMLP-stimulated PMNs increased intracellular calcium in CHO-biosensors. This effect could be attenuated by an antagonist to the NOP receptor (TRAP-101), by a combination of TRAP-101 and a non-specific antagonist to P2 receptors (PPADS), but not by PPADS alone. This suggests that the supernatant contains N/OFQ peptide. Further, there was some preliminary evidence for receptor desensitisation, with repeated administrations of supernatant in the presence and absence of antagonists reducing CHO-biosensor fluorescence. Whilst these data need to be taken in the context of the issues described previously, there was a statistically significant difference in fluorescence response between CHO-cells perfused with TRAP-101 compared with PPADS.

These supernatant data were necessary because of the native expression by CHO cells of purinergic receptors that increase intracellular calcium in response to nucleotides (e.g. ATP, ADP). As discussed in Chapter 5.5, PPADS is not an ideal antagonist. Whilst its low selectivity means that it can block both P2Y and P2X receptors, it has low potency and slow kinetics. It is possible residual blockade persisted in experiments where PPADS was used as the first antagonist. This would mean that in those experiments the biosensors were in effect blocked by both PPADS and TRAP-101 during subsequent perfusion with TRAP-101. However, the data from those experiments suggest that CHO responses were minimally affected by PPADS alone; N/OFQ-mediated calcium signalling was predominant. Alternatives to PPADS including using apyrase to degrade nucleotides within the supernatant, or a combination of PPADS and a specific P2X antagonist like oxidised ATP (oATP).

There was an indication in the confocal experiments that CHO receptors, both purinergic and hNOP, underwent desensitisation, as discussed above. The decrease in responsiveness, however, may have been due to phototoxicity or reduced viability of the cells in the perfusion system. The main implication of this was that the supernatant experiments became limited in time, and that TRAP-101 was used most frequently as the first antagonist as it appeared most effective at blocking the stimulatory actions of supernatant. Whilst further studies could be performed on the NOP receptor in this model, there are already published data confirming the presence and mechanisms of NOP desensitisation.^{113 143}

6.4. Further work

The conclusions and discussion from this thesis point to important areas of further research to clarify and confirm the presented findings. First in assessing the genomic response to LPS and other mimics of sepsis, a thorough and robust validation of housekeeping or reference genes should be undertaken. Ideally this should be performed in purified subpopulations of granulocytes isolated either by MACS or FACS, and from whole blood samples that had been exposed to concentrations of LPS. It would

also be useful to compare the results of whole blood mRNA expression and isolated granulocyte expression. These data could form the basis of a larger clinical observational study of patients admitted to ICU with a diagnosis of sepsis according to Sepsis-3 criteria. Comparing the results of whole blood mRNA with isolated granulocyte mRNA would help make sense of the conflicting results of Stamer and Thompson.^{69 70}

There are areas of the confocal bioassay that can be refined, particularly with regards the variable response of the CHO-biosensors. In the first instance, assessing whether the addition of probenecid improves measured fluorescence would be a relatively simple first step. Beyond that, analysing surface expression of the hNOP- $G\alpha_{i/q}$ receptor could help identify those CHO cell passages with the most even distribution of receptor. Having established a more reliable biosensor response, concentration-response curves could be generated at the start of each experiment.

Examination of N/OFQ secretion from granulocytes could then proceed. Granulocytes could be purified (MACS would be most feasible), and / or immunofluorescence markers used with different lasers in the confocal system to identify different types of granulocyte. Different stimulants of neutrophils and eosinophils could be used (e.g. PMA, LPS, RANTES), and cytochalasin B added to fMLP-treated samples. The data in this thesis demonstrated a significant response to ATP by CHO-biosensors, so either more specific antagonists of P2 receptors and / or apyrase could be added to the perfusion system when performing co-imaging experiments.

Finally, data analysis of fluorescent responses could be enhanced. Assuming non-confluent CHO-biosensor samples, automated identification of cells is possible within ImageJ and other software. These techniques find the edges of cells by comparing pixel colour and marks edges in areas of high contrast (e.g. between black and green). Further, this allows measurement of fluorescence from the whole cell, as opposed to a region of interest within the cytoplasm as described in this thesis. Peak analysis using

software such as MATLAB or analysis of non-linear regression would assist the throughput of data generated from these experiments.

6.5. Concluding thoughts

This thesis has established for the first time a viable and reproducible live cell assay for observing and measuring real-time single cell release of N/OFQ from PMNs. Further, data from this assay, as well as information gleaned from studying mRNA expression in PMNs and individual granulocyte populations, has raised the intriguing question of whether eosinophils are the source of PMN-secreted N/OFQ peptide. Traditionally eosinophils have been viewed as having a relatively minor role in the host's acute immune response to pathogens. It is, however, becoming increasingly recognised that they have an important immunomodulatory function demonstrated by complex interactions with other leukocytes. Similarly, there is an increasing appreciation that the nociceptin system has an important immunomodulatory function in sepsis and inflammation. This bioassay enables visualisation of single cell release and cell signalling, and forms the basis of ongoing studies examining N/OFQ and leukocytes. These studies will further develop the assay, and perhaps answer the follow-up question: N/OFQ and which granulocyte?

7. References

1. Daniels R, UK Sepsis Trust. Survive sepsis: the official training programme of the UK Sepsis Trust. Sutton Coldfield: UK Sepsis Trust; 2014.
2. Alexander SP, Christopoulos A, Davenport AP, et al. THE CONCISE GUIDE TO PHARMACOLOGY 2017/18: G protein-coupled receptors. *Br J Pharmacol* 2017; **174 Suppl 1**: S17–129
3. Reinscheid RK, Nothacker HP, Bourson A, et al. Orphanin FQ: a neuropeptide that activates an opioidlike G protein-coupled receptor. *Science* 1995; **270**: 792–4
4. Meunier JC, Mollereau C, Toll L, et al. Isolation and structure of the endogenous agonist of opioid receptor-like ORL1 receptor. *Nature* 1995; **377**: 532–5
5. Henderson G, McKnight AT. The orphan opioid receptor and its endogenous ligand--nociceptin/orphanin FQ. *Trends Pharmacol Sci* 1997; **18**: 293–300
6. McDonald J, Lambert D. Opioid receptors. *BJA Educ* 2015; **15**: 219–24
7. Lambert DG. The nociceptin/orphanin FQ receptor: a target with broad therapeutic potential. *Nat Rev Drug Discov* 2008; **7**: 694–710
8. Szalay F, Hantos MB, Horvath A, et al. Increased nociceptin/orphanin FQ plasma levels in hepatocellular carcinoma. *World J Gastroenterol* 2004; **10**: 42–5
9. McDonald J, Leonard AD, Serrano-Gomez A, et al. Assessment of nociceptin/orphanin FQ and micro-opioid receptor mRNA in the human right atrium. *Br J Anaesth* 2010; **104**: 698–704
10. Chiou LC, Liao YY, Fan PC, et al. Nociceptin/orphanin FQ peptide receptors: pharmacology and clinical implications. *Curr Drug Targets* 2007; **8**: 117–35
11. King MA, Rossi GC, Chang AH, Williams L, Pasternak GW. Spinal analgesic activity of orphanin FQ/nociceptin and its fragments. *Neurosci Lett* 1997; **223**: 113–6
12. Sakurada T, Katsuyama S, Sakurada S, et al. Nociceptin-induced scratching, biting and licking in mice: involvement of spinal NK1 receptors. *Br J Pharmacol* **127**: 1712–8
13. Ko M-C, Naughton NN. Antinociceptive effects of nociceptin/orphanin FQ administered intrathecally in monkeys. *J Pain Off J Am Pain Soc* 2009; **10**: 509–16
14. Ding H, Hayashida K, Suto T, et al. Supraspinal actions of nociceptin/orphanin FQ, morphine and substance P in regulating pain and itch in non-human primates. *Br J Pharmacol* 2015; **172**: 3302–12
15. Chuang TK, Killam KF, Chuang LF, et al. Mu opioid receptor gene expression in immune cells. *Biochem Biophys Res Commun* 1995; **216**: 922–30

16. Williams JP, Thompson JP, McDonald J, et al. Human peripheral blood mononuclear cells express nociceptin/orphanin FQ, but not mu, delta, or kappa opioid receptors. *Anesth Analg* 2007; **105**: 998–1005, table of contents
17. Mellon RD, Bayer BM. The effects of morphine, nicotine and epibatidine on lymphocyte activity and hypothalamic-pituitary-adrenal axis responses. *J Pharmacol Exp Ther* 1999; **288**: 635–42
18. McCarthy L, Wetzel M, Sliker JK, Eisenstein TK, Rogers TJ. Opioids, opioid receptors, and the immune response. *Drug Alcohol Depend* 2001; **62**: 111–23
19. Hussey HH, Katz S. Infections resulting from narcotic addiction; report of 102 cases. *Am J Med* 1950; **9**: 186–93
20. Charles A Janeway J, Travers P, Walport M, Shlomchik MJ. Principles of innate and adaptive immunity. *Immunobiol Immune Syst Health Dis 5th Ed* 2001;
21. Williams JP, Thompson JP, Rowbotham DJ, Lambert DG. Human peripheral blood mononuclear cells produce pre-pro-nociceptin/orphanin FQ mRNA. *Anesth Analg* 2008; **106**: 865–6, table of contents
22. McDonald J, Howells LM, Brown K, Thompson JP, Lambert DG. Use of preparative fluorescence activated cell sorting (FACS) to profile opioid receptor and peptide mRNA expression on human granulocytes, lymphocytes and monocytes. *Br J Anaesth* 2010; **105**: 707
23. Fiset M-E, Gilbert C, Poubelle PE, Pouliot M. Human neutrophils as a source of nociceptin: a novel link between pain and inflammation. *Biochemistry* 2003; **42**: 10498–505
24. Serhan CN, Fierro IM, Chiang N, Pouliot M. Cutting edge: nociceptin stimulates neutrophil chemotaxis and recruitment: inhibition by aspirin-triggered-15-epi-lipoxin A4. *J Immunol Baltim Md 1950* 2001; **166**: 3650–4
25. Trombella S, Vergura R, Falzarano S, Guerrini R, Calo G, Spisani S. Nociceptin/orphanin FQ stimulates human monocyte chemotaxis via NOP receptor activation. *Peptides* 2005; **26**: 1497–502
26. Anton B, Leff P, Meissler JJ, et al. Nociceptin/orphanin FQ suppresses adaptive immune responses in vivo and at picomolar levels in vitro. *J Neuroimmune Pharmacol Off J Soc Neuroimmune Pharmacol* 2010; **5**: 143–54
27. Singh SR, Sullo N, Matteis M, et al. Nociceptin/orphanin FQ (N/OFFQ) modulates immunopathology and airway hyperresponsiveness representing a novel target for the treatment of asthma. *Br J Pharmacol* 2016; **173**: 1286–301
28. Kato S, Tsuzuki Y, Hokari R, et al. Role of nociceptin/orphanin FQ (Noc/oFFQ) in murine experimental colitis. *J Neuroimmunol* 2005; **161**: 21–8

29. Brookes ZLS, Stedman EN, Guerrini R, Lawton BK, Calo G, Lambert DG. Proinflammatory and vasodilator effects of nociceptin/orphanin FQ in the rat mesenteric microcirculation are mediated by histamine. *Am J Physiol Heart Circ Physiol* 2007; **293**: H2977-2985
30. Giuliani S, Tramontana M, Lecci A, Maggi CA. Effect of nociceptin on heart rate and blood pressure in anaesthetized rats. *Eur J Pharmacol* 1997; **333**: 177-9
31. Singer M, Deutschman CS, Seymour CW, et al. The Third International Consensus Definitions for Sepsis and Septic Shock (Sepsis-3). *JAMA* 2016; **315**: 801-10
32. Thomas L. Germs. *N Engl J Med* 1972; **287**: 553-5
33. Hotchkiss RS, Karl IE. The pathophysiology and treatment of sepsis. *N Engl J Med* 2003; **348**: 138-50
34. Jean-Baptiste E. Cellular Mechanisms in Sepsis. *J Intensive Care Med* 2007; **22**: 63-72
35. Tidswell M, Tillis W, LaRosa SP, et al. Phase 2 trial of eritoran tetrasodium (E5564), a Toll-like receptor 4 antagonist, in patients with severe sepsis *. *Crit Care Med* 2010; **38**: 72-83
36. Devi Ramnath R, Weing S, He M, et al. Inflammatory mediators in sepsis: Cytokines, chemokines, adhesion molecules and gases. *J Organ Dysfunct* 2006; **2**: 80-92
37. Rittirsch D, Hoesel LM, Ward PA. The disconnect between animal models of sepsis and human sepsis. *J Leukoc Biol* 2007; **81**: 137-43
38. Walley KR, Lukacs NW, Standiford TJ, Strieter RM, Kunkel SL. Balance of inflammatory cytokines related to severity and mortality of murine sepsis. *Infect Immun* 1996; **64**: 4733-8
39. Abraham E, Wunderink R, Silverman H, et al. Efficacy and safety of monoclonal antibody to human tumor necrosis factor alpha in patients with sepsis syndrome. A randomized, controlled, double-blind, multicenter clinical trial. TNF-alpha MAbs Sepsis Study Group. *JAMA* 1995; **273**: 934-41
40. FDA. Xigris [drotrecogin alfa (activated)]: Market Withdrawal - Failure to Show Survival Benefit [Internet]. 2011 [cited 2013 Jan 1]. Available from: <http://www.fda.gov/Safety/MedWatch/SafetyInformation/SafetyAlertsforHumanMedicalProducts/ucm277143.htm>
41. Bernard GR, Vincent JL, Laterre PF, et al. Efficacy and safety of recombinant human activated protein C for severe sepsis. *N Engl J Med* 2001; **344**: 699-709

42. Cavaillon J-M, Adib-Conquy M, Cloëz-Tayarani I, Fitting C. Review: Immunodepression in sepsis and SIRS assessed by ex vivo cytokine production is not a generalized phenomenon: a review. *J Endotoxin Res* 2001; **7**: 85–93
43. Silhavy TJ, Kahne D, Walker S. The bacterial cell envelope. *Cold Spring Harb Perspect Biol* 2010; **2**: a000414
44. Brinkmann V. Neutrophil Extracellular Traps Kill Bacteria. *Science* 2004; **303**: 1532–5
45. Hayashi F, Means TK, Luster AD. Toll-like receptors stimulate human neutrophil function. *Blood* 2003; **102**: 2660–9
46. Kumar A, Ray P, Kanwar M, Sharma M, Varma S. A comparative analysis of antibody repertoire against *Staphylococcus aureus* antigens in Patients with Deep-Seated versus Superficial staphylococcal Infections. *Int J Med Sci* 2005; **2**: 129–36
47. Perianayagam MC, Balakrishnan VS, Pereira BJG, Jaber BL. C5a delays apoptosis of human neutrophils via an extracellular signal-regulated kinase and Bad-mediated signalling pathway. *Eur J Clin Invest* 2004; **34**: 50–6
48. Arraes SMA, Freitas MS, Silva SV da, et al. Impaired neutrophil chemotaxis in sepsis associates with GRK expression and inhibition of actin assembly and tyrosine phosphorylation. *Blood* 2006; **108**: 2906–13
49. Unsinger J, McDonough JS, Shultz LD, Ferguson TA, Hotchkiss RS. Sepsis-induced human lymphocyte apoptosis and cytokine production in “humanized” mice. *J Leukoc Biol* 2009; **86**: 219–27
50. Fink MP, Heard SO. Laboratory models of sepsis and septic shock. *J Surg Res* 1990; **49**: 186–96
51. Ayala A, Deol ZK, Lehman DL, Herdon CD, Chaudry IH. Polymicrobial Sepsis but Not Low-Dose Endotoxin Infusion Causes Decreased Splenocyte IL-2/IFN- γ Release While Increasing IL-4/IL-10 Production. *J Surg Res* 1994; **56**: 579–85
52. Fink MP. Animal models of sepsis. *Virulence* 2014; **5**: 143–53
53. Seok J, Warren HS, Cuenca AG, et al. Genomic responses in mouse models poorly mimic human inflammatory diseases. *Proc Natl Acad Sci U S A* 2013; **110**: 3507–12
54. Hubbard WJ, Choudhry M, Schwacha MG, et al. Cecal Ligation And Puncture. *Shock* 2005; **24**: 52–7
55. Eskandari MK, Bolgos G, Miller C, Nguyen DT, DeForge LE, Remick DG. Anti-tumor necrosis factor antibody therapy fails to prevent lethality after cecal ligation and puncture or endotoxemia. *J Immunol* 1992; **148**: 2724–30

56. Camerota AJ, Creasey AA, Patla V, Larkin VA, Fink MP. Delayed treatment with recombinant human tissue factor pathway inhibitor improves survival in rabbits with gram-negative peritonitis. *J Infect Dis* 1998; **177**: 668–76
57. Abraham E, Reinhart K, Opal S, et al. Efficacy and Safety of Tifacogin (Recombinant Tissue Factor Pathway Inhibitor) in Severe Sepsis: A Randomized Controlled Trial. *JAMA* 2003; **290**: 238–47
58. Michie HR, Manogue KR, Spriggs DR, et al. Detection of Circulating Tumor Necrosis Factor after Endotoxin Administration. *N Engl J Med* 1988; **318**: 1481–6
59. von der Möhlen MA, van der Poll T, Jansen J, Levi M, van Deventer SJ. Release of bactericidal/permeability-increasing protein in experimental endotoxemia and clinical sepsis. Role of tumor necrosis factor. *J Immunol Baltim Md 1950* 1996; **156**: 4969–73
60. Calvano SE, Xiao W, Richards DR, et al. A network-based analysis of systemic inflammation in humans. *Nature* 2005; **437**: 1032–7
61. Verbon A, Dekkers PEP, Hove T ten, et al. IC14, an Anti-CD14 Antibody, Inhibits Endotoxin-Mediated Symptoms and Inflammatory Responses in Humans. *J Immunol* 2001; **166**: 3599–605
62. van der Poll T, Coyle SM, Levi M, et al. Effect of a recombinant dimeric tumor necrosis factor receptor on inflammatory responses to intravenous endotoxin in normal humans. *Blood* 1997; **89**: 3727–34
63. Mayr FB, Jilma B. Coagulation interventions in experimental human endotoxemia. *Transl Res* 2006; **148**: 263–71
64. Kruif MD de, Lemaire LC, Giebelen IA, et al. Prednisolone Dose-Dependently Influences Inflammation and Coagulation during Human Endotoxemia. *J Immunol* 2007; **178**: 1845–51
65. Maini AA, George MJ, Motwani MP, Day RM, Gilroy DW, O'Brien AJ. A Comparison of Human Neutrophils Acquired from Four Experimental Models of Inflammation. *PloS One* 2016; **11**: e0165502
66. Cockrell RC, An G. Examining the controllability of sepsis using genetic algorithms on an agent-based model of systemic inflammation. *PLOS Comput Biol* 2018; **14**: e1005876
67. Carvalho D, Petronilho F, Vuolo F, et al. The nociceptin/orphanin FQ-NOP receptor antagonist effects on an animal model of sepsis. *Intensive Care Med* 2008; **34**: 2284–90
68. Williams JP, Thompson JP, Young SP, et al. Nociceptin and urotensin-II concentrations in critically ill patients with sepsis. *Br J Anaesth* 2008; **100**: 810–4

69. Thompson JP, Serrano-Gomez A, McDonald J, Ladak N, Bowrey S, Lambert DG. The Nociceptin/Orphanin FQ System Is Modulated in Patients Admitted to ICU with Sepsis and after Cardiopulmonary Bypass. *PLOS ONE* 2013; **8**: e76682
70. Stamer UM, Book M, Comos C, Zhang L, Nauck F, Stuber F. Expression of the nociceptin precursor and nociceptin receptor is modulated in cancer and septic patients. *Br J Anaesth* 2011; **106**: 566–72
71. Grange RD. Development of an ILMA for N/OFQ. IBSC Dissertation University of Leicester; 2013.
72. Barnes TA, Lambert DG. Editorial III: Nociceptin/orphanin FQ peptide-receptor system: are we any nearer the clinic? *BJA Br J Anaesth* 2004; **93**: 626–8
73. Brown KA, Brain SD, Pearson JD, Edgeworth JD, Lewis SM, Treacher DF. Neutrophils in development of multiple organ failure in sepsis. *Lancet* 2006; **368**: 157–69
74. Al-Hashimi M, McDonald J, Thompson JP, Lambert DG. Evidence for nociceptin/orphanin FQ (NOP) but not μ (MOP), δ (DOP) or κ (KOP) opioid receptor mRNA in whole human blood. *BJA Br J Anaesth* 2016; **116**: 423–9
75. Livak KJ, Schmittgen TD. Analysis of Relative Gene Expression Data Using Real-Time Quantitative PCR and the $2^{-\Delta\Delta CT}$ Method. *Methods* 2001; **25**: 402–8
76. Zhang X, Ding L, Sandford AJ. Selection of reference genes for gene expression studies in human neutrophils by real-time PCR. *BMC Mol Biol* 2005; **6**: 4
77. Andersen CL, Jensen JL, Ørntoft TF. Normalization of Real-Time Quantitative Reverse Transcription-PCR Data: A Model-Based Variance Estimation Approach to Identify Genes Suited for Normalization, Applied to Bladder and Colon Cancer Data Sets. *Cancer Res* 2004; **64**: 5245–50
78. Xie F, Xiao P, Chen D, Xu L, Zhang B. miRDeepFinder: a miRNA analysis tool for deep sequencing of plant small RNAs. *Plant Mol Biol* 2012;
79. Mane VP, Heuer MA, Hillyer P, Navarro MB, Rabin RL. Systematic Method for Determining an Ideal Housekeeping Gene for Real-Time PCR Analysis. *J Biomol Tech JBT* 2008; **19**: 342–7
80. Bustin SA, Benes V, Garson JA, et al. The MIQE Guidelines: Minimum Information for Publication of Quantitative Real-Time PCR Experiments. *Clin Chem* 2009; **55**: 611–22
81. Dedrick RL, Conlon PJ. Prolonged expression of lipopolysaccharide (LPS)-induced inflammatory genes in whole blood requires continual exposure to LPS. *Infect Immun* 1995; **63**: 1362–8

82. Zhang L, Stuber F, Stamer UM. Inflammatory Mediators Influence the Expression of Nociceptin and Its Receptor in Human Whole Blood Cultures. *PLoS ONE* 2013; **8**
83. Gomes NE, Brunialti MKC, Mendes ME, Freudenberg M, Galanos C, Salomão R. Lipopolysaccharide-induced expression of cell surface receptors and cell activation of neutrophils and monocytes in whole human blood. *Braz J Med Biol Res* 2010; **43**: 853–8
84. Moulding DA, Walter C, Hart CA, Edwards SW. Effects of Staphylococcal Enterotoxins on Human Neutrophil Functions and Apoptosis. *Infect Immun* 1999; **67**: 2312–8
85. Kuo C-F, Lin Y-S, Chuang W-J, Wu J-J, Tsao N. Degradation of Complement 3 by Streptococcal Pyrogenic Exotoxin B Inhibits Complement Activation and Neutrophil Opsonophagocytosis. *Infect Immun* 2008; **76**: 1163–9
86. Karlsson A, Nixon JB, McPhail LC. Phorbol myristate acetate induces neutrophil NADPH-oxidase activity by two separate signal transduction pathways: dependent or independent of phosphatidylinositol 3-kinase. *J Leukoc Biol* 2000; **67**: 396–404
87. Cannell IG, Kong YW, Bushell M. How do microRNAs regulate gene expression? *Biochem Soc Trans* 2008; **36**: 1224–31
88. Kimball SR. Eukaryotic initiation factor eIF2. *Int J Biochem Cell Biol* 1999; **31**: 25–9
89. Camarda V, Fischetti C, Anzellotti N, et al. Pharmacological profile of NOP receptors coupled with calcium signaling via the chimeric protein G alpha q α 5. *Naunyn Schmiedebergs Arch Pharmacol* 2009; **379**: 599–607
90. Eglen RM. G Protein Coupled Receptors and High Throughput Screening at G Protein Coupled Receptors. Bentham Science Publishers; 2005.
91. Charlton SJ, Vauquelin G. Elusive equilibrium: the challenge of interpreting receptor pharmacology using calcium assays. *Br J Pharmacol* 2010; **161**: 1250–65
92. Zhang R, Xie X. Tools for GPCR drug discovery. *Acta Pharmacol Sin* 2012; **33**: 372–84
93. Coward P, Chan SDH, Wada HG, Humphries GM, Conklin BR. Chimeric G Proteins Allow a High-Throughput Signaling Assay of Gi-Coupled Receptors. *Anal Biochem* 1999; **270**: 242–8
94. Linden JM. Purinergic Receptors. *Basic Neurochem Mol Cell Med Asp 6th Ed* 1999;
95. Michel AD, Chessell IP, Hibell AD, Simon J, Humphrey PPA. Identification and characterization of an endogenous P2X7 (P2Z) receptor in CHO-K1 cells. *Br J Pharmacol* **125**: 1194–201

96. Marcet B, Chappe V, Delmas P, Verrier B. Pharmacological and Signaling Properties of Endogenous P2Y1 Receptors in Cystic Fibrosis Transmembrane Conductance Regulator-Expressing Chinese Hamster Ovary Cells. *J Pharmacol Exp Ther* 2004; **309**: 533–9
97. Ralevic V, Burnstock G. Receptors for Purines and Pyrimidines. *Pharmacol Rev* 1998; **50**: 413–92
98. Eltzschig HK, MacManus CF, Colgan SP. Neutrophils as sources of extracellular nucleotides: Functional consequences at the vascular interface. *Trends Cardiovasc Med* 2008; **18**: 103–7
99. Lew DP. Receptor signalling and intracellular calcium in neutrophil activation. *Eur J Clin Invest* **19**: 338–46
100. Gupta AK, Giaglis S, Hasler P, Hahn S. Efficient Neutrophil Extracellular Trap Induction Requires Mobilization of Both Intracellular and Extracellular Calcium Pools and Is Modulated by Cyclosporine A. *PLOS ONE* 2014; **9**: e97088
101. Lambert DG, Rainbow RD, editors. Calcium signaling protocols. 3rd ed. New York: Humana Press; 2013.
102. Grynkiewicz G, Poenie M, Tsien RY. A new generation of Ca²⁺ indicators with greatly improved fluorescence properties. *J Biol Chem* 1985; **260**: 3440–50
103. Schindelin J, Arganda-Carreras I, Frise E, et al. Fiji: an open-source platform for biological-image analysis. *Nat Methods* 2012; **9**: 676–82
104. Sato T, Hongu T, Sakamoto M, Funakoshi Y, Kanaho Y. Molecular Mechanisms of N-Formyl-Methionyl-Leucyl-Phenylalanine-Induced Superoxide Generation and Degranulation in Mouse Neutrophils: Phospholipase D Is Dispensable. *Mol Cell Biol* 2013; **33**: 136–45
105. Lukawska JJ, Livieratos L, Sawyer BM, et al. Real-time differential tracking of human neutrophil and eosinophil migration in vivo. *J Allergy Clin Immunol* 2014; **133**: 233-239.e1
106. Yazdanbakhsh M, Eckmann CM, Koenderman L, Verhoeven AJ, Roos D. Eosinophils do respond to fMLP. *Blood* 1987; **70**: 379–83
107. Alam R, Stafford S, Forsythe P, et al. RANTES is a chemotactic and activating factor for human eosinophils. *J Immunol* 1993; **150**: 3442–8
108. Ponath PD, Qin S, Ringler DJ, et al. Cloning of the human eosinophil chemoattractant, eotaxin. Expression, receptor binding, and functional properties suggest a mechanism for the selective recruitment of eosinophils. *J Clin Invest* 1996; **97**: 604–12

109. Trapella C, Guerrini R, Piccagli L, et al. Identification of an achiral analogue of J-113397 as potent nociceptin/orphanin FQ receptor antagonist. *Bioorg Med Chem* 2006; **14**: 692–704
110. Erb L, Weisman GA. Coupling of P2Y receptors to G proteins and other signaling pathways. *Wiley Interdiscip Rev Membr Transp Signal* 2012; **1**: 789–803
111. Coddou C, Yan Z, Obsil T, Huidobro-Toro JP, Stojilkovic SS. Activation and Regulation of Purinergic P2X Receptor Channels. *Pharmacol Rev* 2011; **63**: 641–83
112. Donica CL, Awwad HO, Thakker DR, Standifer KM. Cellular Mechanisms of Nociceptin/Orphanin FQ (N/OFQ) Peptide (NOP) Receptor Regulation and Heterologous Regulation by N/OFQ. *Mol Pharmacol* 2013; **83**: 907–18
113. Thakker DR, Standifer KM. Induction of G protein-coupled receptor kinases 2 and 3 contributes to the cross-talk between μ and ORL1 receptors following prolonged agonist exposure. *Neuropharmacology* 2002; **43**: 979–90
114. Dickinson BC, Chang CJ. Chemistry and biology of reactive oxygen species in signaling or stress responses. *Nat Chem Biol* 2011; **7**: 504–11
115. Kennedy C. PPADs. *XPharm Compr Pharmacol Ref* New York: Elsevier; 2007. p. 1–4
116. Wick MJ, Minnerath SR, Roy S, Ramakrishnan S, Loh HH. Expression of alternate forms of brain opioid ‘orphan’ receptor mRNA in activated human peripheral blood lymphocytes and lymphocytic cell lines. *Brain Res Mol Brain Res* 1995; **32**: 342–7
117. Peluso J, LaForge KS, Matthes HW, Kreek MJ, Kieffer BL, Gavériaux-Ruff C. Distribution of nociceptin/orphanin FQ receptor transcript in human central nervous system and immune cells. *J Neuroimmunol* 1998; **81**: 184–92
118. Kato A, Ogasawara T, Homma T, Saito H, Matsumoto K. Lipopolysaccharide-Binding Protein Critically Regulates Lipopolysaccharide-Induced IFN- β Signaling Pathway in Human Monocytes. *J Immunol* 2004; **172**: 6185–94
119. Holt LM, Olsen ML. Novel Applications of Magnetic Cell Sorting to Analyze Cell-Type Specific Gene and Protein Expression in the Central Nervous System. *PLOS ONE* 2016; **11**: e0150290
120. McCracken JM, Allen L-AH. Regulation of Human Neutrophil Apoptosis and Lifespan in Health and Disease. *J Cell Death* 2014; **7**: 15–23
121. Yousefi S, Green DR, Blaser K, Simon HU. Protein-tyrosine phosphorylation regulates apoptosis in human eosinophils and neutrophils. *Proc Natl Acad Sci U S A* 1994; **91**: 10868–72

122. Sharma M, Hegde P, Aimanianda V, et al. Circulating human basophils lack the features of professional antigen presenting cells. *Sci Rep* 2013; **3**
123. Degel J, Shokrani M. Validation of the efficacy of a practical method for neutrophils isolation from peripheral blood. *Clin Lab Sci J Am Soc Med Technol* 2010; **23**: 94–8
124. Hu P, Zhang W, Xin H, Deng G. Single Cell Isolation and Analysis. *Front Cell Dev Biol* 2016; **4**
125. Kozera B, Rapacz M. Reference genes in real-time PCR. *J Appl Genet* 2013; **54**: 391–406
126. Mehta R, Birerdinc A, Hossain N, et al. Validation of endogenous reference genes for qRT-PCR analysis of human visceral adipose samples. *BMC Mol Biol* 2010; **11**: 39
127. Vandesompele J, De Preter K, Pattyn F, et al. Accurate normalization of real-time quantitative RT-PCR data by geometric averaging of multiple internal control genes. *Genome Biol* 2002; **3**: RESEARCH0034
128. Pfaffl MW, Tichopad A, Prgomet C, Neuvians TP. Determination of stable housekeeping genes, differentially regulated target genes and sample integrity: BestKeeper–Excel-based tool using pair-wise correlations. *Biotechnol Lett* 2004; **26**: 509–15
129. Derveaux S, Vandesompele J, Hellemans J. How to do successful gene expression analysis using real-time PCR. *Methods* 2010; **50**: 227–30
130. Rapacz M, Stępień A, Skorupa K. Internal standards for quantitative RT-PCR studies of gene expression under drought treatment in barley *Hordeum vulgare*: the effects of developmental stage and leaf age. *Acta Physiol Plant* 2012; **34**: 1723–33
131. Jacob F, Guertler R, Naim S, et al. Careful selection of reference genes is required for reliable performance of RT-qPCR in human normal and cancer cell lines. *PLoS One* 2013; **8**: e59180
132. Mehrotra P. Biosensors and their applications – A review. *J Oral Biol Craniofacial Res* 2016; **6**: 153–9
133. Korchak HM, Eisenstat BA, Hoffstein ST, Dunham PB, Weissmann G. Anion channel blockers inhibit lysosomal enzyme secretion from human neutrophils without affecting generation of superoxide anion. *Proc Natl Acad Sci* 1980; **77**: 2721–5
134. Karmakar M, Katsnelson MA, Dubyak GR, Pearlman E. Neutrophil P2X7 receptors mediate NLRP3 inflammasome-dependent IL-1 β secretion in response to ATP. *Nat Commun* 2016; **7**

135. Clemens RA, Newbrough SA, Chung EY, et al. PRAM-1 Is Required for Optimal Integrin-Dependent Neutrophil Function. *Mol Cell Biol* 2004; **24**: 10923–32
136. Bang S, Kim KY, Yoo S, Lee S-H, Hwang SW. Transient receptor potential V2 expressed in sensory neurons is activated by probenecid. *Neurosci Lett* 2007; **425**: 120–5
137. Parenti A, De Logu F, Geppetti P, Benemei S. What is the evidence for the role of TRP channels in inflammatory and immune cells? *Br J Pharmacol* 2016; **173**: 953–69
138. Heiner I, Einfeld J, Halaszovich CR, et al. Expression profile of the transient receptor potential (TRP) family in neutrophil granulocytes: evidence for currents through long TRP channel 2 induced by ADP-ribose and NAD. *Biochem J* 2003; **371**: 1045–53
139. Salmon MD, Ahluwalia J. Pharmacology of receptor operated calcium entry in human neutrophils. *Int Immunopharmacol* 2011; **11**: 145–8
140. Itagaki K, Kannan KB, Singh BB, Hauser CJ. Cytoskeletal reorganization internalizes multiple transient receptor potential channels and blocks calcium entry into human neutrophils. *J Immunol Baltim Md 1950* 2004; **172**: 601–7
141. Björk S, Vainio M, Scheinin M. Uneven cellular expression of recombinant α 2A-adrenoceptors in transfected CHO cells results in loss of response in adenylyl cyclase inhibition. *Biochim Biophys Acta BBA - Mol Cell Res* 2005; **1744**: 38–46
142. Kelly E, Bailey CP, Henderson G. Agonist-selective mechanisms of GPCR desensitization. *Br J Pharmacol* 2008; **153**: S379–88
143. Donica CL, Awwad HO, Thakker DR, Standifer KM. Cellular Mechanisms of Nociceptin/Orphanin FQ (N/OFQ) Peptide (NOP) Receptor Regulation and Heterologous Regulation by N/OFQ. *Mol Pharmacol* 2013; **83**: 907–18
144. Sun D, Zhang M, Liu G, et al. Real-Time Imaging of Interactions of Neutrophils with *Cryptococcus neoformans* Demonstrates a Crucial Role of Complement C5a-C5aR Signaling. *Infect Immun* 2016; **84**: 216–29
145. Brunel SF, Bain JM, King J, et al. Live Imaging of Antifungal Activity by Human Primary Neutrophils and Monocytes in Response to *A. fumigatus*. *J Vis Exp JoVE* 2017;
146. Hoppenbrouwers T, Autar ASA, Sultan AR, et al. In vitro induction of NETosis: Comprehensive live imaging comparison and systematic review. *PLOS ONE* 2017; **12**: e0176472
147. Nauseef WM. Isolation of Human Neutrophils from Venous Blood. *Neutrophil Methods Protoc* Humana Press, Totowa, NJ; 2014. p. 13–8

148. Allen L-AH. Immunofluorescence and Confocal Microscopy of Neutrophils. *Methods Mol Biol Clifton NJ* 2014; **1124**: 251–68
149. de Buhr N, von Köckritz-Blickwede M. How Neutrophil Extracellular Traps Become Visible. *J. Immunol. Res.* 2016.
150. McCaffrey RL, Allen L-AH. Pivotal Advance: *Francisella tularensis* LVS evades killing by human neutrophils via inhibition of the respiratory burst and phagosome escape. *J Leukoc Biol* 2006; **80**: 1224–30
151. Casbon A-J, Allen L-AH, Dunn KW, Dinauer MC. Macrophage NADPH Oxidase Flavocytochrome b Localizes to the Plasma Membrane and Rab11-Positive Recycling Endosomes. *J Immunol Baltim Md 1950* 2009; **182**: 2325–39
152. Baker JG, Hall IP, Hill SJ. Pharmacology and direct visualisation of BODIPY-TMR-CGP: a long-acting fluorescent β 2-adrenoceptor agonist. *Br J Pharmacol* 2003; **139**: 232–42
153. Schaff UY, Yamayoshi I, Tse T, Griffin D, Kibathi L, Simon SI. Calcium Flux in Neutrophils Synchronizes β 2 Integrin Adhesive and Signaling Events that Guide Inflammatory Recruitment. *Ann Biomed Eng* 2008; **36**: 632–46
154. Thomas TA, Dragas-Graonic S, Holmes R, Perez HD. Signal Transduction by the Formyl Peptide Receptor STUDIES USING CHIMERIC RECEPTORS AND SITE-DIRECTED MUTAGENESIS DEFINE A NOVEL DOMAIN FOR INTERACTION WITH G-PROTEINS. *J Biol Chem* 1995; **270**: 28010–3
155. Lou L-G, Zhang Z, Ma L, Pei G. Nociceptin/Orphanin FQ Activates Mitogen-Activated Protein Kinase in Chinese Hamster Ovary Cells Expressing Opioid Receptor-Like Receptor. *J Neurochem* **70**: 1316–22
156. Haskell MD, Moy JN, Gleich GJ, Thomas LL. Analysis of signaling events associated with activation of neutrophil superoxide anion production by eosinophil granule major basic protein. *Blood* 1995; **86**: 4627–37
157. Masterson JC, McNamee EN, Fillon SA, et al. Eosinophil-mediated signalling attenuates inflammatory responses in experimental colitis. *Gut* 2015; **64**: 1236–47
158. Al Hashimi M, Thompson JP, Calo G, Guerrini R, Lambert DG. Nociceptin/orphanin FQ receptor stimulation reduces human polymorphonuclear cell migration in vitro; Abstracts of the Spring Anaesthetic Research Society Meeting (ARS). *Br J Anaesth* 2015; **115**: e950–62
159. Merino CA, Martínez FT, Cardemil F, Rodríguez JR. Absolute eosinophils count as a marker of mortality in patients with severe sepsis and septic shock in an intensive care unit. *J Crit Care* 2012; **27**: 394–9

160. Abidi K, Khoudri I, Belayachi J, et al. Eosinopenia is a reliable marker of sepsis on admission to medical intensive care units. *Crit Care* 2008; **12**: R59
161. Rosenberg HF, Dyer KD, Foster PS. Eosinophils: changing perspectives in health and disease. *Nat Rev Immunol* 2012; **13**: 9–22
162. Acharya KR, Ackerman SJ. Eosinophil Granule Proteins: Form and Function. *J Biol Chem* 2014; **289**: 17406–15
163. Mantovani A, Cassatella MA, Costantini C, Jaillon S. Neutrophils in the activation and regulation of innate and adaptive immunity. *Nat Rev Immunol* 2011; **11**: 519–31

8. Publications and grants relating to this thesis

Publications

1. Al-Hashimi M, Scott SWM, Thompson JP, Lambert DG. Opioids and immune modulation: more questions than answers. *Br J Anaesth* 2013; **111**: 80–8
2. Scott S, Thompson JP, Lambert DG. Investigating nociceptin/orphanin FQ signalling in immunocytes: preliminary studies using live cell imaging.; Proceedings of the Anaesthetic Research Society Meeting: Merton College, Oxford, UK, April 11–12, 2013. *Br J Anaesth* 2013; **111**: 309P-320P
3. S.W. M. Scott, J. M. Willets, J. P. Thompson and D. G. Lambert. Lipopolysaccharide stimulation modifies nociceptin/orphanin FQ mRNA expression in immunocytes; Proceedings of the Anaesthetic Research Society Meeting Aberdeen Exhibition Centre, Aberdeen, 21–22 June 2012. *Br J Anaesth* 2012; **109**: 655P-668P

In preparation:

1. Bird MF, Hebbes CP, Scott SWM, Willetts J, Thompson JP, Lambert DG. A bioassay to detect nociceptin release from granulocytes. *PLOS Biology*.
2. Scott SWM, Thompson JP, Lambert DG. NOP and ppNOC expression in PMNs and whole blood is modulated by LPS.

Grants

1. 2016: BBSRC Biosensor based approach to measure release of Nociceptin/Orphanin FQ from live single immune cells and consequences for immune cell function. (Data acquired in this thesis formed the basis of this application). D G Lambert, J M Willets: **£338,432**
2. 2012: Intensive Care Foundation, Young Investigator Award: **£12,836**
3. 2011: Heath Family Grant Award, Anaesthetic Research Society: **£12,815**